Characterising Chinese Hamster Ovary Cell Extracellular Vesicle Production in Biopharmaceutical Manufacturing

Fergal O'Donnell

A thesis submitted for the Degree of Doctor of Philosophy

Department of Chemical and Biological Engineering

University of Sheffield

Supervisor: Prof. David C. James

Secondary Supervisor: Dr. Stuart Hunt

Sponsored by: Lonza, Slough, UK

Declaration

I, Fergal O’Donnell, declare that the research and findings contained within this thesis are entirely my own. All experimental work and techniques, unless clearly stated otherwise, have been performed by me.

Acknowledgements

There are several people I would like to acknowledge in helping me along this journey.

My parents, Elizabeth and Colm. Your love, guidance and encouragement is what has given me the confidence to go after every ambition I've had in life. Without it, I very much doubt I would have had the strength and bravery to pursue this and the many other amazing life experiences I have had.

My brother, Cormac, who I always look to as a standard-bearer for hard work and how to carry oneself around others.

Then there is my uncle, Mel. I am not able to put into words my gratitude for the support you have given me over the years. I can only hope that you take pride in anything I achieve.

I would like to thank everyone in the DCJ and AJB lab groups. There have been so many Post Docs and PhD students (both former and current) who freely gave up their time to give help and advice when it was needed. I feel privileged to be able to count you as friends for life. A particular mention has to go to my C14 office mates: Molly Smith and Thilo Pohle. My fellow Paddies: Pamela O'Neill, Adrian Bourke and Alex Tsimperdonis (my housemate and Greek Paddy). You made going to work every day a joy and I wish you all the success you deserve in your careers.

To Prof. David James, I can't thank you enough for the opportunity to do this PhD. You were always available and willing to give invaluable direction and knowledge throughout the project. Know that I really enjoyed learning from throughout my time in the DCJ group.

A special thanks has to go to Dr. Stuart Hunt for all his support and technical knowledge for all things EV related – particularly earlier on in the project when I was new to the EV World. If the title of "EV-Sage" ever becomes a thing, you will definitely have earned it.

Thank you also to Andy Racher, Bernie Sweeney and Frida Grynspan at Lonza for their advice and guidance during the project. Especially in the latter half of the project where Bernie and Frida were always willing to go over data and give excellent feedback. This was a massive contribution to the outcomes of the project and they could not have been achieved without you.

Lastly, I would like to thank Leona. You were there throughout it all. Dating a scientist isn't easy (or so you tell me). I love you and hope I make you proud.

Acronyms and Abbreviations

μ Specific Growth Rate

AB Apoptotic Body

Actb ß-Actin

ACTN1 Alpha-actinin-1

AIX Anion Exchange Chromatography

AKI Acute Kidney Injury

Anxa2 Annexin A2

ARF6 ADP ribosylation factor 6

ARRDC1 arrestin domain-containing protein 1

BCA Pierce™ BCA Protein Assay Kit

Becn1 Beclin-1

cDNA complimentary DNA

CE Cholesteryl Ester

CHMP Charged Multivesicular Body Protein

CHO Chinese Hamster Ovary

CMV cytomegalovirus

CRISPR clustered regularly interspaced palindromic repeats

Cryo-EM Cryo Electron Microscopy

CSI Clone Select Imager

DA Diacylglycerol

DE Differential Expression

DHFR Dihydrofolate reductase

Dnm2 Dynamin 2

DOPC Dioleoyl-phosphatidylcholine

DSB Double strand breaks

DTE Difficult to Express

EM Electron Microscopy

EPO Erythropoietin

ER Endoplasmic Reticulum

ERK extracellular signal regulated kinase

ESCRT endosomal sorting complexes required for transport

ETE Easy to Express

EV Extracellular Vesicle

EVB Extracellular Vesicle Biogenesis

Ex-Cell Ex-Cell CHO Cloning Media

Flot1 Flotilin 1

GFP Green Fluorescent Protein

GOI Gene of Interest

GS Glutamine Synthase

GSKO-Host CHO-K1SV Glutamine Synthase Knock-Out - Host

GSTM1 Gluthatione S-transferase Mu 1

GSTM7 Glutathione S-transferase Mu 7

HCP Host Cell Protein

HDR Homology Directed Repair

HexCer hexoscylceramide

Hspa8 Heat shock protein 70

Icam1 Intercellular Adhesion Molecule 1

ILV Intraluminal Vesicles

IRES internal ribosomal entry site

IVCD Integral Viable Cell Density

lEV large Extracellular Vesicle

lncRNA long non-coding RNA

LPL Lipoprotein Lipase

MA Monoacylglycerol

mAb Monoclonal Antibody

MHC-I Major Histocompatibility Complex I

miRNA microRNA

MLCK Myosin Light Chain Kinase

mRNA messenger RNA

MS Mass Spectrometry

MSC Mesenchymal Stem Cell

MSX Methionine Sulfoximine

MTX Methotrexate

MV microvesicle/ microparticle/ ectosome

MVB Multivesicular Body

NaBu Sodium Butyrate

NANA N-acetylneuraminic acid

NEFA Non-esterified fatty acids

NGNA N-glycoylneuraminic acid

NHEJ Non-homologous end joining

NTA Nanoparticle tracking analysis

PAM photospacer-adjacent motif

PBS Phosphate Buffered Saline

PC Phosphatidylcholine

PE Phosphatidylethanolamine

PI3P phosphatidylinositol-3-phosphate

piRNA piwi interacting RNA

PTM Post translational modification

qGLU specific glucose consumption rate

RCME Recombinase mediated cassette exchange

rDNA recombinant DNA

RFU Relative Fluorescent Units

RHOA Ras homolog gene family, member A

RPS27A Ubiquitin-40S ribosomal protein 27a

rRNA ribosomal RNA

Sdc1 Syndecan 1

SEC Size Exclusion Chromatography

SEM Scanning Electron Microscopy

sEV small Extracellular Vesicle

SM sphingomyelin

SOD1 Superoxide Dismutase 1

Stx17 Syntaxin-17

Stx4 Syntaxin-4

Stx5 Syntaxin-5

TALENS transcription activator-like effector nucleases

TB Tuberculosis

TEM Transmission Electron Microscopy

TFF Tangential Flow Filtration

TFRE transcription factor regulatory element

tRNA transfer RNA

TSG101 Tumour Susceptibility Gene 101

TUBA1B Tubulin alpha-1B

UC Differential Ultracentrifugation

UCOE ubiquitous chromatin opening element

Vcam1 Vascular Cell Adhesion molecule 1

VCD Viable Cell Density

VtRNA vault RNA

YBX1 nuclease-sensitive element binding protein 1

ZFN Zinc Finger Nuclease

Abstract

Extracellular Vesicles (EVs) are lipid bilayer bound particles containing several classes of protein, lipid and nucleic acid that are secreted by cells. Depending on the subclass of EV in question, they range from 30 – 1,000nm in size. Over the last decade, their utility in cell-to-cell communication has been described in detail in literature. This has ranged from use as biomarkers in cancer to tissue regeneration in stem cell therapies.

Chinese Hamster Ovary (CHO) cells are one of the most commonly used host cell lines in biopharmaceutical manufacturing; particularly in the case of monoclonal antibody (mAb) production. They can be grown to large cell densities, are less susceptible to viruses which infect human cells and can glycosylate proteins in a human-like-manner. These characteristics, amongst many others, have enabled industrial processes to be created that maximise mAb production in CHO cells.

Whilst it is known that CHO cells secrete EVs, little is understood about the influence of EVs in a biopharmaceutical manufacturing context or what factors impact EV secretion. This thesis established if CHO cells utilised EVs in biopharmaceutical manufacturing by sampling EVs from different time-points in a CHO fed-batch process. This determined if the quantity, size or composition of those EVs change as a fed-batch progresses through different stages of growth. It also looked to see what impact EVs have on their recipient cells; particularly through characterisation of the EV RNA content.

By comparing the EV profile of a non-producing host cell line to a producer cell line, differences in the RNA and lipid composition of EVs between cell lines were investigated. There was also an analysis of what factors drive EV biogenesis in CHO. This assessed whether a particular stage in the cell line development process impacts EV secretion or if there are distinct cellular characteristics which correlate with EV secretion. This was done both by physical quantification of EVs and by transcriptomic analysis of genes involved in EV Biogenesis.

Lastly, the thesis looked to determine if CHO EVs could be used for cellular engineering purposes through promotion of cell growth or by enhancing single cell cloning efficiency.

Taken together, this thesis shows that EV secretion in CHO is largely a conserved process. It reveals that while the EV RNA content may serve to provide anti-apoptotic stimuli, the nucleic acid composition remains largely consistent throughout the manufacturing process. Interestingly, the quantities of EVs secreted and transcriptional activity of EV biogenesis genes does vary considerably between cell lines; with a significant negative correlation with mAb secretion. There is also variation in lipid composition depending on the cell line the EVs are derived from. Cellular engineering attempts which involved using purified EVs to promote growth in low density cell cultures and survival of single cell clones were unsuccessful. Again, this further alludes to EV biogenesis in CHO being evolutionarily conserved with limited utility for biopharmaceutical manufacturing purposes.

Table of Contents

List of Tables

List of Figures

Chapter 1

Literature Review

This chapter is to give a general overview of biopharmaceutical production. It will briefly discuss the history of biologics and how biopharmaceuticals are manufactured in CHO cells. There will also be an overview of extracellular vesicles (EV). This will include their classifications, biogenesis, applications, isolation techniques, characterization techniques and how they are being studied in the context of CHO.

1.1 CHO cells in Biopharmaceutical Manufacturing

The use of biologically derived agents as a source of medicines has long been an established practice. Edward Jenner's discovery that inoculation with cowpox could ve used as a means to prevent the contraction of the deadlier small pox is well documented (Esparza, 2020). Similarly, the use of sphagnum moss in bandages for wounded soldiers during World War One because of its antimicrobial properties is credited with saving many lives (Drobnik and Stebel, 2017). However, biologically derived therapeutics such as Alexander Fleming's discovery of penicillin in 1928, didn't become commercially available until much later. When it did in the 1940's, the research drive was towards chemical synthesis of the drug rather than the fermentation process that was in use (Wright, Seiple and Myers, 2014; Gaynes, 2017). Up until the 1990s, chemically synthesised drugs would make up the near entirety of drug approvals. This was until it became technologically possible to manufacture drugs produced by living organisms at large scale – referred to as "biologics" (Morrow and Felcone, 2004; Kinch, 2015).

The way in which biologics are manufactured began in the 1950s with the first vaccines for adenovirus using primary cell lines from animal donors. This was progressed to using diploid cells with finite lifespan in the 1960s to produce polio vaccine. Despite

the creation of immortalized cell lines from cancer cells, such as the HeLa cell line in the 1950s, there was initially fear in the scientific community about approving immortalize cell lines for the production of biologics. This was due to the lack of knowledge surrounding cancer at the time. Diploid cells were also hesitantly approved as it was believed they had an unquantifiable possibility to become cancerous. It wasn't until the 1970s that the first cancer cell line, Namalwa, was used in clinical trials for the production of interferon (Petricciani and Sheets, 2008).

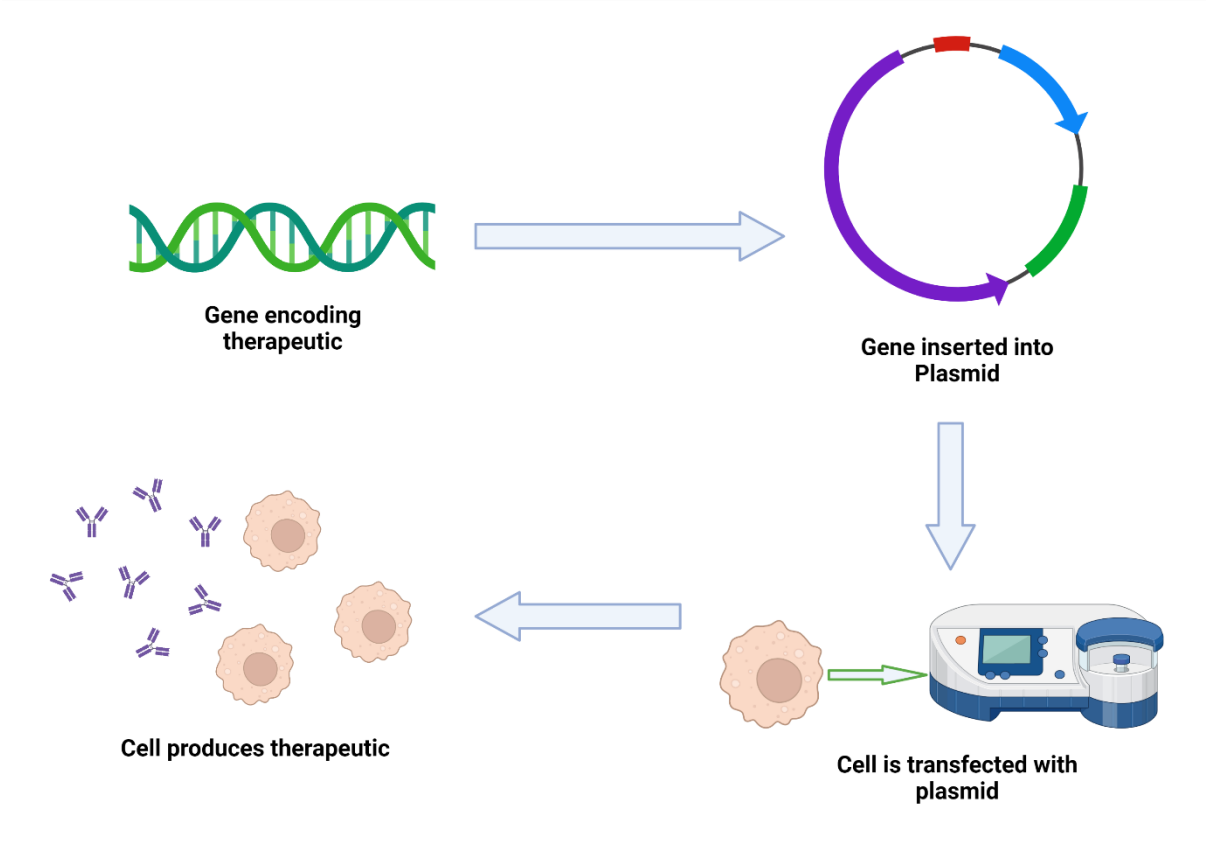

Fig 1.1 Genetic Engineering of Cells with Recombinant DNA to Produce a Protein Therapeutic. *The gene encoding a protein drug or nucleic acid drug is inserted into a plasmid which is transfected into the cell. The cell then transcribes and translates the plasmid containing the gene to produce the drug.*

The development of recombinant DNA (rDNA) technology in the 1980s brought forth the possibility of engineering cell lines that were ideal for manufacturing biologics. rDNA technology enabled the fusion of genes which meant a host cell could be genetically modified to produce a desired product rather than relying on the product being naturally produced by the cell – as was previously the case (Petricciani and

Sheets, 2008). These biologics derived from cells which are genetically engineered to produce them are referred to as “biopharmaceuticals”. According to Walsh (2002), the definition of a biopharmaceutical is: “a protein or nucleic acid based pharmaceutical substance used for therapeutic or in vivo diagnostic purposes, which is produced by means other than direct extraction from a native (non-engineered) biological source”. In biopharmaceutical manufacturing, a cell produces the desired drug after a transgene encoding the product/ gene of interest (GOI) is integrated into the cell’s genome. Examples of biopharmaceuticals include, but are not limited to, monoclonal antibody (mAb), gene therapies, recombinant hormones, vaccines and cytokines (Walsh, 2002).

It was also in the 1980s that CHO cells were first identified as a good host cell line for manufacturing purposes. Subsequently, the cell line was immortalised (Petricciani and Sheets, 2008). The reasons CHO were chosen are numerous. They are relatively immune to human viruses and able to grow in chemically defined serum-free media to large densities. These attributes gave them advantages over human cell lines (Lai *et al.,* 2013; Dumont *et al.*, 2016). Their human-like glycosylation, amongst other post-translational modifications (PTMs), meant they could produce a wider range of complex products compare to those secreted by other non-human cell lines such bacteria. Glycosylation is the addition of glycans to the drug. This glycan addition varies in pattern from species to species and it determines the stability of the drug in the patient’s body and is therefore a crucial PTM. In addition to this, proteins secreted by CHO do not aggregate to the same degree as those produced by bacteria making them easier to manufacture on a large scale (St Amand *et al.*, 2014; Dumont *et al.*, 2016; Lalonde and Durocher, 2017; Peng *et al.*, 2017).

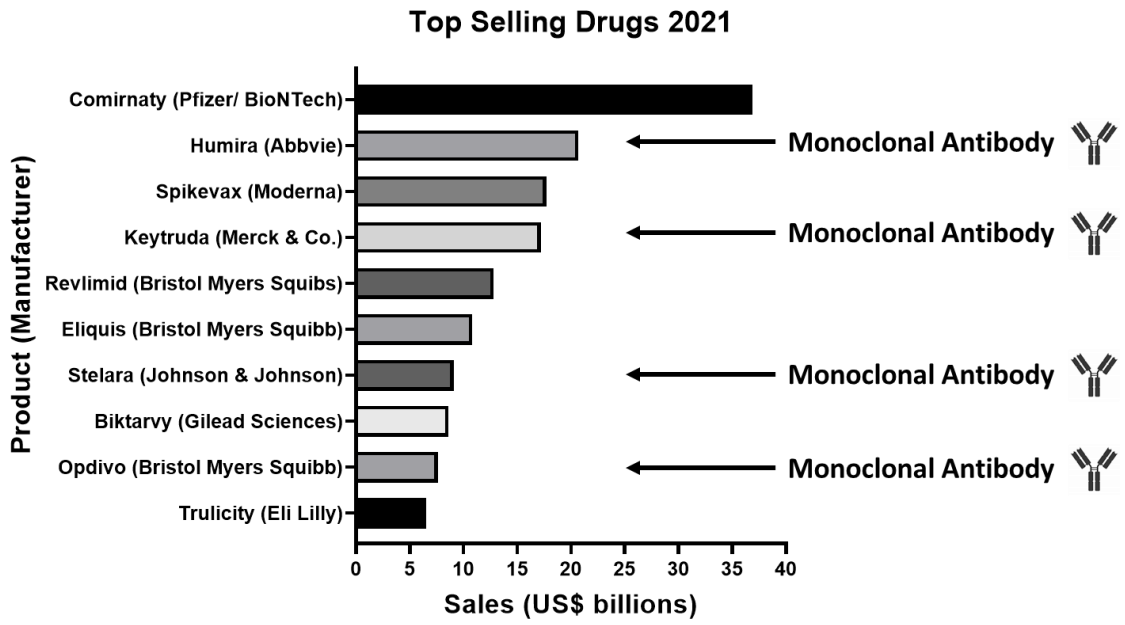

Fig 1.2 Top selling drugs of 2021 (Urquhart, 2022). mAbs represented four of the top 10 selling drugs of 2021. Covid-19 vaccines, Cominarty and Spikevax, are anticipated to sharply decline in sales revenue from 2022 onwards.

Today, biopharmaceutical manufacturing is almost equal to traditional pharmaceuticals in terms of new drug approvals. From the period of 2014 to 2018, biopharmaceuticals accounted for 47% of new drug approvals in the US. This is compared to 21% in 2010 and 26% in 2014 which indicates a substantial shift towards their manufacture over traditional pharmaceuticals. Of those biopharmaceutical drugs approved, 53% of these were mAbs (Walsh, 2018). As recently 2021, mAbs represented eight of the 4 of the top 10 highest selling drugs (See Fig) (Urquhart, 2022). The utility of CHO cells for manufacturing mAbs in particular is reflected in that 84% of the mAbs approved were produced in CHO (Walsh, 2018). It is also worth noting that 48% of biopharmaceuticals approved in the 2014-2018 period are biosimilars – “a biological product that is approved based on the totality of evidence demonstrating that it is highly similar to an approved biological product (originator) in terms of structure, function, quality, and clinical efficiency and safety” - Declerck *et al.* (2017). It is most likely that biosimilars for novel CHO derived biopharmaceuticals will also be manufactured in CHO. This again emphasizes the prevalence of CHO in biopharmaceutical manufacturing (Declerck *et al.*, 2017; Walsh, 2018).

1.2 Biopharmaceutical Manufacturing in CHO – An Overview

The manufacture of mAb in CHO requires a cell line development process which considers every facet of the cell's capability to produce the drug product. There are several factors both intrinsic and extrinsic which can influence the product yield. The approaches to utilising these factors are also continuously improved upon to maximise drug yield.

1.2.1 Transgene Plasmid Design

The first consideration when manufacturing a mAb in CHO is the design of the plasmid containing the GOI encoding the protein product. Variations in plasmid design can depend on both the product being expressed and whether it is being optimised for a transient expression system or a stable one. Transient expression systems are where the plasmid is not incorporated into the genome and therefore product expression is lost over time due to cell division and other cytoplasmic events. A stable system is where a cell has the plasmid incorporated into its genome and will continue to strongly express the product after many cell divisions. However, to create a stable expression system is time consuming and involves screening processes to identify the best producing single clones (Kim and Eberwine, 2010).

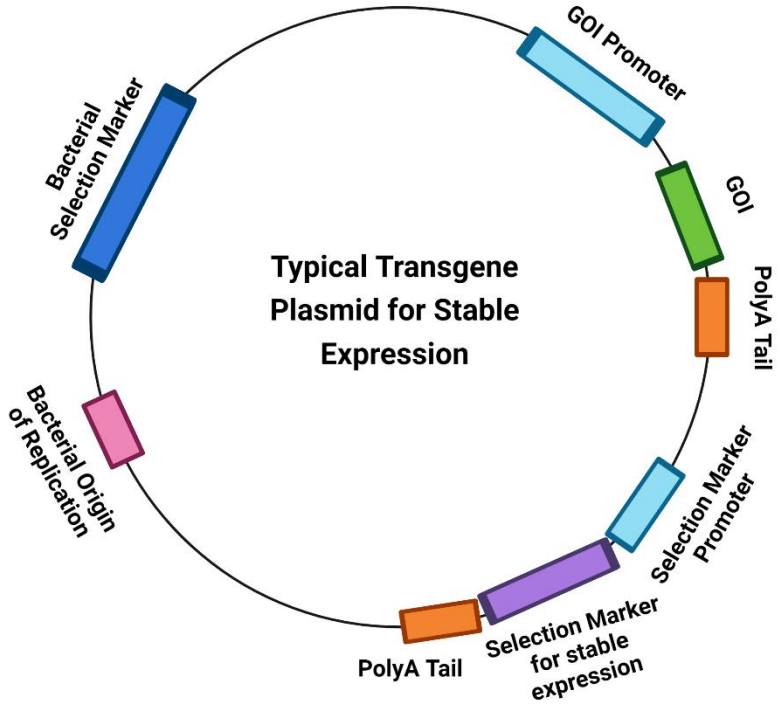

Fig 1.3 A basic map of a plasmid containing a transgene encoding a product (GOI). *The plasmid contains the GOI. Upstream of this is the promoter sequence which initiates transcription with a PolyA Tail downstream of the GOI that terminates transcription. There is also a selection marker gene which allows selection of cells which have stably incorporated the plasmid into their genome. In order to propagate the plasmid (i.e. make more of it for transfecting mammalian cells), the plasmid contains a bacterial origin of replication. This allows bacteria to replicate it whilst the bacterial selection marker means on bacteria which have incorporate the plasmid will grow in the media used to propagate the plasmid. This maximises the numbers of bacteria making copies of the plasmid.*

Constituents of a plasmid include an origin of replication and an antibiotic resistance gene for propagation of the plasmid in bacteria. For expression of the GOI in eukaryotic cells, the first major feature is the promoter sequence for initiating transcription. Then there is the GOI encoding the actual product. Lastly, there's the terminator sequence which stops transcription – usually a polyA tail at the end of the GOI. In the generation of stable systems, selection markers, accompanied with their own promoter and terminator sequences, enable differentiation and selection of CHO cells which have incorporated the plasmid into their genome from transient producers. There are also plasmid designs which have an internal ribosomal entry site (IRES); a small linker

sequence between the GOI and selection marker. It enables the GOI and selection marker to be transcribed and translated at the same time. This ensures that the expression of a selection marker can be correlated to strong product expression (Williams, Carnes and Hodgson, 2009; Kim and Eberwine, 2010; Voronina *et al.*, 2016; Carrara *et al.*, 2021).

Plasmid design has been improved upon over many years. Promoter sequences and their elements have been manipulated significantly to improve GOI expression. Classically, viral promoters such as the cytomegalovirus (CMV) and SV40 promoters have been used in CHO. However, these promoters do not utilize the full suite of transcriptional machinery present in the cell. More recent designs, described as "synthetic promoters", incorporate a number of transcription factor regulatory elements (TFREs) that are designed to maximize the transcriptional capabilities of the cell. Minimal CMV promoters have had copies of TFREs such as nuclear factor kappa B and enhancer box added upstream. These two TFREs, amongst others, have been demonstrated to significantly outperform standard CMV promoters 24 hours post transfection in CHO-S cells in the production of both SEAP and Green Fluorescent Protein (GFP) (Brown *et al.*, 2014).

A significant challenge of transgene expression in CHO has been their propensity to become epigenetically silenced; resulting in lower titres over time. This refers to modifications to the cell's chromatin containing the DNA sequence in which GOI has integrated. An example of one such modification is DNA methylation which can inhibit the activity of transcription enzymes at the promoter sequence. To prevent modifications such as these from occurring, ubiquitous chromatin opening elements (UCOEs) have been added to plasmid designs. They act as regulatory elements which keeps the chromatin around the GOI in a transcriptionally active state. An example is the murine ribosomal protein S3 UCOE. This is a 3 kb single promoter element surrounded by CpG islands – approximately 1000 base pair long segments of DNA highly abundant in cytosine and guanine nucleic acids. CpG islands are frequently reported to be absent of DNA methylation. This demethylated state enhances transcription initiation at the promoter (Deaton and Bird, 2011; Veith *et al.*, 2016; Neville *et al.*, 2017).

Selection markers for the generation of stable systems have also evolved over time. The most common selection marker to date is the dihydrofolate reductase (DHFR) gene. This encodes an enzyme which converts dihydrofolate to tetrahydrofolate. Methotrexate (MTX) can inhibit this gene in CHO but cells which have taken up a plasmid containing DHFR and integrated it into their genome can become resistant to MTX. Amplification of the DHFR gene is done through multiple screening rounds of MTX media addition to select only CHO cells which have strong DHFR expression. Strong selection marker expression is correlated to strong and stable GOI product expression. Therefore only cells that are stably making the product are selected for (Chusainow *et al.*, 2009). A newer selection system uses glutamine synthase (GS) as the selection marker. Glutamine synthase is required for the synthesis of glutamine; an essential nutrient in CHO. The gene can be inhibited by methionine sulfoximine (MSX). However, CHO cells which have incorporated a plasmid containing GS into their genome can be resistant to MSX. Therefore, like the DHFR selection system, only CHO with amplified GS expression are selected for during screening. Further stringency can be added to the system with the use of CHO cell lines with endogenous GS expression knocked-out using zinc finger nucleases (ZFNs) (Fan *et al.*, 2012). The advantage of the GS selection system over the DHFR system is that GS selection only requires one round of MSX addition to culture media for the selection process compared to multiple rounds using the DHFR/ MTX system. This significantly shortens the cell line development timeline. An additional bonus is that ammonia accumulation is minimized as the excess GS activity catalyses its conversion to glutamine (Fan *et al.*, 2013; Noh *et al.*, 2018). Ammonia is a toxic metabolite of CHO which can accumulate during a bioprocess (Rita Costa *et al.*, 2010).

1.2.2 Transgene Integration

The next consideration in generating a stable mAb producing CHO cell line is in the integration of the plasmid to the genome. This too is another aspect of cellular engineering to have improved. Advancements in both genome sequencing and editing technologies have enabled control and specificity in where the transgene plasmid integrates into a host cell's genome. This has been reflected in identification of

genomic transcriptional “hot spots” in CHO such as the BMP5 or CLCC1 loci (Hamaker and Lee, 2018). Conventionally, the plasmid encoding the GOI is integrated at random using a variety of transfection methods. However, this often results in integration happening at sites which are either not transcriptionally active or unstable in their transcriptional activity. Newer approaches look to harness nuclease enzymes with a guide sequence that enables targeted integration at transcription hotspots. Examples include transcription activator-like effector nucleases (TALENS), ZFNs and clustered regularly interspaced palindromic repeats (CRISPR) with a Cas nuclease. In the case of CRISPR/ Cas, a guide RNA strand is used to localize towards a particular sequence of DNA. The target sequence is located adjacent to a photospacer-adjacent motif (PAM) for recognition by the Cas nuclease which then cuts the DNA to form a double strand break (DSB). The strand then repairs itself either by non-homologous end joining (NHEJ) or, if a donor plasmid containing the gene of interest is present, homology directed repair (HDR). HDR results in the GOI being transcribed from the location in the genome where the DNA was cut. One caveat the targeted integration method is that CHO cells have an inclination towards NHEJ over HDR. This can result in undesired gene deletions and truncations. However, combining nucleases with recombinases can overcome this. Recombinase mediated cassette exchange (RCME) technology such as the Bxb1 cassette can be targeted to specific locations in the genome using CRISPR/Cas. These cassettes contain landing pads which are flanked by recombinase target sites. These include frt sites for Flp recombinases and loxP sites for Cre recombinases. The landing pads can contain selection markers which allow cells that have successfully integrated the cassette to be screened for. Once identified, the RMCE tagged CHO cells can be transfected with a plasmid encoding a gene of interest and selection marker that is also flanked by recombinase target sites. In the cell, recombinase enzymes then mediate the exchange of the gene of interest with the landing pad sequence. The sequence has then been successfully targeted to the desired loci; avoiding the need for HDR to occur (Lee *et al.*, 2015; Hamaker and Lee, 2018; Gleditzsch *et al.*, 2019).

1.2.3 The Influence of The Extracellular Environment

Productivity in CHO manufacturing is not just dictated by the genetic engineering strategies employed in cell line development; the culture conditions that affect the extracellular environment are critical determinants of cell growth, titre and product quality. In large scale upstream manufacturing, CHO cells are grown in large bioreactors in media that has been optimised for production. Depending on the cell line or product, the media may not need to be fed (batch culture) or fed at regular intervals (fed-batch culture). The bioreactors contain in-process controls capable of monitoring and maintaining the culture environment by constantly checking and adjusting pH, dissolved oxygen content, CO_2 content and temperature amongst other factors (Hong *et al.*, 2018; Mitra and Murthy, 2022). These factors form part of a list of what are defined as process parameters and have fixed set-points. This is because deviations from their desired set-points will negatively impact the titre obtained or the product quality (Randek and Mandenius, 2017).

Consistent and high product quality is crucial from a regulatory standpoint as it ultimately dictates the safety and efficacy of the drug (Das *et al.*, 2020). An example of how this is the case is the glycosylation profile the product protein – otherwise known as the glycoform. The glycoform of a protein determines its half-life in the blood. Sialylated erythropoietin (EPO) has a half-life of 5-6 hours in rodents vs 2 minutes when desialylated. In humans, asialylated proteins are cleared from the blood in the kidney. The same occurs for proteins with exposed galactose monosaccharides (Hossler *et al.*, 2009). A disadvantage of CHO produced biopharmaceuticals is that there can often be high N-glycoylneuraminic acid content (NGNA). This is a derivative of N-acetylneuraminic acid (NANA). While NANA is commonly found on human proteins, NGNA is not and can induce an immunogenic response which results in rapid removal of the protein from the blood. Thus, for both the production of a therapeutically effective and safe product, it is imperative that majority of the product made is composed of the one glycoform. By increasing pCO_2 of a culture, it was found that higher quantities of the NANA glycoform could be obtained (Hossler, Khattak and Li, 2009).

Other extrinsic factors can modulate the glycoform obtained also. The pH of the culture can alter both galactosylation and sialylation of a mAb. High ammonia content can inhibit or alter glycosylation; the recommended culture content shouldn’t be more than

2mM. In addition, while shown to increases culture lifespan, cultures ran at 30°C can have decreased sialylation on their product (Hossler *et al.*, 2009).

Glycosylation isn't the only attribute of product quality affected by the culture environment. For instance, pH and ion content of the media and shear stress from the bioreactor's agitator can all cause the protein product to unfold and aggregate. Therefore, tight monitoring and control of the extracellular environment when manufacturing mAb in CHO cell culture is necessary to achieve both high titre and the desired product quality (Pandey, 2022).

1.2.4 Engineering the Extracellular Environment Composition

1.2.4.1 Improving mAb titre with additives to the media

Given the influence of extracellular environment on the cell, it has been utilised to control GOI expression. Some promoters are tetracycline inducible. That is where they require the small molecule, tetracycline, to be present in the media before transcription of the transgene can occur. The promoter can then be inhibited by another small molecule, doxycycline. The benefit of such promoters is evident where the cell is producing a difficult-to-express (DTE) protein. Quite often the accumulation of these proteins is toxic to the cell so it is therefore desirable to control when expression of these proteins occur. The product protein can also be stressful to the cellular compartments involved in protein synthesis; such as the endoplasmic reticulum (ER). This results in low product titres. The small molecules can therefore inhibit expression of the DTE protein until the cell density of the culture has met a required level. At which point, a higher product yield can be obtained because the number of cells secreting the protein is maximised (Tadauchi *et al.*, 2019).

Small molecules aren't just effective with promoters designed specifically to harness them. Sodium butyrate (NaBu) media supplementation can effectively enhance GOI expression irrespective of the promoter design. It does so by inhibiting histone deacetylase enzymes. Histones are protein constituents of chromatin. By keeping histones acetylated, chromatin stays in a transcriptionally active conformation. The

enhanced transcriptional activity, in turn, results in greater titres of product (Jiang and Sharfstein, 2008). However, a caveat to using NaBu is it can inhibit cell growth and induce apoptosis which can damage the product being made by the cell. One way in which this can be overcome is by shifting the temperature of the culture from 37°C to 30°C a few days after seeding. These are known as biphasic cultures. While doing so without NaBu supplementation has been effective in prolonging the length of a bioprocess, in the case of NaBu, it mitigates the apoptotic effects of the chemical (Chen *et al.*, 2011).

1.2.4.2 Removing HCPs from the Extracellular Environment

Strategies have also been employed to remove unwanted constituents of the extracellular environment during manufacturing; particularly Host Cell Proteins (HCPs). There is large consideration when developing both upstream and downstream bioprocesses as to how to minimize their presence in both the final product and in the culture itself. The accepted industry standard is 100 ppm or fewer in the final product. This is because they can generate an immunogenic response in patients – which is particularly important for those taking anti-inflammatories or immunosuppressants as they may have a potentially dangerous response (Jawa *et al.*, 2016; Gilgunn and Bones, 2018).

However, their presence during culture and subsequent harvest can also have negative impacts to yield and product quality. Proteinases such as cathespin D or matrix metalloproteinase-19 can degrade the product while it is still in culture. Other HCPs can hinder the effectiveness of downstream processes like the use of protein A columns. High amounts of chromatin has been found to spoil the resin. The removal of chromatin from the harvest prior to protein A chromatography has been shown to markedly enhance HCP removal from the end product (Gilgunn and Bones, 2018).

Over 116 HCPs in CHO have been characterized as difficult to remove from the final product (Chiu *et al.*, 2017). Although there is a large number of difficult to remove HCPs, it appears as those many of them are common irrespective of the cell line or product being made (Yuk *et al.*, 2015; Gilgunn and Bones, 2018). This has allowed the development of strategies to inhibit their accumulation in the culture. One way is

to look at culture conditions and modify them so as to alter the HCP profile. In particular, the use of biphasic culture temperatures has a significant effect on the HCP profile at harvest. This was demonstrated by Goey *et al.*, (2017) where the culture was grown at normal temperature (36.5-37°C) and shifted to mild hypothermia (32°C) during mid-exponential phase. It was found that despite overall HCP concentration being similar at harvest, the variety of HCPs was significantly lower in the mild hypothermic cultures. They also found 44% less protease HCP species.

Other methods have pursued removing the genes expressing specific HCPs. Genome editing techniques have made this possible. Chiu *et al.*, (2017) employed both CRISPR and TALENS to knock-out lipoprotein lipase (LPL) expression in CHO; a difficult to remove HCP. This was done as LPL was shown to degrade polysorbates. These are surfactants added to the final mAb product that aid in long-term storage of the drug by competing with the drug for surface adsorption. LPL removal was shown to reduce polysorbate degradation by 41%.

1.3 Extracellular Vesicles – An important constituent of the Extracellular Environment

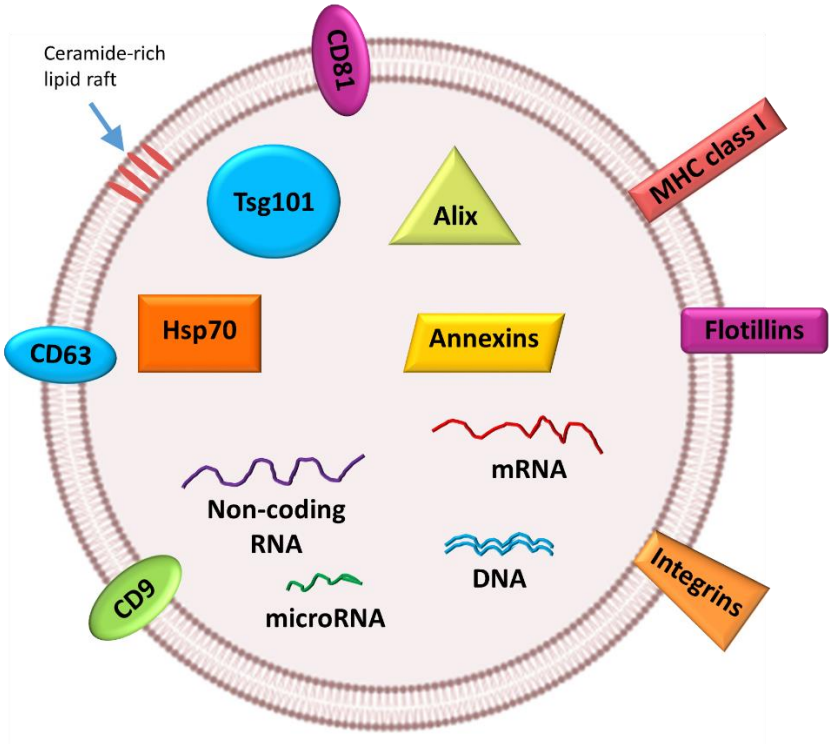

Fig 1.4 Composition of an Extracellular Vesicle based on description from Théry et al., (2018). *The composition of an EV can vary depending on the cell of origin as well as the subclass of EV in*

question. In general, they are lipid bilayer bound nanoparticles and contain several proteins such as TSG101, Hsp70, Annexins and Alix in their cytosol. Their membranes also have transmembrane proteins such as the tetrapsanins (CD63, CD81 and CD9) and embedded proteins such as Major-Histocompatibility Complexes (MHC), Flotillins and Integrins. EV membranes are also reported to be enriched in ceramide relative to cellular membranes. The nucleic acid composition is reported to contain mRNA, DNA and both long and short non-coding RNA.

Given the influence of the extracellular environment on biopharmaceutical manufacturing, the role of Extracellular Vesicles (EVs) in that environment comes into focus. Little is known about the function of EVs in a mAb manufacturing context. They are present in significant quantities – between ~1 $x10^9$ – 1 x 10^{11} particles/ml depending on the phase of culture (Belliveau and Papoutsakis, 2022). This project aims to characterise CHO EVs and their function. Therefore, the remainder of this review will discuss what EVs are, their biogenesis, their utility in other cell types, the techniques associated with their purification and function and what is known about them in context to CHO so far.

1.3.1 Extracellular Vesicles – Composition and Function

EVs are lipid bilayer bound particles secreted by the cell ranging from 30nm in size to 1µm in size. They are enriched in numerous proteins, DNA, messenger RNA (mRNA), microRNA (miRNA) and other small RNA classes (see Fig) and are divided into numerous classes based on their location of origin within the cell (Kao and Papoutsakis, 2019; Mathieu *et al.*, 2019; Paolicelli *et al.*, 2019). A lot of their possible functions in the CHO extracellular environment can be hypothesized from their influence on other cell lines. While originally thought to be “dumps” for cellular waste, there is ever increasing evidence that they facilitate cell-to-cell or paracrine communication. This is where cells secret different molecules that signal other cells in a culture to produce a response. In the case of EVs, their paracrine effects can be attributed to their DNA, RNA or protein cargo depending on the biological process occurring (Torralba *et al.*, 2018; Whitham *et al.*, 2018; Haimovich and Gerst, 2019).

Some of the strongest evidence for their paracrine effects is in how they enable cancer progression. The contents of tumour derived EVs have been demonstrated numerous times to promote angiogenesis and metastasis. They can also induce differentiation of healthy fibroblasts into myofibroblasts (Xu *et al.*, 2018).

The utility of their paracrine signalling is also evident in other cell types. EVs released by immune cells are known to regulate immune stimulation and suppression as well as drive inflammatory responses (Robbins and Morelli, 2014; Kakarla *et al.*, 2020). This has prompted studies which looked to manipulate their role in immune responses. One example is where EVs taken from macrophages treated with mycobacterium tuberculosis (TB) culture filtrate protein were shown to bare TB antigens that could prime the immune response against TB in mice – comparable to a standard vaccine. They were also able to boost the immune response in of mice already vaccinated against TB (Cheng and Schorey, 2013). Similar studies and clinical trials have looked at using the contents of EVs as potential anti-tumour vaccines. The exosomes from immature dendritic cells were shown to contain major histocompatibility complexes that could, in combination with the right co-stimulatory molecules such as CD40 and B7.2, prime T-cells to inhibit tumour growth (Viaud et al., 2011).

Stem cells are another cell type where the cell-to-cell communication facilitated by EVs has been intensely studied. Given that the tissue regenerative capabilities of a mesenchymal stem cell (MSC) is often attributed to their paracrine signalling, EVs isolated from MSCs have been investigated in preclinical models for their therapeutic properties. In the case of cardiac diseases, MSC EVs reduced myocardial infarction sizes by up to 40% in mice. Effective regeneration has also been demonstrated in acute kidney injury (AKI) in mice. MSC EVs were even shown to be comparable to MSCs themselves in regulating the inflammatory response of AKI. Other beneficial effects have been observed in preclinical models treated with MSC derived EVs for lung and liver disease as well as wound healing (Rani *et al.*, 2015). There are currently many MSC EV based therapies undergoing clinical trials (Chen *et al.*, 2020).

Overall, there are several cell types where EVs have been shown to facilitate paracrine signalling. These include liver cells, kidney cells, brain cells and cardiac cells (Szabo and Momen-Heravi, 2017; Badhwar and Haqqani, 2020; Lee, Choi and Yoo, 2021; Saheera *et al.*, 2021).

Such is their potency in being able to transfer cargo from cell to another that EVs are being proposed as vehicles for drug delivery. As EVs can be derived from the organism they are treating, they generate a lower immunogenic response compared to other drug delivery methods requiring a vector that isn't native to the body. They also have cell targeting capabilities and can pass the blood-brain barrier; increasing bioavailability of the drug to the tissue which needs it. EVs have been successfully loaded with small RNAs, mRNA, small chemical drugs and enzymes. There are two processes by which EVs can be loaded with material. The first is pre-isolation whereby the cell secreting them is treated with a high dosage of the molecule that is to be loaded into the EVs. This has been done with the drug Paclitaxel in mesenchymal stromal cells. The second process involves isolating the EVs from the cell secreting them and then incorporating the drug. In the case of anti-inflammatory drug, curcumin, direct mixing of EVs with the drug at room temperature for 5 minutes can sufficiently incorporate the drug. Other drugs, such as RNA based drugs and enzymes which are hydrophilic and won't cross the EV lipid bilayer, require methods like electroporation and sonication which make the EV membrane porous and accessible. Saponin, a glycoside that complexes with cholesterol in the EV membrane to make them porous, is another loading method used. Catalase enzymes have successfully been loaded into EVs by Saponin treatment and used to protect neurons from reactive oxygen species (Gray *et al.* 2015; Vader *et al.*, 2016).

1.3.2 EV Subclasses

The intercellular message carried by an EV may depend on the subclass of EV in question (Tkach *et al.*, 2017). There are two main subclasses secreted by healthy cells that are distinguished by both their size and biogenesis pathways: exosomes and microvesicles/ microparticles/ ectosomes (MVs) (Mathieu *et al.*, 2019). Exosomes are generally 50-150nm in size whilst MVs are 100nm-1000nm in size (Moghadasi *et al.*, 2021). In addition to these, there are Apoptotic Bodies (ABs) which are EVs shed from the membrane of cells undergoing apoptosis and are >500nm in size (Kakarla *et al.*, 2020; Moghadasi *et al.*, 2021). Traditionally, the attribution of these subclasses to EVs in literature was based on their observed physical size, the fact they were isolated by

a certain purification technique or simply the authors' discretion due to a lack of fixed terminology for different EV subclasses (Théry *et al.*, 2018). An example being how Kumar *et al.* (2016) use "microvesicles" as an umbrella term for both microvesicles and exosomes. However, there are no specific markers for each EV subclass and they can easily overlap in their physical attributes depending on the cell line e.g. a large exosome could be 150nm and a small MV could be 100nm and both have the same protein markers. Therefore, it is difficult to state with certainty what subclass of EV is being investigated unless the EV's biogenesis is directly observed. To overcome this, it is now preferable to refer to EVs based on their physical nature (e.g. size), biochemical composition (e.g. CD63+ EVs) or cell of origin (Théry *et al.*, 2018). For the purposes of results chapters in this thesis, and in accordance with Théry *et al.* (2018), an EV population with an observed mode size of ≤100nm will be referred to as a small EV (sEV) and an EV population with an observed mode size >100nm will be called a large EV (lEV) (Hood *et al.*, 2014; Tricarico *et al.*, 2017; Hessvik and Llorente, 2018; McAndrews and Kalluri, 2019).

1.3.3 Extracellular Vesicle Biogenesis

There are numerous routes for Extracellular Vesicle Biogenesis (EVB) to occur. The biogenesis of exosomes can be divided into the endosomal sorting complexes required for transport (ESCRT) dependent and ESCRT independent pathways. Briefly, these involve inward budding of endogenous membranes to form intraluminal vesicles (ILVs). This results in the creation of multivesicular bodies (MVBs). MVBs fuse with the plasma membrane to release their ILVs into the extracellular space; generating exosomes. For MV biogenesis, vesicles are formed through outward budding and shedding of the plasma membrane (Latifkar *et al.*, 2019).

1.3.3.1 ESCRT Pathway

1.3.3.1.1 ESCRT-0 and EV Cargo Recruitment

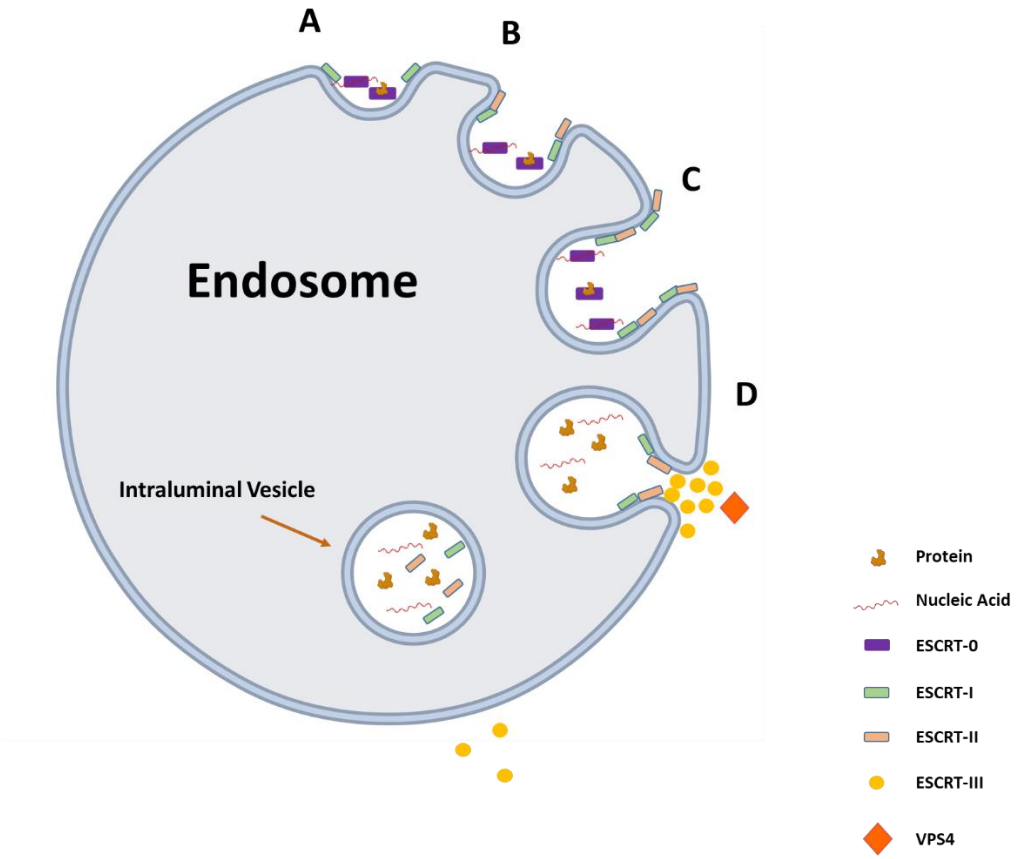

Fig 1.5 ESCRT Pathway. *(A) ESCRT-0 recruits and localises proteins and nucleic acids to endosomal membrane within the cell. It also recruits ESCRT-I. (B) ESCRT-I recruits ESCRT-II and promotes inward budding of endosomal membrane. (C) The accumulation of ESCRT-I and ESCRT-II further buds the membrane inwards. (D) ESCRT-II recruits ESCRT-III which accumulates at the neck of the inward budding and causes fission of the neck which generates the intraluminal vesicle (ILV). ESCRT-III is a transient complex and is disassembled and recycled to the cytoplasm by VPS4. This process recurs numerous times until there are multiple ILVs within the endosome. The endosome is then referred to as a Multivesicular Body (MVB). MVBs fuse with the plasma membrane to release their ILVs as EVs to the extracellular environment.*

The ESCRT pathway involves four protein complexes: ESCRT-0, ESCRT-I, ESCRT-II and ESCRT-III along with accessory proteins. The pathway begins with ESCRT-0 which is involved in selection and recruitment of cargo to endogenous membranes called endosomes. There are two potential fates of cargo recruited to endosomes. The first is to be packaged into exosomes. The other is where the endosome fuses with a

lysozyme to form a lysosome and has its contents degraded. The mechanisms by which cargo is recognized and distinguished for exosome packaging rather than lysosomal degradation is poorly understood. In the case of proteins, PTMs such as ubiquitination, phosphorylation, ISGylation and glycosylation are all thought to be key in distinguishing cargo for exosomes packaging. Often, it can be a lack of a certain PTM which may be a determinant. An example is ANNEXIN A2 which undergoes lysosomal degradation rather than exosome packaging in the absence of phosphorylation of its Tyr23 residue. ISGylation of TSG101, normally found in EV cytosol, causes it to aggregate and be degraded in a lysosome. The ESCRT-0 subunits are designed to recognize PTMs. The core ESCRT-0 proteins STAM1/2 and HRS both contain ubiquitin binding domains which enable them to bind and recruit ubiquitinated cargo to the endosome (Frankel and Audhya, 2018; Anand *et al.*, 2019).

It is thought that RNA, particularly miRNAs, are recruited to EVs by proteins with RNA binding domains. ANNEXIN A2 binds to miRNAs irrespective of their sequence and this enables their subsequent packaging into EVs (Hagiwara *et al.*, 2015a). There is also evidence that the accessory protein, ALIX, shuttles miRNA into EVs. It does so by binding to AGO2, an argonaute protein that is involved in transporting miRNAs around the cell (Iavello *et al.*, 2016). Not unlike proteins, how RNA is distinguished for packaging into EVs is not fully understood. However, the 3’ end of miRNAs may aid in dictating whether or not they become packaged into EVs. 3’ end adenylated miRNAs were found to be enriched in B cells. However, in EVs derived from B cells, 3’ end uridylated isoforms of these miRNAs were more abundant (Anand *et al.*, 2019). Some miRNAs also contain seed sequences or motifs that enable their binding to RNA binding proteins which have been shown to facilitate sEV formation. This is the case with miR-198 which binds to hnRNPA2B1 through a specific motif. Mutation of this motif hinders its binding to hnRNPA2B1 and subsequent loading into EVs (S. P. Li *et al.*, 2018). There are also genes which have been identified as influencers of which miRNAs and mRNAs are found in EVs. This is the case in colorectal cancer cells which have a mutant KRAS gene. Cells with this mutation have distinct miRNA and mRNA profiles from their wild type counterparts (Hinger *et al.*, 2018).

1.3.3.1.2 ESCRT-I

After the recruitment of cargo proteins and nucleic acids, ESCRT-0 localizes to the endosome. It does so by binding to phosphatidylinositol-3-phosphate (PI3P) which is a phospholipid found abundantly on the endosome membrane (Schmidt and Teis, 2012). ESCRT-I then binds to ESCRT-0. This is a complex consisting of the subunits TSG101, VPS28, VPS37A-D and UBAP1. It can also contain MVB12 but this appears to be more prevalent in HIV budding than in MVB formation. The ESCRT-0/ ESCRT-1 interaction is mediated by TSG101. UBAP1 can also bind ubiquitin present on ESCT-0 cargo which may promote the interaction. VPS28 then recruits ESCRT-II to the endosome (Morita *et al.*, 2007; Stefani *et al.*, 2011; Agromayor *et al.*, 2012).

1.3.3.1.3 ESCRT-II

ESCRT-II comprises of VPS36, VPS22 and two VPS25 subunits. It is the GLUE domain of VPS36 which binds to the VPS28 present on ESCRT-I. It is unclear as to whether cargo is passed along ESCRT-0, ESCRT-I and ESCRT-II like a conveyor belt or if they interact with different proteins on the endosome membrane to form a sorting complex. This complex initiates MVB formation. Aggregation of ESCRT-I and ESCRT-II has the effect of budding the endosome membrane inwards. While budding is occurring, the two VPS25 subunits on ESCRT-II each bind to VPS36 and VPS22 to form a Y-shape confirmation. This enables them to recruit ESCRT-III (Schmidt and Teis, 2012).

1.3.3.1.4 ESCRT-III

ESCRT-III is composed of four core subunits: charged multivesicular body protein (CHMP) 6 (which mediates binding to VPS22 of ESCRT-II), CHMP4, CHMP3 and CHMP2. It also has accessory proteins: CHMP1, CHMP5 and hlst1. Unlike the other ESCRT complexes, ESCRT-III is a transient complex and only when its subunits combine to form the complex do they have high affinity for membranes. Once bound,

ESCRT-III further drives the inward budding of the endosome membrane. While the mechanism has yet to be fully described, it also causes fission of the inward budding membrane to create ILVs. VPS4A, an ESCRT-associated protein, then binds to ESCRT-III. Its N-terminal contains a microtubule-interacting and transport domain which can bind to domains present in the C-terminals of ESCRT-III subunits. It is an ATPase associated with various cellular activities that functions to disassemble ESCRT-III and recycle it to the plasma membrane. This process continues until the endosome contains numerous ILVs and can now be classed as a MVB (Alonso Y Adell, Migliano and Teis, 2016; Jackson *et al.*, 2017).

1.3.3.1.5 MVB Mobilisation to Plasma Membrane

The MVB then mobilizes to the plasma membrane to fuses and release its ILVs as exosomes. This mobilization and fusion is thought to be regulated by Rab GTPases. Fusion with the plasma membrane, in particular, is facilitated by Rab27a and Rab27b. The Rab GTPases may also have a role in whether MVBs fuses with the plasma membrane or a lysozyme. It is thought that over expression of Rab5 promotes lysosomal degradation as it inhibits sEV secretion (Ostrowski *et al.*, 2010).

1.3.3.1.6 Plasma Membrane Fusion and Uptake in Recipient Cells

Docking and fusion of MVBs for release into the extracellular environment is dictated through the action of soluble NSF attachment protein receptor (SNARE) proteins. For EVB, these include VAMP7, SYNTAXIN-1a, YKT6 and SNAP-23 (Teng and Fussenegger, 2021) .

Once released to the extracellular environment, EVs are taken up by recipient cells through several mechanisms including: endocytosis, clathrin-dependent endocytosis, caveolin-dependent endocytosis, lipid raft-dependent endocytosis, micropinocytosis, phagocytosis or membrane fusion. How cells recognise and bind to EVs is controlled by proteins present on the EV membrane and the type of uptake. Examples include the tetraspanins (CD9, CD81, CD63) for recognition by the recipient cell. In the case

of lipid raft dependent endocytosis, FLOTILLIN-1 binds the EV to the lipid raft on the cell membrane (Mulcahy, Pink and Carter, 2014)..

1.3.3.2 Non-Classical Exosome Biogenesis:

1.3.3.2.1 ESCRT Associated

MVB formation can also occur through both ESCRT associated and ESCRT independent methods. The former is the case in the ALIX-SYNTENIN-SYNDECAN pathway. ALIX is responsible for loading syndecan into EVs. It does this by binding syntenin which in turn binds syndecan. Not only does ALIX serve as a cargo recruiter, in this way it also stimulates ILV bud formation when bound to syntenin (Baietti *et al.*, 2012). The tetraspanins such as CD9 and CD63 are also thought to influence EV secretion. Studies which have either enhanced or knocked-out their expression reported changes in the quantity of EVs measured. This implies a role for tetraspanins in sEV biogenesis, however, whether they work independently or synergistically with ESCRT machinery is unclear (Hessvik and Llorente, 2018).

1.3.3.2.2 ESCRT Independent

Lipid modifying enzymes can also generate EVs such as neutral sphingomyelinase 2 (nSmase) and phospholipase D2. nSmase converts sphingomyelin to ceramide. Inhibition of nSmase has been shown to reduce sEV secretion (Hessvik and Llorente, 2018). Ceramide is thought to be a critical component of the sEV membrane. It has been shown to be enriched in sEV membranes 1.3-3 times more than in cell membranes. This enrichment occurs in domains or “lipid rafts” at different points in sEV membrane. The lipid rafts are also reported to play a significant role in cargo sorting to the EV as many proteins associate with them; such as major histocompatibility class I (MHC-I) and FLOTILLIN-1. These proteins can in turn facilitate interactions with other cargo. (S. P. Li *et al.*, 2018). Therefore, diminishing

cellular ceramide levels is believed to impact negatively on sEV formation (Elsherbini and Bieberich, 2018).

In the case of phospholipase D2, it releases phosphatidic acid (PA) from phospholipids which may favour ILV formation. In addition, it acts as an effector for ADP ribosylation factor 6 (ARF6), a small GTPase. ARF6 is a regulator for the previously discussed Alix-syntenin-syndecan pathway of EVB and its inhibition can inhibit EVs generated by this pathway (Baietti *et al.*, 2012; Hessvik and Llorente, 2018).

1.3.4. lEV Biogenesis

The major difference that distinguishes lEVs from sEVs is that they are shed directly from the plasma membrane. There are domains in the plasma membrane referred to as lipid “rafts” which are enriched in sphingolipids and tetraspanins that promote interactions which stimulate vesicle budding (Pollet *et al.*, 2018). The domains are asymmetric which can cause curvature of the membrane. The asymmetry is created through the action of ATP dependent enzymes called flippases and floppases (Muralidharan-Chari *et al.*, 2010). Cargo is recruited to these domains by proteins such as ARF6 and Rab22a. ARF6 in particular is thought to recruit VAMP3, ß-1 integrin and MHC-1 (Tricarico *et al.*, 2017).

The mechanism by which shedding occurs is when ARF6-GTPases activates phospholipase D which in turn phosphorylates extracellular signal regulated kinase (ERK). The phosphorylated ERK phosphorylates a Ca^{2+} / calmodulin dependent kinase called myosin light chain kinase (MLCK). MLCK lastly phosphorylates myosin II light chains (MLC) which cause the actin-based cytoskeleton to contract. Phosphorylated myosin II light chains have been observed to accumulate at the necks of lEVs at the cell surface. This actomyosin-based contraction allows the lEV to be “pinched” from the cell membrane and shed (Muralidharan-Chari *et al.*, 2009).

ARF1 also phosphorylates MLC in a similar manner to ARF6. RHOA facilitates phosphorylation of MLC for both ARF1 and ARF6 and can be regulated by DIAPH3 (Kim *et al.*, 2014; Tricarico, Clancy and D’Souza-Schorey, 2017)

ESCRT proteins can sometimes also generate lEVs. This is the case with TSG101 which can be translocated from the endosome membrane to the plasma membrane

through its association with arrestin domain-containing protein 1 (ARRDC1). TSG101 then promotes budding of the plasma membrane (Nabhan *et al.*, 2012).

Elevated concentrations of Ca^{2+} in the cell can increase lEV shedding. It is believed that Ca^{2+} dependent scramblases in the cell cause lipid asymmetry which effectively creates lipid domains. This in turn promotes lEV biogenesis (Crawford *et al.*, 2010; Muralidharan-Chari *et al.*, 2010).

1.4 EV isolation methods

1.4.1 Differential Ultracentrifugation

According to Théry *et al.* (2018), differential ultracentrifugation (UC) is the purification technique most used in EV research. Typically, this involves three centrifugations speeds used on cell culture supernatants: 1,500 – 2,000g for 10 minutes to removes large cell debris, 10,000 – 20,000g for 30 minutes to pellet smaller cell debris (this speed has also been used to isolate lEVs) and 100,000g spin for 70 minutes to isolate sEVs (Livshts *et al.*, 2015; Momen-Heravi, 2017; Deville *et al.*, 2021). A further step can be added where the sEV pellet is re-suspended in PBS and centrifuged again at 100,000g for 70 minutes. This can increase the purity of the sEVs 2-fold, however, it will also result in loss of yield (Webber and Clayton, 2013).

Variations on this method include using sucrose and iodixanol gradients to separate EVs from non-EV proteins and particles. This is known as density gradient ultracentrifugation. In this method, prior to spinning at 100,000g, the spin tube is set up so that it contains higher concentrations of iodixanol or sucrose at the bottom of the tube and lower concentrations near the top. This means higher density particles fractionate towards the bottom of the tube whilst lower density particles fractionate at the top. Therefore, this obtains a greater degree of EV purity than a standard 100,000g ultracentrifugation where everything that's dense enough to pellet at 100,000g is obtained in one pellet. Another benefit is it can better maintain the biophysical properties of the sEVs. However, density gradient ultracentrifugation requires the EV sample to undergo a concentration step prior to addition to the gradient which can

result in a loss of yield. The 100,000g spin can also take up to 24 hours with this method which lowers its throughput (Momen-Heravi, 2017; K. Li *et al.*, 2018). Another consideration for all UC techniques is the volume capacity of the ultracentrifuge being used. This reduces its utility in large scale studies where greater quantities of EVs are desired (Heath *et al.*, 2018).

1.4.2 Size Exclusion Chromatography

Size exclusion chromatography (SEC) is a technique which separates particles as they move through a column based on their size. The column is packed with beads which have pores of specific size. Larger particles will not fit into these pores and therefore move through the column quickly while smaller particles fit into the pores and have their movement through the column slowed down. Typically, samples are added to the column and are moved through it with a running buffer. Once it reaches the bottom of the column, the sample can be gathered in several fractions. Earlier fractions usually contain the larger cellular debris which is not retained by the column. Middle fractions are where sEVs are recovered. Later fractions usually contain small HCPs which move very slowly through the column. The benefits of using this technique are that it can effectively isolate sEVs from both larger and smaller particles and has minimal impact of their physical characteristics compared to other purification techniques. The disadvantages of this method are that particles which happen to be the same size as the EVs can co-isolate with them. In addition, samples can require concentration steps using techniques like diafiltration both prior to addition to the column and afterwards which reduces the throughput (Gámez-Valero *et al.*, 2016; Benedikter *et al.*, 2017; Liangsupree, Multia and Riekkola, 2021).

1.4.3 Immunoprecipitation and Immunocapture

EVs can be isolated using protein markers present on their surface. These markers can range from generic tetraspanins (CD9, CD81, CD63) to markers that isolate EVs from cells of a particular disease state e.g. HER2 being used to isolate EVs from

tumour cells. This method usually involves coating magnetic beads with antibodies specific to the marker of interest. The beads can either be floating freely in a tube or stacked into a column. Once sample is added to the mix/ column with antibody coated beads, the EVs bind to the beads and a wash step removes all unbound sample. This is followed by an elution step to dissociate the EVs from the beads. If the beads are floating freely, a magnet is used to hold them in position during the wash and elution steps. The benefit to this isolation method is its specificity – it will obtain very pure EV samples. The caveats are that EVs which may lack the protein marker on the capture beads will be removed during the wash steps. There is also the limitation that the amount of beads and capture antibody used will limit the quantity of EVs obtained. This causes the method to be high in cost if a large quantity of EVs are desired (Nakai *et al.*, 2016; Heinzelman, 2018; Beekman *et al.*, 2019; Carnino, Lee and Jin, 2019; Logozzi *et al.*, 2020).

1.4.4 Commercially Available Kits

Several EV isolation kits have been brought to market which aim to provide user friendly, quick purifications of EVs. Kits such as ExoQuick (Systems Biosciences), Total Exosome Purification Kit (Invitrogen) and PureExo (101 Bio AMS Biotechnology) all use polymers to precipitate EVs from a sample. While a high yield is often obtained, the purity of the EVs tends to be lower relative to other purification methods (Lucchetti, Fattorossi and Sgambato, 2019).

Other kits such as Exospin (Cell Guidance Systems) and exoEasy (Qiagen) utilise SEC and membrane affinity respectively. Other kits, such as Exo-Flow (Cell Guidance Systems), combine polymer precipitation with immunoprecipitation. The performance of these kits can be highly variable and their suitability for use is often dependent on the requirements of the user (Macías *et al.*, 2019).

1.4.5 Tangential Flow Filtration

Tangential flow filtration (TFF) involves moving sample across a filter horizontally rather than perpendicularly as is the case with classical filtration techniques. The benefit of doing this is that filters are slower to clog and the physical properties of the sample are better maintained as they are not packed against the pores in the filter. This technique has been used to purify and concentrate EVs; usually with two filters. The first filter is greater in size than sEVs (>200nm) and this separates sEVs from larger cell debris in a sample. Once the sEVs have passed this initial filter, they enter a chamber where they accumulate and face a filter that is smaller than them (<30nm). This next filter retains the sEVs but allows small HCPs and waste media to pass through (Kim *et al.*, 2021). The advantage of this method is that it is scale-able and enables the relatively quick purification of EVs from large volumes of supernatant (McNamara *et al.*, 2018). A disadvantage is that anything within the size range of the two filters will be retained which may diminish EV purity depending on the cell source. It also requires the use of pumps and equipment which may not be available to research groups which do not specialise in purification (McNamara *et al.*, 2018; Kim *et al.*, 2021).

1.4.6 Anion Exchange Chromatography

In anion exchange chromatography (AIX), there is a solid phase and a mobile phase. The mobile phase contains the EV sample which moves along the solid phase – usually a monolith or a resin. In the case of AIX, the solid phase is positively charged. As the membrane of EVs are negatively charged, they bind to the solid phase as the liquid mobile phase containing the EVs moves along it. The EVs can then be eluted by changing the ionic strength of the mobile phase which weakens the binding of the EVs to the solid phase (Heath *et al.*, 2018; Staubach *et al.*, 2021).

1.5 EV Analysis Techniques

1.5.1 Nanoparticle Tracking Analysis

Nanoparticle Tracking Analysis (NTA) allows for both the quantification and size measurement of EVs. It involves passing the liquid sample containing EVs through a flow cell. As the EVs pass through the flow cell, light from a laser is aimed at them. Upon contact with the EV, the light scatters. This light scatter enables detection of individual EVs for quantification. To measure the size of the EVs, the camera on the NTA equipment tracks the light scatter of the EV as it moves through the liquid medium it is suspended in. This is referred to as Brownian Motion and correlates with the size of the EV (Gardiner *et al.*, 2013). A caveat of NTA is that it isn't an EV specific measurement - all non-EV particles present in the sample will be detected. To overcome this, NTA instruments are sold with fluorescent filters; such as the Nanosight NS300. However, most fluorophores lack the photostability (stability of the fluorophore upon excitation) to be measured by NTA. EVs can be labelled with antibodies conjugated fluorescent quantum dots which are very photostable to distinguish them from non-EV particles. The difficulty with this method is that antibodies have reduced reactivity when conjugated with quantum dots. It also requires a step to remove unbound antibody-quantum dot conjugates which can vary in its effectiveness (Thane, Davis and Hoffman, 2019).

Another consideration when using NTA is the variability in quantification between instruments from different manufacturers. Indeed, variability in quantification measurements on the same instrument is often very high – up to 25% when samples are measured on different days. Further variation can also be created depending on the settings different users choose when measuring a sample (Vestad *et al.*, 2017; Bachurski *et al.*, 2019).

1.5.2 Western Blotting

There are several protein markers which are enriched in EVs. It is expected that all studies detailing EVs show that their samples contain some of these markers to confirm the presence of EVs (Théry *et al.*, 2018). One way in which the presence of these markers can be tested for is through western blotting. Western blotting involves lysing the protein from a sample, loading to a bis-tris gel and running the gel at 150-200V for ~40 minutes to separate the proteins by their molecular weight. Once this is

done, the proteins in the gel are transferred to a membrane (e.g. a PVDF membrane) using a machine which runs a current through the gel that causes the proteins to migrate from the gel to the membrane (e.g. iBlot dry blotting system). The membrane is then blocked with a milk buffer to prevent non-specific binding, washed and then incubated with primary antibody. Post incubation, the membrane is washed and secondary antibody is added. This secondary "detection" antibody is conjugated to either an enzyme or a fluorophore which enables detection of the protein. While the method is mostly used for qualitative purposes, it can be used quantitatively when using fluorophores for detection (Eaton *et al.*, 2014; Kowal *et al.*, 2017).

1.5.3 Flow Cytometry

Flow cytometry is a technique where particles scatter light as they move through a flow channel. As light from a laser hits the particles, they produce a forward scatter which enables their detection and quantification. They also produce a side scatter which is proportional to their size and enables size measurement. Flow cytometers can also quantify fluorescently labelled particles by detecting the signal emitted once the dye/ fluorophore has been excited by the flow cytometer's laser. This allows for targeted quantification of an analyte of interest (Wang *et al.*, 2010).

There are two ways in which EVs can be analysed by flow cytometry. The first uses conventional flow cytometers in a way which bypasses the fact that their lower limit of detection is larger than the size of an EV. In a method very similar to immunoprecipitation in 1.5.3., EVs are bound to free floating beads coated with antibodies that bind to EV markers. However, instead of eluting the EVs from the beads, secondary antibody with a fluorophore conjugated are added to the EVs bound to the beads. The detection antibody can be specific for the same marker as the capture antibody or for another EV marker. The beads are of a size that is well above the lower limit of detection of the flow cytometer (4-9 microns in diameter). As several EVs bind to a single bead, the combined fluorescent single is detectable to the flow cytometer. The abundance of the EV marker being detected for can be quantified. This enables relative quantification between samples, however, absolute EV quantification

can’t be achieved (Campos-Silva *et al.*, 2019; Bano, Ahmad and Mohsin, 2021; Belliveau and Papoutsakis, 2022).

The second method of flow cytometry utilises a flow cytometer with a smaller flow channel that reduces background noise e.g. NanoFCM’s NanoAnalyzer. This enables the detection and resolution of particles >40nm in size. Therefore, EVs can be quantified absolutely by this method. In addition, the EVs can be fluorescently labelled which allows the user to determine what percentage of their particles are actually EVs or are the subset of EVs they are interested in (Arab *et al.*, 2021; Fortunato *et al.*, 2021).

1.5.4 Electron Microscopy

Electron microscopy (EM) involves exposing EVs to electron beams which are either transmitted or diffracted by the EVs. As EM has a resolution of 0.5nm, it allows for highly detailed structural images of EVs to be obtained. There are the three main types of EM used in EV research. The first is transmission electron microscopy (TEM). This is where the sample is fixed and dehydrated. The EVs are then cut into nanometer thin sections and placed on a carbon coated grid for imaging. At this point, an electron beam illuminates the sample. Brightfield images are generated using a fluorescent screen or charge-couple device which collects transmitted electrons whilst scattered electrons are collected to generated dark-field images. This allows visualization of the EV structure (Chuo, Chien and Lai, 2018).

Scanning electron microscopy (SEM) is similar to TEM in that samples are fixed and dehydrated. However, rather than being sliced, the EVs are coated with a conductive material. The sample is then exposed to an electron beam and detected in the same manner as TEM. While SEM is easier to set-up, the thing layer of conductive material has the potential to interfere with the EV structure (Chuo, Chien and Lai, 2018).

The third form of EM is cryo-electron microscopy (Cryo-EM). This is where liquid ethane cooling allows samples to remain in their hydrated state when they are fixed. The benefits of keeping EVs in their hydrated state are that it will give more accurate EV sizes as well as being able track EV uptake by cells (Chuo, Chien and Lai, 2018).

1.5.5 Mass Spectroscopy

The aforementioned techniques look at methods of EV detection, quantification and single marker analysis. Mass spectroscopy (MS) allows for the characterization of the entire EV proteome and lipidome. In the case of proteomics, the most common form of MS employed is bottom up mass spectrometry which involves cleaving proteins into small peptides using digestion agents such as Trypsin. The sample is then loaded onto a gel for electrophoresis and is separated. Alternatively, sample can be separated by liquid chromatography. Different forms of MS analysis can then be used to identify the proteome of the samples. Label free MS which identifies the most abundant precursor ions and determines their peptides using software tools such as Proteome Discoverer Software (Yao *et al.*, 2019). This analysis can be advanced further to determine characteristics such as the protein conformation as well as levels of ubiquitination, glycolysation and phosphorylation. However, large quantities of protein are necessary for such analyses which can be difficult to obtain from EVs (de Menezes-Neto *et al.*, 2015; Rosa-Fernandes *et al.*, 2017).

For lipidomic analyses, the lipid content of EVs is extracted and separated out using liquid chromatography. When ran through the mass spec, this generates peaks depending on the mass to charge ratio of the lipid in question. The raw data containing these peaks is aligned to identify the lipids using software such as Compound Discoverer (Nishida-Aoki *et al.*, 2020; Sun, Saito and Saito, 2022).

1.5.6 RNA-sequencing and Small RNA-sequencing

As previously mentioned, the functionality of EVs can be attributed to their RNA cargo. For this reason, many groups have attempted characterisation of EV RNA including mRNA, long non-coding RNAs (lncRNAs) and small non-coding RNA such as miRNAs, piwi-interacting RNAs (piRNAs), transfer RNAs (tRNAs) and vault RNAs (vtRNAs) (O'Brien *et al.*, 2020). Sequencing of each of these RNA classes involves a similar protocol which variations depending on the class of RNA that is being focused on. The RNA is first isolated from the EVs using a lysis buffer. Library preps are then made where the RNA is converted to cDNA and amplified before sequencing. The

library kit used can vary depending on what class of RNA is desired for sequencing. For example, small RNA and mRNA will often require different library prep kits (Sha, Bhatia and Yoon, 2018; Benesova, Kubista and Valihrach, 2021). Once library prep is complete, the samples are moved to a flow cell for sequencing such as an Illumina HiSeq platform. The number of times a sequence is read on the platform or "read depth" will vary between RNA classes with small RNA requiring less read depth than mRNA due to their shorter length. When sequencing is complete, samples are demultiplexed and raw fastq files are generated. These are subjected to quality controls which involves library prep adapter trimming and read quality measurement. Read quality is measured by a metric called Q score or Phred and a score of 30 or greater is considered acceptable. After this, reads are aligned to a reference genome using bioinformatic tools such as Bowtie. To compare mRNA or small RNA quantities between samples, differential gene expression is performed where the read counts for the samples are normalized and compared. Bioinformatic tools such as Deseq2 are used for this (Rizzetto *et al.*, 2017; Buschmann *et al.*, 2018; Ge *et al.*, 2019; Potla, Ali and Kapoor, 2021; Busch *et al.*, 2022).

1.6 Extracellular Vesicles in the context of Chinese Hamster Ovary cells

1.6.1 Facilitation of Cell to Cell communication

As has been the case with other cell lines discussed, CHO cells utilise EVs for widespread transport of both protein and RNA cargo from one cell to another. Belliveau and Papoutsakis (2022) revealed how CHO cells use EVs to homogenise a culture. They set-up co-cultures containing 51% of cells labelled with SYTO RNASelect fluorescent dye, a RNA dye, and 49% un-labelled cells. When measured after 24 hours, 98% of the cells in the culture were positive for the dye. Confocal and SEM revealed that the RNA was being transferred by EVs.

This ability to facilitate rapid transfer of cargo can be leveraged to manufacture CHO EVs containing therapeutic proteins. Alphas galactosidase A is an enzyme used to treat lysosomal storage disorders and has been successfully packaged into CHO EVs. The EV-encapsulated enzyme was shown to be active when administered to mice via

intra-arterial injection. While this also highlights the stability of CHO EVs and how they can be internalised by different species, it further emphasizes their ability to efficiently move cargo from one cell to another (Seras-Franzoso *et al.*, 2021).

1.6.2 Potential to Inhibit Apoptosis and Promote Proliferation

Literature detailing the functionality of CHO EVs in manufacturing remains limited, however, there are a few indications that EVs may play some role in preventing cell death and promoting proliferation. The first of these comes from an investigation by Kumar *et al.* (2016) which looked at the proteome of CHO sEVs pelleted at 100,000g. The sEVs were isolated from lag, log, stationary and death phase of batch culture and contained cell stress mediators such as nuclease-sensitive element binding protein 1 (YBX1), Superoxide dismutase (SOD1), Gluthatione S-transferase Mu 1 (GSTM1) and Glutathione S-transferase Mu 7 (GSTM7). In particular, the lag and log phase had Ras homolog gene family, member A (RHOA) and Ras homolog gene family member B (RHOB), polyubiquitin (UBB), Ubiquitin-40S ribosomal protein 27a (RPS27A). RHOA and RHOB are regulators of cell proliferation whilst UBB and RPS27A are can induce cell proliferation. The lag phase also had structural proteins known to be important to cell proliferation such as Alpha-actinin-1 (ACTN1) and Tubulin alpha-1B (TUBA1B). This indicates that EVs can promote proliferation in recipient cells.

Studies characterizing the nucleic acid content of CHO EVs suggest a similar functionality (Keysberg *et al.*, 2021; Busch *et al.*, 2022). While Keysberg *et al.* (2021) identified miRNAs and piRNAs present at different stages in batch culture, Busch *et al*. (2022) looked at what mRNAs and miRNAs are present at late stage fed-batch and what pathways they were involved in or target. They observed that lEVs and sEVs were distinct in their mRNA profiles but both contained mRNAs that belonged to the TGFß and PI3K/AkT pathways which are pro-proliferative. Busch *et al*. (2022) also identifies miR-196a-5p, an anti-apoptotic miRNA, as highly abundant in sEVs.

There is also experimental evidence which demonstrates the pro-proliferative and anti-apoptotic properties of CHO EVs. Han and Rhee (2018) showed that culture supplementation with EVs could protect cells treated with staurosporine from undergoing apoptosis. In addition to this, Takagi *et al.*, (2021) reported that a fraction

of polymers from cell culture supernatant containing sEVs enhanced the growth of cells in batch cultures. However, neither of these studies investigated what property of EVs may be inducing these affects.

1.7 Project Objectives

This project aims to characterise and further understand EV production in CHO in context to mAb production. It will do so over four chapters which have been described in brief below:

Chapter 2 – Materials and Methods: Details of all reagents, equipment and protocols followed.

Chapter 3 – Characterising EV Production in a CHO Fed-Batch Process: This chapter investigates EV production at different time-points in a CHO fed-batch. The quantities of EVs secreted in a fed-batch process will be detailed and how the rate of EV secretion changes with respect to cell growth and productivity. It will identify the optimal time-point at which to purify EVs from fed-batch that maximises yield and purity for use in functional experiments. It will also look at the miRNA content of CHO EVs at different time-points in the fed-batch and see how the information they contain may change during the fed-batch. Lastly, the function of EVs in fed-batch will be predicted based on their miRNA content using bioinformatics tool, miRWalk.

Chapter 4 – Comparing EV Profiles of Different CHO cell lines: This chapter will provide an in-depth comparison of EVs isolated from a Producer cell line and a Non-Producer Host CHO cell line. It will compare the quantity, protein content, miRNAs present and lipid content of the EVs. This will determine if non-producer and producer CHO cells vary in their EV secretion and composition and whether the cell line development process influences the EV profile of the cell.

Chapter 5 - Investigating the Variability of CHO sEV Secretion in Monoclonal Antibody Production. The chapter will quantify sEVs from 8 CHO cell lines grown in Lonza's fed-batch process and compare the transcriptional activity of EVB genes in those cell lines. This will look to see if EV secretion is correlated with other cellular characteristics and what implications sEV secretion may have when selecting a cell line for biopharmaceutical manufacturing.

Chapter 6 – Utilising sEVs to Improve CHO Cloning Efficiency: In this chapter, the ability of EVs to promote the growth of low density cultures and single cell clones post sorting will be investigated.

Chapter 2

Materials and Methods

This chapter details all techniques and materials used for the experimental work described in this thesis. Cell culture work was performed in a Biological Safety Cabinet to maintain sterility. This was done in a separate lab from all molecular and EV analysis work to minimise risk of contamination.

2.1. CHO Cell Culture

2.1.1 CHO Culture Maintenance

CHO cells grown thawed from vials banked and stored in liquid nitrogen. Cells were grown in CD-CHO (Thermo Fisher Scientific, Massachusetts, USA). If the cell line did not express GS, it was grown in CD-CHO containing 6mM L-Glutamine (Thermo Fisher Scientific, Massachusetts USA). Cells were passaged in either TubeSpin Bioreactor 50 TPP cultiflasks (Scientific Laboratory Supplies, Nottingham, UK) or Corning® Erlenmeyer Cell Culture flasks (Merck Life Science, Gillingham, UK) depending on volume requirements. If passaged in Erlenmeyer cell culture flasks (erlenmeyers), cells were incubated at 37°C, 5% CO_2 and 140 RPM in an Infors HT Multitron (Infors, USA). If passaged in TubeSpin Bioreactor 50 TPP cultiflasks (50ml cultiflasks), cells were incubated at 37°C, 5% CO_2 and 240 RPM. All cell lines were passaged four times every three or four days prior to use in any study. Viable cell density (VCD) and viability were measured using a Vi-Cell (Beckman Coulter, Wycombe, UK).

2.1.2 Cryopreservation and Vial Thaw

Cells were passaged at least four times prior to cryopreservation and banking. The cells were moved to a VWR Mega Star 1.6 R centrifuge (VWR, Pennsylvania, USA) and centrifuged at 200g for five minutes to remove spent cell culture supernatant. They were then re-suspended in fresh CD-CHO containing 7.5% DMSO (Merck Life Science, Gillingham, UK) at a density of 1 x 10^7 cells/ ml and a volume of 1.5ml aliquoted to cryogenic vials (StarLab, Milton Keynes, UK). The vials were then stored at -80°C overnight prior to moving them to liquid nitrogen for long-term storage. When removing vials from liquid nitrogen storage, the vial was thawed at 37°C for four minutes in a water bath. Once thawed, the contents of the vial were moved to a 50ml falcon tube (Thermo Fisher Scientific, Massachusetts USA) and diluted to 45ml with CD-CHO. This was then centrifuged 200g for five minutes to pellet the cells and remove DMSO containing media. The cells were then re-suspended in 10ml of CD-CHO. The 10ml of CD-CHO was supplemented with 6mM L-Glutamine should the cell not express GS. A vi-cell measurement was taken to confirm VCD and viability and a volume at a density of 0.3 x 10^6 cells/ml was transferred to either a cultiflask or Erlenmeyer shake flask for incubation.

2.1.3 Fed-batch of CHO-K1SV Glutamine Synthase Knock-Out - Host (GSKO-Host) and CHO-K1SV Producer (CHO-A) cell lines

Proprietary cell lines GSKO-Host (Lonza, Slough, UK) and CHO-A (Lonza, Slough, UK) were both seeded at 0.2 x 10^6 cells/ml in CD-CHO and incubated at 37°C, 140 RPM and 5% CO_2 in a humidified incubator when grown in Erlenmeyer flasks. For CHO-A fed-batch done in 50ml culitflasks cells were seeded at 0.2 x 10^6 cells/ml in CD-CHO and incubated at 37°C, 230 RPM and 5% CO_2 in a humidified Infors HT Multitron incubator. In the case of GSKO-Parental fed-batch, the CD-CHO was supplemented with 6mM L-Glutamine (Thermo Fisher Scientific, Massachusetts, USA) whilst CHO-A was not supplemented. Both cell lines were fed on Days 3, 6 and 9 10% V/V. GSKO-Host was fed Efficient Feed B (Thermo Fisher Scientific, Massachusetts, USA) and CHO-A fed a custom formulation of Efficient Feed B which was absent in L-arginine, L-arginine HCl, L-lysine, L-lysine HCl, uridine, Uracil and Uridine 5-

triphosphate (Thermo Fisher Scientific, Massachusetts, USA). Viability and VCD was measured on the vi-cell daily.

2.1.4 Fed-batch of Lonza CHO-X cell lines

Lonza CHO-X cell lines were grown and passaged prior to fed-batch by Dr. Ryan Taylor in CD-CHO. The cell lines were then grown in fed-batch in E250 erlenmeyer flasks as per Lonza's proprietary protocol and all proprietary base media and feeds were kindly supplied by Lonza, UK. With the exception of the CHO-X Parental cell line which required glutamine supplementation in its base media, all cells were grown in the same conditions. The culture volume was 50ml. Flasks were sampled daily in co-ordination with Dr. Ryan Taylor. VCD, viability and cell diameter were measured on the Vi-Cell. Glucose consumption was measured by Accu-Chek Mobile meter (Roche, Basel, Switzerland) and the glucose was replenished in the cultures as per Lonza's protocol based on these measurements. On day 5 and day 10 of fed-batch, sample was taken for titre measurement which was performed for flasks used in transcriptomic analysis by Dr. Ryan Taylor. Day 5 titre sample was also taken and measured from sEV flasks by the author. Samples were taken for RNA-seq also on Day 5 where 5 $x10^6$ cells were pelleted per replicate and stored at -80°C prior to shipping.

The following formulae were used to calculate integral viable cell density (IVCD), cell specific productivity (qP), specific glucose consumption rate (qGLU) and specific growth rate (μ):

Equation 1: IVCD

$$IVCD_y = \Delta IVCD_y + IVCD_{y-1}$$

Where y is the IVCD for a particular time-point, $\Delta IVCD_y$ is the change in IVCD at that time-point and y-1 is the IVCD for the previous time-point.

$$\Delta IVCD = VCD_{y-1} \times (t_y - t_{y-1}) + [\ (VCD_y - VCD_{y-1}) \times (t_y - t_{y-1}) / 2\ ]$$

Where t_y is cultivation time at y and t_{y-1} is the cultivation time at a previous time-point. VCD_y is the viable cell density at y and VCD_{y-1} is the viable cell density at a previous time-point.

Equation 2: qP

$$qP = [(T_y – T_{y-1}) / (VCD_y - VCD_{y-1})] \times \mu$$

Where T_y is the titre at time-point y and T_{y-1} is the titre at a previous time-point. VCD_y is the viable cell density at time-point y and VCD_{y-1} is the viable cell density at a previous time-point. The formula for qP is as described by Clarke *et al.*, (2011) and Zboray *et al.*, (2015).

Equation 3: qGLU

$$qGLU = (GLU_y – GLU_{y-1}) / [(VCD_y + VCD_{y-1} /2) \times \Delta t]$$

Where GLU_y is the glucose concentration at time-point y and GLU_{y-1} is the glucose concentration at a previous time-point. VCD_y is the viable cell density at y and VCD_{y-1} is the viable cell density at a previous time-point.

Equation 4: μ

$$\mu = [\ln(VCD_y) – \ln(VCD_{y-1}) / t_y - t_{y-1}]$$

Where ln is the natural logarithm. VCD_y is the viable cell density at y and VCD_{y-1} is the viable cell density at a previous time-point. Where t_y is cultivation time at y and t_{y-1} is the cultivation time at a previous time-point.

2.1.4.1 sEV Analysis by NanoAnalyser

For measurement of sEV samples by NanoAnalyzer (NanoFCM, Nottingham, UK), sEV samples were sent to Lonza, Toscana Life Sciences Foundation, Siena, Italy. At Lonza, they were prepared, stained with CFSE dye and ran on the NanoAnalyzer by Dr. Ilaria Passalacqua.

2.2. Single Cell Clone Generation and Maintenance

2.2.1 Flow Cytometry Sorting of Single CHO Clones

All cell sorting was conducted at the University of Sheffield Medical School with the assistance of Sue Clarke and Kay Hopkinson. Prior to sorting, CHO-A cells were grown in CD-CHO and passaged between four and ten times in 50ml cultiflasks with VCD and viability measured on the vi-cell. They were then centrifuged at 200g for 5 minutes, supernatant removed and re-suspended in fresh CD-CHO at a volume where the cell density was 7-10 x 10^6 cells/ml. Once transferred to the medical school, the cells sorted using a FACS Melody (BD, UK). Singlets were gated away from doublets and cell debris using forward scatter and side scatter as shown in Fig shown below.

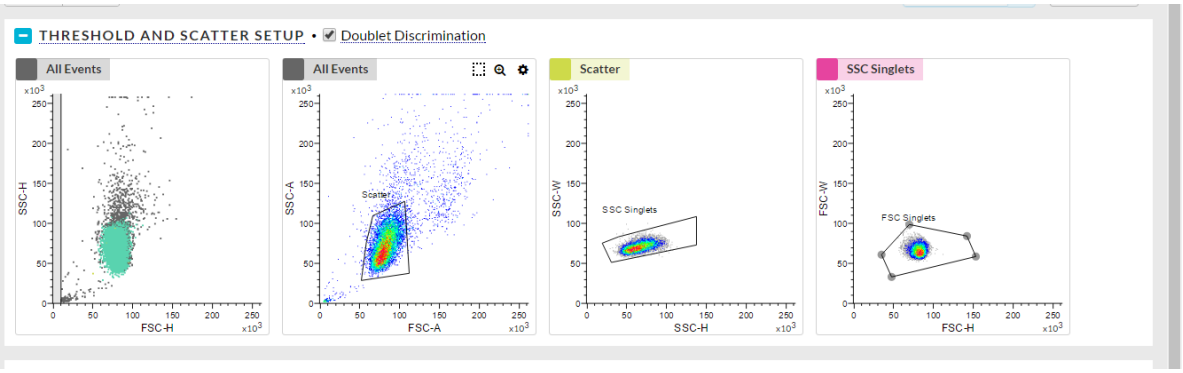

Fig 2.1 Gating performed to isolate single cells from cell debris and clumped cells for sorting.

2.2.2 Culturing of Single Cell Clones and Analysis

Prior to sorting, EV supplemented and blank 96-well CELLSTAR cell culture plates (Greiner Bio-One Ltd, Stonehouse, UK) were seeded with 100µl of either CD-CHO or Ex-Cell CHO Cloning medium (Merck Life Sciences, Gillingham, UK) containing 0.7% Penicillin-Streptomycin (10,000 U/mL) (Thermo Fisher Scientific, Massachusetts, USA). For plates supplemented with EVs, purified EVs were diluted to the desired concentration in either CD-CHO or Ex-Cell CHO Cloning medium containing 0.7% Penicillin-Streptomycin (10,000 U/mL). The plates were then placed in a humidified static Midi 40 CO_2 incubator (Thermo Fisher Scientific, Massachusetts, USA) at 37°C and 5% CO_2 until sorting as described in 2.2.1. After sorting, the plates were returned to the static incubator and left until feeding on Day 7 with 50µl CD-CHO or Ex-Cell CHO Cloning medium. On Day 14, the plates were imaged with a Clone Select Imager (Molecular Devices, California, USA) to examine for growth. Each well on every plate was individually examined and any visible clonal outgrowths recorded.

2.3 EV Purification

EVs were isolated using UC. In brief, cell cultures were harvested by centrifuging in a VWR Mega Star 1.6 R centrifuge with a TX-400 (Thermo Fisher Scientific, Massachusetts USA) rotor at 300g for 6 minutes. To maintain sterility, the supernatants were then poured into 50ml falcon tubes in the biological safety cabinet and stored at -80°C until required for further purification. For further purification steps, the supernatants were thawed in water bath at 37°C. Once thawed, they were moved to a VWR Mega Star 1.6 R centrifuge with a Highconic Fixed Angle rotor (Thermo Fisher Scientific, Massachusetts, USA) and centrifuged at 2,000g for 10 minutes to remove large debris. The 2,000g supernatant was then centrifuged at 10,000g for 30 minutes to pellet small cell debris as well as lEVs. The 10,000g supernatant was centrifuged at 100,000g for 70 minutes in a Optima Max XP ultracentrifuge (Beckman Coulter, Wycombe, UK) using a MLS-50 rotor (Beckman Coulter, Wycombe, UK). 5 mL, Open-Top Thinwall Ultra-Clear Tubes (Beckman Coulter, Wycombe, UK) were used to load supernatant to the Ultracentrifuge. Once the initial 100,000g centrifugation was completed, the pellets obtained were re-suspended in 0.22µm filtered 1X Phosphate Buffered Saline (PBS) (Alfa Aesar, Massachusetts, USA) and

pooled. Once pooled, they were re-diluted to 5ml and centrifuged again at 100,000g for 70 minutes. The re-suspension buffer of the resulting pellet depended on its purpose. For protein quantification, transcriptomic analysis, lipidomic analysis and TEM, the pellet was re-suspended in 0.22µm filtered 1X PBS. Where western blotting was performed after protein quantification, the pellet was re-suspended in RIPA buffer (Merck Life Science, Gillingham, UK) to lyse the EV membrane. If the pellet was used for EV supplementation experiments, it was re-suspended in 600µl CD-CHO and 0.22µm PES membrane (Sartorius Stedim, Göttingen, Germany) filtered in a biological safety cabinet. 50µl aliquots were then made with 1 aliquot used for NTA analysis and 1 aliquot used for sterility testing. This was where the aliquot was diluted to 5ml in fresh CD-CHO in a 50ml cultiflask and incubated for 2 days at 37°C, 5% CO_2 and 240 RPM. If the media remained clear and absent of any obvious signs of contamination, the EV pellet was deemed sterile.

2.4 Nanoparticle Tracking Analysis of EVs

NTA analysis was performed on a Nanosight NS300 (Malvern Panalytical, Worcestershire, UK) equipped with a 488nm laser and syringe pump. The Nanosight NS300 was running NTA 3.4 software. All samples, regardless of re-suspension buffer (1X PBS or CD-CHO) were diluted with PBS for counting so that there were between 20 – 80 particles per frame. When measuring sEVs, the settings used were Camera Level 15, Detection Threshold 5. LEVs were measured at Camera Level 12, Detection Threshold 5. Six 1-minute videos were recorded per measurement and either technical duplicate or triplicate measurements were taken of each sample. The following script was used on the NTA software:

RECORDDILUTION *(insert dilution factor)*

SYRINGELOAD 1000

DELAY 5

SYRINGELOAD 500

DELAY 1

SYRINGELOAD 250

DELAY 1

SYRINGELOAD 100

DELAY 1

SYRINGELOAD 50

SETTEMP 25

REPEATSTART

CAPTURE 60

DELAY 1

SYRINGELOAD 1000

DELAY 3

SYRINGELOAD 50

REPEAT 5

SYRINGESTOP

TEMPERATURECONTROLOFF

PROCESSBASIC

EXPORTRESULTS

2.5 Transcriptomic Analysis of EVs and Cells

2.5.1 RNA Isolation and quantification

RNA was extracted from cell pellets and EVs using a Total RNA Purification kit (Norgen Biotek, Ontario, Canada). This kit has two separate protocols from the manufacturer which were followed for the extraction of RNA from cell pellets and purified EVs re-suspended in PBS which both. Both protocols included DNase

treatment using a RNase-Free DNase1 Kit (Norgen Biotek, Canada). After purification and elution, a 5µl aliquot of the RNA was taken for quantification on an Agilent 2100 Bioanalyser (Agilent, California, USA). The purified RNA and aliquots were stored at -80°C until use. The aliquots were measured on the Bioanalyser by Dr. Matthew D. Wyles using a RNA 6000 pico chip (Agilent, California USA).

2.5.2 Small RNA-sequencing and analysis

Both small RNA-sequencing libraries were performed by Azenta (Genewiz), Massachusetts, USA.

2.5.2.1 Library Preparation for small RNA and HiSeq Sequencing

For Library 1 in Chapter 3, libraries were prepared by using Illumina TruSeq Small RNA library Prep Kit (Illumina, California, USA). For Library 2 in Chapter 4, libraries were preprared using a NEBNext® Small RNA Library Prep Set for Illumina® (New England Biolabs, Massachusetts, USA). For both library prep kits, the manufacturer's protocol was followed. After this point, both Library 1 and Library 2 were treated identically. In brief, Illumina 3' and 5' adapters were added to RNA molecules with a 5'-phosphate and a 3'-hydroxyl group sequentially. A reverse transcription reaction was used to create single stranded cDNA. The cDNA was then PCR amplified using a common primer and a primer containing the index sequence. Amplified cDNA construct was purified by polyacrylamide gel electrophoresis, the correct band (~145 – 160 bp) excised from the gel and eluted with water. The eluted cDNA was concentrated by ethanol precipitation, and resulting in the final sequencing library. The sequencing library was validated on the Agilent TapeStation 4200 (Agilent Technologies, Palo Alto, CA, USA), and quantified by using Qubit 2.0 Fluorometer (Invitrogen, Carlsbad, CA**)** as well as by quantitative PCR (KAPA Biosystems, Wilmington, MA, USA).

The sequencing libraries were multiplexed and clustered on a single lane of a flowcell. After clustering, the flowcell was loaded on the Illumina HiSeq (4000 or equivalent)

instrument according to manufacturer's instructions. The samples were sequenced using a 2x150bp Paired End configuration. Image analysis and base calling were conducted by the HiSeq Control Software. Raw sequence data (.bcl files) generated from Illumina HiSeq was converted into fastq files and de-multiplexed using Illumina's bcl2fastq 2.17 software. One mismatch was allowed for index sequence identification.

2.5.2.2 Small RNA-seq Data Analysis

The raw sequence reads were quality and adapter trimmed using CLC Genomics Server 10. The trimmed reads with a length of 15 to 31 bp were retained. These trimmed reads were compared and annotated using the small RNA database (miRbase 21). In Sheffield, with the assistance of Adrian Bourke, principal component analysis of the annotated reads, heatmaps of samples and number of annotated reads per sample were calculated using R Studio. Differential expression (DE) analysis carried out using Deseq2 in R Studio. Downstream analysis to identify predicted targets of miRNA identified was done using online tool miRWalk (http://mirwalk.umm.uni-heidelberg.de/).

2.5.3 Transcriptomic Analysis of Lonza CHO-X cell lines

Samples were sent to Novogene (Cambridge, UK) for RNA sequencing analysis who returned Raw Fastq files. Dr. Cristina Alexandriu used FastQC to check for high quality reads, STAR to read alignment to Lonza's proprietary CHO genome and FeatureCounts for transcript quantification. DE analysis was then performed using DeSeq2 in R Studio with GS-Null and Parental cell lines being used to normalise between different fed-batches. Dr. Alexandriu also produced the normalised log counts of genes and principal component analysis in R. Lists of genes involved in the biological processes investigated were sourced from literature by the author.

2.6 Lipidomics Analysis

Lipidomics Analysis was performed by Creative Proteomics, New York, USA. EV Samples were shipped on dry ice to their facility at which point they performed the following protocol supplied by Creative Proteomics:

2.6.1 Sample Extraction

1) Samples were thawed on ice and spiked with an internal standard and calibration mixture consisting of di-myristoyl phospholipids (PG, PE, PS, PA), PC(46:0), SM(30:1) and TG(14:1) to give a final sample concentration of 5 uM of each standard.

2) To each sample, 300 microliters of -20C chilled methanol containing 1 mM BHT (an antioxidant) was added Then one mL of MTBE was added to each sample, and samples were then vortexed for 60 minutes at room temperature.

3) 150 microliters of water were added, and the samples were vortexed for an additional 15 minutes and then centrifuged for 15 minutes.

4) The supernatants were collected to new test tubes and precipitated proteins were re-extracted as above.

5) Pooled extracts were dried overnight in a speedvac, and resuspended in 100 microliters of isopropanol containing 0.01% BHT...

2.6.2 Instrument and Sample Analysis Parameters

Immediately prior to analysis, aliquots of each lipid extract were diluted in isopropanol:methanol (2:1, v:v) containing 20 mM ammonium formate. Full scan MS spectra at 100,000 resolutions (defined at m/z 400) were collected on a Thermo Scientific LTQ-Orbitrap Velos mass spectrometer in both positive and negative ionization modes. Scans were collected from m/z 200 to m/z 1200. For each analysis, 5 µL of sample was directly introduced by flow injection (no LC column) at 10 µL/min using an electrospray ionization source equipped with a fused silica ESI needle to minimize intrasource accumulation of triglycerides and very long chain fatty acids. A Shimadzu Prominance HPLC served as the sample delivery unit. The sample and

injection solvent were 2:1 (v: v) isopropanol: methanol containing 20 mM ammonium formate. The spray voltage was 4.5 kV, ion transfer tube temperature was 275 °C, the S-lens value was 50 percent, and the ion trap fill time was 100 ms. The autosampler was set to 15 degrees °C. After two minutes of MS signal averaging, the LC tubing, autosampler, and ESI source were flushed with 1 mL of isopropanol, prior to injection of the next sample. Samples were analyzed in random order, interspersed by solvent blank injections, extraction blank injections, and pooled QC samples derived from all study samples. Following MS data acquisition, offline mass recalibration was performed with the "Recalibrate Offline" tool in Thermo Xcalibur software according to the vendor's instructions, using the theoretical computed masses for the internal calibration standards and several common endogenous mammalian lipid species. MS/MS confirmation and structural analysis of lipid species identified by database searching were performed using higher-energy collisional dissociation MS/MS at 60,000 resolution and a normalized collision energy of 25 for positive ion mode, and 60 for negative ion mode. MS/MS scans were triggered by inclusion lists generated separately for positive and negative ionization modes.

2.6.3 Lipid Peak Finding, Identification, and Quantitation

Lipids were identified using the Lipid Mass Spectrum Analysis (LIMSA) v.1.0 software linear fit algorithm, in conjunction with an in-house database of hypothetical lipid compounds, for automated peak finding and correction of 13C isotope effects. Peak areas of found peaks were quantified by normalization against an internal standard of a similar lipid class. The top ~300 most abundant peaks in both positive and negative ionization mode were then selected for MS/MS inclusion lists and imported into Xcalibur software for structural analysis on the pooled QC sample as described above. For this untargeted analysis, no attempt was made to correct for differences in lipid species ionization due to the length or degree of unsaturation of the esterified fatty acids. Therefore, lipid abundance values are inherently estimates rather than true 'absolute' values.

2.8 Protein Extraction and Quantification

EV Protein was extracted using RIPA buffer (Merck Life Science, Gillingham, UK) with 0.2% Proteinase Inhibitor (Merck Life Science, Gillingham, UK). For simple protein quantification of EVs re-suspended in PBS, the volume of RIPA was added in a 1:1 ratio. For western blotting, the sEV pellet was re-suspended in RIPA immediately after purification to ensure a concentrated protein sample. EV protein used for western blotting was quantified using a Pierce™ BCA Protein Assay Kit (BCA) (Thermo Fisher Scientific, Massachusetts, USA) following the manufacturer's protocol. EVs which had been re-suspended in PBS prior to treatment in RIPA were more dilute and required use of a Micro BCA™ Protein Assay Kit (Thermo Fisher Scientific, Massachusetts, USA) following the manufacturer's protocol.

2.9 Western Blot Analysis

The following primary antibodies were used: rabbit polyclonal TSG101 (Catalogue Number: 14497-1-AP, Proteintech, Manchester, UK), rabbit polyclonal Alix (Catalogue Number: 12422-1-AP, Proteintech, Manchester, UK), rabbit polyclonal CD63 (Catalogue Number: PA5-92370, Thermo Fisher Scientific, Massachusetts, USA), mouse monoclonal Syntenin-1 (Catalogue Number: 27105, Signalway Antibody, Maryland, USA) and rabbit polyclonal HSP90ß1 (Catalogue Number: 100613-T32, Sino Biological, Beijing, China). For detection of rabbit primary antibodies, goat anti-rabbit Alexa Fluor™ Plus 800 secondary antibody (Catalogue Number: A32735, Thermo Fisher Scientific, Massachusetts, USA). For detection of mouse primary antibodies, goat anti-mouse Alexa Fluor™ 700 secondary antibody (Catalogue Number: A-21036, Thermo Fisher Scientific, Massachusetts, USA) was used. Chameleon Duo Pre-stained Protein Ladder (Li-Cor, New England, USA) was used for visualisation of the blots.

Samples were diluted to 14µl using deionised H_2O. They were denatured and reduced by adding 5µl NuPAGE LDS Sample Buffer (4X) (Thermo Fisher Scientific, Massachusetts, USA) and 2µl NuPAGE Sample Reducing agent (10X) (Thermo Fisher Scientific, Massachusetts, USA) to give a final volume of 21µl and heated at

80°C for 10 minutes. They were then loaded to a NuPAGE 4-12% Bis-Tris Gel (Thermo Fisher Scientific, Massachusetts, USA) in deionised water diluted NuPAGE MOPS SDS Running Buffer 20X (Thermo Fisher Scientific, Massachusetts, USA). The samples were then separated on the gel at 180V until the protein sample had visibly migrated to the bottom of the gel.

After separation, the samples were transferred to a PVDF membrane (Thermo Fisher Scientific, Massachusetts, USA) using a iBlot Gel Transfer Device (Thermo Fisher Scientific, Massachusetts, USA) at P3 for 7 minutes.

Once transferred, the blots were immediately transferred to blocking buffer containing 5% dried skimmed milk (Tesco, UK) in TBS (Geneflow, Lichfield, UK) and left on a rocker for 1 hour at room temperature. After blocking, the blot was washed with TBS-T. TBS-T was made up using 0.05% Tween20 (Scientific Laboratory Supplies, Nottingham, UK) in TBS. The blot was washed for 3 5-minute intervals on a rocker. Primary antibody was then diluted in TBS-T as recommended by the manufacturer's protocol and added to the blot. Primary staining was allowed to occur, rocking, overnight at 4°C. Once complete, the blot was again washed and secondary antibody added. Secondary antibody staining was performed at room temperature for 1 hour. After secondary staining the blot was again washed and blotted dry with Whatman® gel blotting papers, Grade GB005 (Merck Life Science, Gillingham, UK) before imaging.

Imaging of blots was performed using a Li-Cor Odyssey SA (Li-Cor, New England, USA) running Image Studio V 5.2 software. Densitometry analysis was also performed using the same software.

2.10 Transmission Electron Microscopy Analysis

Transmission Electron Microscopy analysis was performed on the EVs by Dr. Chris Hill. In brief, 5µl of EV sample was added to the upper surface of a glow discharge carbon coated 400 mesh copper:molybdenum electron microscopy grid (Agar Scientific, Essex, UK) and left for 1 minute. The grid was blotted dry with Whatman qualitative filter paper (grade 1) (Whatman plc, Buckinghamshire, UK) to remove

excess sample. Then 5µl of distilled water was added to the grid and again it was blotted dry with Whatman qualitative filter paper. 5µl of 1% aqueous Phosphotungtic Acid (PTA) was used to stain the grid and left for 20 seconds before blotting dry. The grid was stored in a box and left in the dark until analysis under a FEI Tecnai Spirit Biotwin Transmission Electron Microscope (Field Electron and Ion Company, Oregon, USA) operated at 80Kv. Images were recorded using a Gatan Orius 1000B camera (Gatan, California, USA) and Digital Micrograph software.

2.11 Titre Measurements

Monoclonal Antibody Titre from fed-batch experiments was measured using Valita®Titer plates (ValitaCell, Dublin, Ireland) following the manufacturer's protocol. Plates were read on a SpectraMax ID5 Multi-Mode Microplate reader (Molecular Devices, California USA).

2.12 Statistical Analysis

All statistical analysis was performed in Graphpad Prism (version 9). Independent Two-tailed t-tests were used to compare between two samples. For comparison of 3 or more samples, standard one-way ANOVA was used with Tukey post hoc test to correct for multiple comparisons. For DE analysis in small RNA-seq and transcriptomic analyses, Deseq2 used Wald's test for statistical significance with a Benjamini Hochberg correction for multiple comparisons. All graphs show standard deviation as error bars unless otherwise stated. P-values on graphs are denoted as "ns" when greater than 0.05, "*" when less than or equal 0.05, "**" when less than or equal to 0.01, "***" when less than or equal to 0.001 or "****" when less than or equal to 0.0001.

Chapter 3

Characterising EV Production in a CHO Fed-Batch Process

3.1 Introduction

A CHO fed-batch process has distinct stages of growth: early growth phase/ lag phase, middle growth phase/ exponential phase, stationary phase and late stationary/ death phase (Becker *et al.*, 2019). In each of these stages, cell behaviour varies considerably. In lag phase and exponential, the cells prioritise adaptation to their environment and growth. In early stationary phase, the rate of cell growth equals the rate of cell death as nutrients become less available and metabolite accumulation occurs in the cell culture environment. In late stationary/ death phase, where nutrients in the culture are almost completely depleted and metabolites which negatively impact the extracellular environment are abundant, cell death happens at a far higher rate (Ha *et al.*, 2022). The observed differences in cell state is reflected in transcriptomic analysis demonstrating CHO cells isolated from different stages of fed-batch have differential gene expression (Ha *et al.*, 2022).

Given that intracellular processes vary between these different stages of fed-batch, it was speculated that the ways in which cells communicate with each other also varies throughout a fed-batch. This paracrine signalling may also influence cellular behaviour at the different stages of fed-batch. EVs are a known mediator of cell-to-cell communication yet little is known about how their abundance and composition changes throughout a fed-batch processes. Similarly, little is known about their influence on cell behaviour.

Studies such as Zavec *et al.* (2016) have quantified EV accumulation in fed-batch using flow cytometry and PKH67 lipophilic dye. They noted that EV quantity increases dramatically at late stage fed-batch. However, a caveat to this finding is that raw

sample was measured where the EVs were not isolated from non-EV particles. Lipophilic dyes are also non-EV specific and will stain cell membranes; the debris of which are likely to be more abundant at late stage fed-batch (Nagyova *et al.*, 2014). On the other hand, Belliveau and Papoutsakis (2022) quantified purified EVs from different days of fed-batch by NTA and noted that the rate by which EVs accumulate in the supernatant slows down as fed-batch culture progresses.

How the EV cargo changes throughout the fed-batch process has not been described in literature. Studies by Keysberg *et al.* (2021) provided an in-depth characterisation of the proteomic cargo present in EVs isolated from different stages of CHO batch culture. They noted increased presence of endoplasmic reticulum and cytoskeleton proteins in EV samples from late stage batch culture. This indicated that cellular debris were co-isolating in EV samples as cell death increased. They also characterised the miRNA content of the EVs throughout the batch culture. The miRNA content of EVs is of particular interest as not only can they be a biomarker of cellular health, much of EV mediated cell-to-cell communication is attributable to the miRNAs they contain (Bhome *et al.*, 2018; Dilsiz, 2020; Zheng *et al.*, 2021). miRNAs are short 20-22 nucleotide non-coding RNA sequences. They inhibit gene expression by binding to the 3' untranslated region of mRNA transcripts. In doing so, they inhibit their translation and also signal them for loading and degradation in the miRNA-induced silencing complex (RISC) (O'Brien *et al.*, 2018). Variation in the miRNA content of EVs was observed with the changing stages of growth in batch culture. Whilst Keysberg et al. (2021) do not investigate the function of the miRNAs, Busch *et al.*, (2022) predict the EV miRNAs to have an anti-apoptotic function. However, they only look at EV miRNAs from Day 11 of fed-batch when cell viability was in decline. Therefore, they do not account for the possible differences that may occur between exponential, stationary and death phase; nor do they attempt to test their prediction. Thus there is a lack of literature detailing how EV composition changes during a fed-batch process. There is also an absence of investigations which attempt to understand how they may influence the fed-batch.

In this study, EV accumulation in the cell culture supernatant was measured and the RNA content of sEVs isolated and sequenced. This enabled prediction of the functions sEVs have in cell-to-cell communication and biological processes they affect. In addition, EV depletion experiments were performed to test the hypothesised functions.

3.1.1 Chapter Summary

Lonza cell line CHO-A expressing an easy to express (ETE) mAb was grown in fed-batch. EVs were isolated from exponential phase, early stationary and early death phase by UC. UC was chosen primarily, as outlined in 1.5.1., because it was the most commonly used EV purification technique in literature. It is also used by Lonza for small scale EV studies. Western blotting was used to confirm efficient isolation of EVs using this technique.

NTA, BCA and further western blot analysis were also performed on both sEVs and lEVs to understand both how EVs accumulate throughout a fed-batch and also how their purity and composition may change depending on what stage of fed-batch they are isolated from. This would inform experimental approach carried out in Chapter 4, Chapter 5 and Chapter 6.

The miRNA content of sEVs from exponential, early stationary and early death phase was also isolated and sequenced to determine if there was DE of the sEV miRNAs at these different time-points. The function of these miRNAs was also predicted using two methods: 1) A targeted literature survey of most abundant miRNAs detected. 2) Use of online prediction tool miRWalk to predict the targets of the majority of the miRNAs detected (Sticht *et al.*, 2018).

Lastly, on the basis of the predicted functions of the sEV miRNAs, a fed-batch was set-up where sEVs were depleted to test the hypothesis generated.

3.1.2 Chapter Aims

The following were identified as aims for this chapter:

- Confirm UC successfully isolates sEVs from non-EV cell debris

- Quantify lEV and sEV accumulation in the extracellular space during the fed-batch

- Measure the protein content of purified lEV and sEV samples and use particle: protein ratios, along with western blots of an EV marker, to determine EV purity at different stages in fed-batch. This would inform which stage of fed-batch was optimal for isolating EVs for use in Chapters 4, 5 and 6.

- Identify the miRNAs present in sEVs at different stages in the fed-batch and use these miRNAs to predict possible functions of sEVs in fed-batch.

- Test the hypothesis generated from the predicted function of the sEV miRNAs with a fed-batch in which sEVs were depleted.

3.2 Results

3.2.1 Differential Ultracentrifugation (UC) successfully isolates EVs with consistent EV yields between fed-batches

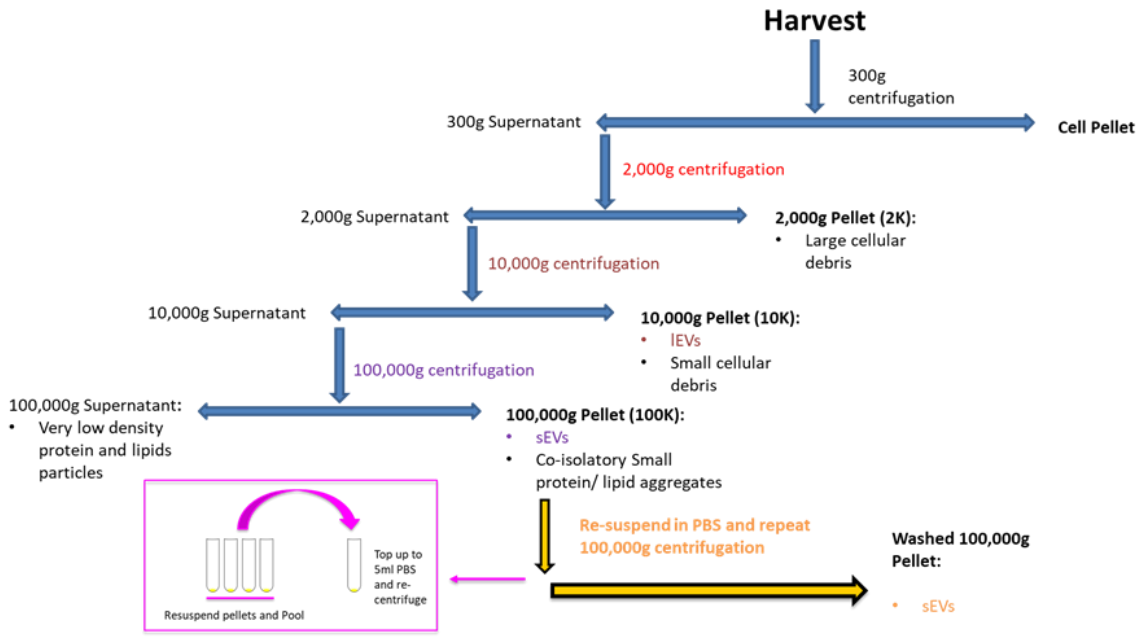

Fig 3.1 Workflow of EV purification steps. *The cell culture is centrifuged at 300g to pellet cells. The supernatant is taken and centrifuged at 2,000g (2K) which removes large cellular debris. The supernatant is then centrifuged at 10,000g (10K) which isolates lEVs as well as smaller cellular debris. A 100,000g centrifugation is then performed on the 10,000g supernatant to pellet sEVs. To concentrate sEVs and reduce the abundance of non-EV co-isolates, 100,000g pellets are pooled and re-suspended in 1X PBS. They are then re-centrifuged at 100,000g to generate the "washed" 100,000g pellet.*

Before attempting to quantify EVs from fed-batch, the capability of UC (see **Fig 3.1**) to purify EV enriched fractions was tested. Western blots were performed on the 10,000g and 100,000g fractions which are reported to contain lEVs and sEVs respectively. The EV samples were taken from Day 5 of CHO-A fed-batch. The presence of EV markers confirmed that the purification process was isolating EVs. Equal concentrations of protein were loaded for the 10,000g and 100,000g pellets in each blot. The EV markers TSG101, Syntenin-1, Alix and CD63 were all found to be present in the 100,000g fraction. TSG101 and CD63 were also present in the 10,000g fraction.

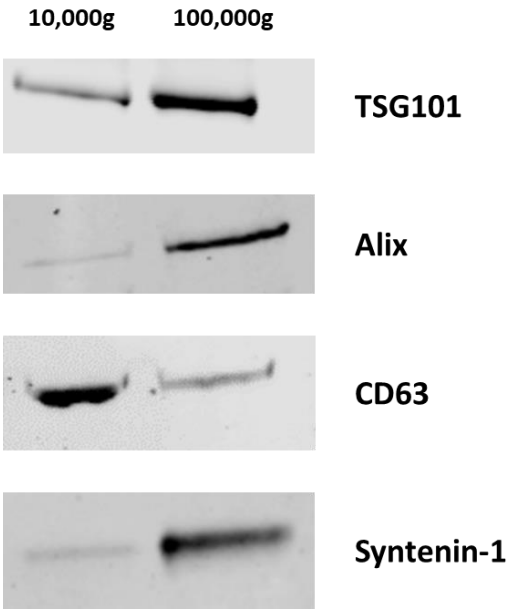

Fig 3.2 EV markers present in UC Fractions. *EV markers TSG101, Alix, CD63 and Syntenin-1 were all identified in the 100,000g (sEV) fraction. TSG101 and CD63 were also found to be abundant in the 10,000g (lEV) fraction. EV samples were purified from Day 5 CHO-A fed-batch and lysed in RIPA buffer with protease inhibitor prior to EV marker detection by western blot.*

To ensure that the EVs were being separated from non-EV cellular debris, a further round of western blotting was performed on EVs. This time taken from Day 11 (late stationary phase) of fed-batch. Blotting was done for non-EV protein marker HSP90B1 which is an endoplasmic reticulum protein as suggested by Théry *et al.* (2018). Three biological replicates were tested with equal protein concentrations loaded for the 2,000g, 10,000g and 100,000g pellets. Cell protein lysate was used as a positive control.

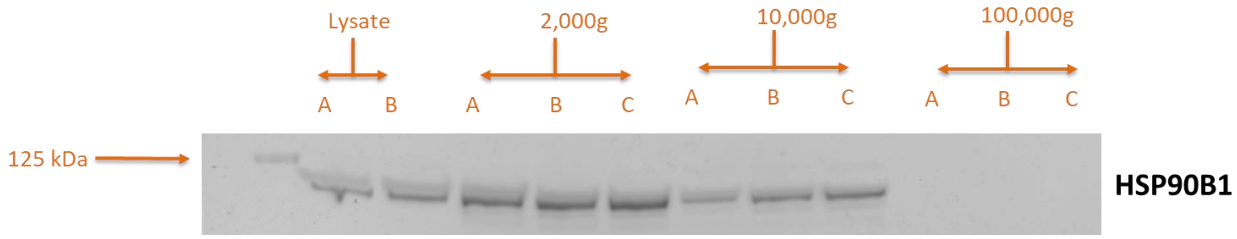

Fig 3.3 Non-EV Protein Marker absent in 100,000g (sEV) fraction. *Western blot for HSP90B1 revealed it was absent in the 100,000g pellet but co-isolated with lEVs and in the cellular debris fraction. The EV samples were purified from Day 11 CHO-A fed-batch culture. A, B and C represent biological replicates.*

The absence of HSP90B1 from the 100,000g pellet isolated at late stage fed-batch culture demonstrated that UC was able to remove sEVs from non-EV cell debris. This provided a high level of confidence that what was being analysed in the 100,000g pellet was mostly EVs with the majority of cellular debris removed in earlier fraction. The presence of EV markers in the 10,000g pellet along with non-EV markers showed that while EVs were present in this fraction, they were less pure than those in the 100,000g fraction.

It was next ascertained if there was large variation in the batch-to-batch yield of EVs obtained; be it due to variation introduced by human error in the UC process or simply batch-to-batch variation. To examine this, three separate fed-batches of the GSKO-Host cell line were grown with duplicate flasks in each fed-batch. The sEVs from each fed-batch were purified on Day 5 and then counted by NTA.

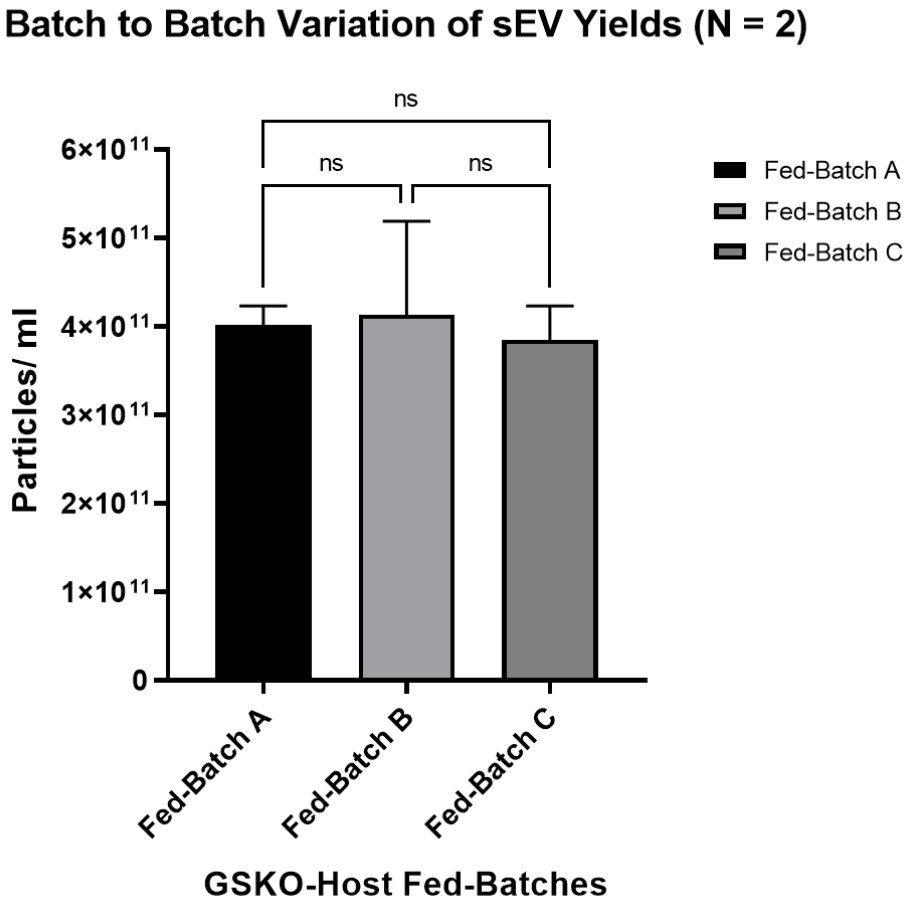

Fig 3.4 Consistent sEV yields between fed-batches. *GSKO-Host cells were grown to Day 5 of fed-batch and sEVs purified by UC with 100,000g pellet re-suspended in 600µl CD-CHO. Cells were grown*

in E1000 erlenmeyer flasks with a culture volume of 160ml. 100ml of this was used for sEV purification. sEVs were counted by NTA Analysis. There were 2 replicates per fed-batch and error bars are standard deviation of mean particle count for each fed-batch. Blank CD-CHO with no sEVs re-suspended in it measured fewer than 3 particles per frame on the Nanosight NS300 which is considered particle free solution. One-way ANOVA applied with Tukey post-hoc test to correct for multiple comparisons as a statistical significance test.

There was little variation in particle count between fed-batches in **Fig 3.4** indicating that cells which were grown in the same conditions and which had the same purification parameters applied to the UC process (i.e. volume purified, re-suspension volume and re-suspension media) and gave a consistent yield of sEVs.

3.2.2 Quantification of EV accumulation in CHO-A fed-batch

To understand how EVs accumulated in the extracellular space during mAb manufacturing, CHO-A was grown in fed-batch. In brief, 12 E500 erlenmeyer flasks with a culture volume of 80ml were set up as shown in **Fig 3.5** (A).

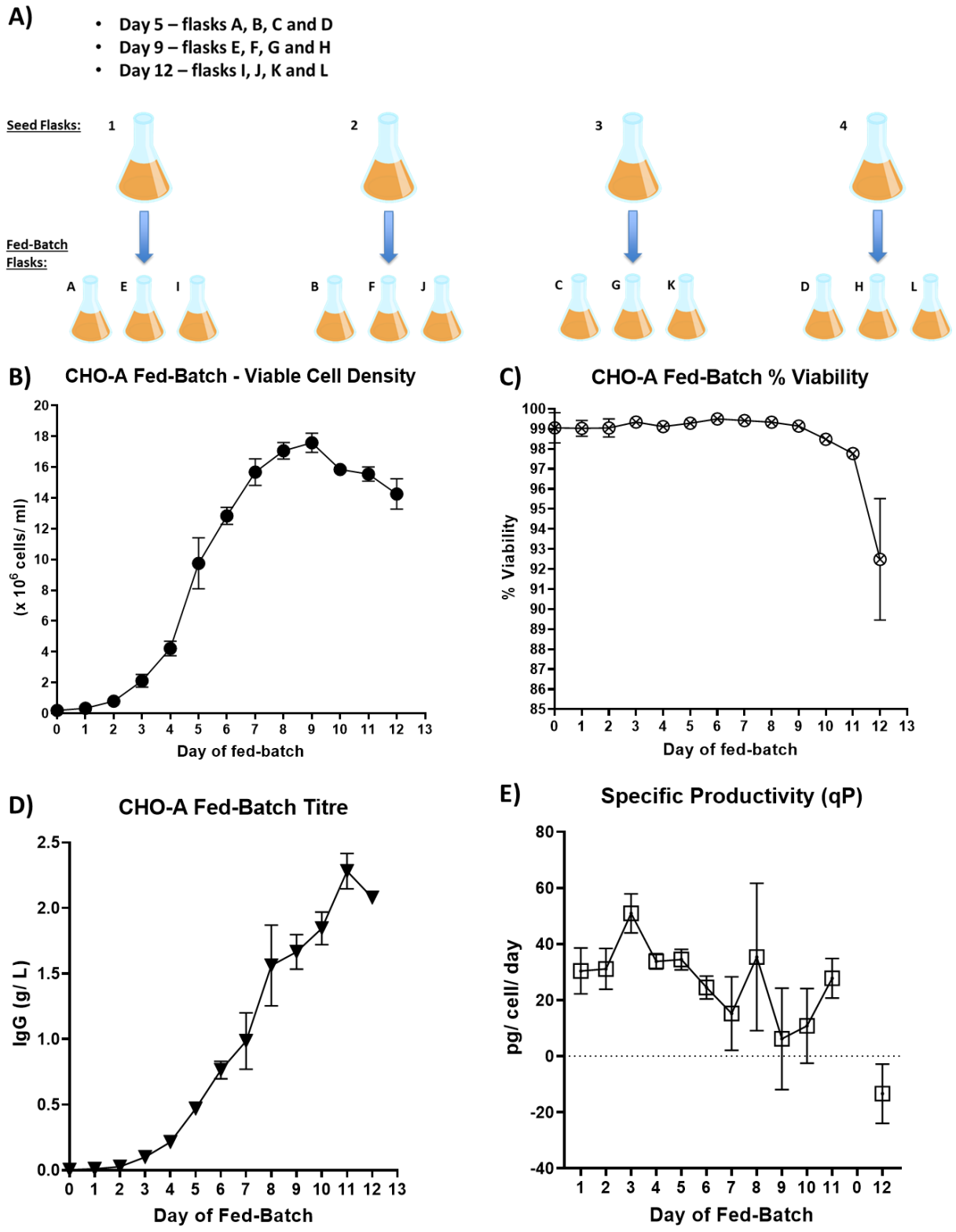

Fig 3.5 Fed-Batch of CHO-A Cell Line. To ensure enough cell culture supernatant volume for EV analysis, flasks were grown to either Day 5, 9 or 12 in the fed-batch and then harvested. *(A) 12 flasks seeded from 4 biological replicate seed flasks passaged separately from passage one until passage four. Four flasks were harvested on Day 5 (replicates A, B, C and D), four harvested on Day 9 (replicates E, F, G and H) and four flasks harvested on Day 12 (I, J, K and L). (B) VCD as measured*

by Vi-Cell. (C) Viability of cells as measured by Vi-cell. (D) IgG titre of fed-batch. All titre samples taken from flasks I, J, K and L. (E) Specific Productivity (qP) on each day of fed-batch. All error bars are standard deviations. For VCD, Viability and Titre 12 replicates were recorded until Day 5, eight replicates until Day 8 and four replicates until Day 12.

On each of Days 5, 9 and 12, four flasks were harvested respectively. This was because the cells were in exponential phase on Day 5, peak VCD/ early stationary phase on Day 9 and late stationary/ early death phase on Day 12. 10ml of cell culture supernatant was purified and the 10,000g and 100,000g pellets were re-suspended in 100µl PBS. Three replicates were then run on the NTA to both quantify and size the EVs.

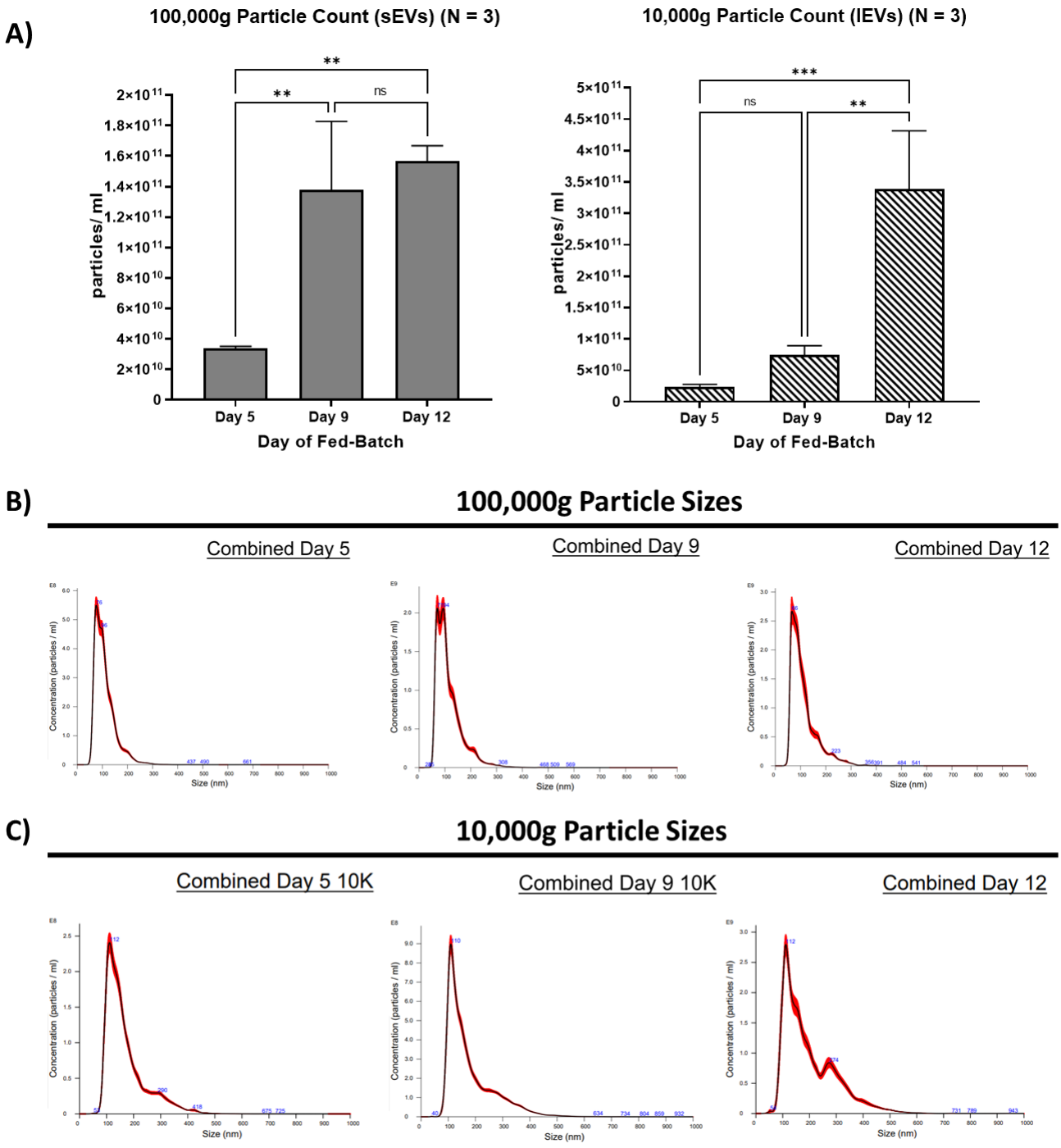

Fig 3.6 NTA Analysis showed EV accumulation up to early stationary fed-batch whilst modal EV sizes remained consistent. *(A) Particle counts for Days 5, 9 and 12 of fed-batch. Three replicates used for each day of fed-batch analysed. Error bars are standard deviation.* One-way ANOVA applied with Tukey post-hoc test to correct for multiple comparisons. *(B) NTA size data for 100,000g pellet. (C) NTA size data for 10,000g pellet. Sizes of the three replicates from each day were combine to get an average size profile for that day of fed-batch for both 100,000g and 10,000g NTA analysis.*

The number of EVs increased significantly between Day 5 and Day 9 in the 100,000g pellet whilst there wasn't a significant increase between Day 9 and Day 12. In the case of the 10,000g pellet, there was only a slight increase in the number of particles from Day 5 to Day 9 relative to the large and significant increase between Day 9 and Day 12. As can be seen in **Fig 3.6** (B), the size of the EVs in the 100,000g pellet stays constant throughout the fed-batch with the majority of particles being classed as sEVs that are smaller than 100nm in size (mode size 70 - 90nm). The particle sizing in (C) shows lEVs which are 100nm or greater in size (mode size 110-112nm). There is a noticeable increase in the number of 200nm+ particles on Day 12.

To better understand EV accumulation in the extracellular space. It was necessary to see how it was changing relative to the number of viable cells. This would indicate if the cellular rate of EV secretion fluctuated as culture progressed. To do this, ratios of the number EVs per cell were generated.

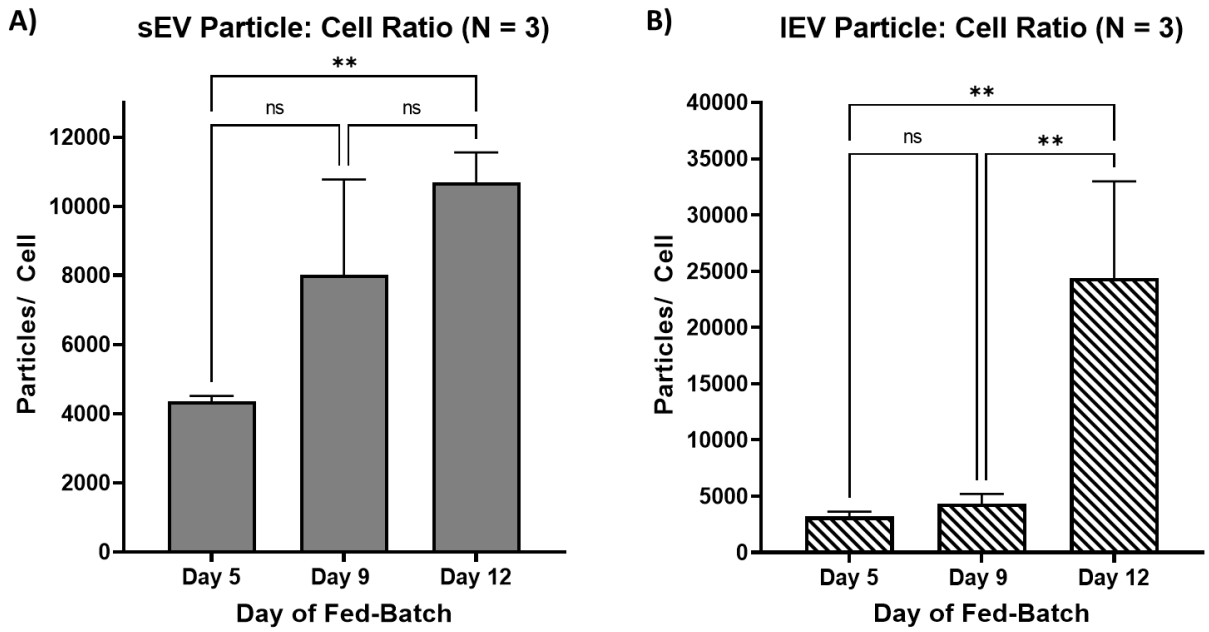

Fig 3.7 The number of EVs/ Cell increases as fed-batch progresses. *The total number of particles counted in each replicate was divided by the total number of cells in each replicate on Days 5, 9 and 12 of fed-batch. Ratio of particles/ cell for (A) sEVs and (B) lEVs. Error bars are standard deviation.* One-way ANOVA applied with Tukey post-hoc test to correct for multiple comparisons.

Although not significant, there does appear to be an increase in the number of sEVs per cell from Day 5 to Day 9 with greater variability on Day 9. There also appears to be an increase from Day 9 to Day 12. However, it is also not significant and less pronounced than between Day 5 and Day 9. In the case of lEVs, the ratio of particles/ cell stays constant between Day 5 and Day 9 but increases considerably on Day 12. These ratios suggest that the rate of sEV secretion increases up to stationary phase and slows somewhat beyond this point. There is a significant increase in the number of sEVs/ cell between exponential and late stage fed-batch. In the case of lEVs, the rate of secretion only increases after stationary phase.

3.2.3 Protein Content of EV Pellets and Purity

In addition to NTA counts, the protein content of the 10,000g and 100,000g fractions were measured by BCA. This was done, firstly, as a form of orthogonal validation for the NTA counts – one would expect to see that two samples of equal purity with different particle counts to have protein content reflecting the difference. Secondly, it was necessary to identify the optimal time-point in fed-batch for obtaining both a high yield and highly pure EV sample. The analysis in 3.2.1 showed that UC effectively separated sEVs from the majority of cellular debris. Yet there may be proteins or debris which co-isolate with EVs in the UC process. The abundance of these co-isolates may differ at different stages in the fed-batch. Quantifying co-isolates was important for subsequent studies comparing EV secretion between cell lines as was done in Chapters 4 and 5 or when attempting to treat CHO cell cultures with EVs as done in Chapter 6. In both scenarios, a high purity was desirable as it gave confidence that what was being analysed were EVs and any subsequent effects on cells treated with EV samples were due the EVs themselves; rather than co-isolates.

Along with the 10,000g and 100,000g fractions, the 2,000g fraction in which large cell debris pellet was also measured. This was to have as a further indicator of EV purity as a high quantity of cellular debris protein would likely translate into less pure EVs.

30ml of cell culture supernatant from the same fed-batch used for NTA counts in **Fig 3.5** was purified and the resulting pellet in each fraction re-suspended in RIPA with proteinase inhibitor prior to measuring by BCA assay.

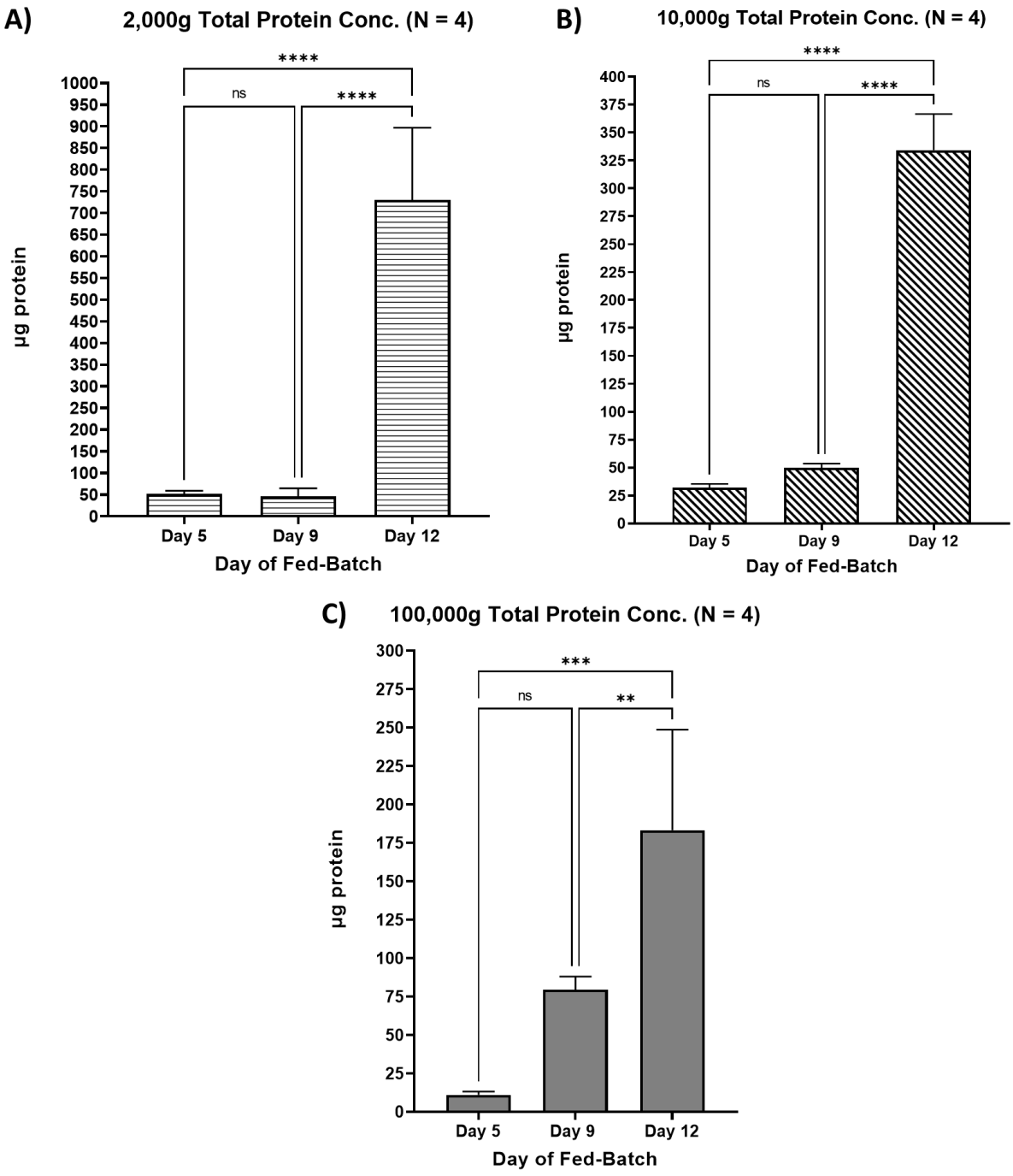

Fig 3.8 Protein content increases at different rates in each fraction. *Total protein content for four replicates on Days 5, 9 and 12 of (A) 2,000g fraction (large cellular debris), (B) 10,000g fraction (lEVs) and (C) 100,000g fraction (sEVs) as measured by BCA assay. Error bars are standard deviation. One-way ANOVA applied with Tukey post-hoc test to correct for multiple comparisons.*

The greatest protein content was found in the 2,000g fraction where large cellular debris pellet (**Fig 3.8** (A)). The amount of protein recoverable in this fraction didn't change between Day 5 and Day 9. However, on Day 12, where VCD and viability had

fallen, there was a very large increase in the amount of protein. The 10,000g fraction in **Fig 3.8** (B) was very similar to the 2,000g fraction whereby there was little change in protein content between Day 5 and Day 9 before a large significant increase on Day 12. The 100,000g fraction in **Fig 3.8** (C) showed that protein gradually accumulated as the fed-batch progressed.

To understand how EV purity was changing during the fed-batch, particle: protein ratios were generated for both the 10,000g and 100,000g fractions by taking the total number of particles, as measured by NTA, and dividing by the total protein content. These ratios have previously been used to measure EV purity when comparing purification techniques (Webber and Clayton, 2013).

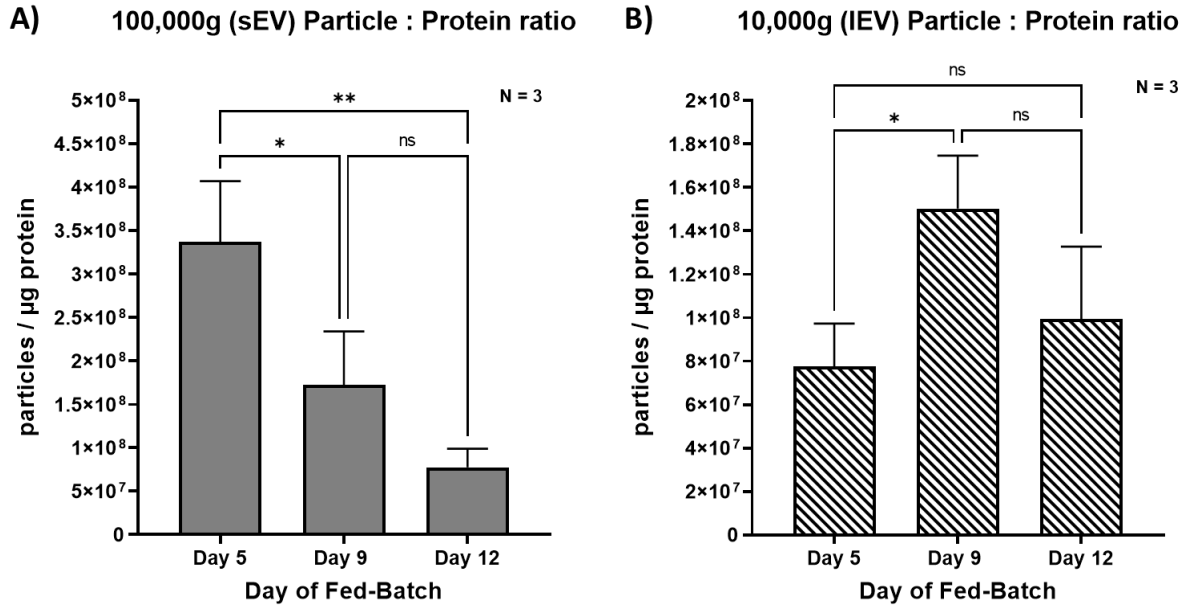

Fig 3.9 The purity of sEVs diminished as fed-batch progresses. *Total particle counts of the three replicates measured by NTA divided by the total protein content of EV samples from those replicates. Ratio of number of particles per µg for (A) sEVs and (B) lEVs. Error bars are standard deviation. One-way ANOVA applied with Tukey post-hoc test to correct for multiple comparisons.*

In **Fig 3.9** (A) there was a clear decline in the purity of the sEVs as fed-batch progressed. Particularly on Day 12 where cell death was occurring at a greater rate and there were large amounts of cell debris; as seen by the increase in protein content in the 2,000g fraction on Day 12. Surprisingly, the 10,000g fraction appeared to show that purity increases from Day 5 to Day 9. On Day 12 the increase in the number of particles was proportional to the increase in protein content as its purity was similar to

Day 5. To understand what may be contributing to the protein content apparent on Day 12 other than EVs. Transmission Electron Microscopy (TEM) images were taken of sEV pellets from this day of fed-batch. This showed how protein aggregates were co-isolating with sEVs in the 100,000g fraction at this stage in fed-batch and were likely contributing to the increased protein content observed.

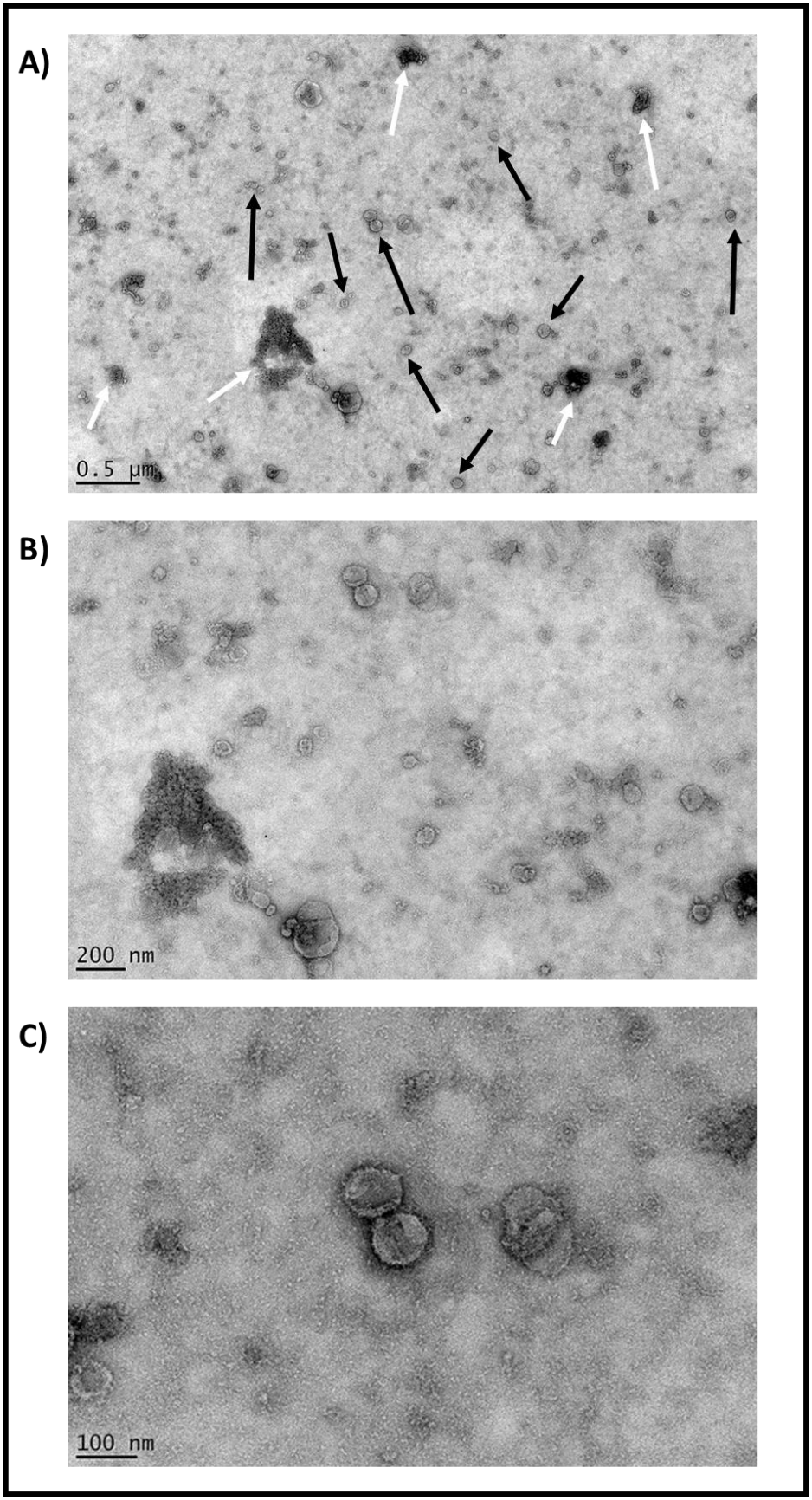

Fig 3.10 TEM imaging of late stage fed-batch sEVs showed samples had protein aggregates co-isolating with the sEVs. *sEVs purified by UC from late stationary/ early death phase of stage fed-*

batch and re-suspended in 1X PBS prior to imaging by TEM. (A) Image at 0.5µm showing sEVs and protein aggregates present. (B) 200nm magnification of the same image. (C) 100nm magnification of the same image. sEVs were distinct by their cupped shape morphology. Protein aggregates appear as dark globular bodies in the image.

Along with particle: protein ratios and TEM analysis, western blots were performed with each day measured in triplicate. This was to determine if the changes in protein content were due to increased EV presence or if there were higher quantities of co-isolate proteins. As TSG101 was found to be abundant in the sEV fraction (see **Fig 3.2**), it was blotted for to measure sEV abundance. CD63 was used for lEVs. Densitometry analysis was then performed to measure band intensity.

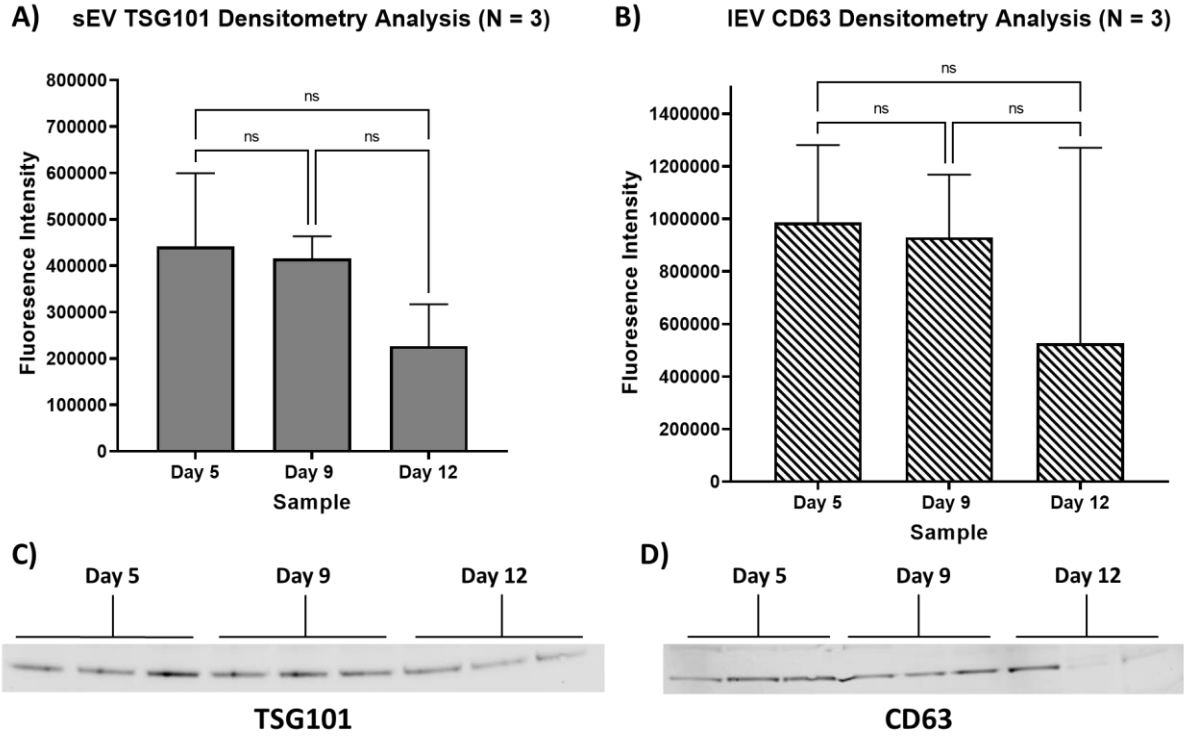

Fig 3.11 sEV and lEV marker abundance decreases on Day 12. *Densitometry analysis of western blot for (A) TSG101 and (B) CD63. Corresponding western blot for densitometry analysis with equal protein concentrations loaded to each lane in (C) TSG101 (7.4 µg per lane) and (D) CD63 (9.8 µg per lane). As no loading control exists that is known to co-isolate with EVs, three replicates from Days 5, 9 and 12 of fed-batch by NTA were loaded to the blot. This was to account for variance in protein transfer during blotting. Error bars are standard deviation. One-way ANOVA applied with Tukey post-hoc test to correct for multiple comparisons.*

Both TSG101 and CD63 are comparable for Day 5 and Day 9 in **Fig 3.10** (A) and (B). TSG101 band intensity fell overall on Day 12, albeit, not significantly. In the case of CD63 in the lEV fraction, it became far more variable on Day 12. This suggested that the fraction of both sEV and lEV protein, as part of the total protein content that is purified by UC, diminishes after the fed-batch has entered stationary phase.

3.2.4. Characterising the miRNA content of CHO sEVs in fed-batch

3.2.4.1 Fed-batch and RNA Isolation

Another CHO-A fed-batch was set-up as per **Fig 3.5** (A). This time in E250 erlemenyers with a culture volume of 40ml. The sEVs were also isolated at the same time-points – Exponential Phase (Day 5), Early Stationary (Day 8) and late stationary/ early death phase (Day 12) (see **Fig 3.12** (A)). The reason sEVs were chosen to examine how miRNA content evolves throughout fed-batch over lEVs is because the UC purification is designed primarily to isolate sEVs from non-EV debris. As seen in 3.2.1, non-EV cellular debris co-isolated in 10,000g fraction. This meant that while UC could isolate fractions enriched with lEVs, there was concern that miRNAs detected in this fraction may be from co-isolates rather than lEVs. Therefore, to have a high degree of confidence what was being measured was EV miRNAs, sEVs were only considered for this analysis.

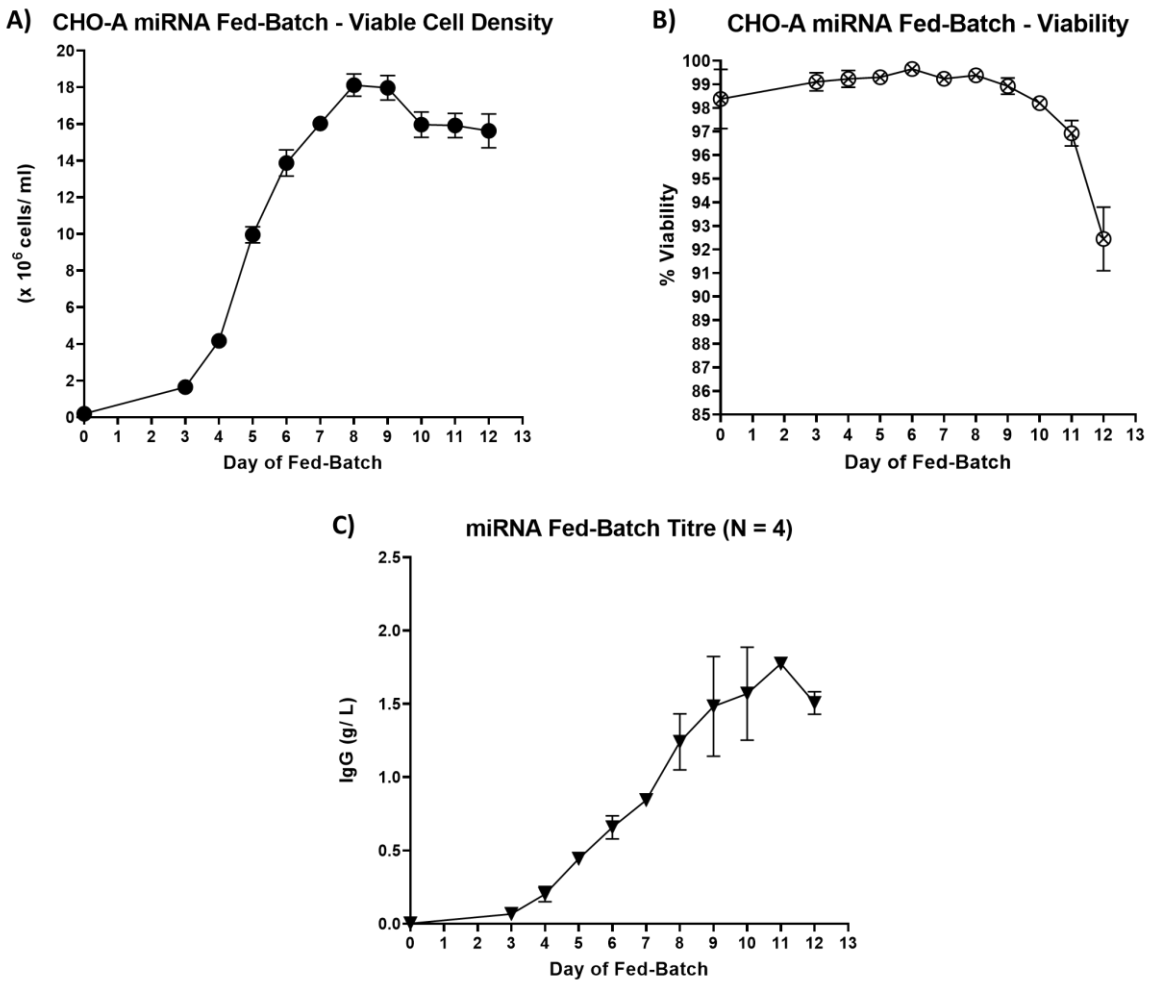

Fig 3.12 Fed-Batch of CHO-A in E250 erlenmeyer flasks for EV RNA Analysis. *(A) VCD and (B) Viability of CHO-A fed-batch. (C) Titre as measured by ValitaTiter assay to confirm IgG yield similar to fed-batch in Fig 3.5. Titre samples taken at time-points shown from the four replicate flasks harvested on Day 12. EVs isolated from Days 5, 8 and 12 with 4 replicate flasks harvested on each of these days. All error bars are standard deviation.*

4 replicates per harvest time-point were used for RNA extraction. 30ml of cell culture supernatant was taken from each harvested flask and purified by UC. sEV pellets were re-suspended in 200µl PBS as recommended by the Norgen Total RNA isolation EV protocol prior to RNA extraction. The isolated RNA was then measured on an Agilent Bioanalyser for both quantity and sizing of RNA isolated.

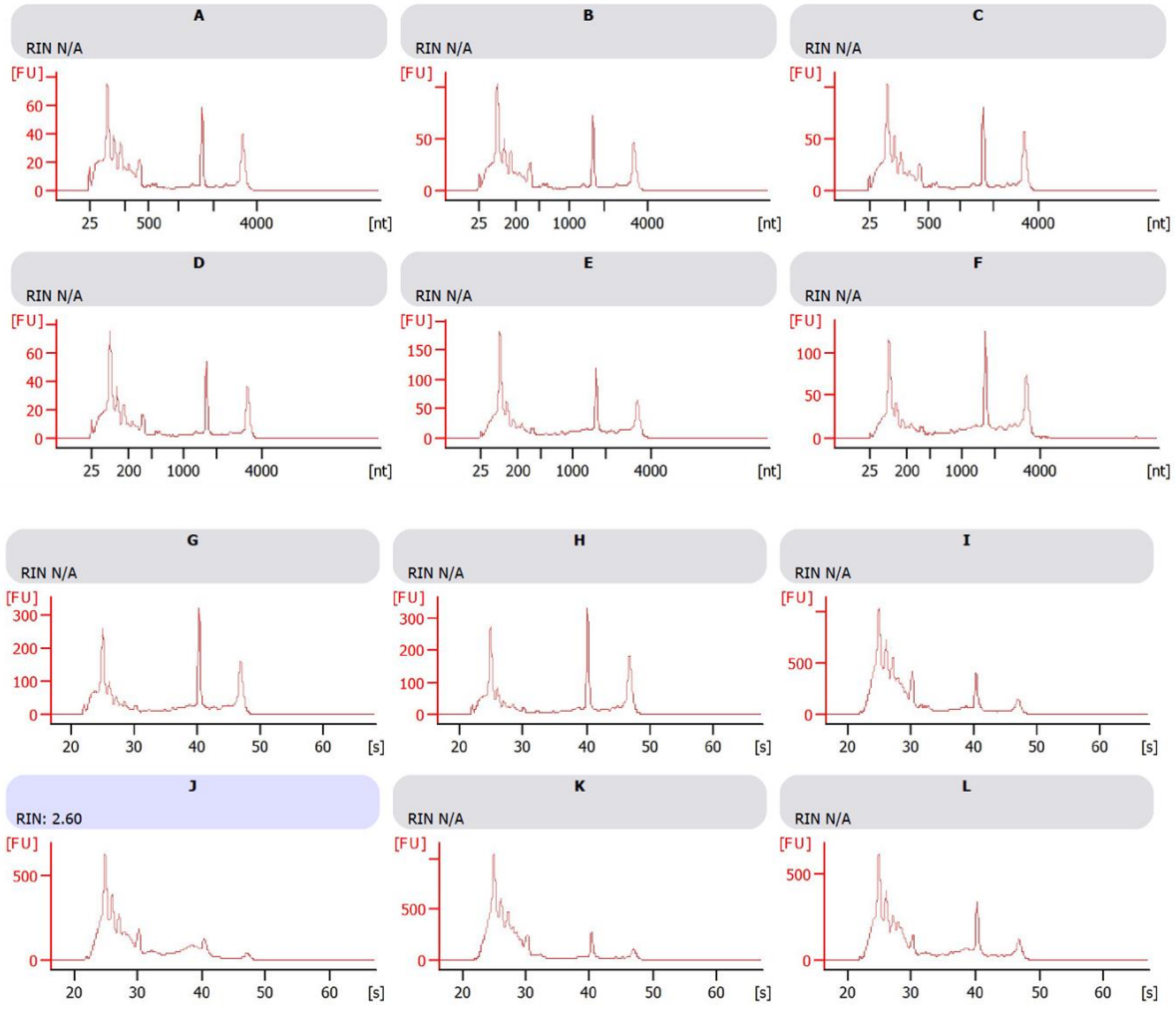

Fig 3.13 Size of the RNA isolated from sEVs is broadly below 200 nt. *Bioanalyser report showing the size of RNA isolated from sEVs. A, B, C and D = Day 5. E, F, G and H = Day 8. I, J, K and L = Day 12. Note: G-L x-axis units given in seconds [s] rather than [nt].*

The majority of sEV RNA was fewer than 200 nucleotides in size. There were also residual 18S rRNA peaks as well as large 5S rRNA peaks in each sample. All samples then underwent Small RNA-sequencing at Genewiz.

3.2.4.2 Small RNA-sequencing and Differential Expression (DE) Analysis

As can be seen in **Fig 3.14** (A) the majority of miRNAs were present at all 3 time-points. Day 12 had the most unique miRNAs with 11 identified on that day alone. Day 8 and Day 12 also shared 11 miRNAs not present on Day 5. This suggests certain

miRNAs were not loaded into EVs until stationary phase of fed-batch. However, the degree to which miRNA expression levels overlap shows that Day 5 and Day 8 were far more similar than Day 12 in **Fig 3.14** (B). Day 5 and Day 12 have little overlap in terms of miRNA expression. The differences between the days was further highlighted by the principal component analysis in **Fig 3.14** (C) which also showed little difference within sample groups.

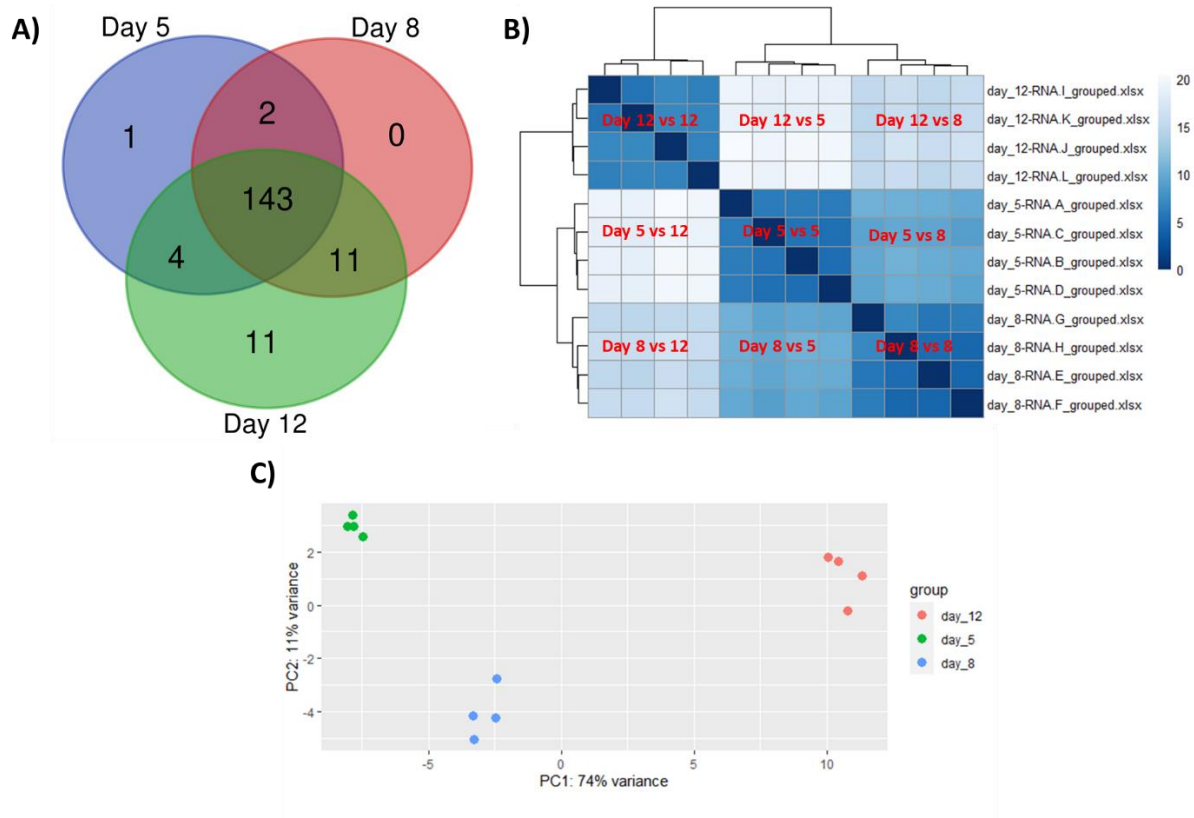

Fig 3.14 The numbers of miRNAs identified on each day of fed-batch and how their expression levels compare on each day. *(A) miRNA overlap on each day of fed-batch. (B) Heatmap of similarities in expression between samples on each day. The fainter the colour, the greater the difference between samples. (C) Principal Component Analysis showing variation between sample groups and within sample groups.*

To compare the quantities of individual miRNAs present on each day, the normalised counts of each miRNA as a percentage of the total miRNA content they occupy were plotted. The top 15 most abundant miRNAs on Day 5 were compared to their quantities on the other 2 days. This revealed that the majority of the total miRNA count in CHO sEVs was taken up by a relatively small number of miRNAs.

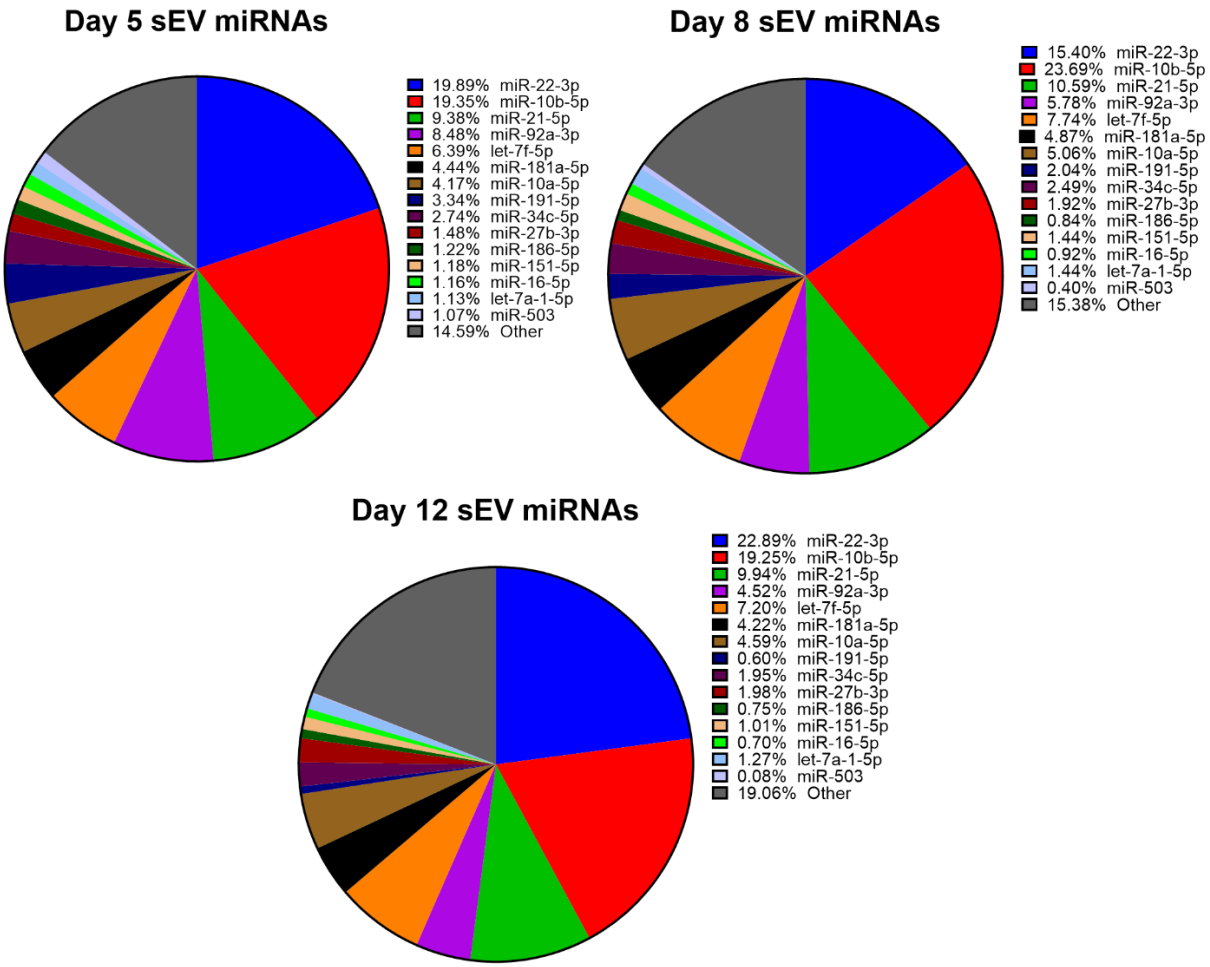

Fig 3.15 Comparison of Individual miRNA Abundances. *Top 15 miRNAs present on Day 5 and their percentage of total miRNA population on Days 5, 8 and 12.*

As much as 85.41% of the total miRNAs present in Day 5 sEVs was composed of the top 15 miRNAs present. The top 5 alone accounted for 63.49%. The proportions of these miRNAs present didn't change either as the fed-batch progressed. While DE analysis revealed significant changes in miRNA quantities, they are relatively small changes as in seen in **Table 1**.

Table 1: DE Analysis of Top 15 most abundant miRNAs on Day 5. *(A) Comparison of Day 5 vs Day 8. (B) Comparison of Day 8 vs Day 12. Wald's test used to check for statistical significance in differences in abundance across the three days of fed-batch with Benjamini Hochberg post-hoc test for multiple comparisons.*

A)

Top 15 miRNA on Day 5	Significant Differential Expression? Day 5 vs Day 8	log2FoldChange on Day 8	padj
miR-22-3p	Yes	-0.374514477	1.42E-07
miR-10b-5p	Yes	0.270574611	0.018399
miR-21-5p	Yes	0.161663599	0.038731
miR-92a-3p	Yes	-0.556894188	9.73E-18
let-7f-5p	Yes	0.25527502	0.026493
miR-181a-5p	No		
miR-10a-5p	Yes	0.263235796	0.000966
miR-191-5p	Yes	-0.70108489	5.51E-10
miR-34c-5p	No		
miR-27b-3p	Yes	0.365481445	1.56E-07
miR-186-5p	Yes	-0.536043759	1.19E-25
miR-151-5p	Yes	0.265288638	8.39E-08
miR-16-5p	Yes	-0.325251403	0.00598
let-7a-1-5p	Yes	0.312434027	0.046382
miR-503	Yes	-1.433426224	1.5E-104

B)

Top 15 miRNA on Day 5	Significant Differential Expression? Day 8 vs Day 12	log2FoldChange on Day 12	padj
miR-22-3p	No		
miR-10b-5p	Yes	-0.328056554	0.001026
miR-21-5p	Yes	-0.153585616	0.036441
miR-92a-3p	Yes	-0.419811598	8.26E-11
let-7f-5p	No		
miR-181a-5p	Yes	-0.26729685	0.006654
miR-10a-5p	Yes	-0.224659119	0.008924
miR-191-5p	Yes	-1.809388137	2.65E-60
miR-34c-5p	Yes	-0.418488515	1.95E-06
miR-27b-3p	No		
miR-186-5p	Yes	-0.23575339	5.43E-06
miR-151-5p	Yes	-0.563913517	6.19E-33
miR-16-5p	Yes	-0.449586362	8.54E-05
let-7a-1-5p	No		
miR-503	Yes	-2.342768548	1.1E-266

Overall, the relative quantities of the most abundant miRNAs stayed the same throughout the fed-batch. Of the miRNAs which made up more than 2% of the total miRNAs present on Day 5, only miR-92a-3p and miR-191-5p had a consistent fall in abundance as the fed-batch progressed. miR-34c and miR-181 had no significant change on Day 8 but had declined on Day 12. It was in the less abundant miRNAs such as miR-503 and miRNAs listed as Other in **Fig 3.14** where the greatest changes in expression were observed. See Appendix A and Appendix B for list of all differentially expressed miRNAs on Day 8 and Day 12.

3.2.5 Predicting the Function of CHO EV miRNAs

There were two approaches taken to hypothesize the functions of CHO sEVs based on their miRNA composition. As most of the top 10 most abundant miRNAs on Day 5 stayed consistent in their expression throughout fed-batch, and occupied such a large

percentage of the total miRNA composition, it was possible that they had the greatest influence on fed-batch culture. Therefore, a search of the literature for each of these 10 miRNA was carried out for building an overall consensus of their function. However, abundance of miRNA does not necessarily equate to functionality in a cell. This may be because the targets the miRNA binds to may be low in their abundance. Even if binding to a target occurs, it may not be strong or stable resulting in minimal degradation of the target sequence (Chipman and Pasquinelli, 2019). Therefore, it was also necessary to consider as many miRNAs present as possible and predict the function of their targets. To do this, all Day 5 sEV miRNAs with a normalised mean count of 50 or more (119 miRNAs) were converted to their mouse orthologues and ran through bioinformatics software, miRWalk (Sticht *et al.*, 2018). This enabled target prediction for 99 of those miRNAs. More importantly, it allowed identification of the biological processes those targets were involved in through gene set enrichment analysis. The reason Day 5 sEV miRNAs were selected is because the majority of miRNAs present on Day 5 were also detected on all 3 days. Any additional miRNAs present on Day 8 and Day 12 may be a result of deteriorating cell health or from possible co-isolates in the EV sample.

3.2.5.1 Top 10 Most Abundant miRNAs literature survey

1) **miR-22-3p:** Shown to activate liver cancer by suppressing ERα and promote proliferation in renal cell carcinoma by inhibiting expression of PTEN (Luo *et al.*, 2017). It was also found to be upregulated in pancreatic cancer patients (Hussein *et al.*, 2017). However, miR-22-3p has been shown to be tumour suppressive in hepatocellular carcinoma as it inhibits expression of CD147 (Wang *et al.*, 2017). Likewise, it inhibits cell growth in lung cancer by targeting the MET/ STAT3 pathway. This suggests that its function is somewhat cell specific (Yang *et al.*, 2021).
2) **miR-10b-5p:** Upregulated in several cancer types. It increases metastasis, invasion and proliferation in breast cancer, pancreatic cancer and lung cancer. It does this targeting HOXD10 which in turn upregulates E-Cadherin (involved in several oncogenic pathways), targeting of HOXD10 and the targeting of NF1

which can also activate the proto-oncogene c-Jun (Sheedy and Medarova, 2018). In recombinant cell lines, miR-10b-5p is upregulated which may explain its high abundance in CHO sEVs (Maccani *et al.*, 2014). In humans, mice and rats, it targets genes involved in TGF-ß action which is involved in cell growth and proliferation (Sadowska *et al.*, 2021).

3) **miR-21-5p:** Associated with being anti-apoptotic and pro-survival, miR-21-5p is upregulated in many cancer types. In breast cancer, it downregulates the tumour suppressor PDCD4. In lung cancer, it targets Spry2 and BTG2 to enhance tumorigenesis (Feng and Tsao, 2016). In mice, miR-21 was shown to be necessary for ERK-MAPK pathway activation and the induction of hypertrophy in cardiomyocytes as well as cardiac fibroblast activation (Dai *et al.*, 2020). Like miR-10b, miR-21 is also upregulated in recombinant cell lines. However, overexpression of miR-21 reduces specific productivity. It was found to cause no increase in cell growth with lower titre (Jadhav *et al.*, 2012). It is also upregulated during stationary phase of growth which is similar to what is seen with the increase in abundance from Day 5 to Day 8. (Gammell *et al.*, 2007).

4) **miR-92a-3p:** Meta-analysis has shown that miR-92a-3p is upregulated in non-small-cell lung cancer and RGS3, a regulator of G-protein signalling 3, is a target of miR-92a (Jiang *et al.*, 2019). It is also upregulated in colorectal cancer (Fu *et al.*, 2018). Li *et al.* (2019) found that it promoted the proliferation of esophageal squamous cell cancer by inhibition of PTEN. In CHO, miR-92a increases productivity by targeting insig1 which results in increased cholesterol levels. This allows for a Golgi apparatus of greater volume which enhances protein secretion (Loh, Yang and Lam, 2017).

5) **Let-7f-5p:** In CHO, let-7f-5p has been demonstrated to inhibit cell growth and induced cell death (Fischer *et al.*, 2015). This is somewhat at odds with a study which found let-7f promoted bone marrow mesenchymal stem cell survival by targeting caspases-3 (Han *et al.*, 2018).

6) **miR-181a-5p:** Anti-apoptotic miRNA which promotes oncogenic pathways through its targeting of STING. This allows the cell to bypass interferon mediated cell death (Knarr *et al.*, 2020).

7) **miR-10a-5p:** In CHO, upregulation of miR-10a-5p was positively correlated with cellular growth (Clarke *et al.*, 2012). Like miR-10b, it also targets TGF-ß (Sadowska *et al.*, 2021). In acute myeloid leukaemia, it is highly abundant and targets both a regulator of p53, MDM4, and p53 itself; thereby inhibiting their expression. These genes are heavily involved in tumour suppression (TT *et al.*, 2021).

8) **miR-191-5p:** In cancer, this miRNA is involved in proliferation, metastasis and stress resistance. However, whether it is tumorigenic or tumour suppressive can depend on the cell line (Nagpal and Kulshreshtha, 2014). In the case of cholangiocarcinoma, inhibiting miR-191 induces apoptosis which suggests an anti-apoptotic function (Kang *et al.*, 2018).

9) **miR-34c-5p:** Identified as a tumour suppressor, it targets c-myc, CDK6 and c-MET which activate cell death. A study involving miRNA sponges in CHO attempted to deplete its isotype, miR-34a. This differs from miR-34c by a single nucleotide outside the seed region (it will therefore bind to the same targets). The authors note miR-34c would also be sequestered by the sponge. Increasing miR-34a expression was shown to inhibit CHO cell growth by 90% (Kelly *et al.*, 2014).

10) **miR-27b-3p:** Strong anti-proliferation effect by targeting CBLB/ GRB2 in breast cancer cells (Chen *et al.*, 2018). It has a similar effect in gastric cancer as it targets tyrosine kinase like orphan 1 receptor (Tao *et al.*, 2015). It also inhibits the proliferation of glioma cells by inhibiting YAP1 (Miao *et al.*, 2020). In CHO, removal of miR-27b-3p by CRISPR-Cas9 improved viability in late stage batch and fed-batch cultures (Kellner *et al.*, 2018).

It is difficult to build an overall consensus from the most abundant miRNA as to what functions they may be attribute to CHO sEVs in terms of cell growth and proliferation. There are a similar number of pro-proliferative (miR-10b-5p, miR-21-5p, miR-92a-3p, miR-10a-5p) and anti-proliferative (miR-22-3p, let-7f, miR-34c-5p, miR-27b-3p) miRNAs. Therefore, it is inconclusive as to how they may influence cell growth during a fed-batch process. However, there is some indication they have an anti-apoptotic/

pro-survival role based on the functions of miR-10b-5p, miR-21-5p, miR-92a-3p, miR-10a-5p and miR-181a-5p.

3.2.5.2 Target Prediction and Functional Analysis Using miRWalk

The online tool miRWalk uses the Target Prediction for miRNAs (TarPmiR) approach for predicting the targets of miRNA. TarPmiR was developed and described in detail by Ding, Li and Hu (2016). Briefly, it works by first considering seed matching of the miRNA (nucleotides 2-7 in the miRNA) to its complementary sequence in the target mRNA. This generates its first list of candidate targets. It also considers the minimal folding energy of the two when binding. Fold energy indicates the stability of the binding of the miRNA to the mRNA transcript and the lower the energy, the more stable the binding. This generates a second list of candidate targets. TarPmiR then calculates the values of the aforementioned features and 11 others. These are:

(i) Accessibility: This is a measure of how open the target mRNA sequence is for miRNA binding to occur.

(ii) AU Content: AU rich elements in the 30 nucleotides upstream or downstream of target site region promote miRNA binding.

(iii) The total number of paired positions in the miRNA 3' end (nucleotides downstream of the seed position).

(iv) Difference between the number of paired positions in the seed region and that in the miRNA 3' end.

(v) Flanking conservation: This measures how evolutionary conserved sequences 40 nucleotides upstream and downstream of the target binding site are using a PhyloP score. The sequences flanking miRNA binding sites are often conserved which means a high PhyloP score increases the likelihood of miRNA binding (Kenny *et al.*, 2015).

(vi) The length of the largest consecutive pairs between the miRNA and mRNA

(vii) The position of the largest consecutive pairs relative to the 5' end of the miRNA

(viii) The length of the target region on the mRNA to which the miRNA binds – the true length of this region should be between 20-24 nucleotides long

(ix) The total number of paired positions between the mRNA and miRNA.

(x) m/e motif: This is the probability of matching (m) or, if not, else (e) for each position in the miRNA.

(xi) Stem Conservation: This is a PhyloP score of the miRNA stem loop precursor.

Having scored these features, TarPmiR finally uses random forest modelling to give the probability of binding (p-value). For this analysis, the p-value threshold was set to 0.95. The miRWalk tool also allowed filtering of predicted miRNA-mRNA pairings to only show those which were also predicted by two other target prediction tools: TargetScan and miRDB. This was therefore utilised to provide greater assurance of target prediction.

Once the genes of the mRNA targets were identified, the genes were put through gene sequence enrichment analysis on miRWalk to obtain a gene ontology of the biological processes most targeted by the miRNAs. They were also subject to KEGG analysis to understand what pathways those genes were involved in.

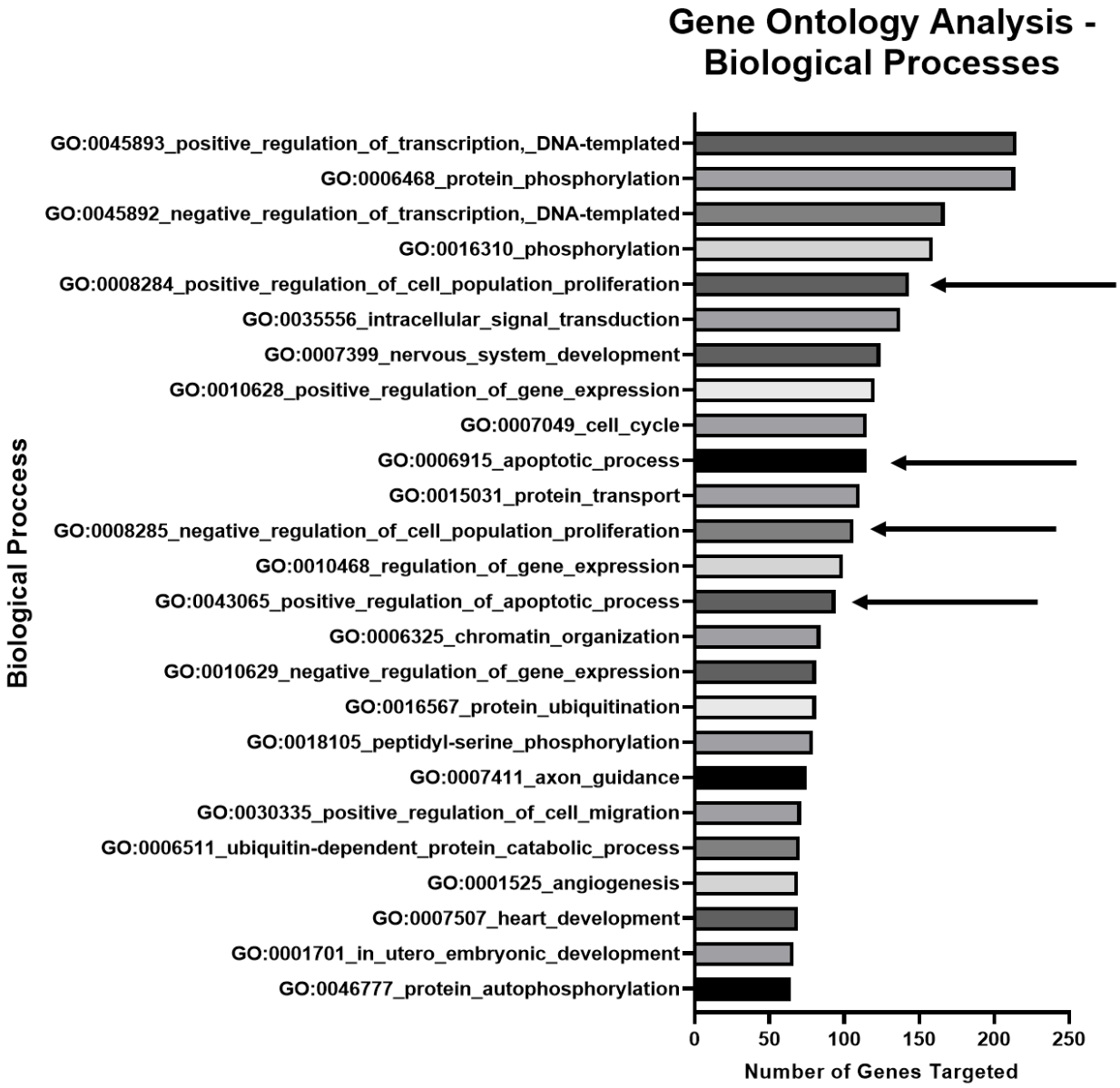

Fig 3.16 Gene set enrichment analysis for the biological processes of the genes targeted by the sEV miRNAs. *Gene Ontology of the top 25 biological processes targeted by Day 5 sEV miRNAs. Processes regulating proliferation and apoptosis (highlighted) amongst those most targeted.*

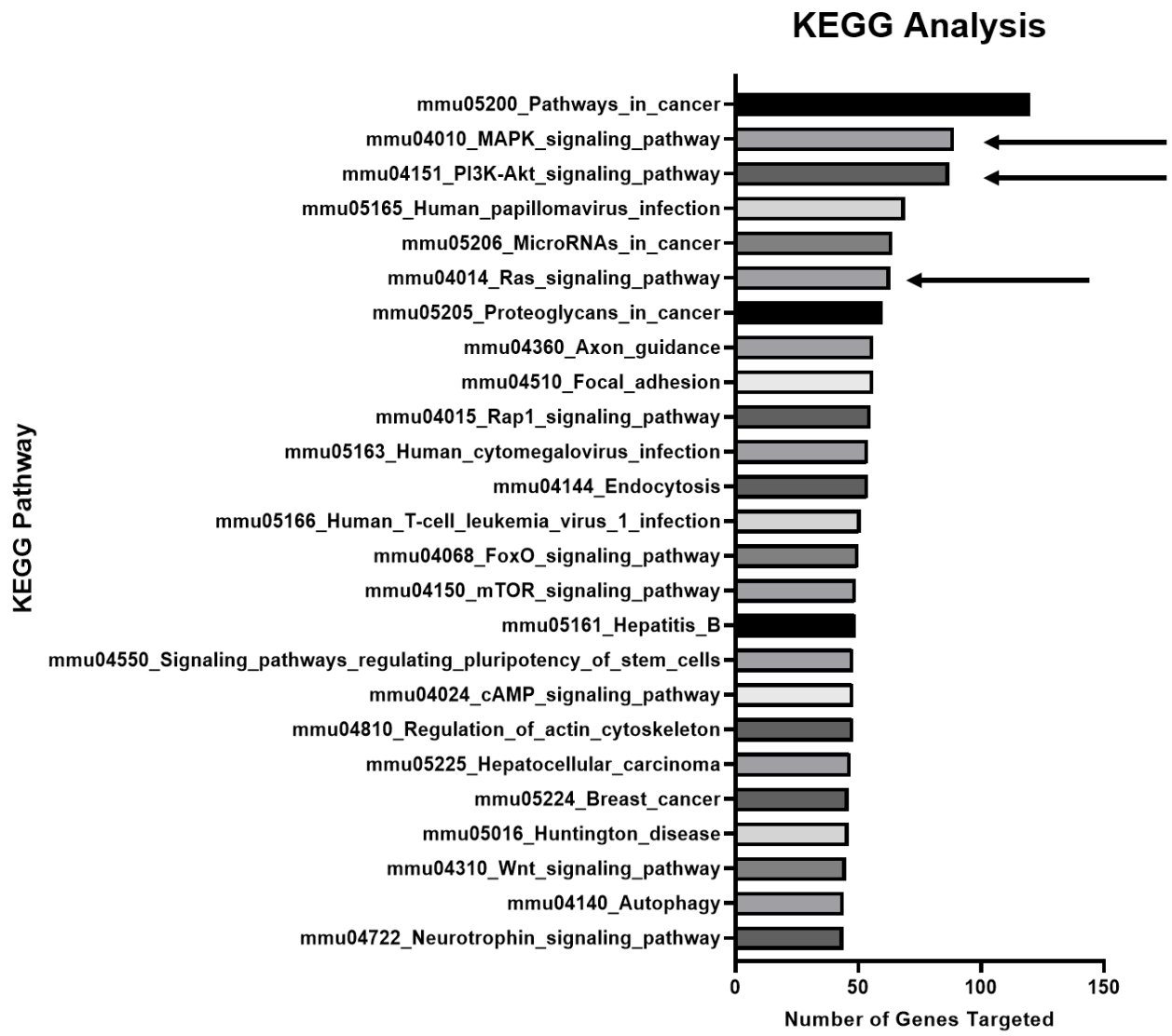

Fig 3.17 KEGG analysis of signaling pathways targeted by sEV miRNAs. *Top 25 pathways targeted by the miRNAs. MAPK, PI3K-Akt and Ras signaling amongst pathways most influenced by sEV miRNAs.*

In **Fig 3.16** the Gene Ontology analysis showed genes involved in cell proliferation, both pro-proliferative and anti-proliferative, were amongst those most targeted by the miRNAs in the sEVs. This suggested a role in modulating cell growth for sEVs. The miRNAs also targeted the processes of DNA transcription, phosphorylation and ubiquitination in the cell. Phosphorylation is often used to activate and deactivate proteins such as cell receptors and enzymes. Having these in an active or inactive state can often dictate the signal transduction of entire pathways which influence cell behaviour (Ardito *et al.*, 2017). Ubiquitination is a post translational modification often

used by the cell to mark a protein for degradation (Tai and Schuman, 2008). The fact sEVs consistently carried these miRNAs which target, and thereby inhibit, these processes suggested they play a role in maintaining cell stasis and viability throughout the fed-batch. Perhaps of greatest interest is that they targeted genes involved in the cell cycle, apoptosis, promoting apoptosis and autophagy. This further hints at a role in maintaining culture viability by preventing the expression of genes which promote cell death. The KEGG analysis also showed how the sEVs are used to maintain cell state by the miRNAs targeting and inhibiting genes involved in MAPK, PI3K-Akt and Ras signaling. All of these pathways modulate cell proliferation and cell death (Wei and Liu, 2002; Ryan and Corcoran, 2018; Shi *et al.*, 2019).

3.2.6 Depleting sEVs from fed-batch process

Given that the miRNAs were predicted to target genes which modulate cell growth, viability and how cells utilise their intracellular cargo, it raised the question as to how the cells may react when sEVs quantities are below their normal concentrations in a cell culture environment. To investigate this, a CHO-A fed-batch set up in cultiflasks (10ml volume) as shown in **Fig 3.18** where EVs were depleted from media at Day 8 in fed-batch by UC:

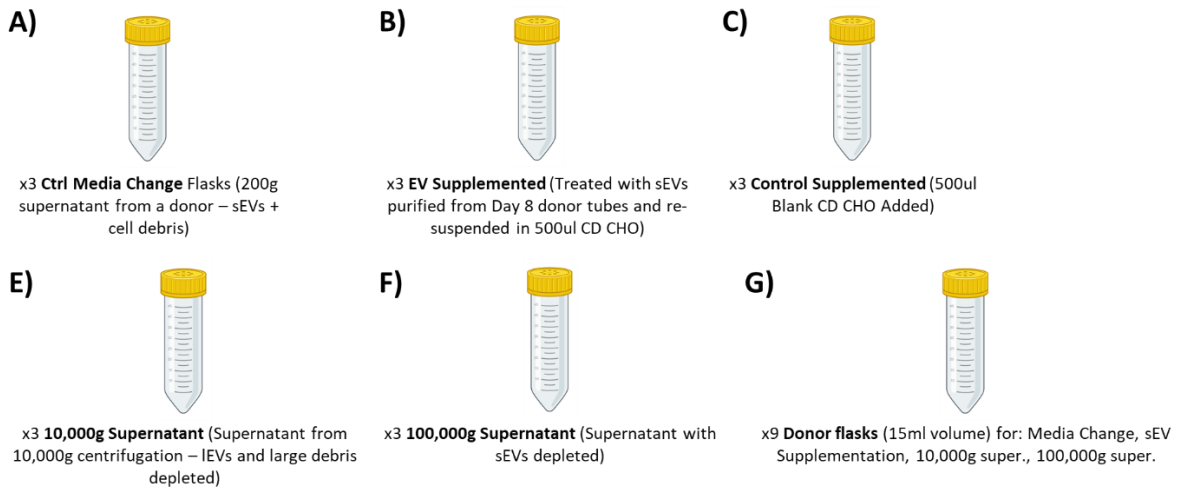

Fig 3.18 Design of EV Depletion Experiment: *Fed-batch was carried out in cultiflasks. All manipulations carried out on Day 8 of fed-batch. All donor flasks and treatment flasks were grown in*

the same fed-batch. Donor flasks were grown in 15ml volume to account for potential loss of volume during centrifugations and filtrations. Treatment flasks grown in 10ml culture volume. (A) Control flasks where cells were centrifuged at 200g and re-suspended in own media. (B) Control flasks where the cells were centrifuged at 200g and re-suspended in media from a donor culture. (C) Flasks supplemented with sEVs re-suspended in 500µl fresh CD-CHO. sEVs taken from donor flasks where sEVs were purified to generate 100,000g supernatant. Cells were not centrifuged and re-suspended in these flasks. (D) Control flasks where 500µl fresh blank CD-CHO was added on Day 8. Cells were not centrifuged and re-suspended in these flasks. (E) Flasks where cells were centrifuged at 200g and re-suspended in supernatant centrifuged at 10,000g to remove lEVs and large cellular debris. The supernatant was 0.22µm PES filtered post centrifugation to sterilise. (F) Cells centrifuged at 200g and re-suspended in media centrifuged at 100,000g to remove sEVs. This was also 0.22µm PES filtered to sterilise prior to re-suspension of cells.

The cells were grown to peak VCD as it was thought that any detrimental or beneficial impacts of altering sEV abundance in the culture would be most evident at this stage. This is where nutrients have been depleted significantly and there is a sizeable accumulation of cellular debris and metabolites. Therefore, any change in the cell stasis would be immediately evident as the cells have fewer resources to recover than they would have in exponential growth where nutrient concentration is high and there is less harmful metabolite accumulation.

At peak VCD (Day 8), the donor flasks were harvested and the supernatants purified as described in **Fig 3.18**. The effect on VCD and viability post Day 8 manipulation was then measured by Vi-Cell. Flasks were sampled until average viability dropped below 70%.

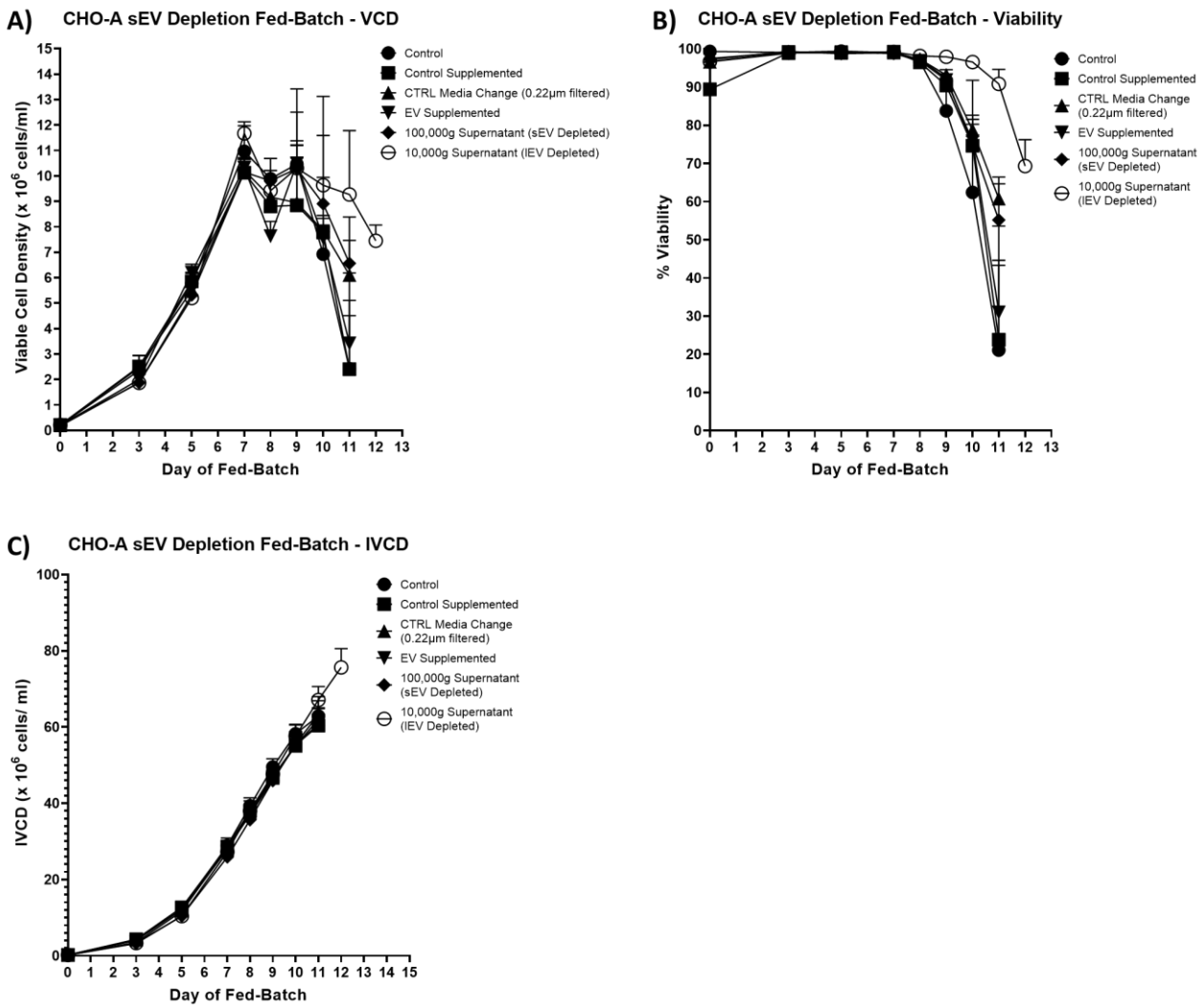

Fig 3.19 EV Depletion Fed-Batch showed 10,000g supernatant flasks had extended viability. *(A) VCD of fed-batch. (B) Viability of fed-batch. (C) Integral Viable Cell Density (IVCD) of flasks in fed-batch. Three replicates per condition. Error bars are standard deviation. All manipulations performed on Day 8. Control flasks had cells centrifuged at 200g and re-suspended in own media. CTRL Media Change (0.22µm filtered) were flasks where the cells were centrifuged at 200g and re-suspended in media from a donor culture. EV Supplemented had sEVs isolated from flasks used to generate 100,000g supernatant re-suspended in 500µl fresh CD-CHO. Cells were not centrifuged and re-suspended in these flasks. Control Supplemented were flasks where 500µl fresh blank CD-CHO was added. Cells were not centrifuged and re-suspended in these flasks. 10,000g Supernatant were flasks which had cells pelleted and re-suspended 10,000g supernatant (lEV depleted media) taken from donor flasks. 100,000g flasks had cells pelleted at 200g and re-suspended in 100,000g supernatant (lEV and sEV depleted media).*

Post treatment of flasks on Day 8 it appeared the flasks had entered stationary phase. There was a gradual decline in VCD until to Day 10. After this, the VCD fell steeply for

all flasks except those re-suspended in 10,000g supernatant. This was also reflected in the culture viability where it started to decline from Day 9 onwards except for 10,000g supernatant flasks which remained constant until Day 10. Even when in decline, the 10,000g supernatant flasks maintained viability above 90% until Day 11. These flasks also remained above 70% viability a full day longer than any other set of flasks. This was in contrast to the other flasks where both VCD and viability fell sharply from Day 9 onwards. The next best performing flasks were where the media change was performed and those that were re-suspended in 100,000g supernatant on Day 8. However, by Day 11 both of these flasks had dropped to below 60% and were far lower in VCD than 10,000g supernatant flasks. The control flasks, control supplemented and EV supplemented were all the worst performing with VCD and viability falling sharply from Day 9 onwards.

To confirm these observations were not unique to a single fed-batch, a second cultiflask fed-batch was set up. This was set up in the same way as shown in **Fig 3.18**. However, the manipulations were performed on Day 7 rather than Day 8. This was because it was noted that the VCD fell on Day 8 and viability had also began falling for some of the flasks on Day 8. While this may have occurred due to some of the flasks being centrifuged and re-suspended, in itself a harsh process on the cells, it may also have been that the fed-batch had already peaked on Day 7 and some of the flasks were already well into stationary phase. If the cells were already in mid stationary phase, this may have contributed to viable cell densities and viabilities witnessed.

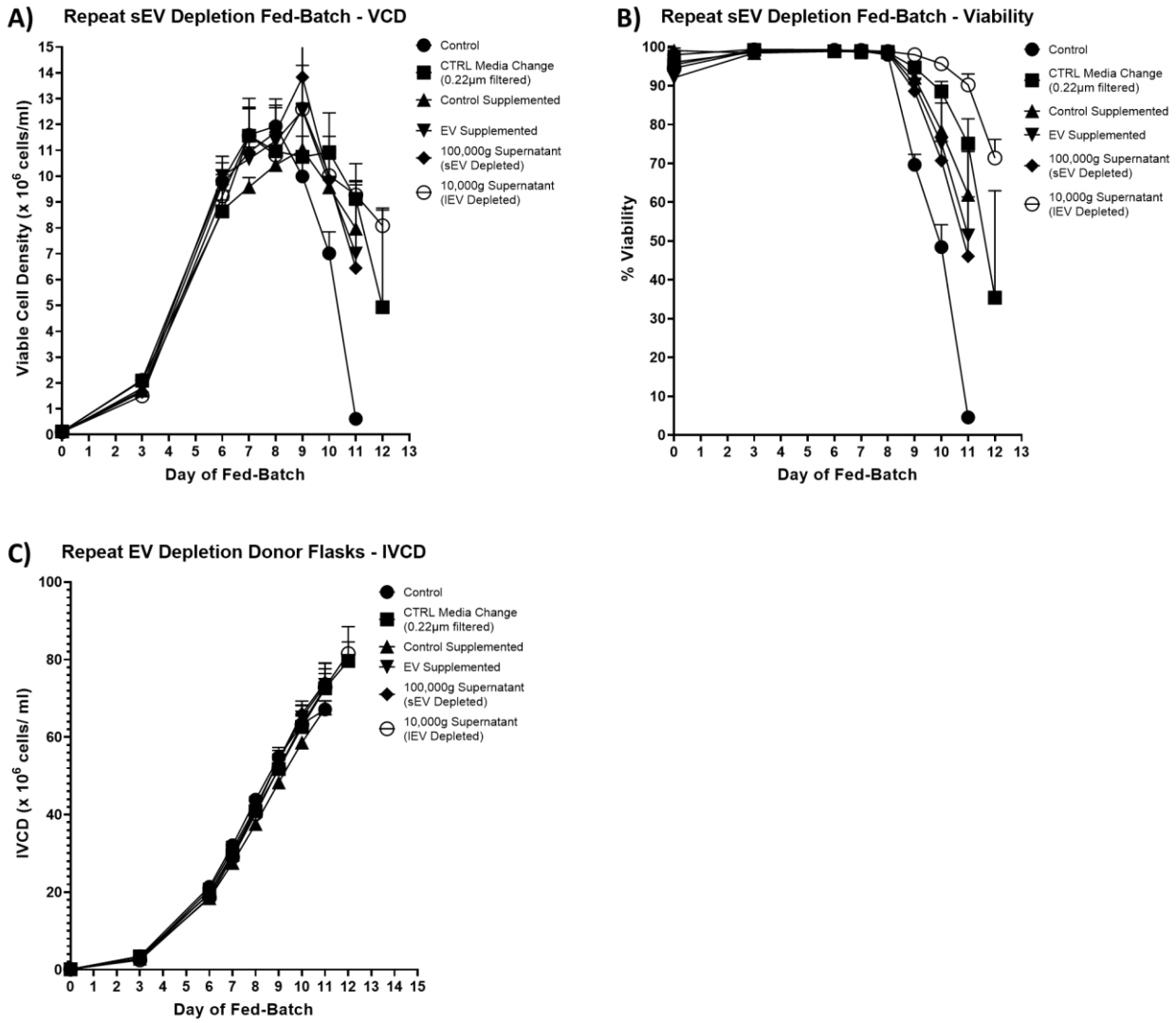

Fig 3.20 Repeat of EV Depletion Fed-Batch showed the same pattern. *(A) VCD of fed-batch. (B) Viability of fed-batch. (C) IVCD of flasks in fed-batch. Three replicates per condition. Error bars are standard deviation. All manipulations performed on Day 7. Control flasks had cells centrifuged at 200g and re-suspended in own media. CTRL Media Change (0.22µm filtered) were flasks where the cells were centrifuged at 200g and re-suspended in media from a donor culture. EV Supplemented had sEVs isolated from flasks used to generate 100,000g supernatant re-suspended in 500µl fresh CD-CHO. Cells were not centrifuged and re-suspended in these flasks. Control Supplemented were flasks where 500µl fresh blank CD-CHO was added. Cells were not centrifuged and re-suspended in these flasks. 10,000g Supernatant were flasks which had cells pelleted and re-suspended 10,000g supernatant (lEV depleted media) taken from donor flasks. 100,000g flasks had cells pelleted at 200g and re-suspended in 100,000g supernatant (lEV and sEV depleted media).*

A repeat of the fed-batch showed a very similar pattern to the first. It appeared that the centrifugations and treatments performed on Day 7 had less initial impact than those

witnessed in the first fed-batch. VCD increased slightly on Day 8 and some of the flasks only reached peak VCD on Day 9. However, again the 10,000g supernatant maintained a high VCD for the longest duration; albeit with a sharper decline from peak VCD than the first fed-batch. Viability was consistent with the first fed-batch with it being greater than 90% until Day 11. The next best performing flasks were the media change flasks. The viability of both the 10,000g supernatant and media change flasks stayed above 70% until Day 12. Interestingly the control flasks, control supplemented, EV supplemented and 100,000g supernatant flasks again had viability below 70% by Day 11 and had a sharp decrease in VCD post Day 9. Based on the two fed-batches, depleting lEVs and large cellular debris extends the duration of the culture. However, further depletion of the sEVs in the culture largely reduced this effect; suggesting that the sEVs are necessary for maintaining the viability of the culture. While the 100,000g supernatant flasks outperform the control flasks, they have comparable performance to the control supplemented and EV supplemented. Given that the control supplemented and EV supplemented flasks had similar viable cell densities and viabilities, supplementing cultures with additional EVs did not extend culture length.

3.3 Discussion

It is clear that both sEVs and lEVs accumulate in the culture environment as the VCD increases up to peak VCD. After this point, there is only a slight increase in the rate of sEV secretion. The fact that there were more sEVs/ cell in early stationary phase of fed-batch than in exponential phase suggests the cells either increase sEV secretion or decrease sEV uptake as fed-batch progresses. This increase in sEVs/ cell coincides with a general decrease in qP after Day 5 of fed-batch; suggesting the number of sEVs/ cell is negatively correlated with qP.

The increase in sEVs/ cell at early stationary phase and late stationary/ early death phase may be in response to the culture environment becoming harsher for the cell. There is evidence that cells increase EV production in response to stress stimuli (Atienzar-Aroca *et al.*, 2016; Harmati *et al.*, 2019; Vulpis *et al.*, 2019). It was notable in the case of sEVs that there is less of an increase in the number of sEVs/ cell from Day 9 to Day 12 as there was from Day 5 to Day 9. The additional sEVs/cell measured

on Day 12 may well be co-isolated cellular debris due to higher cell death rather than sEVs. This is somewhat in agreement with what Belliveau and Papoutsakis (2022) observed in that sEV accumulation plateaus after peak VCD is achieved. However, they also see a plateau to in lEVs whereas the CHO-A fed-batch in this study had a dramatic increase in lEVs at late stationary phase. This again is could be due to increased amount of cell death in the CHO-A fed-batch on Day 12. As the western blots for HSP90B1 demonstrated, non-EV material can co-isolate in this fraction and there may be several intracellular components detectable by NTA that pellet at 10,000g at late stationary phase.

The protein content of EV samples from different stages in fed-batch gave a further indication of cellular debris co-isolating with sEVs as fed-batch progresses. Particularly in late stationary/ early death phase, the dramatic increase in protein content for the 2,000g, 10,000g and 100,000g pellets on this day highlighted that there was a lot more cellular debris present at this time-point; most likely due to elevated cell death. Despite the dramatic increase in accumulation of protein in the 2,000g and 10,000g fraction on Day 12, purification by UC meant that the sEV count was only slightly impacted by the additional debris. None the less, there was a marked decrease in the particle : protein ratio as the fed-batch progressed. This, in combination with the western blot for TSG101 and TEM images, indicates that sEV purity diminishes at later stages of fed-batch.

The lEVs perhaps display a limitation of the particle : protein ratio as a measure of EV purity. If one was to look at the particle : protein ratio for lEVs, it would be easy to conclude that the increased particle count is proportional to the increase in protein. Yet this does not necessarily equate to an increase in lEV abundance. When band intensity for lEV CD63 on Day 12 was compared to Day 5 and Day 9, it was far more variable on Day 12. Therefore, while there may be elevated lEV concentration at late stage fed-batch, the non-EV specific count provided by NTA cannot be considered reliable. It is difficult to ascertain from these analyses what proportion of the content pelleted at 10,000g on Day 12 is actually lEVs.

The particle : protein ratio identified Day 5 (exponential growth) as the ideal time-point for harvesting EV material from a CHO fed-batch. Not only have the particles less co-isolated protein than at later stages but a high concentration of EVs can be obtained.

The cells the EVs are derived from are in a highly viable state with minimal stress relative to later stages in fed-batch. This should reduce the potential for variability in terms of EV composition. There is also the consideration that a fed-batch requiring only 5 days of growth enables quicker generation of EV stocks than waiting until later phases.

The bioanalyser analysis showed that the majority of sEV RNA was small RNA fewer than 200 nucleotides in size. Small RNA-seq analysis identified several miRNAs, however, only a small fraction of these miRNA make up the majority of the miRNAs present. Surveying literature describing these miRNAs suggests they largely have a role in modulating cell proliferation. There were as many pro-proliferative as growth inhibitory miRNAs so it is difficult to assess whether CHO cells utilise these sEV to promote growth as culture progresses or arrest it. One function which they are likely to perform is inhibition of apoptosis. This is in agreement with what Han and Rhee (2018) and Busch *et al.* (2022) who found that sEVs had anti-apoptotic miRNA and were able to inhibit apoptosis. However, it is worth mentioning that the miRNA predicted to be anti-apoptotic by Busch *et al.* (2022), miR-196-5p, was not found in this study. However, other miRNAs listed by Busch et al. (2022) as the most abundant such as miR-10b-5p, miR-92a-3p and let-7a-5p were detected. It was noted that the composition of the top 10 miRNAs in their study is different to what was found in the sequencing carried out here. This is could be due to two factors. First is that the cell line they used was engineered in house expressing a different product to the CHO-A cell line. This may result in a different miRNA profile in the sEVs. Alternatively, they used the Illumina TruSeq Stranded Total RNA Library Preparation Prep Gold kit in their sequencing which is different to the Illumina TruSeq Small RNA library Prep Kit used in our study. In small RNA sequencing, the choice of library prep kit can determine what miRNAs are detected and their relative abundance may not be truly represented due to adapter biases towards particular miRNAs (Dard-Dascot *et al.*, 2018). This provides a caveat to the literature survey of the most abundant miRNA detected in this study. It also could impact the DE analysis as a library kit may lack sensitivity to changes in miRNA abundance.

Although it does not account for the quantity of a particular miRNA or the number of times a particular gene is targeted, miRWalk provides a broader analysis of what genes are being targeted by the miRNAs. Furthermore, it enables a prediction as to

what functionality those miRNAs give sEVs by investigating what biological processes and pathways those targeted genes are involved in. It returned similar results to the literature survey in that there was a similar number of pro-proliferation and anti-proliferation genes targeted. The fact that genes involved in processes such as autophagy, apoptosis and the promotion of apoptosis were inhibited by sEV miRNAs is yet further evidence they play a role in preventing cell death. While the KEGG analysis doesn't provide specific information, we can see that the main pathways targeted all have function in modulating cell proliferation and cell death.

Having predicted that the sEVs might affect culture growth and viability, the EV depletion fed-batch was carried out to understand what would happen if the stimuli provided by sEVs was removed mid fed-batch. Alternate approaches were considered such as chemical inhibition of EVB with chemicals such as GW4869 and Manumycin A. However, using these chemicals would have had the potential to also interfere with other cellular processes. For instance, GW4869 is a neutral sphingomyelinase inhibitor which prevents the synthesis of ceramide; a lipid used in a several biological pathways (Essandoh *et al.*, 2015; Datta *et al.*, 2017). Therefore, while total sEV removal could not be assured, it was preferable to deplete the sEV content of the fed-batch using UC than attempt to inhibit EVB.

It was perhaps unsurprising that removing material that could be pelleted at 10,000g from cell culture supernatant would increase the longevity of culture viability; especially at peak viable density/ early stationary phase where cell debris begin to accumulate in large quantities. These debris can stimulate cell death and create an adverse environment for the cell. The process of apoptosis, for instance, can be initiated by extrinsic factors present in the extracellular environment (Henry *et al.*, 2020). By centrifuging the media at 10,000g and subsequently filtering with a 0.22µl filter, some of the debris which may carry these extrinsic factors may have been removed from the cell culture supernatant. Alternatively, it may be the case that lEVs contain stimuli which promote cell death at this stage in the fed-batch and are removed by 10,000g centrifugation. The fact that the control media change flasks outperformed the control flasks was unexpected and suggests that simply using media from a donor culture can extend culture lifespan somewhat. However, this was only evident in the second fed-batch where the control media change flasks were next best performing after the 10,000g supernatant. What was consistent in both fed-batches is that depleting sEVs

by further centrifuging the 10,000g supernatant at 100,000g removed the fed-batch life-span extending effect seen in the 10,000g supernatant flasks. This gives further credence to the hypothesis that the sEVs carry anti-apoptotic miRNAs which have an important function in maintaining CHO cell viability.

A caveat to this study is that there may also be other factors present in the supernatant that are removed at 100,000g which maintain cell viability. Another consideration is that not all sEVs present in the cell culture supernatant may have been depleted by UC. It may only be a particular subclass of sEV which pellets at 100,000g. Yet it is difficult to further ensure smaller or less dense EVs are depleted without also removing other constituents of the cell culture supernatant. The fact that centrifugation at 100,000g does not appear to co-isolate small proteins and particles fewer than 50nm in size from cultures with high viability gives further confidence that sEVs are the major agent depleted from the supernatant in this case.

Given the clear negative effect of removing sEVs from fed-batch, it was expected that supplementing cultures with sEVs might be beneficial to culture viability and extend fed-batch longevity. Yet the flasks supplemented with sEVs had similar growth and viability profiles as those supplemented with 500µl CD-CHO. These sEVs were purified from donor cultures at the same-stage in fed-batch. In theory, this should mean that adding them to the supplemented flasks should double the sEV concentration in these flasks. Yet doing so has no observable effect on the cells. This leads to the conclusion that CHO cells only require a threshold quantity of stimuli from the sEVs and anything beyond this is not beneficial to the stasis of the culture.

Chapter 4

Comparing EV Profiles of Different CHO Cell Lines

4.1 Introduction

The previous chapter discussed how a single producer CHO cell line secreted EVs throughout a fed-batch process and how it utilised the stimuli contained within sEVs to maintain cell viability. However, this raised the question as to whether the EV secretion observed was unique to that cell line or was it consistent amongst different CHO cell lines. It is well established that CHO cell lines vary in their composition and cellular traits. For instance, large variations in miRNA expression, lipid content and proteome are well documented (Johnson *et al.*, 2011; Széliová *et al.*, 2020). While direct comparisons of EVs isolated from different CHO cell lines do not exist in literature, evidence from other cell lines suggests differences in EV profile can occur where cells are either exposed to different culture environments or are genetically differentiated. This is especially true in the case of cancer cell lines which often have altered EV miRNA expression profiles compared to their non-cancerous counterparts (de Paula Silva *et al.*, 2021). It was therefore hypothesised that the EVs derived from different CHO cell lines may also differ substantially in quantity and composition where genetic engineering has occurred.

It is known that EVB can be altered depending on the conditions the cell is exposed to. One example is how the cell culture media (Li *et al.*, 2015; Andrews *et al.*, 2021; Bost *et al.*, 2022). In generating a mAb producing CHO cell line, typical cell line development involves several steps; all of which expose the cell to different external stimuli. This begins with the initial transfection which may alter transcriptional activity within the cell. Then there is selection for a stable producing pool of cells followed by cloning which are both stressful processes to the cell and require it to adapt the new

environments (Noh, Shin and Lee, 2018). Likewise, a clonal mAb producing CHO cell line is selected for its ability to secrete mAb in large quantities. It is unknown to what degree pathways which result in upregulated mAb production impact EV secretion. There are genes in mAb product secretion such as syntaxin 4, SNAP-23, VAMP8 and VAMP2 that are also involved in EV secretion as they enable fusion of the MVB to the plasma membrane (Peng, Abellan and Fussenegger, 2011; Colombo, Raposo and Théry, 2014; Yu *et al.*, 2020). However, to what degree these genes influence overall EV secretion in CHO is unknown. Therefore, it was decided to compare the EV profiles of the producer cell line, CHO-A with a non-producing host CHO cell line, GSKO-Host. Although genetically engineered to have GS knocked out, GSKO-Host had yet to undergo any of the adaptations required in cell line development for producer cell lines.

4.1.1 Chapter Summary

To investigate possible differences in quantity, size and composition, sEVs and lEVs were isolated from CHO-A (producer cell line) and GSKO-Host (a non-producing host cell line). The two cell lines were grown in fed-batch to Day 5 (exponential phase). The quantity and size of the sEVs and lEVs were compared by NTA and the protein content measured by BCA. In addition to this, TEM imaging enabled visual confirmation of quantity and sizing of sEVs. The miRNA composition was compared using small RNA-seq to see if there was variation in the miRNA content of sEVs from a producer cell line vs a non-producer. As a further layer to this analysis, the miRNA content of the sEVs in the GSKO-Host were compared to the intracellular miRNA content of the GSKO-Host. This was to establish if certain miRNAs were differentially expressed in sEVs relative to those found within the cell. Lastly, the lipidome of the sEVs from both cell lines was compared by mass spectrometry. This examined if sEVs were consistently abundant in certain lipids; similar to other cell lines' EVs. Based on the reports of the lipid content of CHO cells found in literature, it was also possible to estimate which lipids were enriched in sEVs relative to the cell itself.

4.1.2 Chapter Aims

The following were the aims of this chapter:

- Compare the quantity and size of the lEVs and sEVs from each cell line

- Compare the protein content of the lEVs and sEVs to compare the purity of EV samples from each cell line

- Characterise the miRNA content of sEVs from both cell lines and compare miRNAs to relative abundance of miRNAs found inside the cell

- Characterise the lipodomic content of sEVs from each cell line and compare to lipid content of sEVs from other cell lines.

4.2 Results

4.2.1 Fed-batch of CHO-A and GSKO-Host cell lines

To compare the EV profiles of the CHO-A and GSKO-Host cells, both cell lines were grown in fed-batch in E1000 erlenmeyer shake flasks with a culture volume of 160ml. It was elected that both cell lines should be grown in the same fed-batch rather than compare to previous CHO-A fed-batches. This was to eliminate possible differences due to batch-to-batch variation, differences in UC purification volumes and ensure consistent sample handling prior to small RNA-seq isolation and analysis. The fed-batch was grown until Day 5, at which point the flasks were harvested.

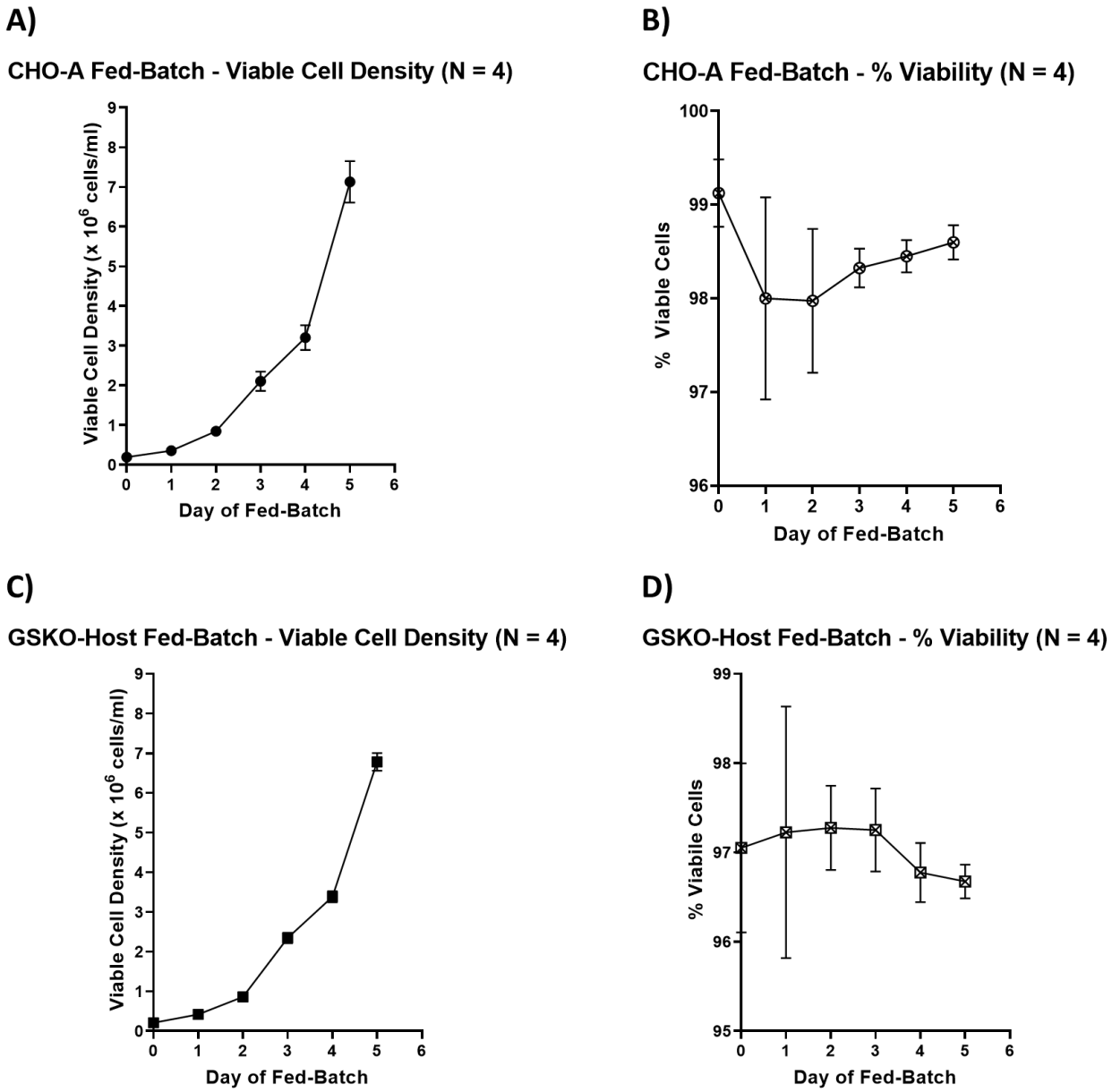

Fig 4.1 Both cell lines grown until Day 5 (exponential growth). *(A) VCD of CHO-A fed-batch. (B) Percentage of viable cells in CHO-A fed-batch. (C) VCD of GSKO-Host fed-batch. (D) Percentage Viable cells of GSKO-Host fed-batch. All error bars are standard deviation. Four replicates were grown until Day 5.*

For NTA, BCA, TEM, small RNA-seq and lipidomic analysis, 100ml of cell culture supernatant was purified by UC per biological replicate. The resulting 10,000g pellets were re-suspended in 200µl 1X PBS and x4 50µl aliquots made. The 100,000g pellets were re-suspended in 600µl 1X PBS. To further enhance purity and to ensure sEV

sterility, the sEVs were put through a 0.22µm filter in a biological safety cabinet and x12 50µl aliquots made. These were stored at -80°C prior to analysis.

4.2.2 Western Blot of GSKO-Host EVs

To confirm GSKO EVs had the same protein markers present as CHO-A EVs, western blots were performed for Alix, CD63 and TSG101 as seen in **Fig 4.2**. 30ml of cell culture supernatant was purified and pellets re-suspended in RIPA with proteinase inhibitor.

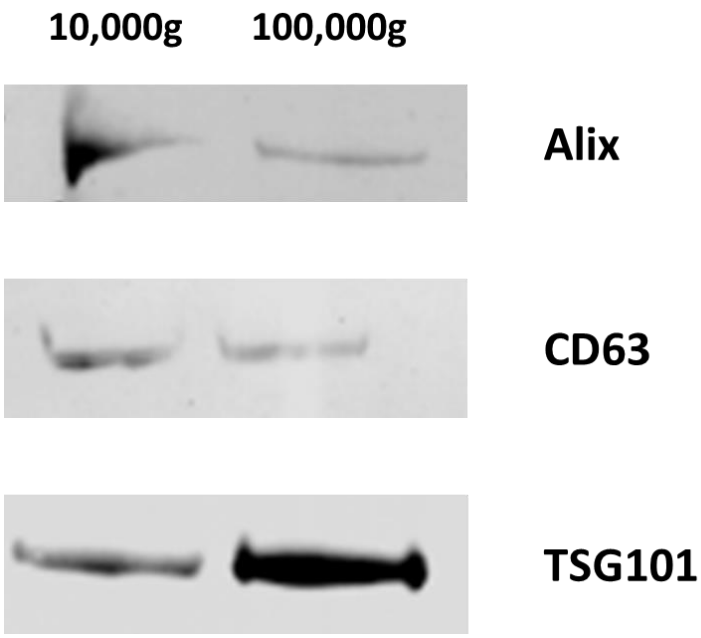

Fig 4.2 EV markers were detected for GSKO-Host EVs. *Western blots for EV markers in GSKO EVs in 10,000g pellet (lEVs) and 100,000g pellet (sEVs). All EV samples are from Day 5 GSKO-Host sEV fed-batch.*

The blots showed that EV protein markers were also present in EVs isolated by UC from the GSKO-Host cell line.

4.2.3 lEV and sEV Particle counts from CHO-A and GSKO-Host fed-batch

Both lEVs and sEVs were counted by NTA to measure EV abundance in the cell culture supernatant. The number of EVs/ cell was then calculated to compare EV secretion between the cell lines.

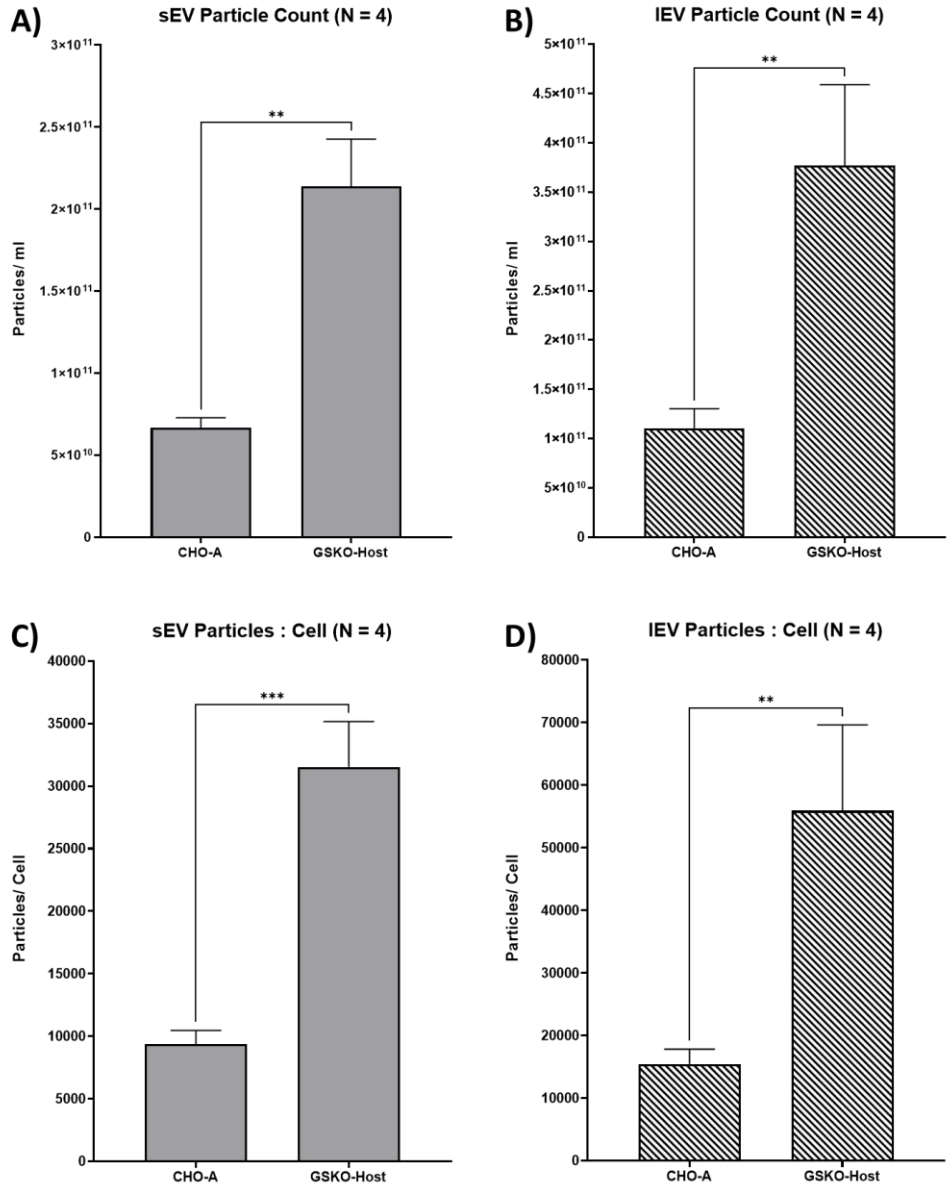

Fig 4.3 NTA Analysis revealed that the GSKO-Host cell line had significantly higher quantities of sEVs and lEVs per cell than CHO-A. *NTA measurement of (A) sEV abundance on Day 5 and (B) lEV abundance on Day 5. (C) The number of sEVs/ cell generated by dividing the total number of sEVs purified on Day 5 of fed-batch from each cell line by the total number of cells on Day 5. (D) the number of lEVs/ cell generated by dividing the total number of sEVs purified on Day 5 of fed-batch from each*

cell line by the total number of cells on Day 5. All error bars are standard deviation. Four replicates per sample. Statistical comparison test is independent two tailed t-test.

NTA analysis showed that for both lEVs and sEVs, there was a significant difference in the quantities secreted between the cell lines. The GSKO-Host had approximately 3-times more lEVs/ cell and sEVs/ cell than CHO-A. This suggested that EVB overall was upregulated in the GSKO-Host cell line rather than a specific subclass of EV. NTA also enabled comparison of the sizes of the EVs secreted which showed little difference (see **Fig 4.4**).

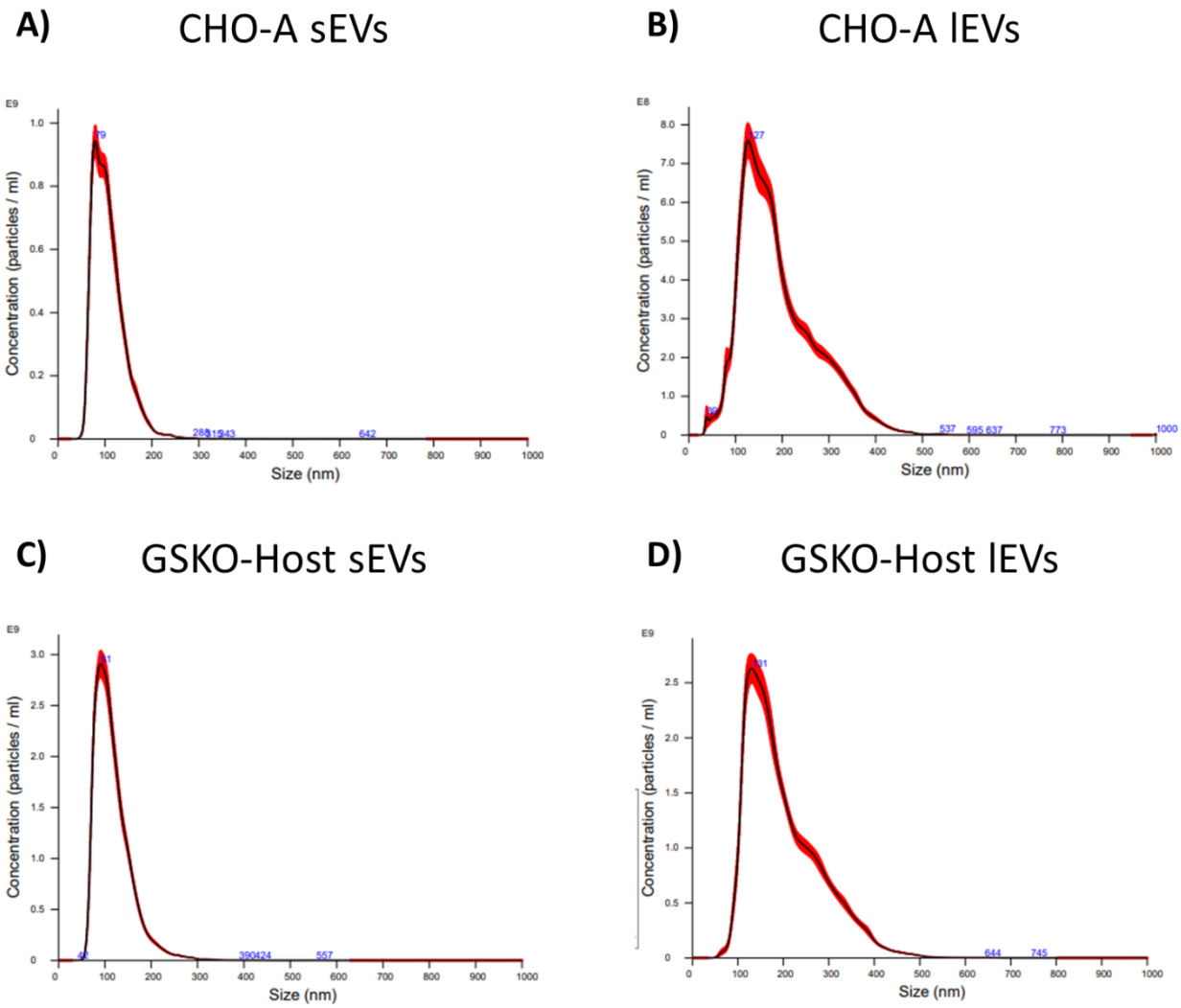

Fig 4.4 EV particle size was broadly similar between both cell lines. *NTA analysis of the size of particles for (A) CHO-A sEVs, (B) CHO-A lEVs, (C) GSKO-Host sEVs and (D) GSKO-Host lEVs from Day 5 fed-batch.*

4.2.4 BCA and TEM Analysis

Whilst NTA had measured significantly more particles of EV size range in the GSKO-Host, it was not known whether the EV samples from each cell line were of equal purity. There was the possibility that the GSKO-Host simply shed more cellular debris which could potentially contribute to the higher particle count observed in the NTA analysis. Two approaches were taken to determine if this was the case. The first was quantitative with the use of BCA analysis to compare the particle : protein ratio of the two cell lines. If the ratio was similar between the cell lines or, if the GSKO-Host EVs had a higher number of particles per µg of protein, then this would indicate that the NTA measurement was quantifying mostly EV abundance. A lower number of particles per µg of protein would be indicative of non-EV co-isolates in the sample (Webber and Clayton, 2013). The second analysis was qualitative using TEM of the sEV pellets. This would not only enable visual quantification of the differences in abundance, but also enable identification of non-sEV particles.

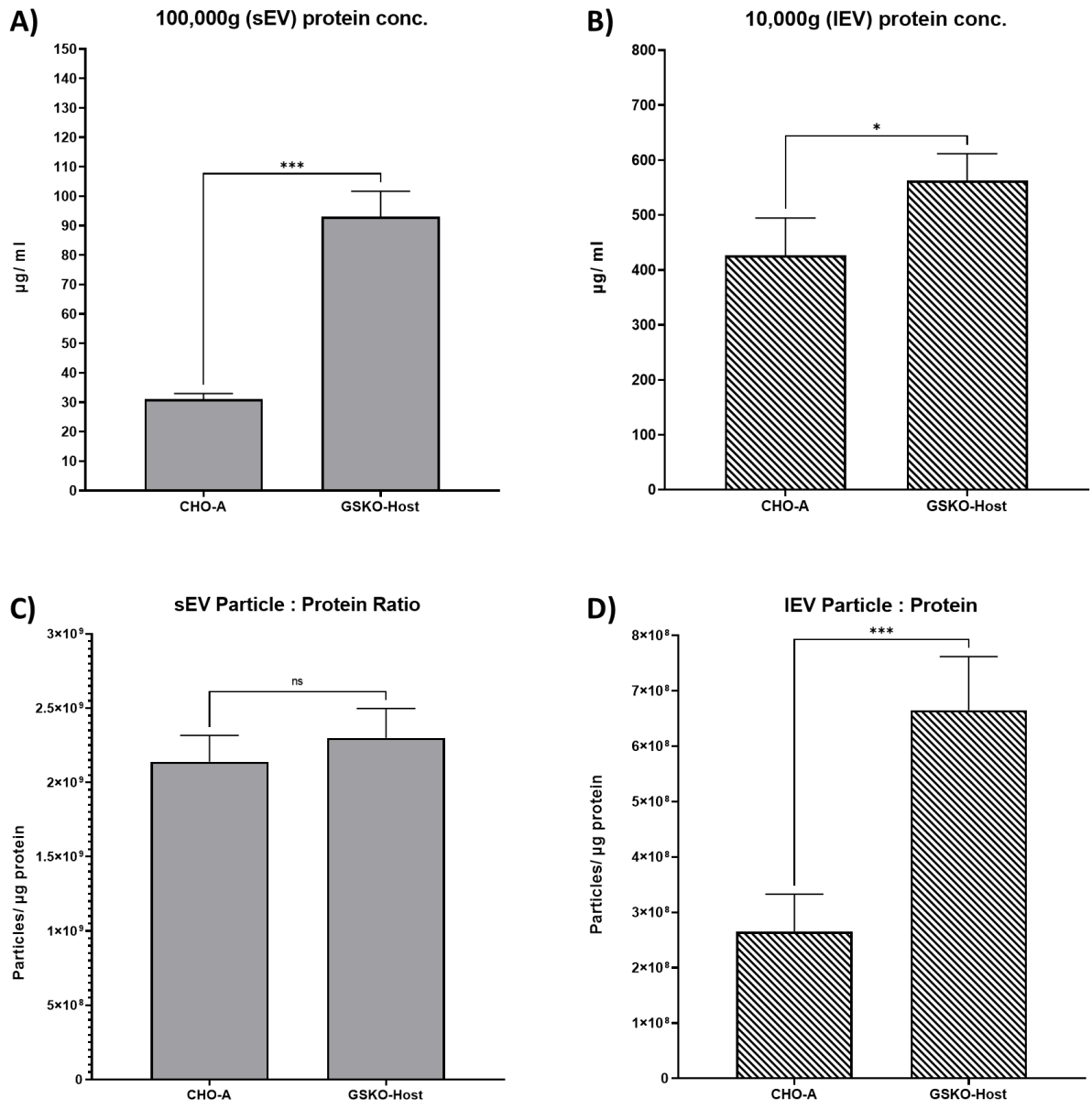

Fig 4.5 BCA Analysis showed that the sEV ratio of particles : protein were equivalent for both cell lines but there was a significant difference in the lEV ratio. *Protein content of (A) sEVs and (B) lEVs. The number of particles per µg of protein was compared for (C) sEVs and (D) lEVs. All samples isolated from Day 5 fed-batch. Four replicates per sample. All error bars are standard deviation. Statistical comparison is independent two-tailed t-test.*

The increase in sEV particle count had the same proportional increase in sEV protein concentration for both cell lines. This gave confidence that the increase in NTA particle count was due to an increase in sEV abundance rather than an increase in non-EV cell debris. For lEVs, there was significantly fewer particles per µg of protein in the CHO-A cell line. As was seen in Chapter 3, this does not necessarily correlate with

lEV purity as UC is not optimal for purifying lEVs. Yet the fact that the GSKO-Host was also shedding greater numbers lEV sized particles per µg of protein, the quantity of which had a proportional increase similar to the sEVs, did strongly suggest that lEV secretion was also upregulated in the GSKO-Host.

TEM provided additional verification that there was an increase in sEV abundance. The images in **Fig 4.6** clearly showed sEVs enriched in both samples with a greater quantity apparent in the GSKO-Host sEV sample.

A)

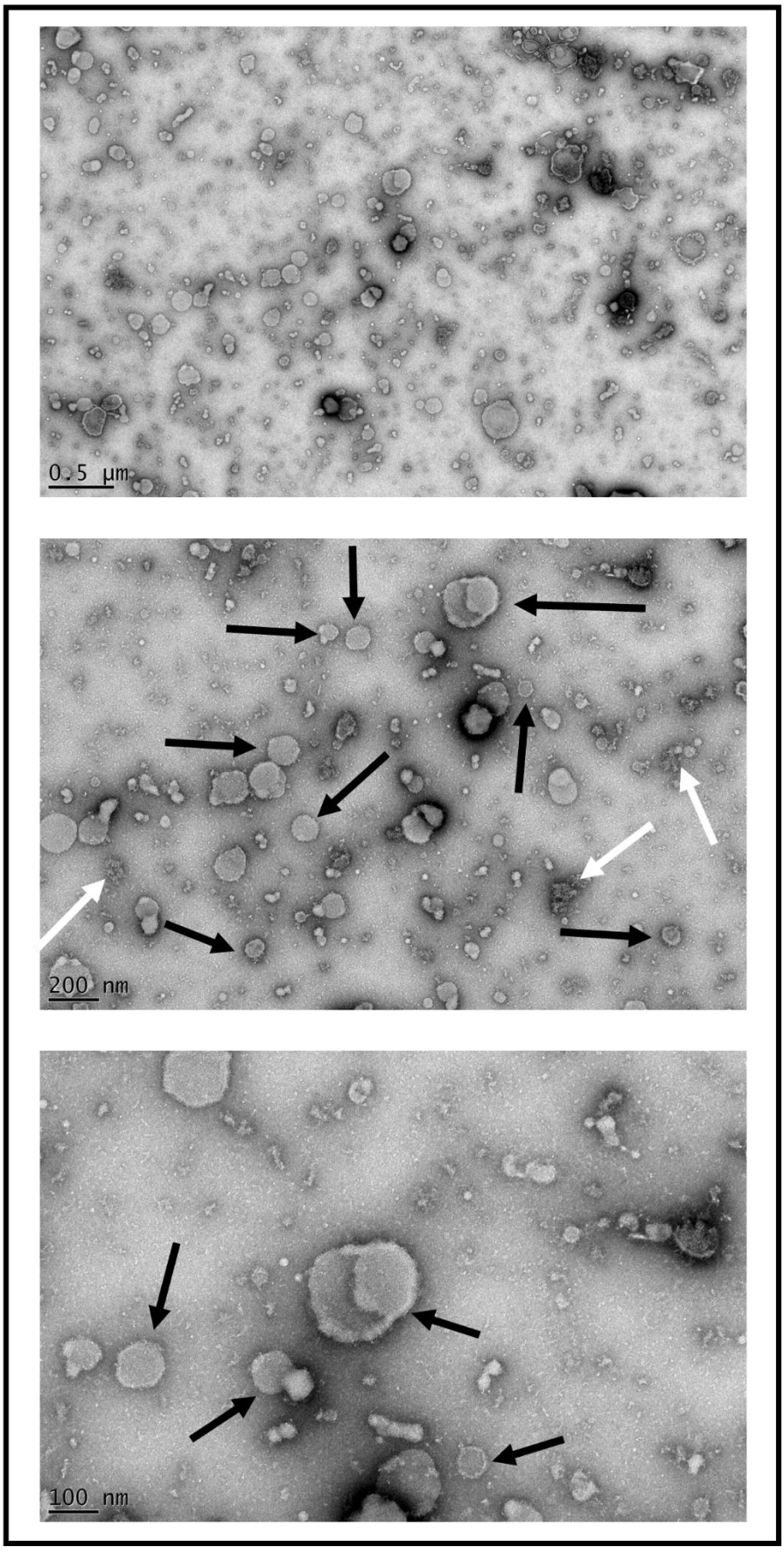

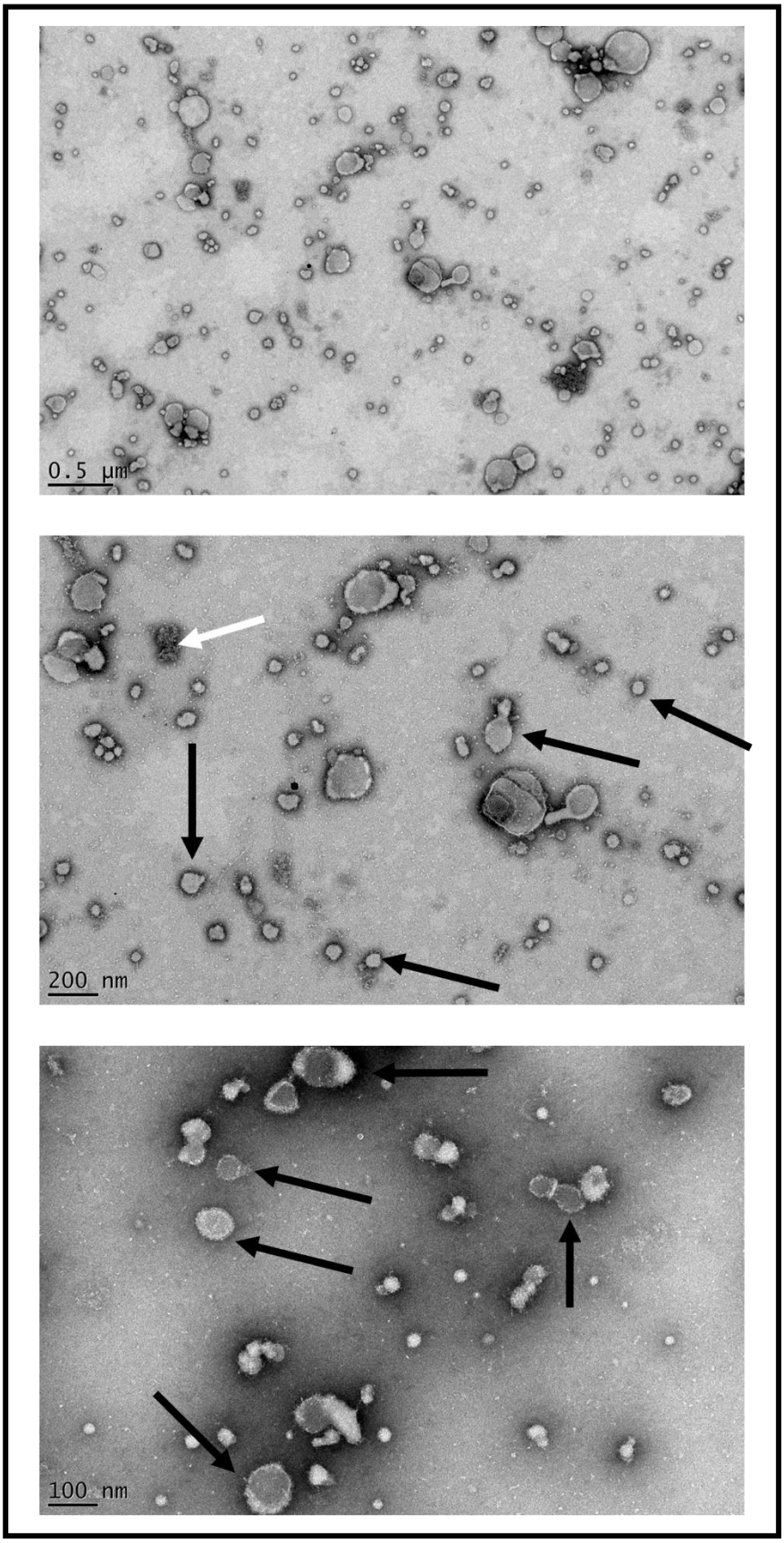

Fig 4.6 TEM analysis showed Day 5 sEV samples from both cell lines were equivalent in purity and the GSKO-Host sEV sample was visibly denser than CHO-A. *TEM images of (A) GSKO-Host*

sEVs at 0.5µm, 200nm and 100nm magnification. (B) CHO-A sEVs with at 0.5µm, 200nm and 100nm magnification. A sample of EVs are highlighted (black arrows) along with protein aggregates (white arrows).

The sEVs were distinctively visible from their “cupped-shape”/ pressed button morphology. The sEVs appeared as this shape due to the fixation and adsorption processes prior to analysis by the electron microscope (Rikkert *et al.*, 2019). The most common diameter was ~100nm which is similar to the size measured by NTA, however, it was noted that there were EVs of sizes closer to 200nm which suggested that some lEVs had co-isolated with the sEVs. Visual inspection of **Fig 4.6** (A) and (B) clearly showed that sEV sample from the GSKO-Host was denser than CHO-A. The TEM images from both samples also had relatively similar proportions of non-EV particles. This agreed with the findings from the NTA and BCA analysis.

4.2.5 Comparison of sEV miRNA content

With it established that the GSKO-Host had elevated EV secretion, a comparison of the RNA content from sEVs of both cell lines was carried out to see if there were differences in sEV nucleic acid composition. The sEV RNA content of the 4 biological replicates from each cell line were extracted with the same protocol used in 3.2.4. The GSKO-Host sEVs replicates were diluted to 200µl in sterile 1X PBS prior to extraction whilst x4 50µl aliquots of each replicate of CHO-A sEVs were pooled to obtain approximately equivalent amounts of RNA. Once the RNA had been isolated, it was sent for quantification and sizing on the Agilent Bioanalyser.

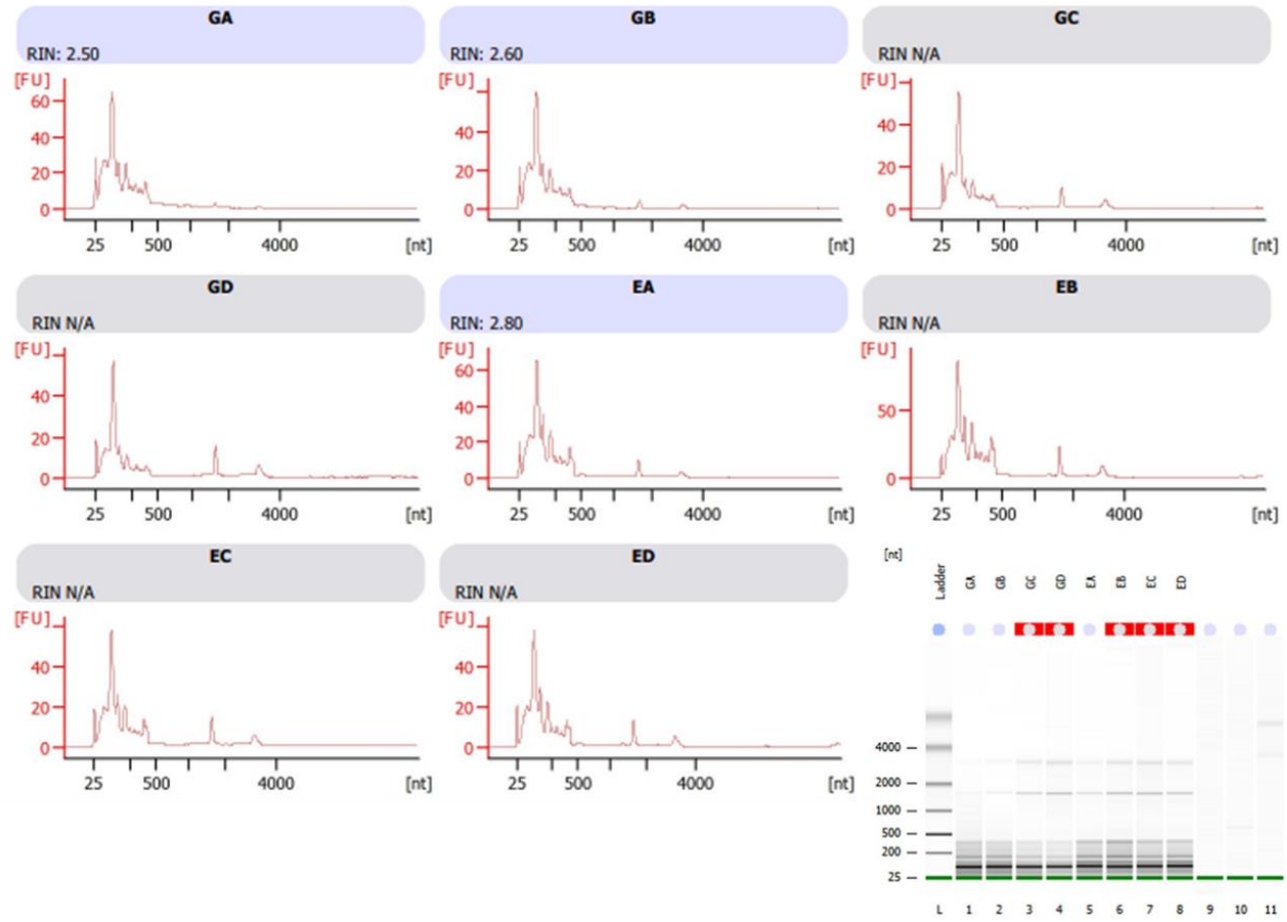

Fig 4.7 Bioanalyser Analysis showed sEVs from both cell lines contained mostly small RNA fewer than 200 nt in size. *Bioanalyser measurement of sEV samples. GA = GSKO-Host replicate A, GB = GSKO-Host replicate B, GC = GSKO-Host replicate C, GD = GSKO-Host replicate D, EA = CHO-A replicate A, EB = CHO-A replicate B, EC = CHO-A replicate C, ED = CHO-A replicate D.*

The majority of the RNA in both cell lines' sEVs was small RNA less than 200 nucleotides in size and was consistent with what was observed in 3.2.4. This was sent to Genewiz for small RNA-sequencing. RNA was also isolated from cells pelleted in the GSKO-Host fed-batch on Day 5. As previously stated, this was an additional analysis to determine if there were miRNAs which were selectively enriched in sEVs relative to the intracellular miRNA content.

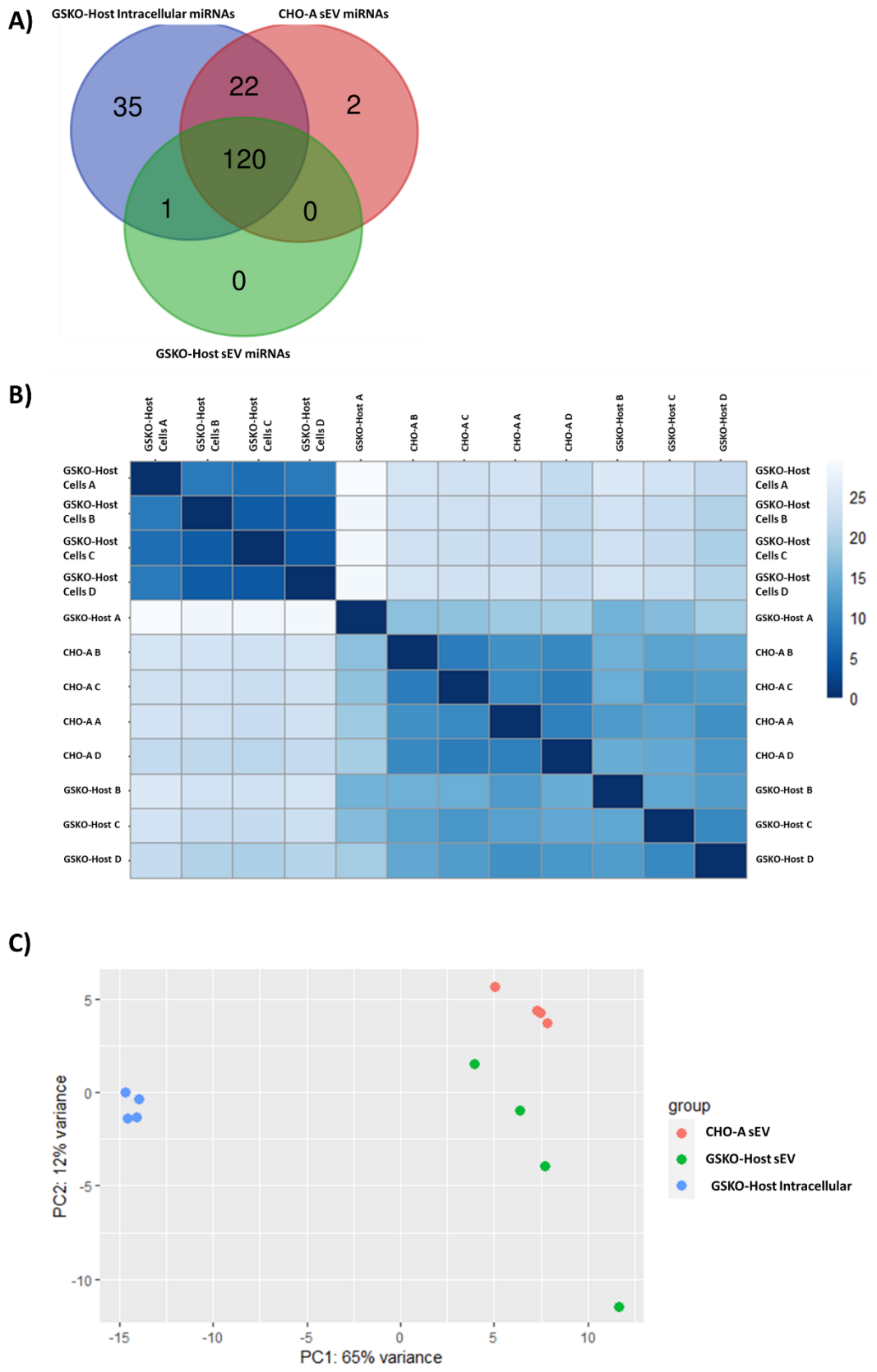

Fig 4.8 Small RNA-seq revealed that majority of miRNAs detected were present in both sets of sEVs and in equivalent quantities. *(A) Overlap of miRNAs identified in GSKO-Host Intracellular*

miRNAs, CHO-A sEVs and GSKO-Host sEVs. (B) Heatmap of the variation in expression between samples. (C) Principal component analysis of the replicates for each sample type.

The vast majority of miRNAs identified in CHO-A sEVs were also present in the GSKO-Host sEVs. Surprisingly, 22 of the 24 miRNAs present in CHO-A sEVs, but not present in GSKO-Host sEVs, were also found in the GSKO-Host intracellular miRNA composition. In **Fig 4.8** (B) that the expression levels of miRNAs were most similar in the sEVs from the two cell lines. There was similar expression variance between the GSKO-Host intracellular miRNAs and the miRNAs in the sEVs of both cell lines. The principal component analysis also showed that the variation in expression was greatest between the intracellular miRNA and the sEV samples. Strangely, both the principal component analysis revealed and the heatmap indicated that GSKO-Host replicate A had sizeable variation from the other GSKO-Host replicates.

DE analysis revealed that 87 of the miRNAs were significantly differentially expressed between the GSKO-Host intracellular miRNAs and the GSKO-Host sEVs miRNAs; 29 of these miRNAs were upregulated in sEVs. Between the GSKO-Host sEVs and the CHO-A sEVs, there were only 33 miRNAs significantly differentially expressed (See Appendix C and Appendix D for full lists of differentially expressed miRNAs). To visualise the relative changes in miRNA abundances, the top 15 most abundant miRNAs in GSKO-Host sEVs and GSKO-Host Intracellular were plotted as percentages of the total miRNA content in each sample. For comparison of the relative abundances, the top 15 miRNAs in GSKO-Host sEVs were plotted as percentages of the total miRNA content in CHO-A sEVs. Likewise, the top 15 GSKO-Host Intracellular miRNAs were also plotted as percentages of the total GSKO-Host sEV miRNA content.

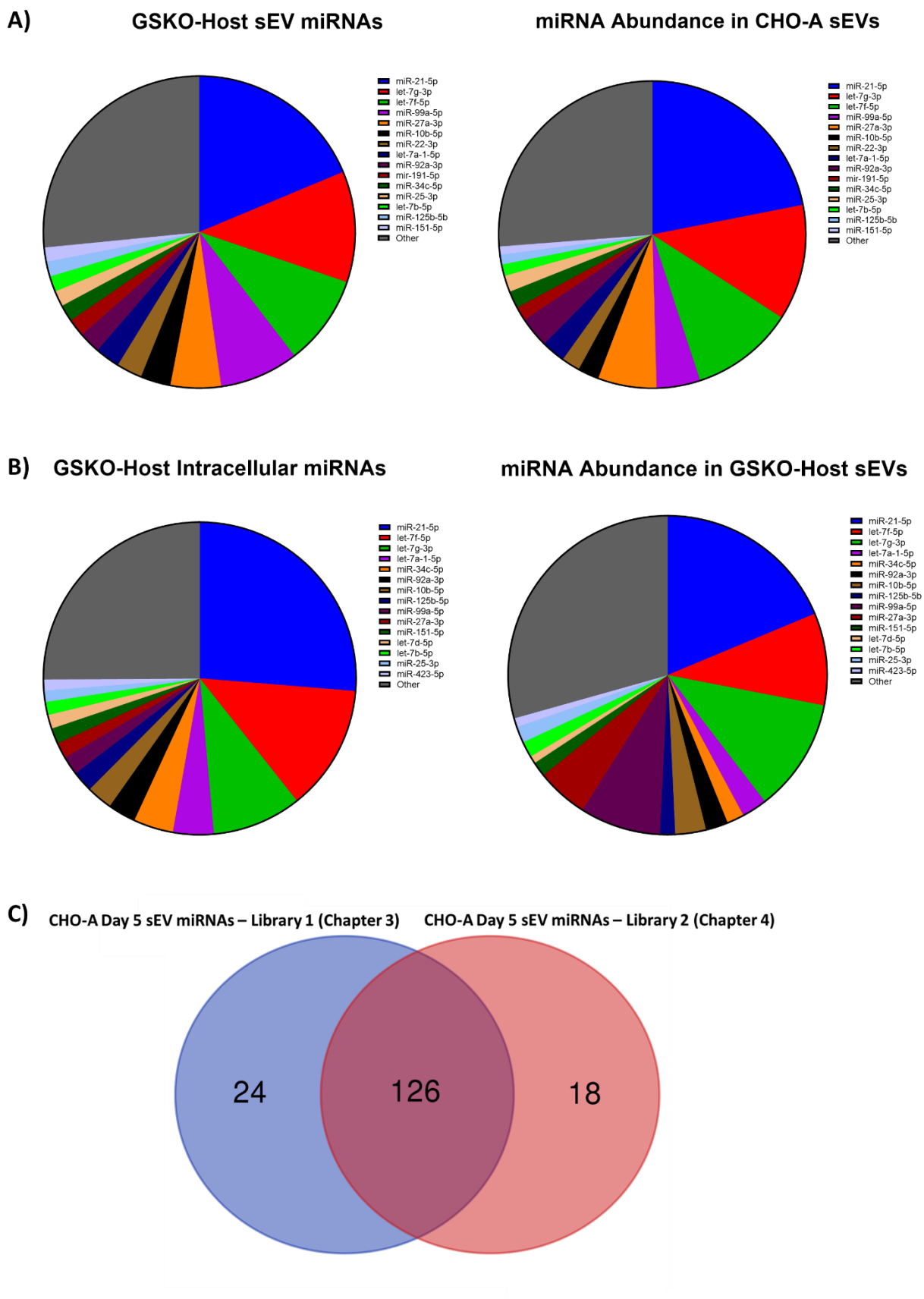

Fig 4.9 GSKO-Host sEVs and CHO-A sEVs have little difference in terms of relative miRNA abundances whereas GSKO-Host Intracellular miRNAs vary in abundance substantially from

GSKO-Host sEVs. *(A) Normalised counts of the most abundant miRNAs in GSKO-Host sEVs as percentages of the total miRNA content. For comparison of relative abundances, those same miRNAs plotted as percentages of the total CHO-A sEV miRNA content. (B) Normalised counts of the most abundant miRNAs in GSKO-Host intracellular content as percentages of the total miRNA content. For comparison, the proportions of the total miRNA content those same miRNAs occupy in GSKO-Host sEVs. (C) Comparison between miRNAs identified in Chapter 3 versus those identified in Chapter 4.*

There was little difference in individual miRNA abundances between sEVs from the two CHO cell lines. Of the top 15 miRNAs detected, only miR-99a-5p (upregulated in CHO-A), miR-92a-3p (upregulated in CHO-A) and miR-27a-5p (upregulated in CHO-A) were differentially expressed. The remainder of the differentially expressed were amongst the least abundant miRNAs. When comparing intracellular miRNA content and the miRNA content of sEVs, there were several of the top 15 detected GSKO-Host Intracellular miRNAs and the top 15 GSKO-Host sEV miRNAs which were significantly altered in their expression (see **Table 2**).

Table 2: Significantly upregulated/ downregulated miRNAs in GSKO-Host sEVs relative to GSKO-Host Intracellular miRNA content. *Wald's test used to determine statistically significant comparisons across all samples with Benjamin-Hochberg test used to correct for multiple comparisons.*

miRNA	log2FoldChange	padj	Upregulated/ Downregulated
miR-21-5p	0.640073	0.021267	Downregulated in GSKO-Host sEVs
let-7f-5p	0.646954	0.000144	Downregulated in GSKO-Host sEVs
let-7a-1-3p	0.881932	1.37E-07	Downregulated in GSKO-Host sEVs
miR-34c-5p	1.399072	7.17E-15	Downregulated in GSKO-Host sEVs
miR-92a-3p	0.518302	0.002432	Downregulated in GSKO-Host sEVs
miR-125b-5p	0.676729	9.45E-11	Downregulated in GSKO-Host sEVs
miR-99a-5p	-1.86544	3.55E-14	**Upregulated in GSKO-Host sEVs**

miR-27a-3p	-1.47564	7.07E-19	**Upregulated in GSKO-Host sEVs**
let-7d-5p	1.073945	1.29E-10	Downregulated in GSKO-Host sEVs
miR-25-3p	-0.30446	0.013093	**Upregulated in GSKO-Host sEVs**
miR-423-5p	0.489917	0.002973	Downregulated in GSKO-Host sEVs
miR-22-3p	-1.42098	1.04E-15	**Upregulated in GSKO-Host sEVs**

It was notable in **Fig 4.9** (C) that while the majority of miRNAs detected in Day 5 CHO-A sEVs in Library 1 of Chapter 3 were also detected in Library 2 of this chapter, the abundances of miRNAs detected differed substantially. This is illustrated in **Table 3** where the top 20 most abundant miRNAs in each library are listed from top to bottom.

Table 3: Top 20 Day 5 CHO-A sEV miRNAs from both small RNA-seq libraries.

Library 1 (Chapter 3)	**Library 2 (Chapter 4)**
miR-22-3p	miR-21-5p
miR-10b-5p	let-7g-3p
miR-21-5p	let-7f-5p
miR-92a-3p	miR-27a-3p
let-7f-5p	miR-99a-5p *
miR-181a-5p *	miR-92a-3p
miR-10a-5p	let-7a-1-5p
miR-191-5p	miR-10b-5p
miR-34c-5p	miR-22-3p
miR-27b-3p	miR-34c-5p
miR-186-5p *	miR-25-3p
miR-151-5p *	miR-27b-3p
miR-16-5p *	miR-191-5p
let-7a-1-5p	miR-146b-5p *
miR-503-5p *	let-7b-5p *
miR-25-3p	miR-29a-3p *
miR-27a-3p	miR-125b-5p *
miR-30e-5p *	miR-3074-2-5p *
miR-486-5p *	miR-3074-1-5p *
let-7g-3p	miR-10a-5p
* = miRNA is unique to that library's top 20	

4.2.6 Comparison of sEV Lipid content

In addition to the miRNA content of the sEVs, the lipid content was also characterized and compared. Not only did this provide an overall picture of the lipid content of sEVs from CHO cells but it also showed that there were significant differences in the quantities of different lipid classes between cell lines.

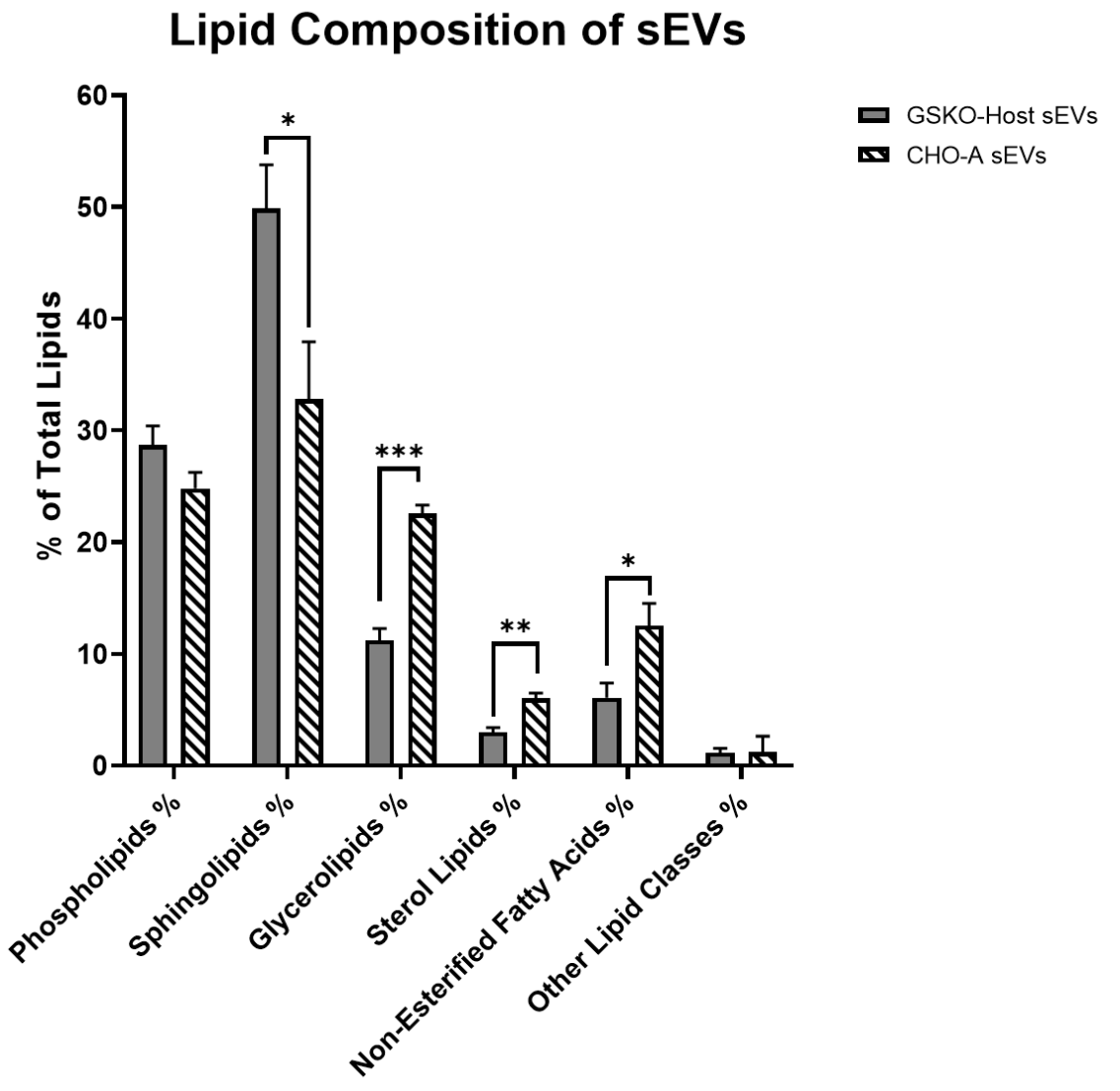

Fig 4.10 Lipidomics analysis showed differences in lipid composition between sEVs from both cell lines. *Overall lipid composition of CHO sEVs from Day 5 of fed-batch. Significant differences were detected in Sphingolipid, Glycerolipid, Sterol Lipid and Non-Esterified Fatty Acid content. Three replicates per cell line. All error bars are standard deviation. Independent two-tailed t-tests used to check for statistically significant differences.*

The lipid characterization shown in **Fig 4.10** highlighted that the majority of lipid in CHO sEVs are sphingolipids, followed by phospholipids and glycerolipids. The GSKO-Host sEVs contained significantly higher quantities of sphingolipids whilst CHO-A sEVs had significantly more glyceroplipids, sterol lipids and non-esterified fatty acids (NEFA). The lipid classes were further broken down to see which lipids in those classes were differentiated in their quantity.

A)

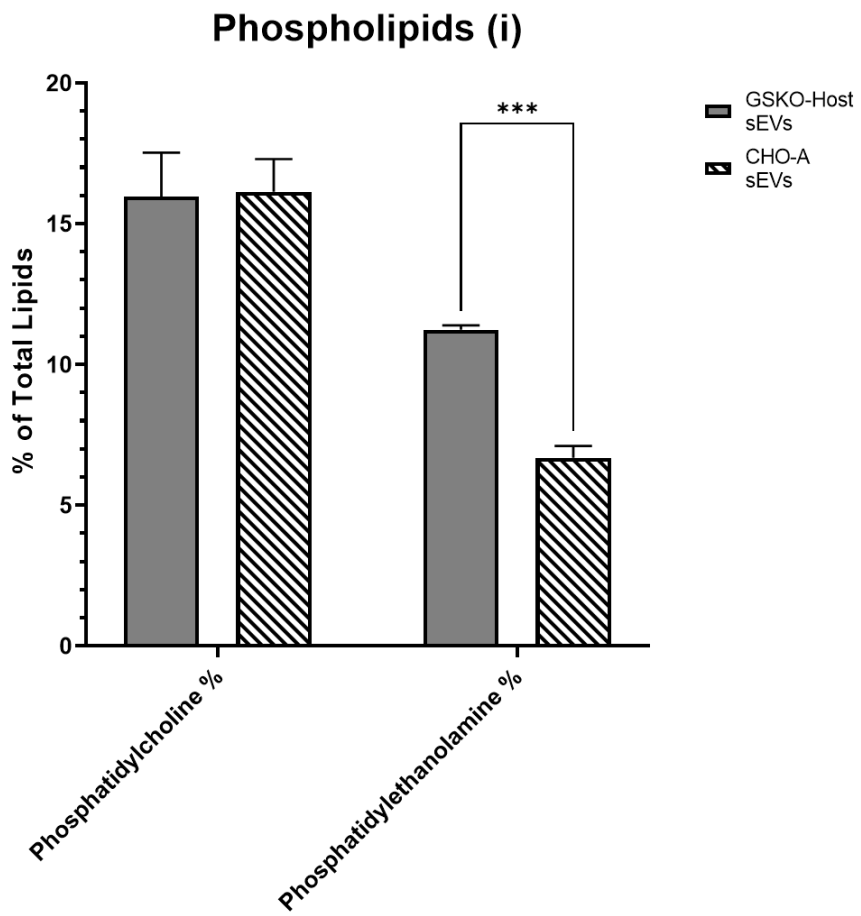
Phospholipids (i)
% of Total Lipids
20
15
10
5
0
***
GSKO-Host sEVs
CHO-A sEVs
Phosphatidylcholine %
Phosphatidylethanolamine %

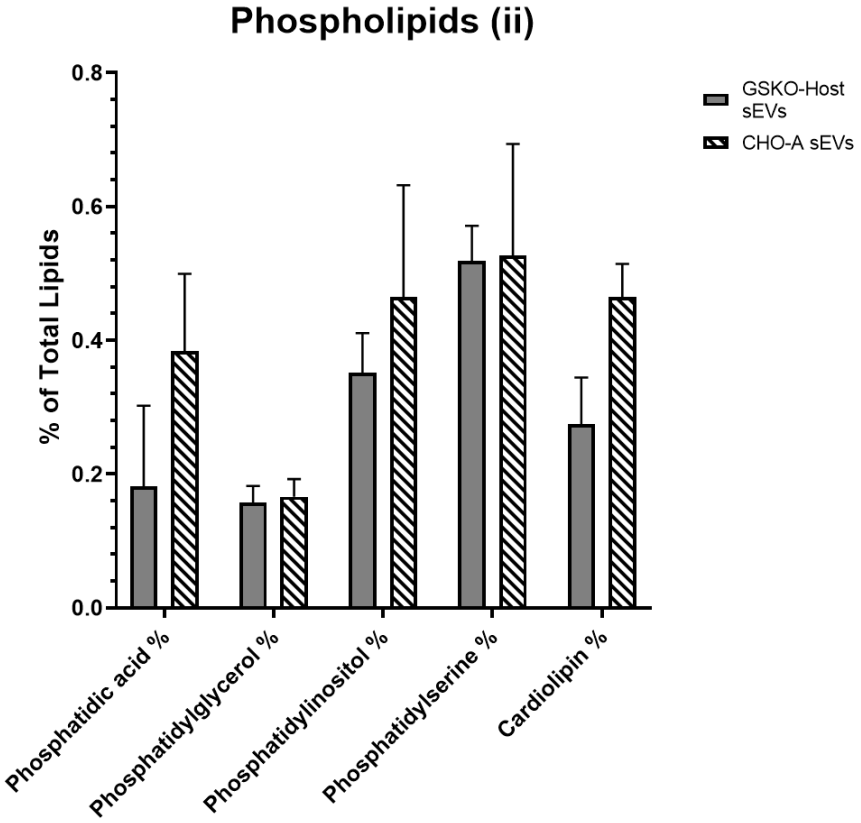
Phospholipids (ii)
% of Total Lipids
0.8
0.6
0.4
0.2
0.0
GSKO-Host sEVs
CHO-A sEVs
Phosphatidic acid %
Phosphatidylglycerol %
Phosphatidylinositol %
Phosphatidylserine %
Cardiolipin %

B)

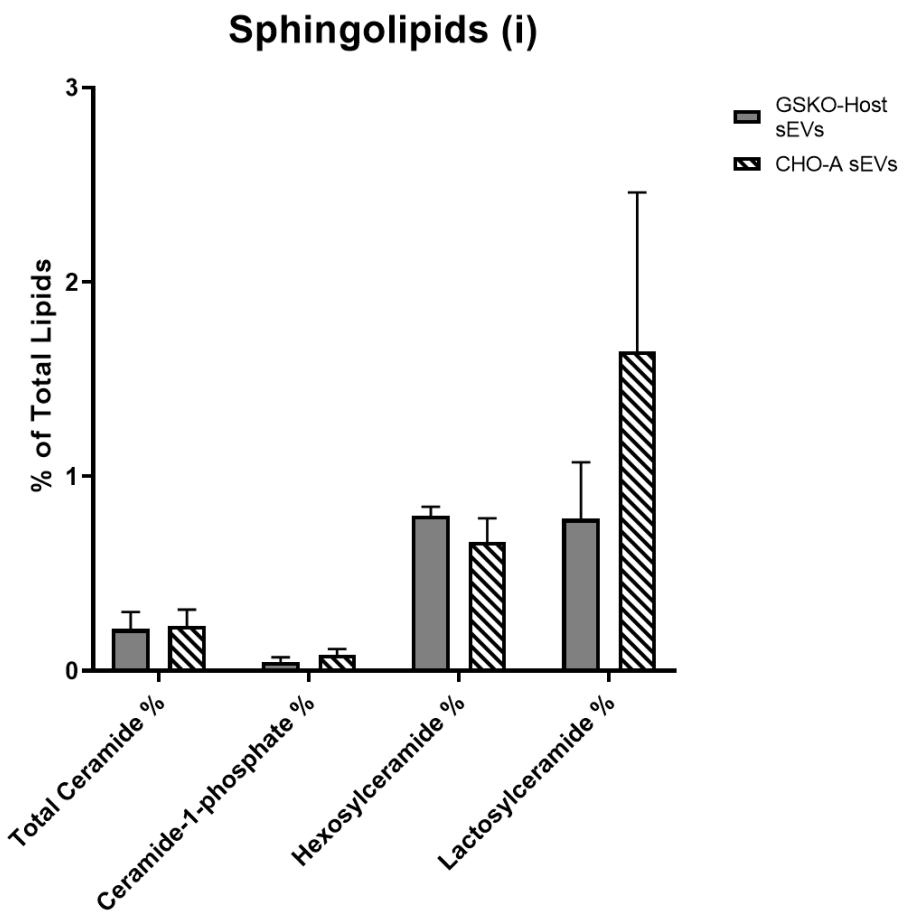
Sphingolipids (i)
% of Total Lipids
3
2
1
0
GSKO-Host sEVs
CHO-A sEVs
Total Ceramide %
Ceramide-1-phosphate %
Hexosylceramide %
Lactosylceramide %

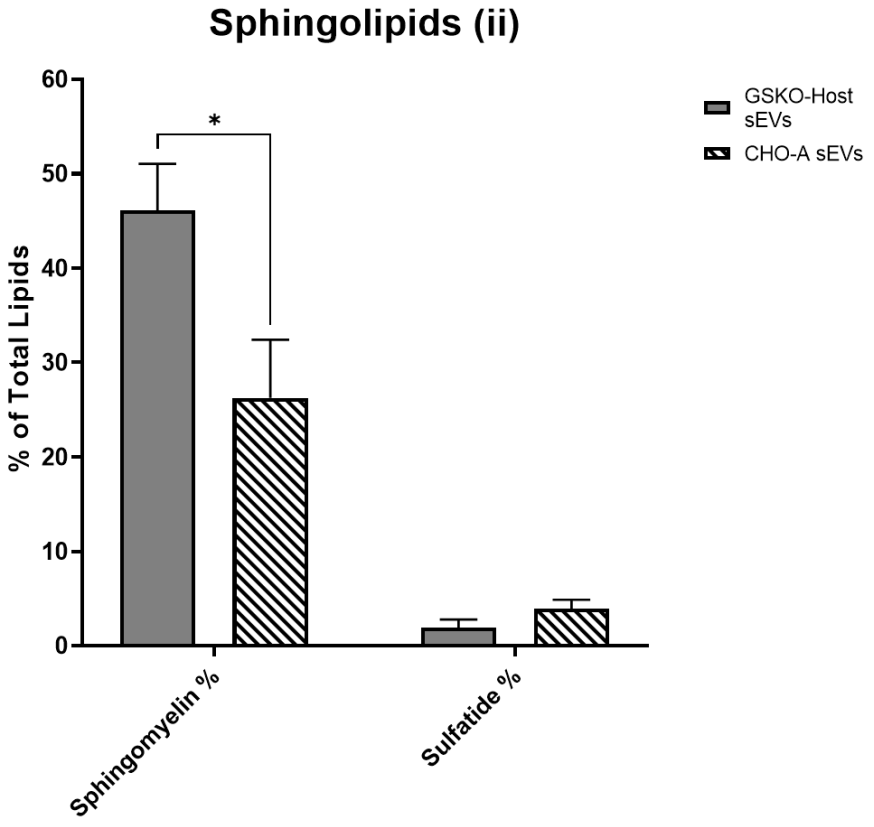
Sphingolipids (ii)
% of Total Lipids
60
50
40
30
20
10
0
*
GSKO-Host sEVs
CHO-A sEVs
Sphingomyelin %
Sulfatide %

C)

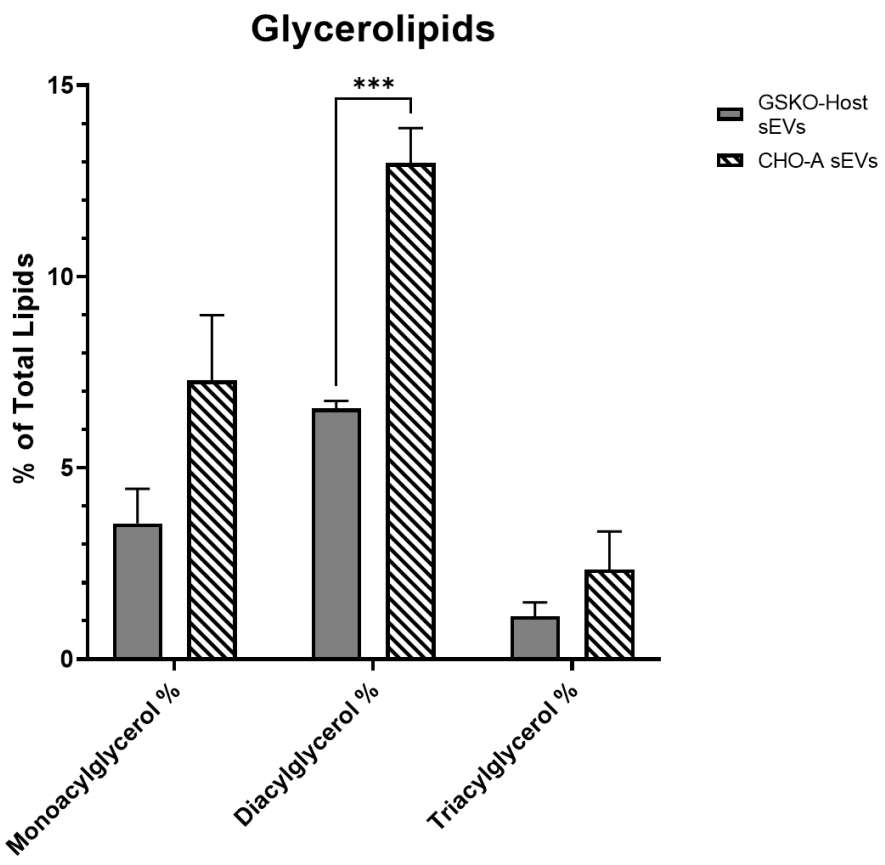
Glycerolipids
***
15
10
5
0
% of Total Lipids
GSKO-Host sEVs
CHO-A sEVs
Monoacylglycerol %
Diacylglycerol %
Triacylglycerol %

D)

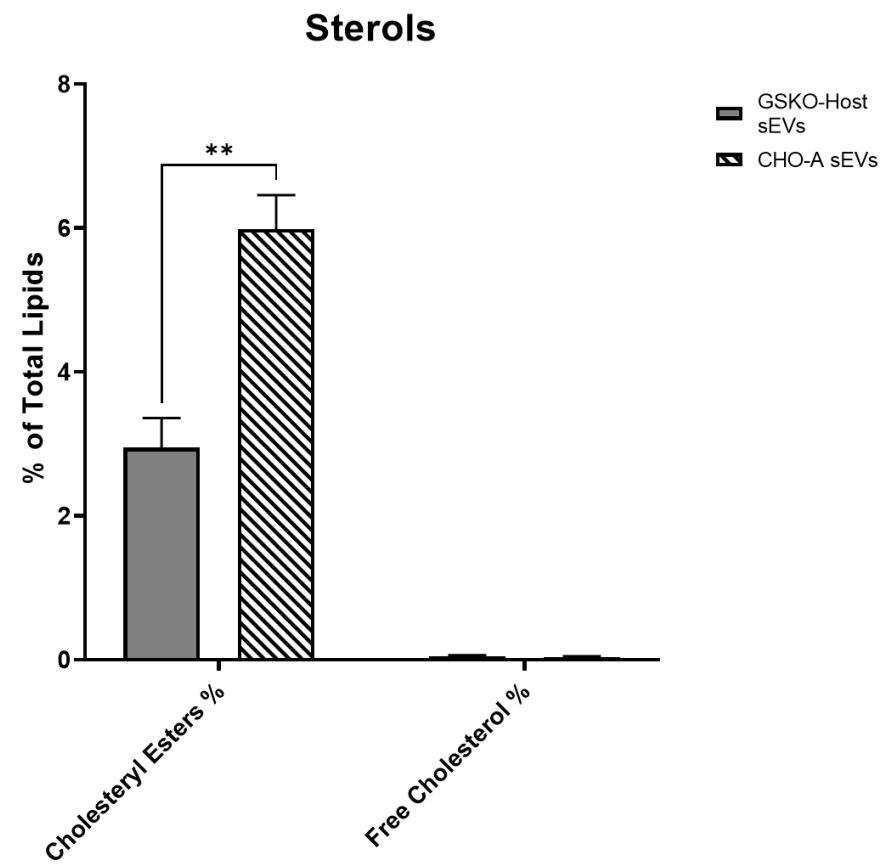
Sterols
**
8
6
4
2
0
% of Total Lipids
GSKO-Host sEVs
CHO-A sEVs
Cholesteryl Esters %
Free Cholesterol %

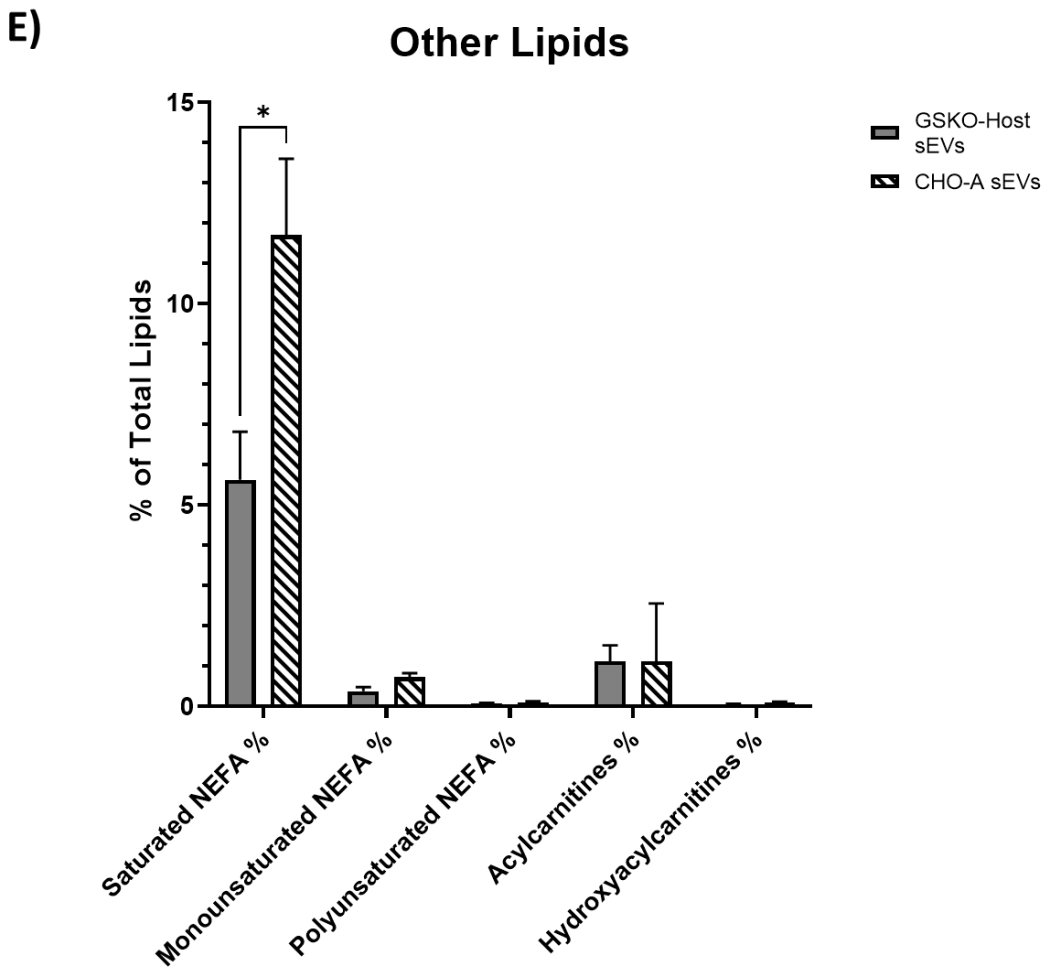

Fig 4.11 Breakdown of the abundances of each lipid as a percentage of the total lipids detected. (A) Phospholipids, (B) Sphingolipids, (C) Glycerolipids, (D) Sterols and (E) Other lipids including NEFA (Non-esterified fatty acids). *Three sEV replicates from each cell line. All error bars are standard deviation. Independent two-tailed t-tests used to check for statistically significant differences.*

Of the phospholipids, phosphatidylcholine (PC) and phosphatidylethanolamine (PE) were the highest in quantity with all other phospholipids only being <1% of the total lipid content. PE was significantly lower in sEVs from the CHO-A cell line. In the sphingolipids, each of the ceramides accounted for fewer than 1% of the total lipid content. The most abundant sphingolipid for both sets of sEVs was sphingomyelin (SM). However, SM was significantly lower in the CHO-A sEVs; approximately half that of the GSKO-Host sEVs. In the case of Glycerolpids, Monoacylglycerol (MA) was somewhat higher, although not significantly, in CHO-A sEVs. Diacylglycerol (DA) was significantly higher in the CHO-A sEVs and double that of GSKO-Host sEVs. The most

abundant of the Sterols was Cholesteryl Esters (CE) and these were approximately twice as abundant in the CHO-A sEVs. With regards Other Lipids, Saturated NEFA made up the majority of these and accounted for significantly more of the total lipid content in CHO-A sEVs.

4.3 Discussion

To the author's knowledge, there has been no studies directly comparing EV secretion between CHO cell lines. The fact that the GSKO-Host had three times the number of lEVs/ cell and sEVs/ cell suggests that EVB might be limited in its utility to the cell. That is to say, in Chapter 3, sEVs from CHO-A were predicted to regulate cell growth and prevent cell death. This was observed when depletion of sEVs from CHO-A fed-batch decreased viability of the cells and shortened fed-batch life-span. Yet it may be the case that the stimuli provided by EVs are only necessary to a certain point. After this point is reached, sEV secretion is in surplus to the cell's requirement and the size of the surplus varies amongst cell lines. Alternatively, an adaptation may occur in producer cell lines to lower the necessary quantity of EVs needed to maintain cell-to-cell communication. Beyond this threshold quantity, the producer cell does not require EVs to mediate cell-to-cell communication and cellular resources in EV secretion may be "exchanged" in order to allow higher protein product secretion. This is potentially indicated by the lEV fraction of CHO-A which had fewer particles per µg of protein than GSKO-Host. This is possibly because the CHO-A cell line can more readily secrete protein than lEVs as a producer cell line.

However, it remains difficult to pinpoint whether this downregulation in EVB could be a direct or indirect consequence of mAb secretion. For example, is known that inhibiting lysosome degradation promotes EVB in other cell lines as a compensatory mechanism and vice versa (Eitan *et al.*, 2016). In this instance, CHO-A could have greater lysosomal activity and therefore secrete fewer EVs as an unintended consequence.

A caveat to this analysis was that the feed medias between the two differed slightly with CHO-A requiring an Efficient Feed B absent in certain amino acids. The impact

this had on the EV secretion is hard to predict or account for as the CHO-A cell line would not grow in standard Efficient Feed B formulation.

The similarity between the sEV miRNA compositions suggests that CHO sEV miRNAs are conserved across cell lines. This is regardless of whether the cell line is a producer or non-producer. Several of the same miRNAs detected in this study were also found by Keysberg *et al.* (2021) and Busch *et al.* (2022) which adds to this assertion. However, both the cell lines tested in their studies and in this study were CHO-K1 derived. It may be that other CHO cell lines such as CHO-S or CHO DG44 have a different sEV miRNA profile. Yet what is clear from this study is that CHO cells conserve their sEV miRNA profile throughout the cell line development process and the signaling those miRNAs provide.

Some miRNAs are enriched in sEVs relative to the intracellular miRNA content. The miRNAs miR-22-3p, miR-99a-5p and miR-27a-3p were all found to be highly abundant in sEVs with a log2 fold change greater than 1.4. Studies from different cancer cell types and immune cells have shown miR-99a-5p to be pro-apoptotic due to its ability to target and inhibit mTOR (Garrido-Cano *et al.*, 2018; Tsai *et al.*, 2018; Wang *et al.*, 2022). On the other hand, through targeting of BTG2 in gastric cancer and Mapk10 in nasopharyngeal carcinoma, miR-27a-3p promotes cell proliferation (Zhou *et al.*, 2016; Li and Luo, 2017). As mentioned in Chapter 3, miR-22-3p has a cell specific functionality.

The differences in miRNA abundances between Library 1 (Chapter 3) and Library 2 (Chapter 4) are most probably explained by the use of different library prep kits at Genewiz (see Appendix E for number of annotated reads generated by each library and Appendix F for Genewiz's QC report). In Library 1, Illumina TruSeq Small RNA library Prep Kit was used. For Library 2 in Chapter 4, a NEBNext® Small RNA Library Prep Set for Illumina® was used. The choice of small RNA library prep kit will affect the quantities of miRNAs detected. This is often due to adapter biases for particular small RNA sequences (Dard-Dascot *et al.*, 2018; Herbert *et al.*, 2020). In this case, the bias is best illustrated in how miR-22-3p is most abundant in Library 1 but only the 9th most abundant Library 2. Similarly, miR-99a-5p is not present in the top 20 most abundant miRNAs in Library 1 but is 5th in Library 2. This perhaps highlights a limitation of small RNA-seq in terms of sensitivity to changes in the quantities of miRNAs;

particularly for low abundance miRNAs. At the same time, with 13 miRNAs being common to the top 20 of both libraries, despite the use of two different library prep kits, there is a degree of assurance that these miRNAs are high in quantity in CHO sEVs.

The variation in the lipid abundance between sEVs from different CHO cell lines was not surprising. It is known that different CHO cell lines vary in their lipid composition and this was likely reflected in the sEV lipid content. When compared to cellular lipid abundance, it appears that sEVs in general have a greater SM content (10-20% of total cell lipid composition) and reduced PC (30-40%) and PS (~5%) relative to CHO cells reported in literature. Yet they have similar cholesterol (10-15%) and PE (10-15%) composition (Széliová *et al.*, 2020). The ceramide (0.1%) composition is also similar to what is reported as the percentage of plasma membrane lipid in literature but there appears to be higher quantities of hexoscylceramide (HexCer) (0.1% in plasma membranes) in sEVs (Tiszlavicz *et al.*, 2022). The increased SM and HexCer along with lower PC content in CHO sEVs is similar to what has been reported in sEVs from other cell lines (Dinkins, Wang and Bieberich, 2017).

When comparing CHO sEVs to EVs from other cell types, there appears to be far less cholesterol. Skotland *et al.*, (2020) report that EVs from PC-3 cells, B-lymphocytes and Mast cells contain 59%, 42.1% and 15% cholesterol, respectively, as part of the total lipid composition. This compares with only 3-6% in the two CHO cell lines investigated here. PC content is similar to PC-3 cells (15.3%) but lower than B-lymphocytes (20.3%) and Mast cells (28%). SM, especially in the case of GSKO-Host sEVs, is far more abundant as it only takes up 16.3% of PC-3 cells, 23% of B-lymphocytes and 12% of Mast cells. PE content is similar to PC-3 cells (15.3%) and B-lymphocytes (14.6%) but lower than Mast cells (24%).

CHO-A sEVs having greater CE content is potentially reflective of it being a producer cell line with upregulated vesicular traffic and stress in the endoplasmic reticulum for which increased cholesterol is needed (Ridsdale *et al.*, 2006). A possible cause for the increased SM in GSKO-Host sEVs could be that lactosylceramide is more abundant in CHO-A sEVs. Conversion of lactosylceramide and SM are two of the possible utilisations of ceramide and the reduced SM in CHO-A sEVs may be a consequence of increased lactosylceramide (Novgorodov *et al.*, 2016). It is difficult to speculate as to why CHO-A sEVs have reduced PE given the many cellular functions it is involved

in. One possible function which may reduce PE synthesis is a change in the rate of autophagy occurring in the CHO-A cell line. PE binds to LC3 in mammalian cells to determine the size of an autophagosome and therefore the rate of autophagy in the cell will impact on PE synthesis (Calzada, Onguka and Claypool, 2016).

In summary, different CHO cell lines can have significantly different EV secretion rates. In this study, the CHO-A producer cell line had far fewer EVs/ cell than the GSKO-Host. The reasons for which this is the case are unknown. What is certain is that the nucleic acid composition of sEVs is not impacted by the cell lines development produce and, although the quantities of sEV derived stimuli may vary between cell lines, the nature of those stimuli remains constant. Where CHO sEVs do vary in terms of composition is in their lipid content. This is likely to be due to them reflecting the lipid composition of the cell line they are derived from based on reports in literature.

Chapter 5

Investigating the Variability of CHO sEV Secretion in Monoclonal Antibody Production

5.1 Introduction

In Chapter 4, there was a clear distinction in the number of lEVs/ cell and sEVs/ cell between CHO-A and the GSKO-Host. This warranted investigation as to what were the factors responsible for this variation. Is it the case that the number of EVs secreted by a CHO cell line is random or is it somehow correlated to other characteristics such as productivity, growth, biomass accumulation, nutrient consumption or cell size? If there is a correlation, does it make EV secretion a “biomarker” of that trait? Does a particular stage in the cell line development process greatly alter the number of EVs/ cell for that cell line? Does a minor difference in feed media formulation, as was the case in Chapter 4, dramatically alter the quantity of sEVs/ cell?

To address these questions, Lonza supplied 8 cell lines. 7 of these cell lines were derived from a proprietary cell line named here as “CHO-X”. These were the CHO-X Parental, 2 GS-Nulls with differing expression levels of glutamine synthase and 4 producer cell lines secreting ETE mAb; X1, X2, X3 and X4. The producer cell lines were all distinguished with differing ability to produce mAb as measured by cell specific productivity (qP). The qP of each cell line had been ranked by Lonza in previous studies where the cell lines were compared directly to each other. In addition to the CHO-X cell lines, a stably transfected GS-Null polyclonal pool derived from a different cell line development process to that of CHO-X was also investigated; Non-X GS-Null. This was to account for the potential that EV profiles observed were unique to the CHO-X cell lines. The background for each of these is summarised in **Table 4.**

Table 4: Cell lines supplied by Lonza and grown in fed-batch.

Producer Cell Lines		Non-Producer Cell Lines	
Cell Line	Lonza qP Ranking	Cell Line	GS Expression Ranking
X1	1	GS-Null 1	1
X2	2	GS-Null 2	2
X3	3	Parental	No GS Expression
X4	4	Non-X GS-Null (pool)	-

By examining these cells lines, each with distinct characteristics, it would guide an understanding as to what factors, if any, influenced EV secretion. EV secretion was measured at two levels. The first being a physical measurement of the number of sEVs/ ml for each cell line. The second was using transcriptomic analysis of genes involved in EVB and pathways which share genes involved in EVB and how these may be differentially expressed amongst cell lines. Cellular characteristics were also recorded such as cell volume, IVCD, average specific glucose consumption, titre and cell specific growth rate to determine what factors correlated with the quantity of sEVs/ cell.

5.1.1 Chapter Summary

8 cell lines supplied by Lonza were grown in fed-batch using Lonza's proprietary base and feed medias and protocol. RNA-seq samples were taken on Day 5 of fed-batch as well samples for sEV quantification and titre. The sEV samples were quantified by two methods: NTA and NanoAnalyzer. A correlations matrix was then generated to see if any of the following traits correlated with the number of sEVs/ cell measured by NTA: Day 5 titre, Day 10 titre, Day 5 qP, Day 10 qP, IVCD, Growth Rate, Cell Volume and Specific Glucose Consumption Rate (qGLU). DE analysis was also performed to see how EVB gene transcription differed amongst the cell lines and if these differences reflected the physical quantities of sEVs measured.

5.1.2 Chapter Aims

- Grow 8 cell lines in fed-batch and measure VCD, Viability, Titre, Cell Volume and average qGLU

- Measure sEV secretion in each cell line by NTA and NanoAnalyzer

- Generate a correlation matrix to ascertain what cellular characteristics correlate with EV secretion

- Compare the transcriptional activity of EVB genes in the different cell lines. Determine if the physical measurement of sEVs is reflected transcriptionally and if pathways which share genes involved in EVB are also transcriptionally differentiated.

5.2 Results

5.2.1 Fed-Batch of Lonza CHO-X cell lines and Titre Analysis

Two fed-batch processes were set-up. The first was a Producer fed-batch containing the cell lines producing the mAb. The second was a Non-Producer fed-batch. In both fed-batches, Parental and Non-X GS-Null cell lines were grown and samples taken for RNA-seq. This was to allow normalisation between fed-batches for transcriptional analysis. However, samples for sEV analysis in the Non-X GS-Null and Parental cell lines were only taken from the second fed-batch. In both fed-batches, four replicates were grown per cell line. Two replicates were harvested on Day 5 for sEV purification and analysis. The other two replicates were used for RNA-seq analysis. In the producer fed-batch, the RNA-seq replicates were grown to Day 12 to verify the qP of the producer cell lines matched Lonza's rankings.

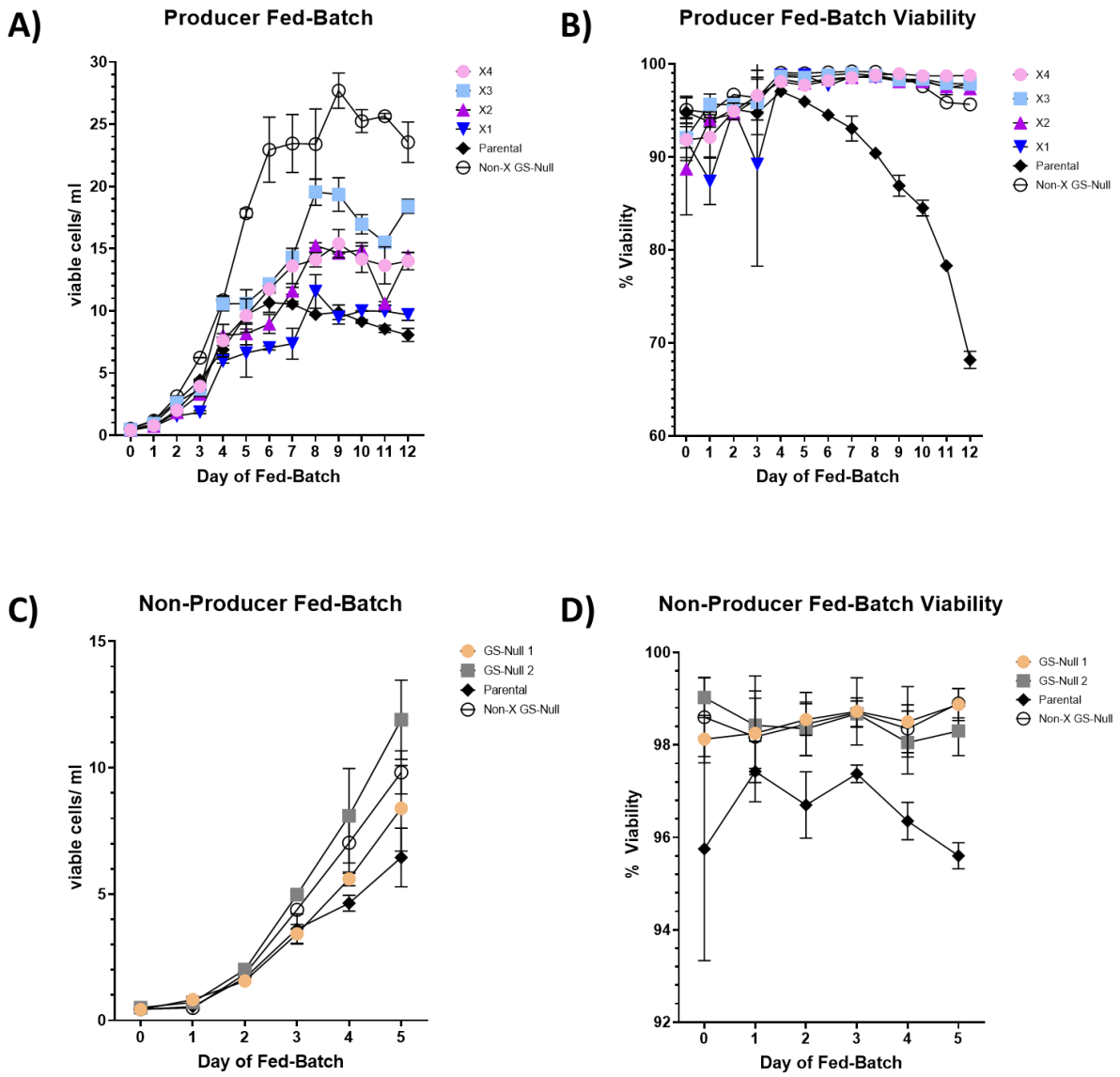

Fig 5.1 Growth and viability of Producer and Non-Producer fed-batches from cell lines supplied by Lonza. *(A) Producer fed-batch VCD. (B) Producer fed-batch viability. (C) Non-Producer Fed-Batch VCD. (D) Non-Producer Fed-Batch Viability. Four replicates were grown to Day 5 in producer fed-batch with two harvested on Day 5 for sEV analysis and the remaining two grown to Day 12 for qP analysis. Only two replicates were grown in the producer fed-batch for Parental and Non-X GS-Null. Titre was taken on Day 5 and Day 10 of the producer fed-batch. RNA-seq samples were taken on Day 5. Four replicates were grown for all cell lines in the Non-Producer fed-batch with two used for RNA-seq analysis and two for sEV analysis. Parental and Non-X GS-Null were grown in both fed-batches with RNA-seq samples taken on Day 5 in both fed-batches to allow normalisation between fed-batches. However, sEV analysis was only performed on Parental and Non-X GS-Null from the non-producer fed-batch. All error bars are standard deviation.*

Titre was measured on Day 5 for all replicates and on Day 10 for the RNA-seq replicates. The qP of the producer cell lines aligned with Lonza's ranking; particularly by Day 10 (See **Fig 5.2** (D)).

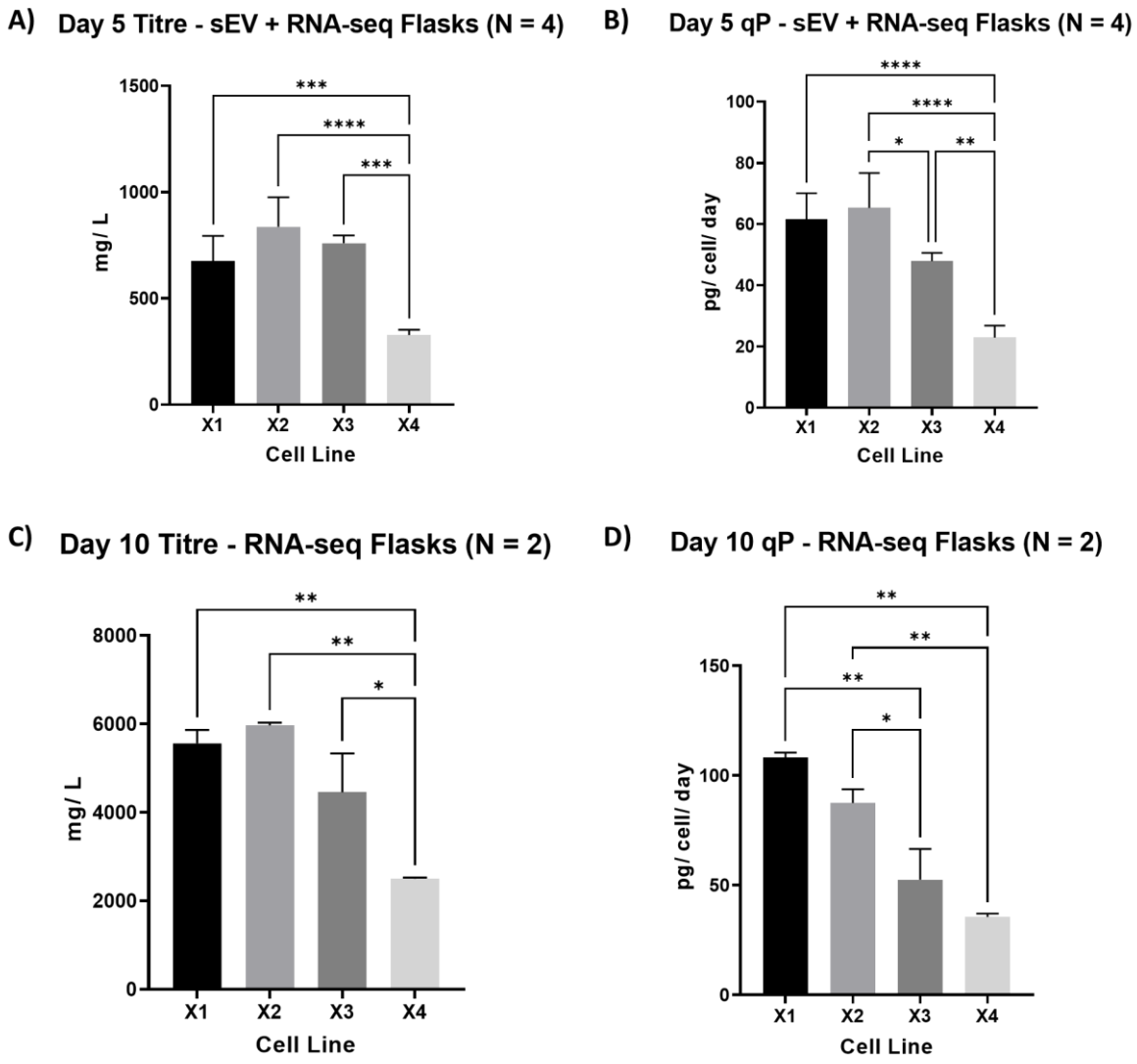

Fig 5.2 Titre and qP of the cells lines in the Producer Fed-Batch. *(A) Day 5 titre of flasks used for sEV and RNA-seq analysis. (B) Day 5 qP of those cell lines. (C) Day 10 titre of flasks used in RNA-seq analysis. (D) Day 10 qP of the flasks used for RNA-seq analysis. Error bars are standard deviation. Four replicates used for Day 5 analysis with two replicates for Day 10 analysis. Statistical comparisons are One-way ANOVA with Tukey post-hoc test used to correct for multiple comparisons.*

By as early as Day 5, higher qP was evident in the X1 and X2 cell lines. X3 appeared to be lower in qP than X1 by Day 5 and was significantly lower by Day 10.

X2 was significantly higher than X3 on both Day 5 and Day 10. X4 was significantly lower in qP on Day 5 compared to all other cell lines and was significantly lower than X1 and X2 on Day 10.

5.2.2 sEV Analysis of CHO-X cell lines

For sEV analysis, 30 ml of cell culture supernatant was purified by UC. A variation was added to the UC process where the initial 100,000g pellets were re-suspended to 1ml in 1X PBS and 0.22µm PES membrane filtered prior to diluting to 5ml in 1X PBS and re-centrifuging at 100,000g. This was because very large pellets were visually observed in the 2,000g and 10,000g fractions and it was anticipated there could be some dissociation from these pellets into the supernatant which would contaminate the 100,000g pellet. The filtration step minimised the chances of these physically large co-isolates pelleting at the 100,000g step. The final 100,000g pellet was then re-suspended to 200µl in 1X PBS and four 50µl aliquots were generated for NTA and NanoAnalyzer analysis. The sEVs of each cell line were first quantified and sized by NTA.

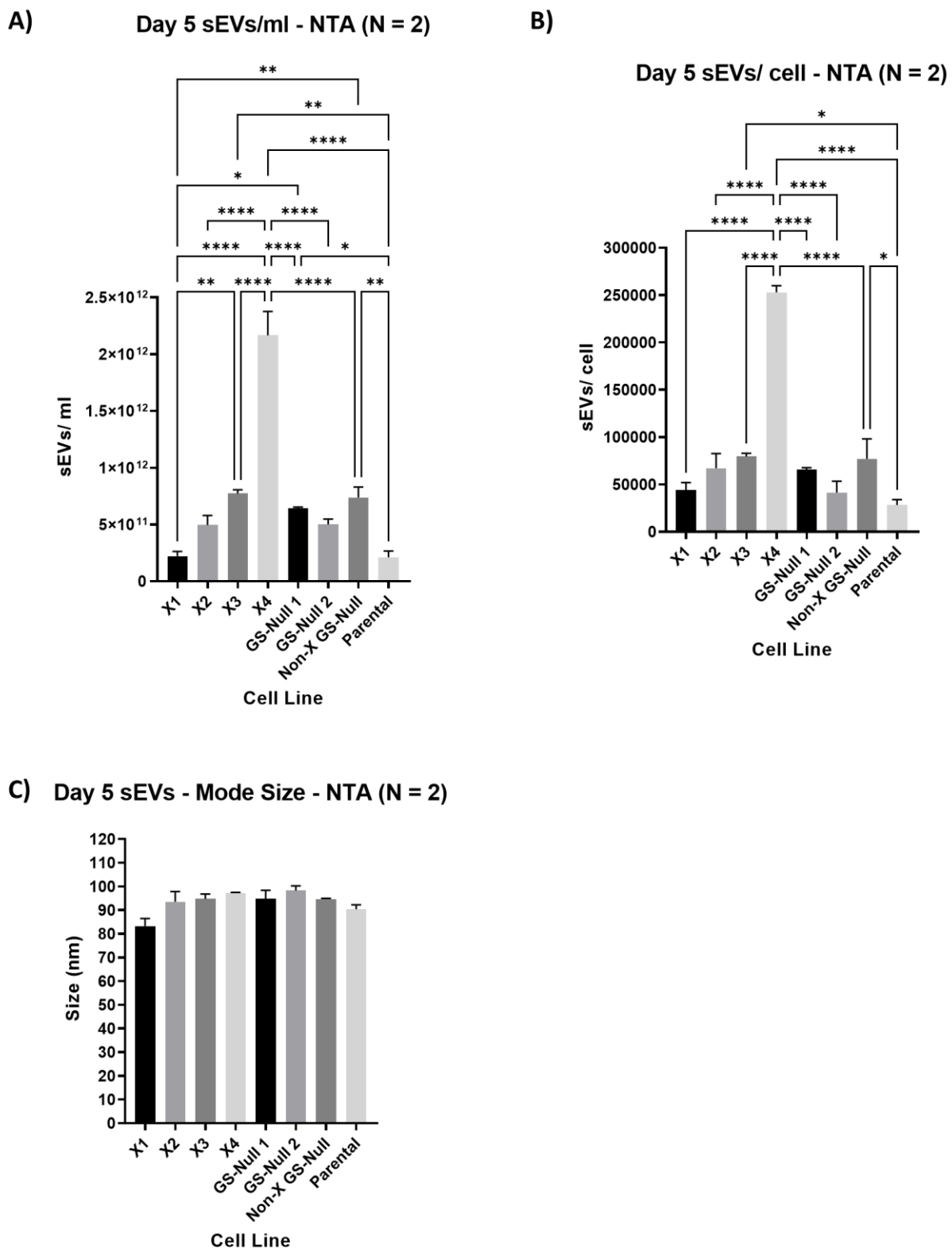

Fig 5.3 NTA counts showed larger sEV quantities secreted by low qP clones. *(A) NTA sEV particle count. (B) The number of sEVs / cell using the Day 5 VCDs of the replicates the sEVs were isolated from. (C) Mode size of the sEVs measured by NTA. All error bars are standard deviation. Statistical significance determined by One-way ANOVA with Tukey post-hoc test used for multiple comparisons.*

The first observation from the NTA sEV counts was, even when accounting for different re-suspension volumes, the quantities of sEVs obtained from these cell lines were far greater than what had been obtained previously with CHO-A and GSKO-Host in previous chapters. The number of sEVs/ cell also varied with each cell line. The X1 and the Parental cell lines had the lowest number of sEVs/ cell with X4 having, by far, the greatest number of sEVs/ cell. The size of the sEVs was very similar to what had been observed with the CHO-A and GSKO-Host cell lines in Chapters 3 and 4.

As a further quantification of sEVs, the sEV samples were also analysed by NanoAnalyzer. The NanoAnalyzer is a flow cytometer which is capable of detecting single sEVs (Fortunato *et al.*, 2021). An advantage to using the NanoAnalyzer was that the sEVs could be stained with CFSE dye. CFSE dye stains sEVs by crossing the sEV membrane and having its acetate groups removed by esterases present in the sEV cytosol. This severely reduces CFSE's membrane permeability and therefore concentrates it inside the sEV. Inside the sEV, CFSE covalently binds to proteins present in the sEV cytosol and the fluorescence, concentrated inside the sEV, is detectable to a flow cytometer. In this way, it specifically detects sEVs from other particles present in the sample which would be otherwise be indistinguishable by NTA. Thus, the NanoAnalyzer could provide both the total particle count for each sample and a purity measurement of each sample.

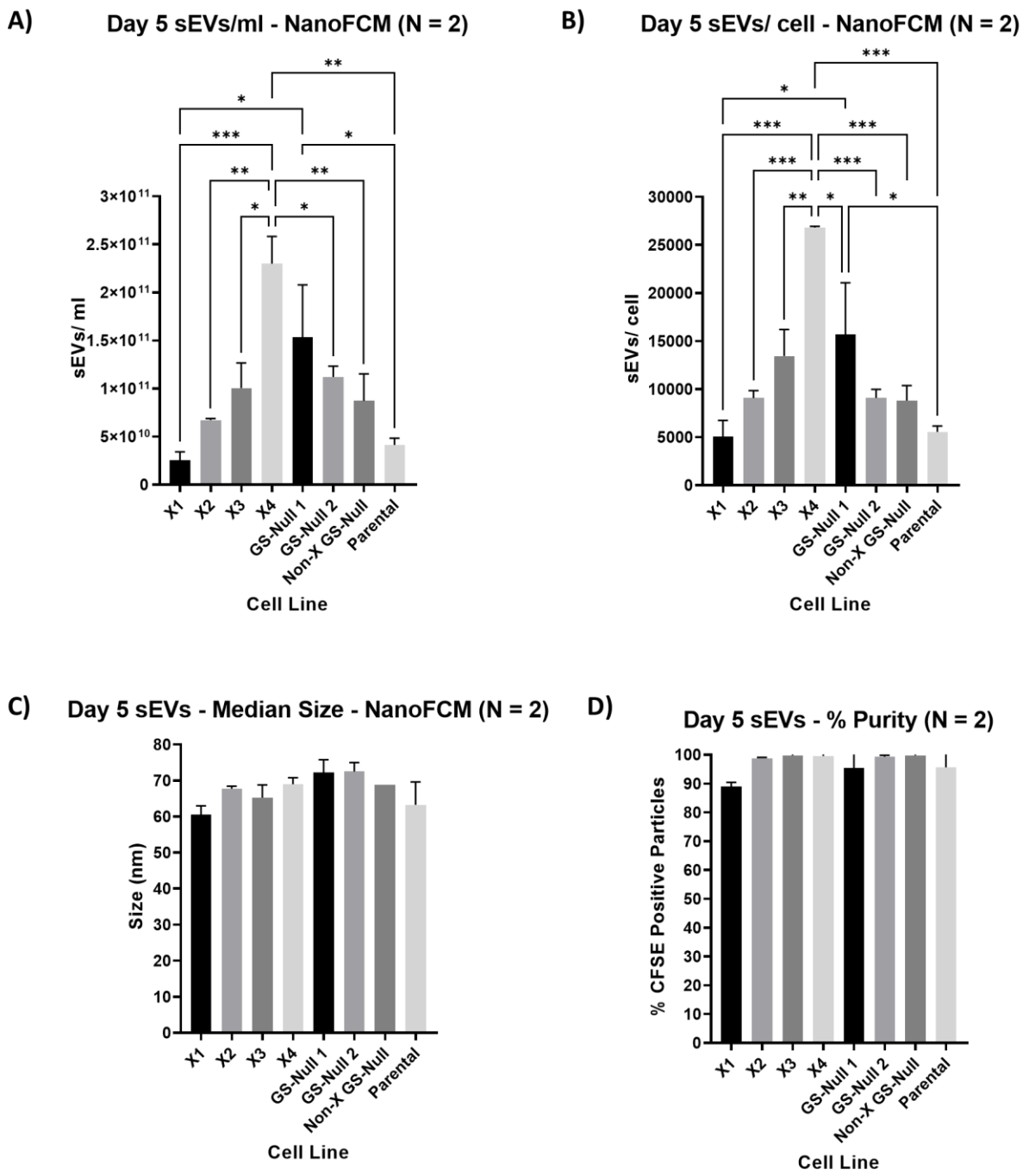

Fig 5.4 NanoAnalyser counts were relatively similar to NTA. *The NanoAnalyzer provided particle counts and sizing as well as determining the percentage of particles which were CFSE-positive for each cell line. (A) The total particle count. (B) The number of sEVs per cell. (C) The median size of the sEVs. (D) The percentage of CFSE-positive particles. Statistical significance determined by One-way ANOVA with Tukey post-hoc test used for multiple comparisons.*

The NanoAnalyzer detected approximately 10 times fewer particles than NTA. However, the pattern observed with the different cell lines in terms of sEVs/ cell was

very similar. A notable difference being that it showed a more staggered differentiation in the sEVs/ cell in the producer cell lines. In the producers, X4 had the highest number of sEVs/ cell, followed by X3, then X2 and X1. Again, the GS-Null cell lines had more sEVs/ cell than the Parental and similar quantities to the producer cell lines. The percentage of CFSE-positive particles was above 90% for all cell lines; suggesting comparable levels of purity and that what was being measured were sEVs for the vast majority of particles.

5.2.3 Correlations Matrix of Cell attributes and EV Secretion

To determine what cellular characteristics correlate with sEV secretion, a correlations matrix was generated in RStudio. This took into account Day 5 sEVs/ cell based on NTA measurements, IVCD as a measure of biomass, Titre, qP, Cell Specific Growth Rate (μ), Cell Volume as a measure of cell size and the average qGLU over the 5 days of fed-batch. The reason the average qGLU was used rather than the qGLU on Day 5 was because glucose was replenished to a specific quantity from Day 3 onwards. In addition to Day 5 Titre and qP, the Day 10 Titre and qP from the RNA-seq flasks were added to the matrix to see how Day 5 sEV measurements correlated with productivity at late stage fed-batch. The matrix used a Pearson correlation co-efficient ranging from -1 to 1. A co-efficient that was closer to -1 was negatively correlated whereas a co-efficient closer to 1 indicated a positive correlation. Only statistically significant relationships were retained in the matrix (See Appendix G for all values used to generate the matrix).

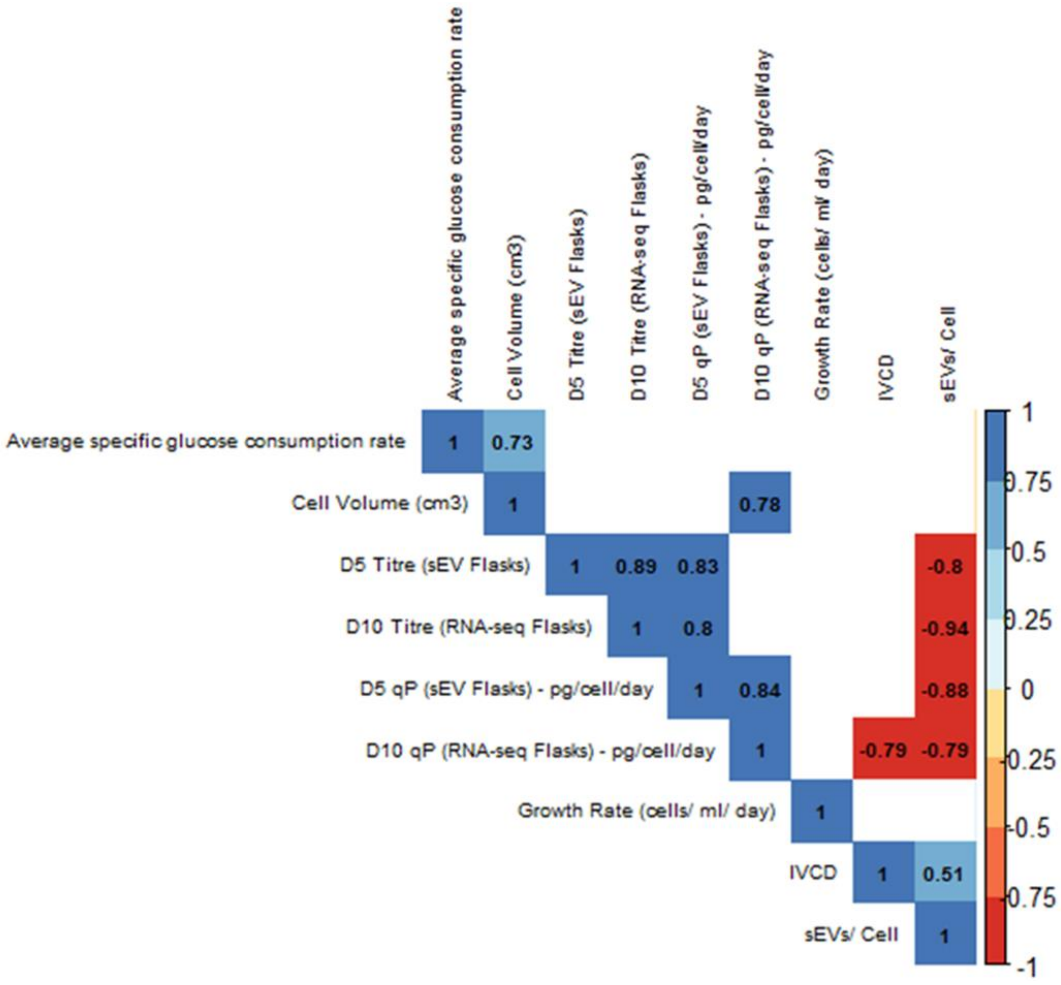

Fig 5.5 Correlations matrix shows negative relationship between qP and sEVs/ cell. *The matrix shows a Pearson correlation co-efficient ranging from -1 to 1 with values close to -1 negatively correlated and values closer to 1 positively correlated. Only significant correlations are shown in the matrix. Of all cellular characteristics measured, sEVs/ cell is negatively correlated with Day 5 titre, Day 10 titre, Day 5 qP and Day 10 qP. There is also positive correlation with the IVCD and the sEVs/ cell. Values for Day 5 titre, qP, average specific glucose consumption rate, cell volume and IVCD are taken from sEV flasks from both producer and non-producer fed-batch. Day 10 titre and qP values taken from RNA-seq flasks from producer fed-batch. The matrix was generated in RStudio using the Hmisc library package. All values and code used to generate matrix are in Appendix G.*

The matrix revealed a strong significant negative correlation between the number of sEVs/ cell and Day 5 titre, Day 5 qP, Day 10 titre and Day 10 qP. There was also a significant, but weaker, positive correlation between the IVCD or biomass of a cell line and the number of sEVs/ cell. There was no significant relationship between a cell line's sEV profile and its growth rate or volume on Day 5 of fed-batch. There was also no significant relationship with the average specific glucose consumption rate.

5.2.4 Transcriptomic Analysis of EV Biogenesis Genes

The genes involved in EVB which were annotatable to the Lonza reference genome were broken down into several categories. This included genes defined as members of the ESCRT pathway, genes associated with members of the ESCRT pathway, Multivesicular Body (MVB) mobilisation to the plasma membrane, MVB fusion and release from the plasma membrane, lEV/ Microvesicle (MV) biogenesis, genes involved in ESCRT independent EVB and genes involved in EV uptake. Some genes were present in multiple categories; especially in the case of EV Uptake where genes had functionality in both EV secretion and uptake (Mulcahy, Pink and Carter, 2014).

To supplement the analysis, genes which are believed to be shared by lysosome formation and EVB were also included in the analysis. EVB and lysosome formation are highly related pathways and it was believed differences in transcriptional activity may either influence, or be a consequence of, lysosome formation in the cell (Tancini *et al.*, 2019; Vidal, 2019). Lipid synthesis genes, although not directly involved in EVB, were also assessed. This was to examine whether the numbers of sEVs/ cell observed may also be attributable to DE in lipid synthesis as EVs are lipid bilayer particles. The lipid synthesis genes were divided into two categories: Phospholipid Synthesis and Other Lipid Synthesis. Similar to EV uptake genes, there were phospholipid synthesis genes which were also used in the synthesis of more than one type of lipid and thus appear in both lipid synthesis categories.

The different categories of genes in EVB are summarised in **Table 5** along with their source literature.

Table 5: Genes involved in different stages of EVB and lipid synthesis were categorised. *The following are EVB genes which could be annotated to Lonza's proprietary CHO genome. ESCRT-0 (Kapuralin et al., 2015; Coudert et al., 2021), ESCRT-I (Schmidt and Teis, 2012), ESCRT-II (Carrasquillo et al., 2012; Ju et al., 2021) and ESCRT-III (Larios et al., 2020; Teng and Fussenegger, 2021) are the four subunits of the ESCRT pathway. MVB_mobilisation are genes required for movement of the MVB/ late endosome containing sEVs to the plasma membrane (Ostrowski et al., 2009; Kowal, Tkach and Théry, 2014). MV or ESCRT-associated are genes which are either associated with the main constituents of the ESCRT pathway and/or are involved in MV biogenesis* (van Niel *et al.*, 2011; Ghossoub *et al.*, 2014a; Kim *et al.*, 2014; Wei *et al.*, 2015; Tricarico, Clancy and D'Souza-Schorey, 2017; Tschuschke *et al.*, 2020)*. ESCRT_independent are genes which initiate EVB without constituents of the ESCRT pathway (Hsu et al., 2010; Ghossoub et al., 2014b; Hyenne, Labouesse and Goetz, 2018; Choezom and Gross, 2022). Lys-EV_formation_overlap (Lys-EV) are genes which are utilised in both lysosome formation and EVB (Mathieu et al., 2021; Xing et al., 2021; Ferreira et al., 2022). Plasma_membrane_fusion genes enable the MVB to dock and fuse with the plasma membrane to release sEVs to the extracellular space (Hessvik and Llorente, 2017; Raja et al., 2019; Keller et al., 2020; Yu et al., 2020; Gurung et al., 2021). EV_uptake genes express both constituents of EVs in their biogenesis and are proteins which enable EV uptake in recipient cells (Mulcahy, Pink and Carter, 2014). Phospholipid_synthesis and Other_lipid_synthesis are genes which are required for phospholipids and other lipids such as sphingolipids, ceramides and glycerolipids (Cockcroft, 2021).*

Gene Set	Genes
ESCRT-0	Stam, Stam 2, Hgs
ESCRT-I	Vps37b, Tsg101, Vps37a, Mvb12a, Mvb12b, Ubap1, Vps28
ESCRT-II	Vps25, Snf8, Vps36
ESCRT-III	Chmp2a, Chmp2b, Chmp3, Chmp4b, Chmp4c, Chmp7, Chmp1a, Chmp5
MVB_mobilisation	Rab27a, Rab27b, Rab35, Rab2b, Rab5a, Rab9a
MV_or_ESCRT-associated	Arf6, Arf1, Diaph3, Rab22a, Myo1a, Rhoa, Anxa2, Vps4a, Cd63, Cd9, Cd81, Rab11a, Rab11b
ESCRT_independent	Smpd3, Pdcd6ip, Sdcbp, Rala, Ralb, Rab35, Pld2
Lys-EV_formation_overlap	Atg12, Atg3, Becn1, Atg16l1, Atg7, Hspa8, Hsp90aa1, Lamp1, Lamp2, Rab7a, Rab7b
Plasma_membrane_fusion	Stx4, Ytk6, Snap23, Stx5, Vamp8, Vamp2, Vamp7, Stx1a, Stx17, Snap29
EV_uptake	Cd9, Cd81, Cd63, Tspan8, Itga4, Vcam1, Icam1, Itgal, Sdc1, Gpc3, Cd209, Ly75, Dnm2, Cav1, Rac1, Actb, Flot1, Anxa2, Anxa6
Phospholipid_synthesis	Fasn, Scd5, Gpam, Agpat4, Cds1, Cds2, Cdipt, Plpp1, Chka, Pcyt1a, Chpt1, Etnk1, Pcyt2, Cept1, Ptdss1, Ptdss2, Pemt, Pisd
Other_lipid_synthesis	Chka, Pcyt1a, CHPT1, Pemt, Etnk1, Pcyt2, Ptdss1, Ptdss2, Pisd, Cds2, Cdipt, Ptpmt1, Crls1, Pla2g5, Sptlc2, Kdsr, Cers1, Degs1, Cerk, Acer1, sphk1, Sgms1, Hmgcr, Srebf1, Scap, Plcb2, Pld3

The normalised counts of each of these categories showed which genes had the highest levels of expression across all cell lines.

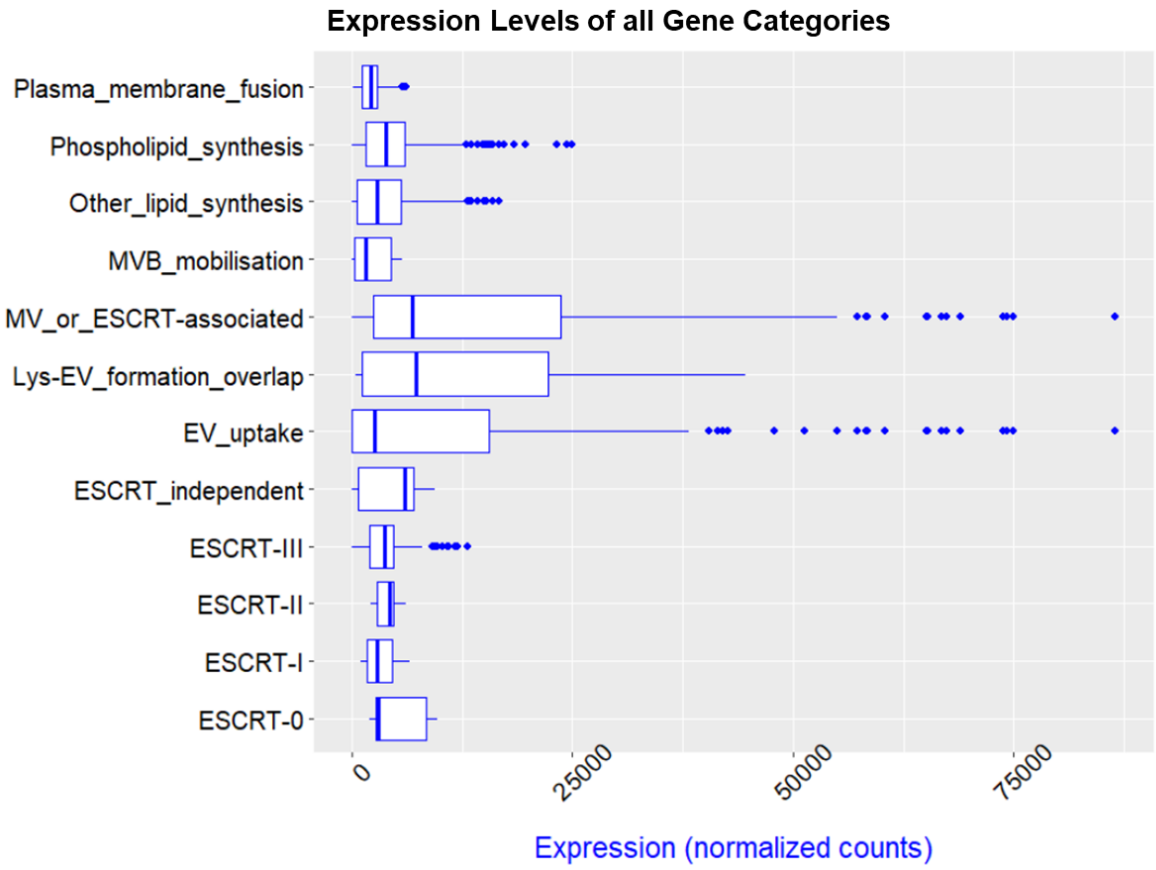

Fig 5.6 Normalised counts of mRNA transcripts of genes involved in MV Biogenesis, ESCRT pathway associated genes, Lys-EV and EV uptake amongst the most transcribed.

With the exception of genes in ESCRT-0, the ESCRT pathway categories all had low levels of expression. Instead, genes for proteins which associate with the ESCRT pathway and regulate MV biogenesis were more transcriptionally active. Likewise, genes which were used in Lys-EV had high expression. Genes involved in lipid synthesis, MVB mobilisation and ESCRT Independent biogenesis all had comparable levels of expression.

5.2.4.1 Differential Expression Analysis of EV genes

Numerous DE comparisons were carried out and are summarised in **Fig 5.7**. Four comparisons were of greatest interest. The first was a straight comparison between all producer cell lines and all non-producer cell lines. The second had GS-Null 1, GS-Null 2 and Non-X GS-Null combined as “GSNulls” in the analysis to clearly distinguish

differentially expressed genes in GSNulls from producer cell lines. The GS-Null cell lines were considered a better comparator than the Parental when attempting to understand differences in transcriptional activity of EVB genes between a mAb producer and non-producer. Although Non-X GS-Null was a stable pool and had not undergone clonal selection, it had undergone GS selection like a producer cell line. GS-Null 1 and GS-Null 2 were both clonal cell lines which had undergone both GS selection and clonal selection as a producer cell line would. Therefore, GSNulls were only distinguished from the producers by the fact they didn't secrete mAb. By contrast, the Parental did not secrete mAb and also had not undergone any of the same processes as the producers. As is seen in **Fig 5.7** (A), the Parental varied massively in terms of overall transcriptional activity to both the producers and the GSNulls. The combined "GSNulls" were then compared to each cell line for the second comparison. The third comparison combined the high qP clones (X1 and X2) and the low qP clones (X3 and X4) to see what EVB genes are differentiated between high qP, low qP and GSNulls cell lines. Lastly, as X1 and X4 had such distinguishable quantities of sEVs/ cell, they were also compared directly to each other to see if this was reflected transcriptionally.

A)

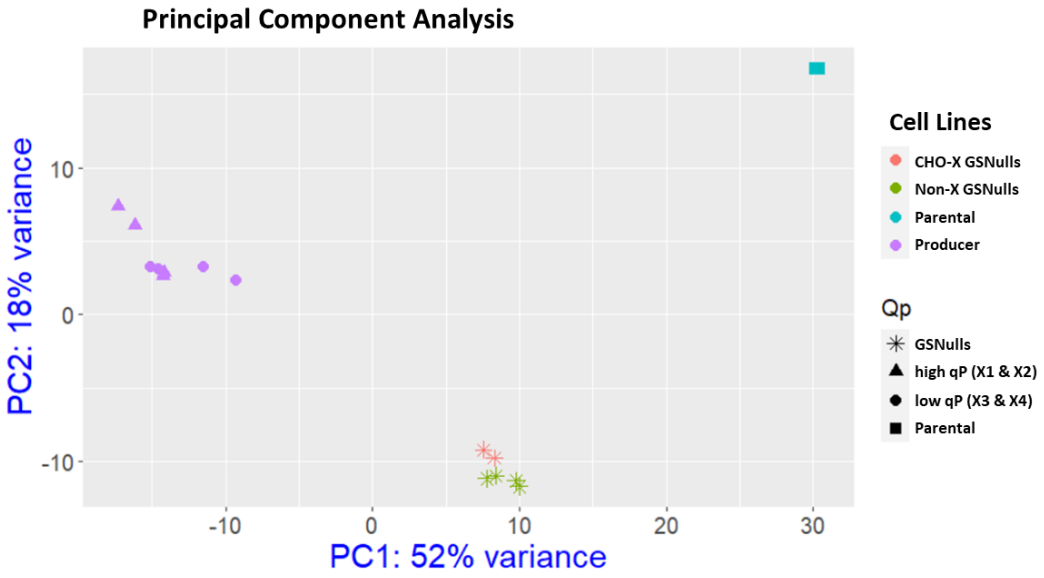
Principal Component Analysis
PC2: 18% variance
PC1: 52% variance
10
0
-10
-10
0
10
20
30
Cell Lines
CHO-X GSNulls
Non-X GSNulls
Parental
Producer
Qp
GSNulls
high qP (X1 & X2)
low qP (X3 & X4)
Parental

B)

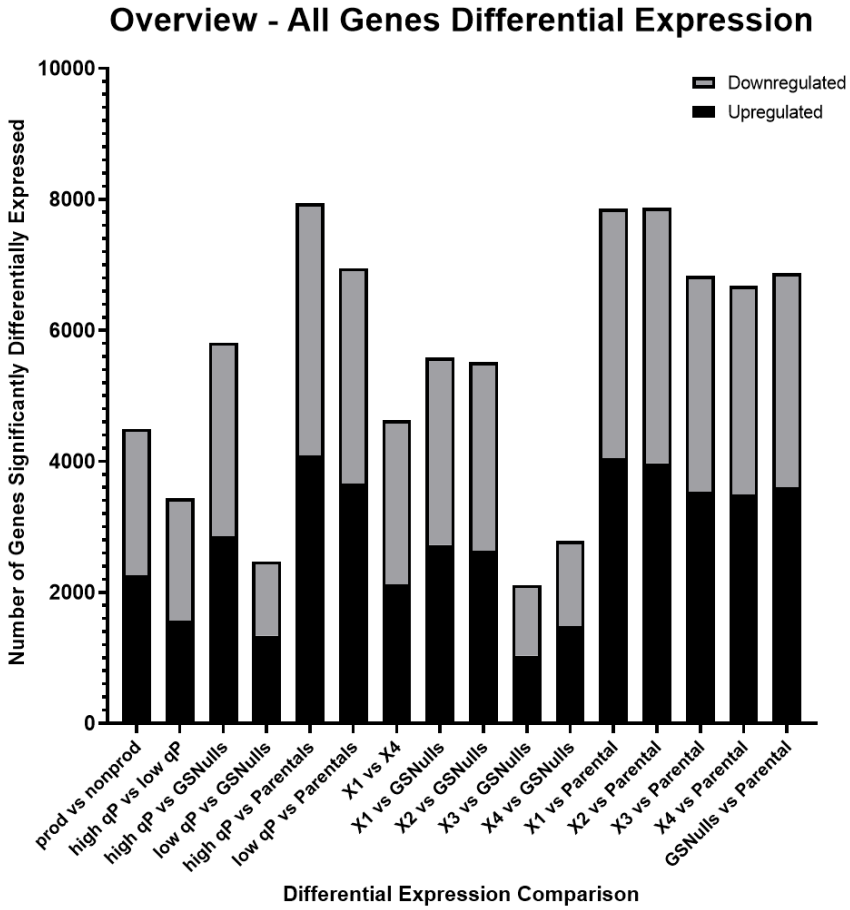
Overview - All Genes Differential Expression
Number of Genes Significantly Differentially Expressed
10000
8000
6000
4000
2000
0
Downregulated
Upregulated
prod vs nonprod
high qP vs low qP
high qP vs GSNulls
low qP vs GSNulls
high qP vs Parentals
low qP vs Parentals
X1 vs X4
X1 vs GSNulls
X2 vs GSNulls
X3 vs GSNulls
X4 vs GSNulls
X1 vs Parental
X2 vs Parental
X3 vs Parental
X4 vs Parental
GSNulls vs Parental
Differential Expression Comparison

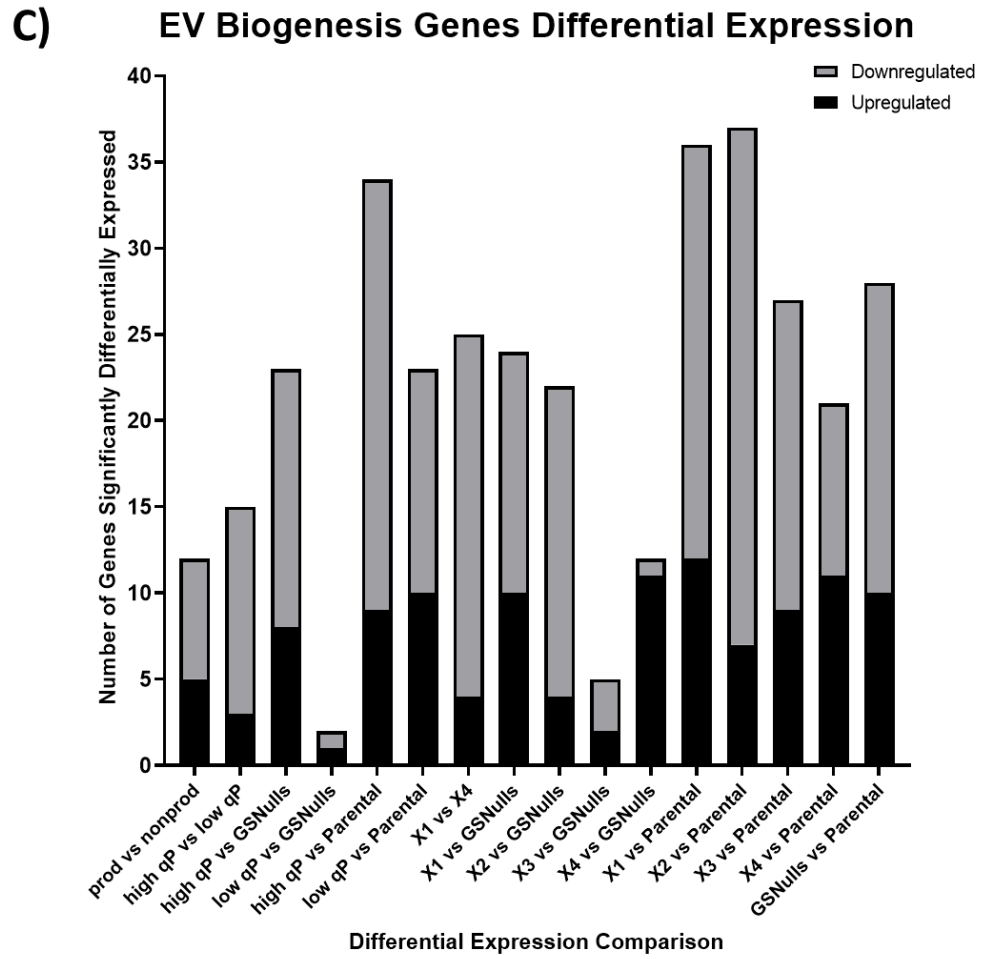

Fig 5.7 The majority of EVB genes are downregulated in high qP clones relative to GSNulls, Parental and low qP cell lines. *(A) Principal component analysis (PCA) showed the degree of variation between replicates and between cell lines. There were two replicates per cell line. (B) Shows the total number of significantly differentially expressed genes in each comparison. The prod vs nonprod comparison comprised of X1, X2, X3 and X4 combined as "prod" and GSNulls and Parental combined as "non-prod". The "high qP" consisted of X1 and X2. The "low qP" consisted of X3 and X4. (C) The number of EVB genes (excludes lipid synthesis genes) which were significantly differentially expressed in each comparison. Wald's Test used to determine statistically significant upregulated and downregulated genes with Benjamini-Hochberg correction for multiple comparisons.*

In **Fig 5.7** (B) the comparisons with the greatest number of genes with significantly different expression were those which involved the Parental cell line. The comparisons between GS-Nulls and producer cell lines then had the next greatest number of differences. Overall, there was a similar ratio of upregulated and downregulated genes for each comparison. However, for genes relating specifically to EVB in **Fig 5.7** (C), the comparisons to both the Parental and GSNulls showed EVB was mostly

downregulated. Unsurprisingly given variation seen in the principal component analysis in **Fig 5.7** (A), the greatest number of significant differences in **Fig 5.7** (C) were comparisons involving the parental cell line.

Individually, X1 and X2 had far greater differentiation to the GS-Nulls relative to X3 and X4. This was also evident when X1 and X2 were combined in the high qP comparisons and X3 and X4 combined in low qP comparisons. The high qP cell lines had more significantly differentiated genes when compared to the GSNulls than the low qP cell lines. The differentiated genes were also mostly downregulated. Both high qP and low qP cell lines, when compared to the Parental cell line, had the majority of DE EVB genes downregulated. In X1 vs X4, the majority of genes were downregulated in X1 which reflected the observed sEVs/ cell.

From the proximity of replicates to each other in **Fig 5.7** (A), there was little between replicates from each cell line. There was also low variation between the CHO-X GS-Nulls and Non-X GS-Null. However, there was some variation amongst the producer cell lines. Yet the largest variation existed between the three groupings of producers, GSNulls and the Parental cell line.

As the overall summary revealed that high qP clones had several EVB genes differentially expressed relative to low qP clones and GSNulls, the EVB were broken down into their different gene categories. This would reveal if a particular category had a greater proportion of genes upregulated or downregulated.

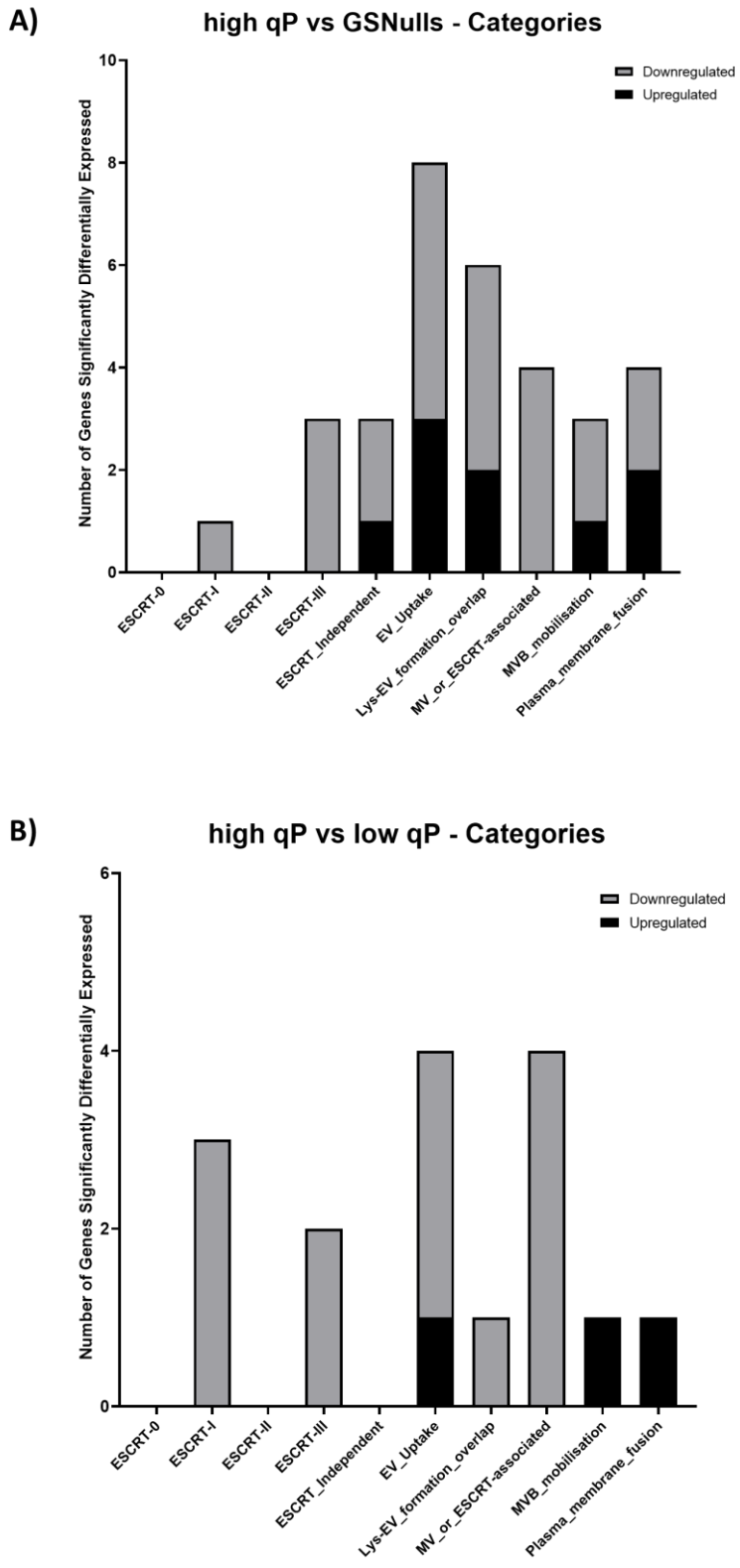

Fig 5.8 ESCRT-I, ESCRT-II, EV Uptake, Lys-EV formation overlap and MV and ESCRT-associated genes downregulated in high qP clones in comparisons with GS-Nulls and low qP clones. *(A) high qP vs GSNulls comparison. (B) low qP vs GSNulls comparison.*

The ESCRT-I and ESCRT-III categories were downregulated in both high qP and low qP cell lines relative to GSNulls. As too were MV and ESCRT associated genes along with EV Uptake genes. A difference between the two comparisons is how Lys-EV had six differentially expressed genes in the high qP vs GSNulls yet only one gene had significantly altered transcription in the high qP vs low qP.

The log of the normalised counts of the genes in each category were plotted. This was to see which individual EVB genes were significantly upregulated or downregulated. Significant DE was denoted in the following comparisons: GSNulls vs Parental, prod vs nonprod, high qP vs GSNulls, high qP vs Parental, low qP vs GSNulls, low qP vs Parental, high qP vs low qP and X1 vs X4.

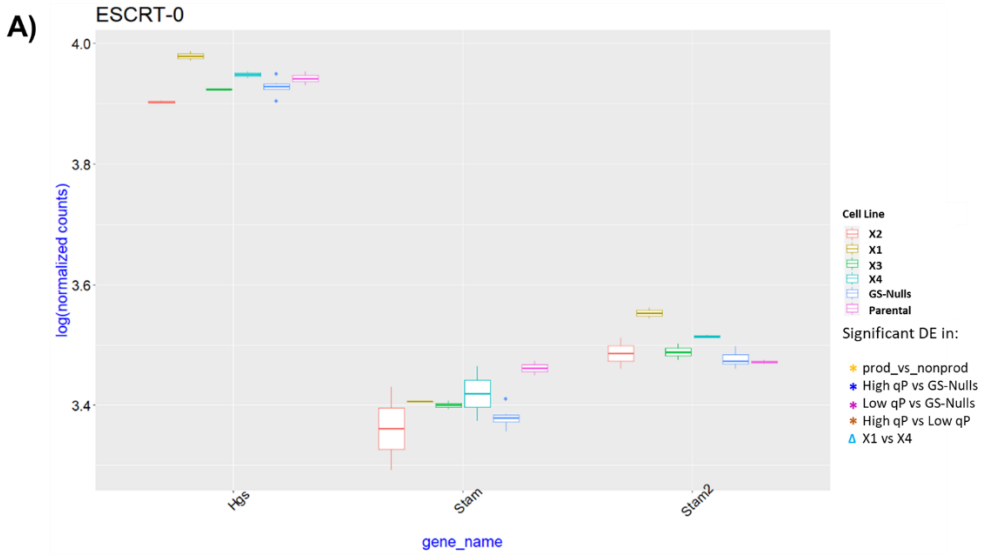
A)
ESCRT-0
log(normalized counts)
4.0
3.8
3.6
3.4
Hgs
Stam
Stam2
gene_name
Cell Line
X2
X1
X3
X4
GS-Nulls
Parental
Significant DE in:
prod_vs_nonprod
High qP vs GS-Nulls
Low qP vs GS-Nulls
High qP vs Low qP
X1 vs X4

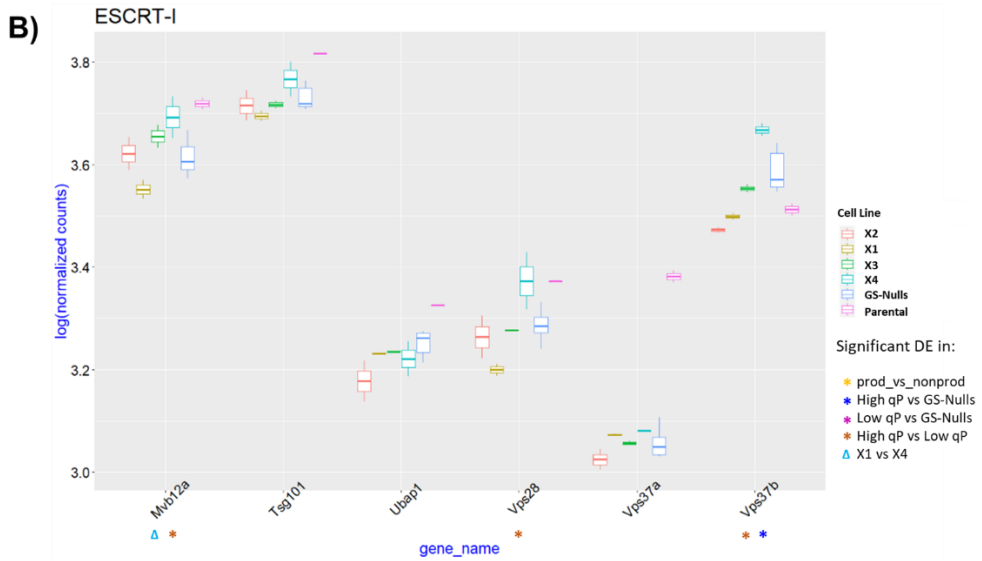
B)
ESCRT-I
log(normalized counts)
3.8
3.6
3.4
3.2
3.0
Mvb12a
Tsg101
Ubap1
Vps28
Vps37a
Vps37b
gene_name
Cell Line
X2
X1
X3
X4
GS-Nulls
Parental
Significant DE in:
prod_vs_nonprod
High qP vs GS-Nulls
Low qP vs GS-Nulls
High qP vs Low qP
X1 vs X4

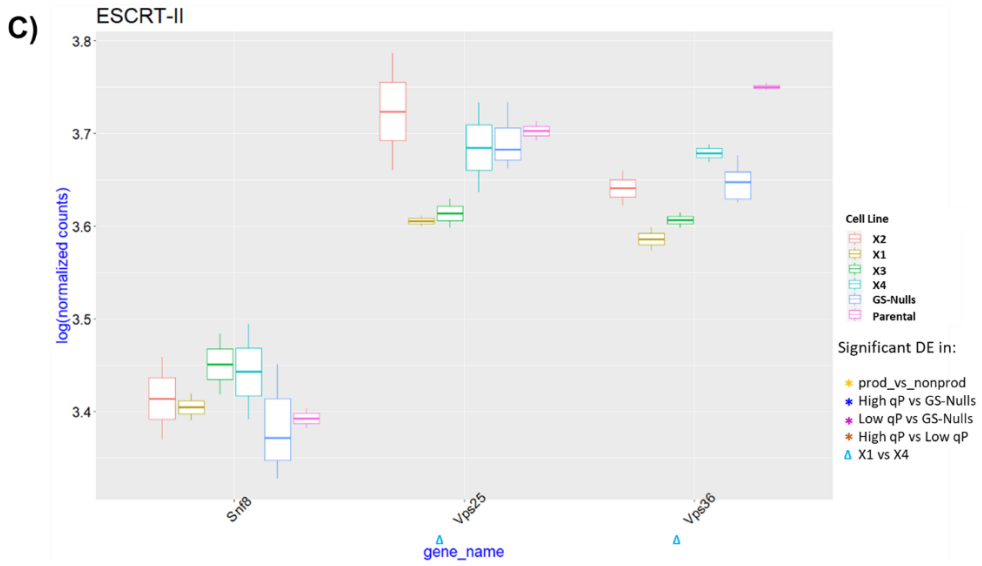
C)
ESCRT-II
log(normalized counts)
3.8
3.7
3.6
3.5
3.4
Snf8
Vps25
Vps36
gene_name
Cell Line
X2
X1
X3
X4
GS-Nulls
Parental
Significant DE in:
prod_vs_nonprod
High qP vs GS-Nulls
Low qP vs GS-Nulls
High qP vs Low qP
X1 vs X4

D)

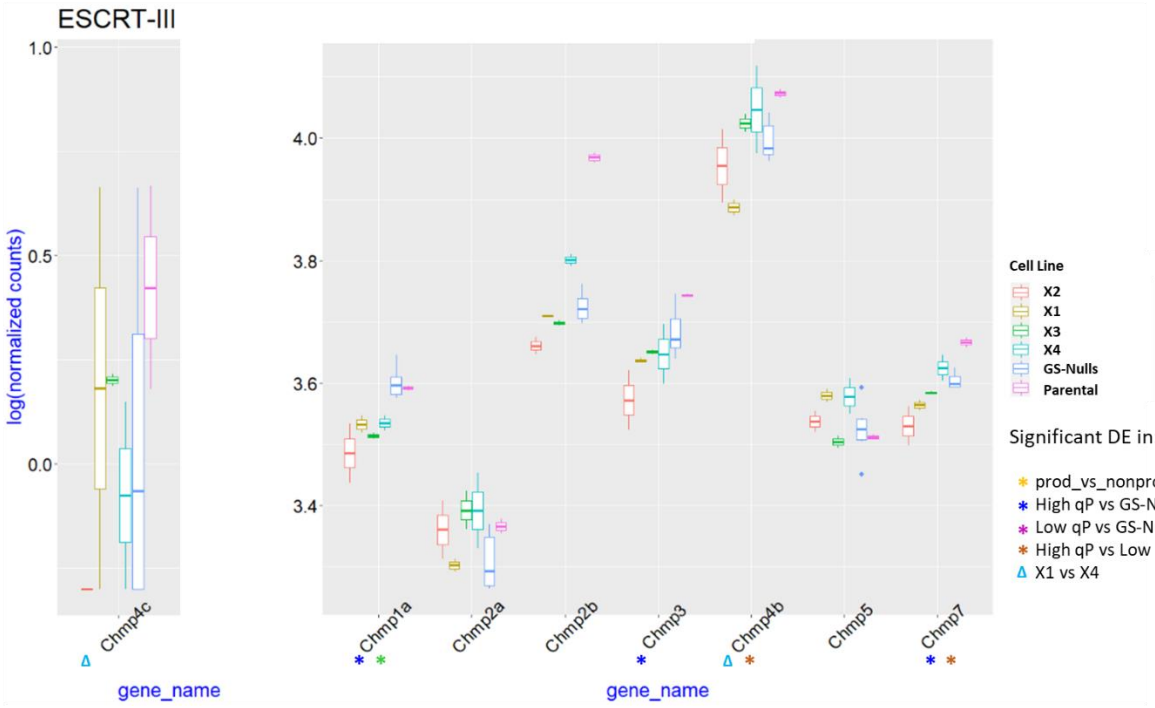
ESCRT-III
log(normalized counts)
1.0
0.5
0.0
4.0
3.8
3.6
3.4
Chmp4c
Chmp1a
Chmp2a
Chmp2b
Chmp3
Chmp4b
Chmp5
Chmp7
gene_name
gene_name
Cell Line
X2
X1
X3
X4
GS-Nulls
Parental
Significant DE in:
prod_vs_nonprod
High qP vs GS-Nulls
Low qP vs GS-Nulls
High qP vs Low qP
X1 vs X4

E)

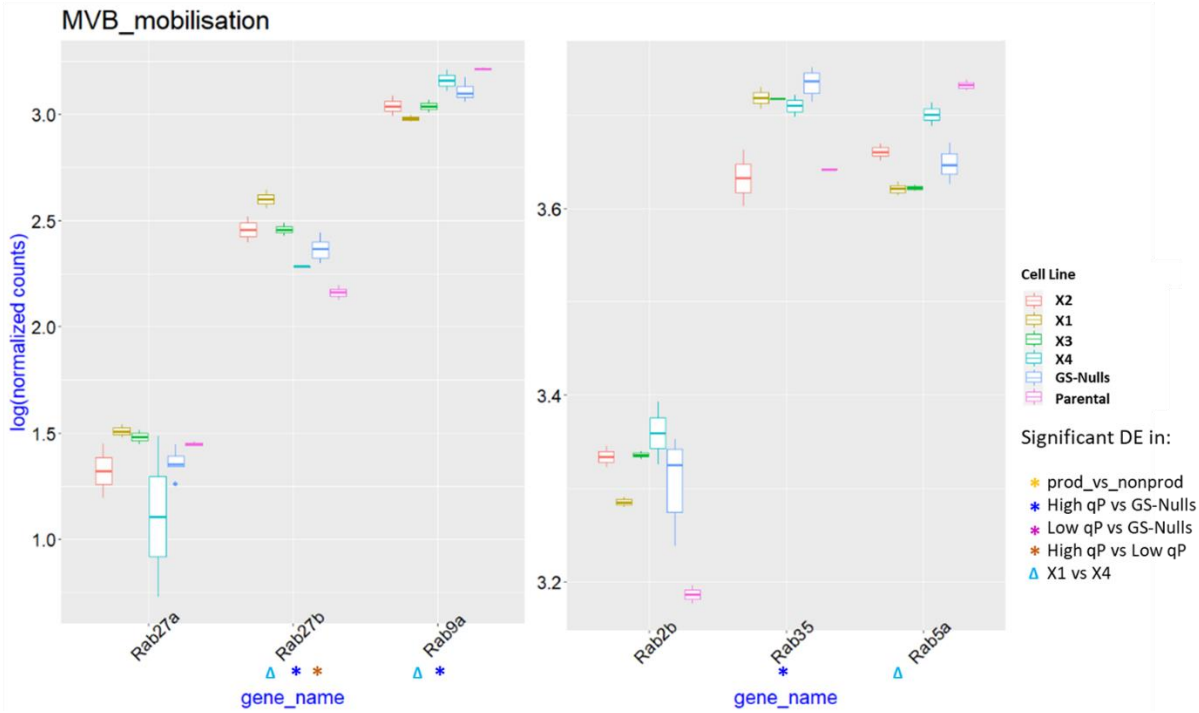
MVB_mobilisation
log(normalized counts)
3.0
2.5
2.0
1.5
1.0
3.6
3.4
3.2
Rab27a
Rab27b
Rab9a
Rab2b
Rab35
Rab5a
gene_name
gene_name
Cell Line
X2
X1
X3
X4
GS-Nulls
Parental
Significant DE in:
prod_vs_nonprod
High qP vs GS-Nulls
Low qP vs GS-Nulls
High qP vs Low qP
X1 vs X4

F)

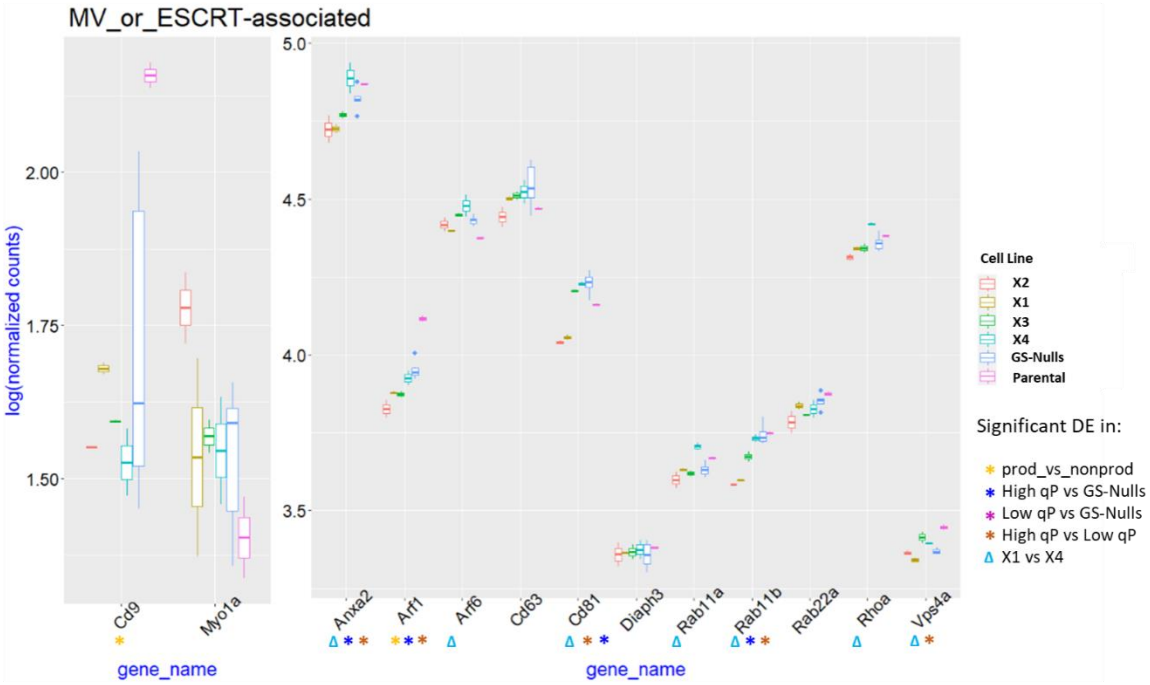
MV_or_ESCRT-associated
log(normalized counts)
2.00
1.75
1.50
5.0
4.5
4.0
3.5
Cd9
Myo1a
Anxa2
Arf1
Arf6
Cd63
Cd81
Diaph3
Rab11a
Rab11b
Rab22a
Rhoa
Vps4a
gene_name
gene_name
Cell Line
X2
X1
X3
X4
GS-Nulls
Parental
Significant DE in:
prod_vs_nonprod
High qP vs GS-Nulls
Low qP vs GS-Nulls
High qP vs Low qP
X1 vs X4

G)

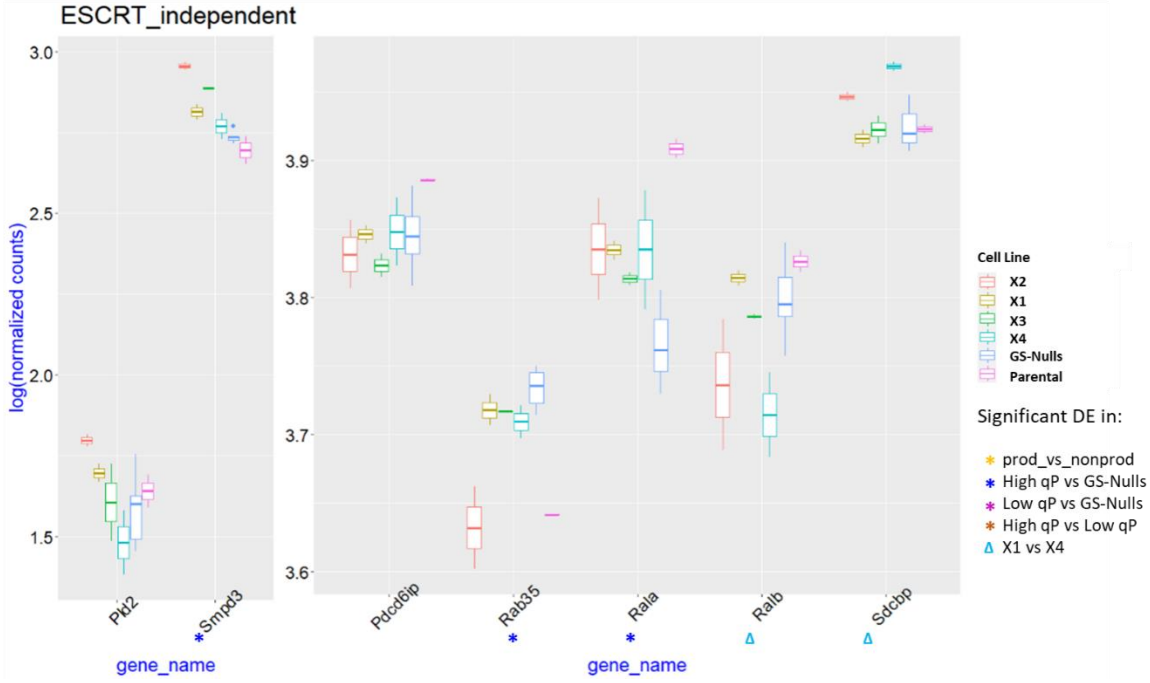
ESCRT_independent
log(normalized counts)
3.0
2.5
2.0
1.5
3.9
3.8
3.7
3.6
Pkl2
Smpd3
Pdcd6ip
Rab35
Ral a
Ralb
Sdcbp
gene_name
gene_name
Cell Line
X2
X1
X3
X4
GS-Nulls
Parental
Significant DE in:
prod_vs_nonprod
High qP vs GS-Nulls
Low qP vs GS-Nulls
High qP vs Low qP
X1 vs X4

H)

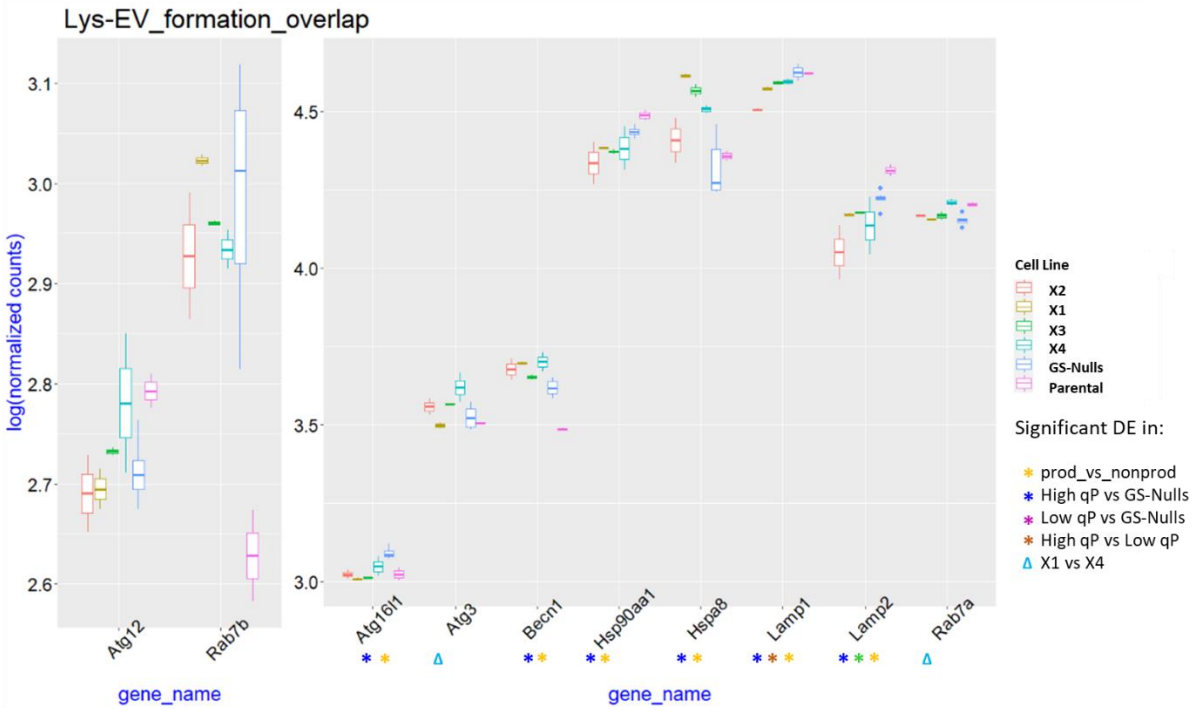
Lys-EV_formation_overlap
log(normalized counts)
3.1
3.0
2.9
2.8
2.7
2.6
Atg12
Rab7b
gene_name
4.5
4.0
3.5
3.0
Atg16l1
Atg3
Becn1
Hsp90aa1
Hspa8
Lamp1
Lamp2
Rab7a
gene_name
Cell Line
X2
X1
X3
X4
GS-Nulls
Parental
Significant DE in:
prod_vs_nonprod
High qP vs GS-Nulls
Low qP vs GS-Nulls
High qP vs Low qP
X1 vs X4

I)

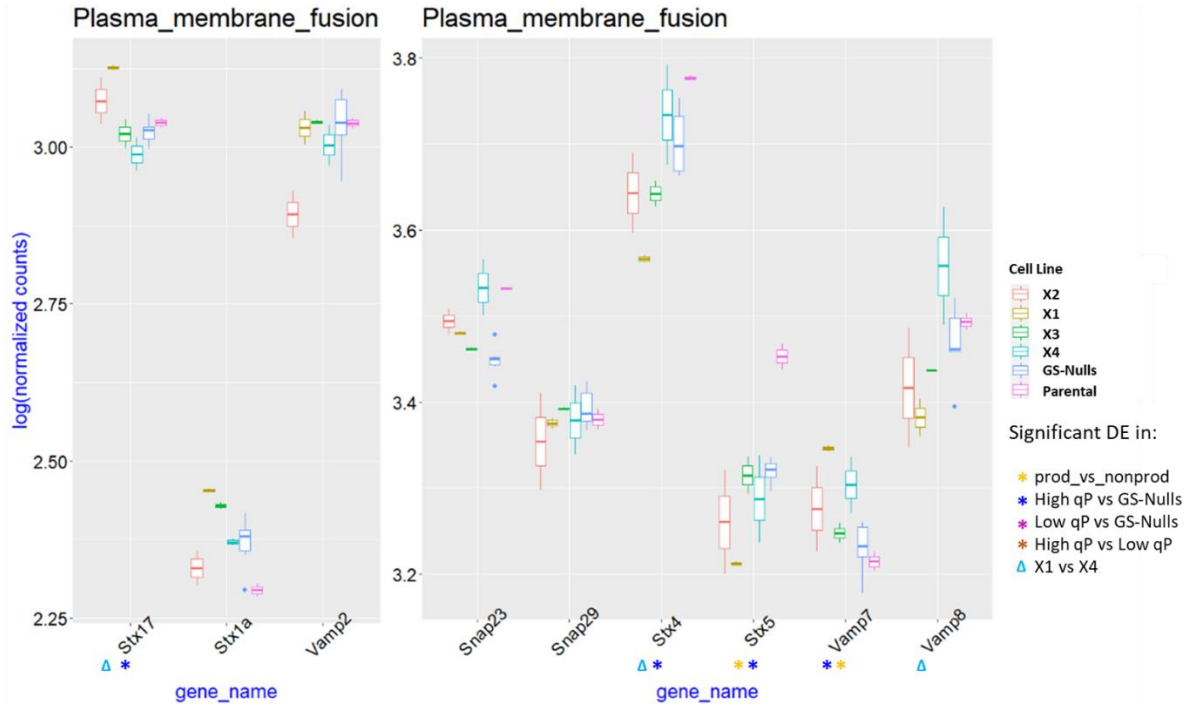
Plasma_membrane_fusion
log(normalized counts)
3.00
2.75
2.50
2.25
Stx17
Stx1a
Vamp2
gene_name
Plasma_membrane_fusion
3.8
3.6
3.4
3.2
Snap23
Snap29
Stx4
Stx5
Vamp7
Vamp8
gene_name
Cell Line
X2
X1
X3
X4
GS-Nulls
Parental
Significant DE in:
prod_vs_nonprod
High qP vs GS-Nulls
Low qP vs GS-Nulls
High qP vs Low qP
X1 vs X4

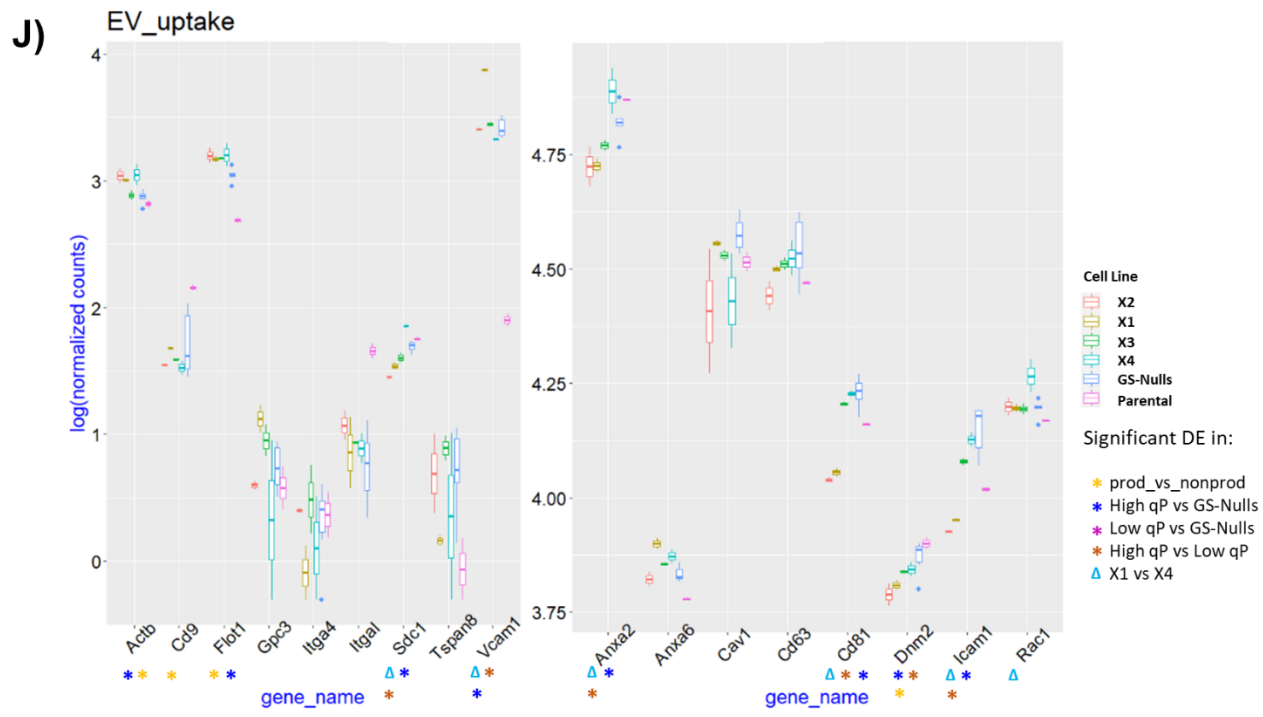

Fig 5.9 Normalised log counts of the genes in each category showed which genes in each category were differentially expressed. *(A) ESCRT-0. (B) ESCRT-I. (C) ESCRT-II. (D) ESCRT-III. (E) MVB mobilisation. (F) MV or ESCRT-associated genes. (G) ESCRT-independent. (H) Lys-EV formation overlap. (I) Plasma membrane fusion. (J) EV uptake. Wald's Test used to determine statistically significant upregulated and downregulated genes with Benjamini-Hochberg correction for multiple comparisons.*

In ESCRT-I, Mvb12a and Vps28 were downregulated in high qP cell lines relative to low qP cell lines. Vps37b was downregulated in high qP cell lines compared to both GSNulls and low qP cell lines. ESCRT-III had Chmp1a and Chmp3 downregulated in high qP cell lines compared to GSNulls whilst Chmp4b was downregulated only relative to low qP cell lines. Chmp7 was also significantly lower in high qP cell lines for both comparisons. In MVB mobilisation genes, Rab27b was upregulated in high qP cell lines compared to both low qP and GSNulls. However, Rab35 and Rab9a were downregulated relative to GSNulls. MV or ESCRT-associated had numerous genes which were downregulated in both high qP cell lines vs GSNulls and high qP cell lines vs low qP cell lines. These were Anxa2, Arf1, CD81 and Rab11b. Vps4a was also downregulated in high qP cell lines when compared to low qP cell lines. ESCRT independent genes had Rab35 downregulated and Rala upregulated in high qP clones compared to GSNulls. For Lys-EV, Atg16l1, Lamp1 and Lamp2 were downregulated

whereas Becn1, Hsp90aa1 and Hspa8 were upregulated in the high qP vs GSNulls comparison. Lamp1 was also downregulated in high qP cell lines relative to low qP cell lines. Stx4 and Stx5 were downregulated whilst Stx17 and Vamp7 were upregulated in high qP cell lines compared to GSNulls in Plasma membrane fusion genes. The EV uptake genes had Actb, Flot1 and Vcam1 upregulated and Sdc1, Anxa2, CD81, Dnm2 and Icam1 downregulated in high qP cell lines compared to GSNulls. Sdc1, Anxa2, CD81 and Icam1 were also downregulated in the high qP cell lines relative to low qP cell lines. Vcam was upregulated relative to the low qP clones. With the exception of Rab27b, Ralb, Stx17 and Vcam1, X1 was downregulated compared to X4 in its transcriptional activity for every EVB gene where there was significant DE. This aligned with the physically observed quantities of sEVs/ cell which confirmed that the transcriptional analysis was reflective physical measurements. The exception to this being the parental cell line which was upregulated in EVB gene expression in the majority of comparisons to other cell lines. When GSNulls and the Parental are combined and compared to all the producers combined in the prod_vs_nonprod, Actb, Flot1, Rab27b, Smpd3 and Vamp7 are all upregulated in the producers. The downregulated genes in this comparison were Cd9, Dnm2 and Stx5.

5.2.4.2 DE analysis of genes involved in lipid synthesis

The observation that high qP cell lines had reduced transcriptional activity for genes involved in EVB raised the question as to whether this was unique to EVB or if other pathways showed similar downregulation. In particular, pathways which have the potential to impact EV secretion such as lipid synthesis. EVs are lipid bilayer bound particles and lipid is therefore a major component in their composition. It would be expected that a decrease in lipid synthesis would have a knock on effect on EVB as one of the key biological building blocks would be less abundant for this process.

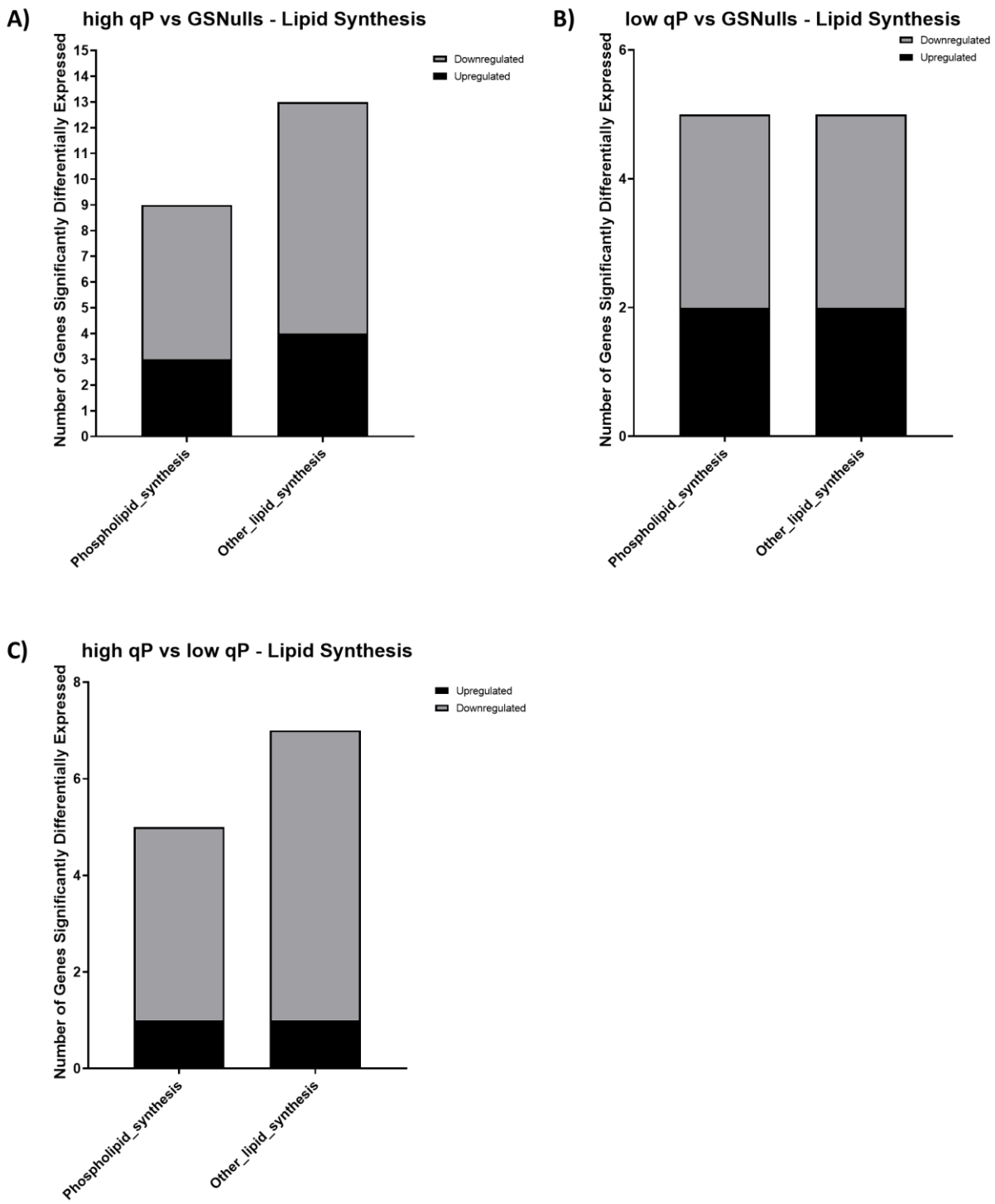

Fig 5.10 Several genes involved in lipid synthesis downregulated in high qP cell lines relative to GSNulls and low qP cell lines. *(A) DE analysis revealed that high qP clones had 6 significantly downregulated phospholipid synthesis genes (Agpat4, Cdipt, Fasn, Pcyt1a, Pcyt2, Pisd) and 3 upregulated genes (Chka, Chpt1 and Etnk1). 9 genes involved in the synthesis of other lipids when compared to GSNulls were downregulated (Cers1, Srebf, Cdipt, Hmgcr, Pcyt1a, Pld3, Ptpmt1, Scap and Pisd) and 4 were upregulated (Chka, Chpt1, Etnk1 and Sgms1). (B) Whilst low qP clones had less DE, there were 3 phospholipid synthesis genes downregulated (Agpat4, Fasn and Pcyt2) and 2 upregulated (Chka and Chpt1). Other lipid synthesis genes also had 3 downregulated (Hmgcr, Pcyt2,*

Pld3) and 2 upregulated (Chka and Chpt1). (C) In the case of high qP cell lines vs low qP cell lines, there were 4 genes downregulated (Agpat4, Cdipt, Pemt and Pisd) and 1 upregulated (Etnk1). For genes involved in other lipid synthesis, 6 were downregulated (Pemt, Cdipt, Pisd, Pld3, Scap and Srebf1) and 1 was upregulated (Etnk1).

DE analysis showed that for lipid synthesis genes, where significant DE was found, it was mostly downregulation of transcriptional activity. There was a large overlap in the genes involved in both phospholipid synthesis and that of other lipids. The majority of those genes downregulated were those which synthesised multiple types of lipid. This suggested that high qP cell lines had lipid synthesis downregulated overall when compared to GSNulls and low qP cell lines. Again this downregulation in lipid synthesis transcriptional activity had a similar pattern to the physical counts of sEVs/ cell. The high qP cell lines had a greater number of downregulated genes compared to GSNulls than low qP cell lines. Of the genes which were downregulated in both the high qP vs GSNulls and low qP vs GSNulls comparisons, Agpat4, Fasn and Pcyt2 were common to both. For the genes that were upregulated in both comparisons, Chka and Chpt1 were significantly differentially expressed.

5.3 Discussion

The sEV counts by both NTA and NanoAnalyzer showed that the number of sEVs/ cell is negatively correlated with the ability of the cell to secrete mAb. The cell line development process also has an impact on EV secretion. GS selection alone of a cell line appeared to increase the number of sEVs/ cell with respect to the CHO-X Parental. The cell line with greater GS expression as ranked by Lonza, GS-Null 1, had a higher NTA and NanoAnalyzer measurement of sEVs/ cell than GS-Null 2. However, this higher count was not significant and was also comparable to the Non-X GS-Null cell lines; a stable pool. This indicated that the level of GS expression was not a determinant of EV secretion but rather that the adaption to glutamine depleted media selected for cells which had higher sEVs/ cell counts than their parental cell line.

It was notable that X1’s sEVs/ cell was comparable to the Parental in both the NTA and NanoAnalyzer analysis. This would suggest the selection process which finds the

strongest producing cell line may actually isolate clones which could adapt to GS selection without the need to increase their sEV production. It also suggests that EVB has limited utility to the cell and may potentially sequester cellular resources from mAb production. No trait other than qP correlated with a cell line's sEVs/ cell with the exemption of IVCD which had a small positive correlation with EV secretion. This is perhaps to be expected given that cell growth is negatively correlated with qP (Torres and Dickson, 2022). Thus cells which have a high sEVs/ cell are also likely to have a large accumulation of biomass.

A caveat to this analysis was that it was not possible to sample sEVs from peak viable cell density of the fed-batch to determine if the relative quantities of sEVs/ cell for each cell line stayed consistent as the fed-batch progressed. None the less, it did suggest that sEV count in early fed-batch can be an indicator of a cell line's productivity even at late stage fed-batch as Day 10 qP had a negative correlation with Day 5 sEVs/ cell.

Another observation was the increased quantity of sEVs/ ml obtained using the Lonza fed-batch system rather than CD-CHO / Efficient Feed B system. Whilst CHO-A or GSKO-Host were not grown in the Lonza system to enable a straight comparison, it is likely the industrial manufacturing optimised base and feed medias, along with regular glucose replenishment, enabled the cells to increase sEV secretion. For instance, high glucose is known to increase EV secretion (da Silva Novaes *et al.*, 2019). The finding that all EV samples had at least 90% of particles CFSE-positive confirms that was being counted were intact sEVs; rather than lipid debris or co-isolates.

The transcriptomic analysis of EVB genes showed that they were mostly downregulated in high qP cell lines compared to low qP cell lines. This was unsurprising given that sEVs/ cell measurements appeared lower in X1 and X2 than in X3 and X4; especially in the NanoAnalyzer analysis. X2 had a similar quantity of sEVs/ cell in the NTA analysis to all the GS-Null cell lines whilst it had a comparable quantity of sEVs/ cell to GS-Null 2 and Non-X GS-Null and was lower than GS-Null 1 in the NanoAnalyzer analysis. X1 appeared lower than GS-Null 1 and Non-X GS-Null in the NTA analysis and all of the GS-Null cell lines in the NanoAnalyser analysis. At odds with this trend of transcriptomic analysis reflecting lower sEV counts was the sEVs/ cell for the Parental. This had the lowest count in both the NTA and NanoAnalyser analysis despite having higher EVB transcriptional activity in every

comparison. However, as previously stated, the large genetic variation from both the producer cell lines and the GS-Null cell lines creates the possibility that there could be other factors which impact EV secretion in the Parental not captured in this study.

ESCRT-I and ESCRT-II had genes downregulated in the high qP clones when compared to low qP and GSNulls. This in itself could account for the lower sEVs/ cell observed as the ESCRT pathway is the classical mode of EV biogenesis for the cell described in literature. Similarly, genes involved in MV biogenesis or are ESCRT-associated were also downregulated. There were no significantly upregulated genes in any of these categories.

The DE observed in high qP cell lines for Lys-EV compared to GSNulls is difficult to account for. Autophagy has been found to be upregulated in strong producer cell lines as increased lysosomal degradation promotes cell survival (Kim *et al.*, 2013). This is at odds with the downregulation observed here. However, Beclin-1 (Becn1) and Heat Shock Protein 70 (Hspa8) were upregulated in the high qP cell lines. Beclin-1 in particular has been reported to be a key regulator of autophagy which may mean autophagy is still upregulated in the high qP cell lines even though other, less impactful, genes are downregulated (Kang *et al.*, 2011).

For genes dictating MVB fusion with the plasma membrane, it is surprising to see syntaxin-4 (Stx4), syntaxin-5 (Stx5) and Vamp7 downregulated in high qP cell lines compared to GSNulls and low qP cell lines. Whilst this further accounts for the decrease in sEVs/ cell, one would expect members the cell's protein secretory pathways to be upregulated in strong producer cell lines. Yet it was noted that Syntaxin-17 (Stx17) was upregulated compared to GSNulls and contributes to protein secretion in the cell (Pérez-Rodriguez *et al.*, 2021).

The reduced transcriptional activity of genes utilised for EV uptake from the extracellular environment in high qP cell lines, if interpreted as genes with solely uptake functionality, is difficult to reconcile with the EV counts. One would expect reduced capability to take in EVs from the extracellular environment to be reflected in higher sEV accumulation in the culture. Yet this was not the case. What is more likely is that these genes serve dual functionality in both EV secretion and uptake. The EV Uptake genes which were downregulated in high qP cell lines compared to GSNulls were Syndecan 1 (Sdc1), Annexin A2 (Anxa2), CD81, Dynamin 2 (Dnm2) and

Intercellular Adhesion Molecule 1 (Icam1). Of these, CD81 is a constituent of the EV membrane whilst Syndecan 1 and Annexin A2 are both present in EVs and have a role in recruiting miRNAs to EVs (Hagiwara *et al.*, 2015b; Parimon *et al.*, 2018). With the exception of Dnm2, all of the genes were also downregulated when compared to low qP cell lines. Thus the impact of these genes being less transcriptionally active in high qP cell lines is as likely to be manifested in lower EV secretion as it is EV Uptake. For the upregulated uptake genes in the high qP vs GSNulls comparison, there was: ß-Actin (Actb), Flotilin 1 (Flot1) and Vascular Cell Adhesion molecule 1 (Vcam1). Vcam1 was also upregulated in high qP cell lines compared to low qP cell lines. Their upregulation may be explained by these genes all having other functions in the cell. Actb has a role in modulating the cell cycle (Bunnell *et al.*, 2011). Flot1 is involved in cytoskeletal organisation (Hu *et al.*, 2021). Vcam1 also has functionality in cell adhesion (Kong *et al.*, 2018).

In summary, sEV secretion was downregulated in high qP CHO cell lines. This was evident with both physical counts and transcriptomic analysis of genes involved in EVB. This finding suggests that high qP cells sequester resources from EVB to facilitate higher mAb secretion. The same can be hypothesised for lipid biogenesis being downregulated in high qP cell lines. Yet possible pathways for which EV secretion and product secretion overlap remain obscure. The genes identified in both protein secretion and EV secretion in the Plasma Membrane fusion category, Stx4, Stx5 and Vamp7 were downregulated. It is unknown if high qP cell lines having downregulated EVB is a product specific observation or if the same is true of cell lines secreting other products/ types of product. Likewise, low qP cell lines should be investigated to determine if extremely high quantities of EV secretion can be an indicator of poor productivity across multiple products. With respect to downstream bioprocessing, both 4.2.3. and the analysis on genes involved in MV biogenesis indicate that sEV secretion correlates with lEV correlation in CHO. This increased lipid content in the extracellular environment is potentially a consideration for product purification. Particularly in the case of lEVs which range from 100 – 1000nm. Given that downstream bioprocessing ranges from 50-80% of the total manufacturing costs, it would be preferable to choose a cell line which contributes less lipid to the culture environment (Boodhoo *et al.*, 2022). An extracellular environment less abundant in

host cell lipid is also likely to benefit product quality as it would mean fewer possible interactions for the product.

Chapter 6

Utilising sEVs to Improve Low Density CHO Cell Growth and CHO Cloning Efficiency

6.1 Introduction

CHO sEVs were next investigated to determine if they could be used as tools in cell engineering. This was done in two ways. The first being supplementation of CHO cell cultures to see if sEVs could be used as media components to promote cell growth. The second looked at whether sEVs could promote either the survival or growth of single cell clones post sorting by flow cytometry.

6.1.1 sEVs to Promote Cell Growth

There is little literature which discusses the functional utility of sEVs. In terms of influencing culture density. Takagi *et al.* (2021) described how a polymer fraction of particles greater than 10 kDa and fewer than 220nm in size could promote growth in batch culture. They detected sEVs in this fraction by NTA and CD81 ELISA. Strangely, however, sub fractionation of the polymer fraction to two groups containing particles between 10 kDa and 100 kDa and one containing particles greater than 100 kDa but smaller than 220nm removed this growth boosting effect. The CD81 was also not detectable in the sub-fractions. Therefore, it's inconclusive whether the growth boosting effect was due to sEVs or another agent present in the polymer fraction. Of the biological processes identified in 3.2.5.2, both positive and negative regulation of cell proliferation were amongst gene sets most targeted. Further investigation is needed with sEVs that have been isolated by a more standardised EV purification protocol such as UC. If sEVs can be used to augment cell growth, they could be

considered as potential additives to media. In this chapter, sEVs were taken from Day 5 of fed-batch/ exponential phase; a stage of fed-batch in which the cell density increases rapidly. These EVs were assessed for their ability to influence growth of low density cell cultures through supplementation.

6.1.2 sEVs to Improve Cloning Efficiency

Of the possible functions of the miRNAs identified in 3.5.2.2, genes involved in apoptosis and genes which promote apoptosis were amongst those most targeted. In addition to these, several genes involved in protein phosphorylation and signal transduction were also targeted. There was also the clear observation that depletion of sEVs from fed-batch culture caused viability to decline at a quicker rate. This raised the question as to how significant are the various communication stimuli exchanged between cells in general in promoting growth and survival. Especially in the context of single cell cloning – a critical part of cell line development.

Typically, when generating a stable producing cell line, cells are transfected and then exposed to a selection agent to identify cells which have the mAb product gene and the selection marker stably incorporated into their genome. This gives a heterogeneous pool of stable producing cells which all have varying abilities to produce the mAb product. For both consistency in mAb titre obtained and a more uniform product quality, single cells are taken from these pools and sorted to wells to generate monoclonal populations (Noh, Shin and Lee, 2018; Weinguny *et al.*, 2020). Post sorting, several of these clones do not grow. The number of clones in a plate which survive sorting to a well and form outgrowths, often termed “cloning efficiency”, can often be very low and is influenced by several factors. This includes the innate ability of the cell to grow as an isolated clone, the media the clone is grown in and the method used to isolate the clone. For instance, different cloning methods such as limiting dilution has a cloning efficiency of 5.7% whilst flow cytometry and commercial sorting platforms like the Beacon Platform are 11% and 52% respectively (Le *et al.*, 2019).

Studies have looked to improve cloning efficiency by using directed evolution where host cells are put through multiple rounds of the sorting process to isolate clones which

have a greater innate ability to become clonal outgrowths post sorting (Weinguny *et al.*, 2020). Others have identified protein growth factors secreted by cells and supplemented them to the media the clones were grown in (Lim *et al.*, 2013). There are also biologically derived additives not natively expressed by the cell which be added to the cloning media (Zhu *et al.*, 2012). It is well known that adding serum and cell culture supernatant/ spent media/ conditioned media to the cloning media can give high cloning efficiency (Zhu *et al.*, 2012; Lim *et al.*, 2013; Kim *et al.*, 2020). However, regulatory bodies disapprove of the use of these as they are not chemically defined and can be potential sources of contamination (Ho *et al.*, 2021). Yet no consideration has been given to purified sEVs which are a natural vector of autocrine signalling secreted by the cell. Furthermore, sEVs are high in quantity both in serum and, as seen in previous chapters, cell culture supernatant (Shelke *et al.*, 2014; Zhao *et al.*, 2020). It is possible that sEVs carry some of the clonal outgrowth stimulation observed in both serum and conditioned media. They have also been shown to prevent cell death suggesting they could provide pro-survival stimuli to the lone cell post sorting (Han and Rhee, 2018). Thus their ability to improve cloning efficiency was investigated in this chapter.

6.1.3 Chapter Summary

Low density CHO-A cells cultures were supplemented with Day 5 fed-batch sEVs. Cells were sorted to 96-well plates by flow cytometry and incubated for 72 hours. The growth was then measured by PrestoBlue assay. The sEVs were also investigated for their ability to promote single cell clone outgrowth post sorting by flow cytometry. This involved sorting the cells to 96-well plates containing media that was supplemented with sEVs. After a 14-day incubation, the number of clonal outgrowths was measured by Clone Select Imager to determine if sEVs increased the number of clonal outgrowths.

6.1.4 Chapter Aims

- Supplement low density cell cultures with sEVs to enhance their growth

- Supplement single cell clones with sEVs to maintain clone survival and outgrowth post sorting by flow cytometry.

6.2 Results

6.2.1 Setting up PrestoBlue Standard Curve to Measure Low Density Cell Growth

To determine what impact sEVs may have on cell growth, low density cell cultures were set-up in 96-well plates. The 96-well format was chosen because high concentrations of sEVs could be added to each well. As was seen in 3.2.6., simply doubling the number of sEVs that can be pelleted at 100,000g at a given time-point in culture didn't affect a high density cell culture's VCD or viability. There was also the observation that different cell lines can have far higher numbers of EVs/ cell than other cell lines and therefore have different thresholds of signaling from sEVs. Thus it was necessary to test as many sEVs per cell as possible. However, the challenge with measuring growth in low density cell cultures was finding a method that was sensitive to such low cell concentrations but also high throughput. PrestoBlue, which detects cell concentration by measuring the metabolic activity in a well, was chosen. For this assay, it was necessary to determine the correct incubation time for which it would be sensitive to changes in the cell concentration at the culture density that was to be treated with sEVs. Standard curves were generated with the following concentrations of CHO-A cells: 0 cells/ ml, 6,250 cells/ ml, 12,500 cells/ ml, 25,000 cells/ ml, 50,000 cells/ ml, 100,000 cells/ ml and 200,000 cells/ ml. These were incubated at 37°C for varying lengths of time.

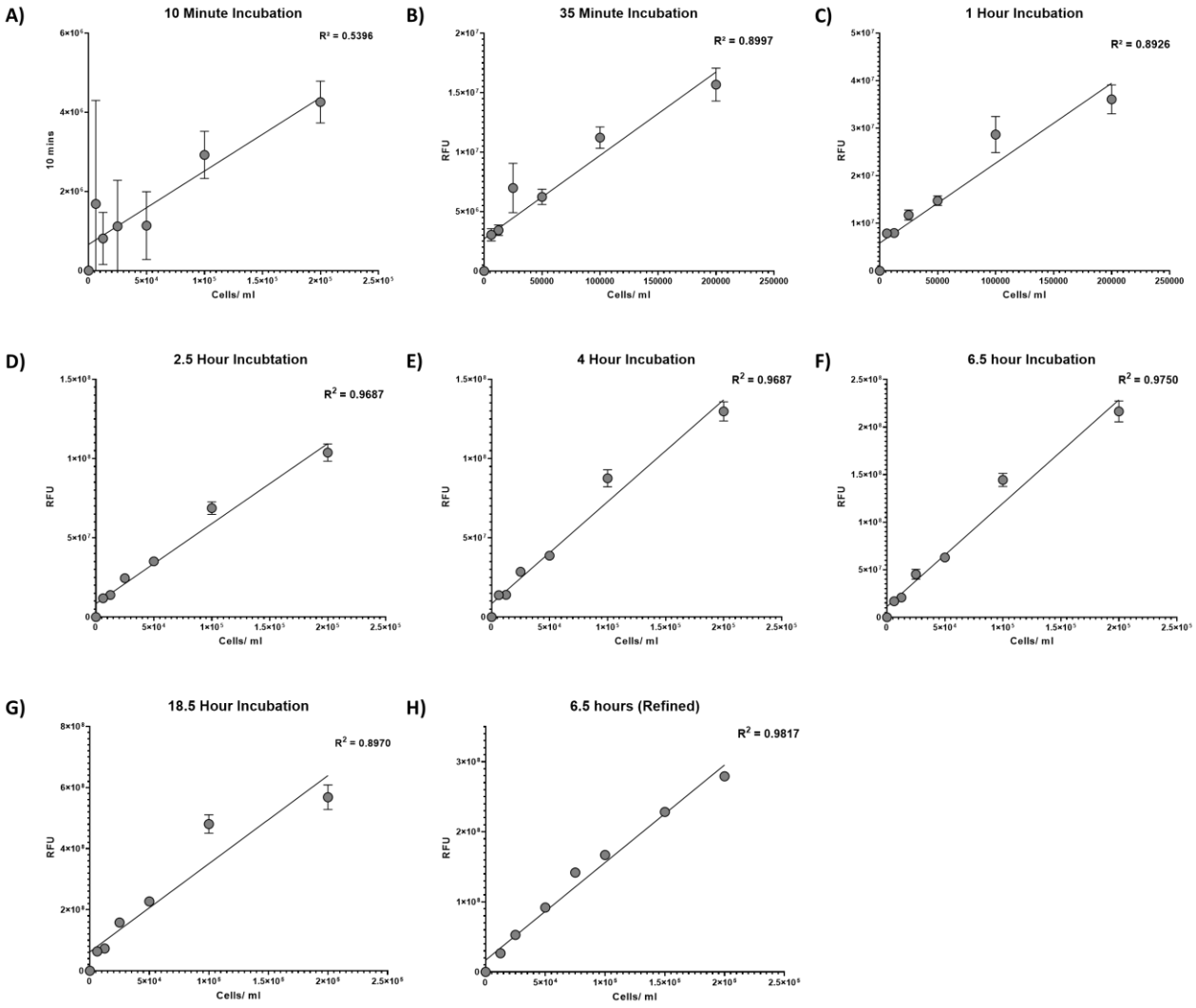

Fig 6.1 PrestoBlue Assay developed to quantify low-density cell growth. *Relative Fluorescence Units (RFU) of Presto Blue standard curve plates incubated at 37°C for (A) 10 minutes, (B) 35 minutes, (C) 1 hour, (D) 2.5 hours, (E) 4 hours, (F) 6.5 hours and (G) 18.5 hours. The assay was later refined with additional cell concentrations added to the standard curve in (H).*

After incubation, the RFU was measured by ID5 plate reader. As is seen in **Fig 6.1** (F), the 6.5-hour incubation produced a line of best fit that was most sensitive to changes in cell concentration. Further concentrations were then added to this (see **Fig 6.1** (H)) which showed high sensitivity to changes in concentration between 25,000 cells/ ml and 200,000 cells/ ml.

6.2.2 Supplementing Low Density Cells with sEVs

Having established an assay for measurement of the low density cell cultures, 96-well plates were seeded by flow cytometry with each well containing 500 cells/ 100 µl CD-CHO (5,000 cells/ ml). The media in each row was supplemented with a defined concentration of sEVs. The sEVs were obtained from both CHO-A and GSKO-Host Day 5 fed-batches which were purified by UC as described in Chapter 4 with the exception that the sEVs were re-suspended in CD-CHO rather than PBS. This was preferable as it removed the need to account for the addition of PBS to the culture. CD-CHO, both unfiltered and post filtration with a 0.22µm filter, measured fewer than 3 particles per frame when measured by NTA which meant accurate particle counts could be obtained for sEVs re-suspended in this media. To ensure no positional bias in the plates or bias for a certain row due to the plate reader, replicates in a sort were set up as shown in **Fig 6.2** with different concentrations of sEVs seeded to different rows.

Replicate 1	1	2	3	4	5	6	7	8	9	10	11	12
A	Conc. A	Conc. A	Conc. A	Conc. A	Conc. A	Conc. A	Conc. A	Conc. A	Conc. A	Conc. A	Conc. A	Conc. A
B	Conc. B	Conc. B	Conc. B	Conc. B	Conc. B	Conc. B	Conc. B	Conc. B	Conc. B	Conc. B	Conc. B	Conc. B
C	Conc. C	Conc. C	Conc. C	Conc. C	Conc. C	Conc. C	Conc. C	Conc. C	Conc. C	Conc. C	Conc. C	Conc. C
D	Conc. D	Conc. D	Conc. D	Conc. D	Conc. D	Conc. D	Conc. D	Conc. D	Conc. D	Conc. D	Conc. D	Conc. D
E	Conc. E	Conc. E	Conc. E	Conc. E	Conc. E	Conc. E	Conc. E	Conc. E	Conc. E	Conc. E	Conc. E	Conc. E
F	Conc. F	Conc. F	Conc. F	Conc. F	Conc. F	Conc. F	Conc. F	Conc. F	Conc. F	Conc. F	Conc. F	Conc. F
G	Conc. G	Conc. G	Conc. G	Conc. G	Conc. G	Conc. G	Conc. G	Conc. G	Conc. G	Conc. G	Conc. G	Conc. G
H	Conc. H	Conc. H	Conc. H	Conc. H	Conc. H	Conc. H	Conc. H	Conc. H	Conc. H	Conc. H	Conc. H	Conc. H

Replicate 2	1	2	3	4	5	6	7	8	9	10	11	12
A	Conc. E	Conc. E	Conc. E	Conc. E	Conc. E	Conc. E	Conc. E	Conc. E	Conc. E	Conc. E	Conc. E	Conc. E
B	Conc. F	Conc. F	Conc. F	Conc. F	Conc. F	Conc. F	Conc. F	Conc. F	Conc. F	Conc. F	Conc. F	Conc. F
C	Conc. G	Conc. G	Conc. G	Conc. G	Conc. G	Conc. G	Conc. G	Conc. G	Conc. G	Conc. G	Conc. G	Conc. G
D	Conc. H	Conc. H	Conc. H	Conc. H	Conc. H	Conc. H	Conc. H	Conc. H	Conc. H	Conc. H	Conc. H	Conc. H
E	Conc. A	Conc. A	Conc. A	Conc. A	Conc. A	Conc. A	Conc. A	Conc. A	Conc. A	Conc. A	Conc. A	Conc. A
F	Conc. B	Conc. B	Conc. B	Conc. B	Conc. B	Conc. B	Conc. B	Conc. B	Conc. B	Conc. B	Conc. B	Conc. B
G	Conc. C	Conc. C	Conc. C	Conc. C	Conc. C	Conc. C	Conc. C	Conc. C	Conc. C	Conc. C	Conc. C	Conc. C
H	Conc. D	Conc. D	Conc. D	Conc. D	Conc. D	Conc. D	Conc. D	Conc. D	Conc. D	Conc. D	Conc. D	Conc. D

Replicate 3	1	2	3	4	5	6	7	8	9	10	11	12
A	Conc. G	Conc. G	Conc. G	Conc. G	Conc. G	Conc. G	Conc. G	Conc. G	Conc. G	Conc. G	Conc. G	Conc. G
B	Conc. H	Conc. H	Conc. H	Conc. H	Conc. H	Conc. H	Conc. H	Conc. H	Conc. H	Conc. H	Conc. H	Conc. H
C	Conc. D	Conc. D	Conc. D	Conc. D	Conc. D	Conc. D	Conc. D	Conc. D	Conc. D	Conc. D	Conc. D	Conc. D
D	Conc. A	Conc. A	Conc. A	Conc. A	Conc. A	Conc. A	Conc. A	Conc. A	Conc. A	Conc. A	Conc. A	Conc. A
E	Conc. B	Conc. B	Conc. B	Conc. B	Conc. B	Conc. B	Conc. B	Conc. B	Conc. B	Conc. B	Conc. B	Conc. B
F	Conc. C	Conc. C	Conc. C	Conc. C	Conc. C	Conc. C	Conc. C	Conc. C	Conc. C	Conc. C	Conc. C	Conc. C
G	Conc. E	Conc. E	Conc. E	Conc. E	Conc. E	Conc. E	Conc. E	Conc. E	Conc. E	Conc. E	Conc. E	Conc. E
H	Conc. F	Conc. F	Conc. F	Conc. F	Conc. F	Conc. F	Conc. F	Conc. F	Conc. F	Conc. F	Conc. F	Conc. F

Fig 6.2 Plate randomization to ensure no positional bias in growth observed. Layout of each replicate where the concentration of sEVs/ ml differed in each plate. *Conc. A = Concentration of A sEVs/ ml, Conc. B = Concentration of B sEVs/ ml, Conc. C = Concentration of C sEVs/ ml, Conc. C =*

Concentration of C sEVs/ ml, Conc. D = Concentration of D sEVs/ ml, Conc. E = Concentration of E sEVs/ ml, Conc. F = Concentration of F sEVs/ ml, Conc. G = Concentration of G sEVs/ ml, Conc. H = Concentration of H sEVs/ ml.

Two rounds of sorting were completed where 96-well plates containing sEVs from either CHO-A or GSKO-Host were seeded at a density of 5,000 cells/ ml. These were left to incubate at 37°C for 72 hours. After incubation, the plates were measured by the PrestoBlue assay.

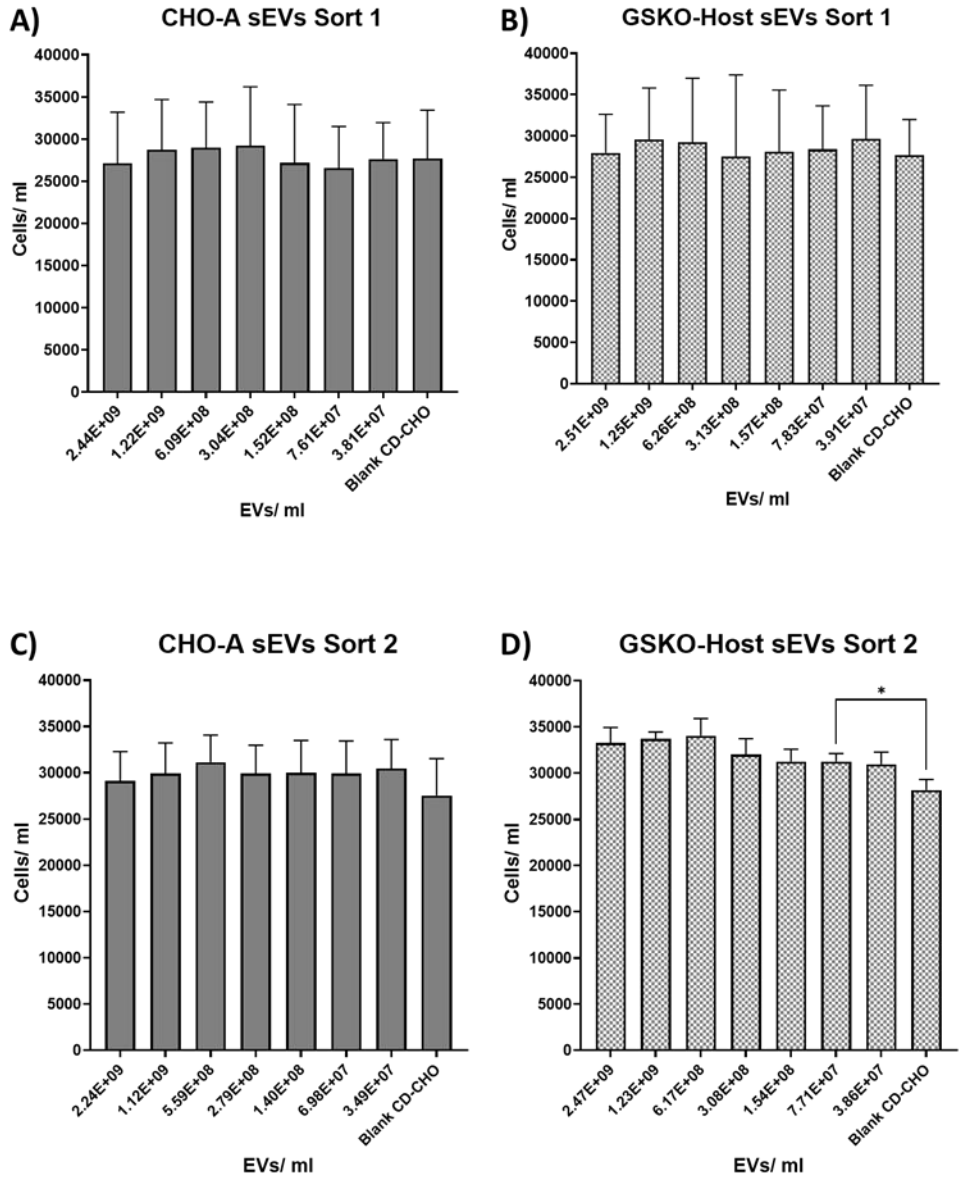

Fig 6.3 sEVs did not increase the growth of low density cell cultures. *CHO-A cells grown in CD-CHO supplemented with different concentrations of sEVs/ ml (three replicates per sort). (A) Plates supplemented with CHO-A sEVs in the first round of sorting by flow cytometry. (B) Plates supplemented*

with GSKO-Host sEVs in the first round of sorting. (C) Plates supplemented with CHO-A sEVs in the second round of sorting. (D) Plates supplemented with GSKO-Host sEVs in the second round of sorting. Error bars are standard deviation. One-way ANOVA with Tukey post-hoc test used to check for statistically significant differences between sEV concentrations.

Irrespective of what concentration of sEVs was used, there was no change in growth observed compared to blank CD-CHO after incubation for 72 hours. There was also no difference in the growth observed between cells treated with CHO-A sEVs and GSKO-Host sEVs. This suggested that sEVs could not be used to enhance the growth of low density CHO cell cultures. However, it was noted that the cells were slow to grow in the static 96-well plates. If they doubled every 24 hours, as is expected in suspension culture, the wells should have been at a density of ~40,000 cells/ml. Yet the densities observed in both sorts are below this.

6.2.3 Cloning in CD-CHO media

Despite their inability to promote the growth of low density cell cultures, sEVs were further investigated to determine if they could promote the survival of single cell clones. As was seen in 3.2.5.2, sEVs contained miRNAs which were implicated in several biological processes. Thus, they were still hypothesised to contain stimuli which could "trick" a single cell clone that it was in a dense culture and either prevent its death or initiate its clonal outgrowth. 96-well plates were supplemented with a concentration of 5×10^8 sEVs/ml. This was estimated to be a similar concentration of sEVs/ ml to what would be found in the extracellular space between exponential growth and peak VCD based on sEV quantities measured on Day 5 CHO-A fed-batch in Chapters 3 and 4. In order to generate a dilution containing the desired concentration of sEVs, 50 – 100µl of purified sEV sample was diluted to 50ml in CD-CHO.

Initially, cloning was attempted with plates seeded with 100µl CD-CHO growth media per well (sEV supplemented or un-supplemented) with 50µl blank CD-CHO feed on Day 7. However, this provided highly variable numbers of clonal outgrowths post sorting and the variability was irrespective of what way the cells were treated. A sample of the rounds of single cell sorting are shown in **Fig 6.4**.

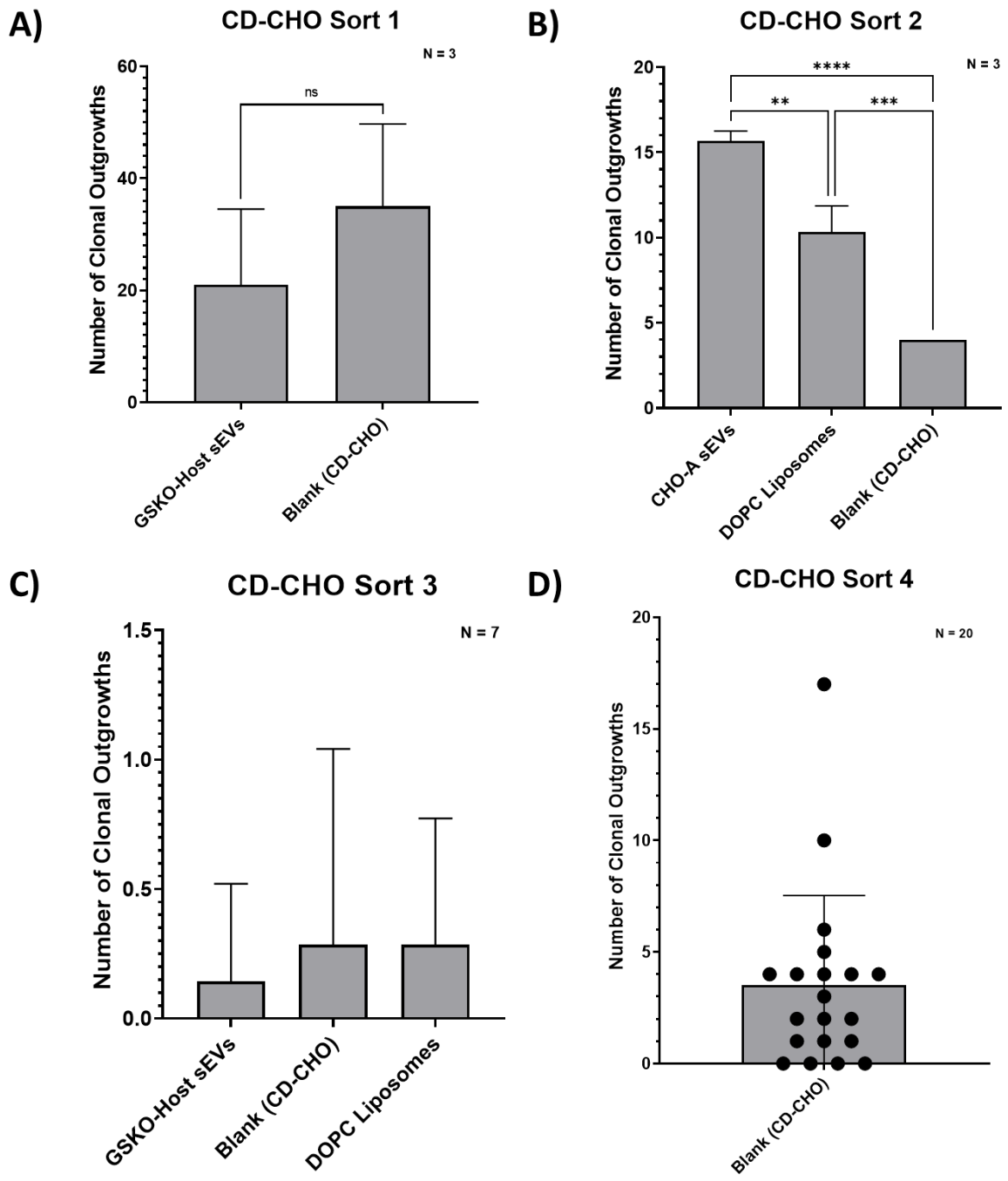

Fig 6.4 Large variation in the number of clonal outgrowths by Day 14 from each round of sorting. *(A) Sort 1 comparing GSKO-Host sEVs to Blank CD-CHO. Independent two tailed t-test used to check for statistical significance. (B) CHO-A sEVs compared to Dioleoyl-phosphatidylcholine (DOPC) liposomes and Blank CD-CHO. One-way ANOVA with Tukey post-hoc test used to check for statistical significance between samples. (C) GSKO-Host sEVs compared to Blank CD-CHO and DOPC liposomes. (D) Blank CD-CHO with large number of plates to capture variability.*

The unsuitability of CD-CHO for single cell cloning was clear from **6.4** (D) where variability in the number of clonal outgrowths ranged from 4 plates having no outgrowths to 1 plate having 17. To confirm that the CD-CHO media was generating the variability and not the FACS Melody instrument used for single cell sorting, 48 images of the wells as viewed with a bottom up microscope were captured.

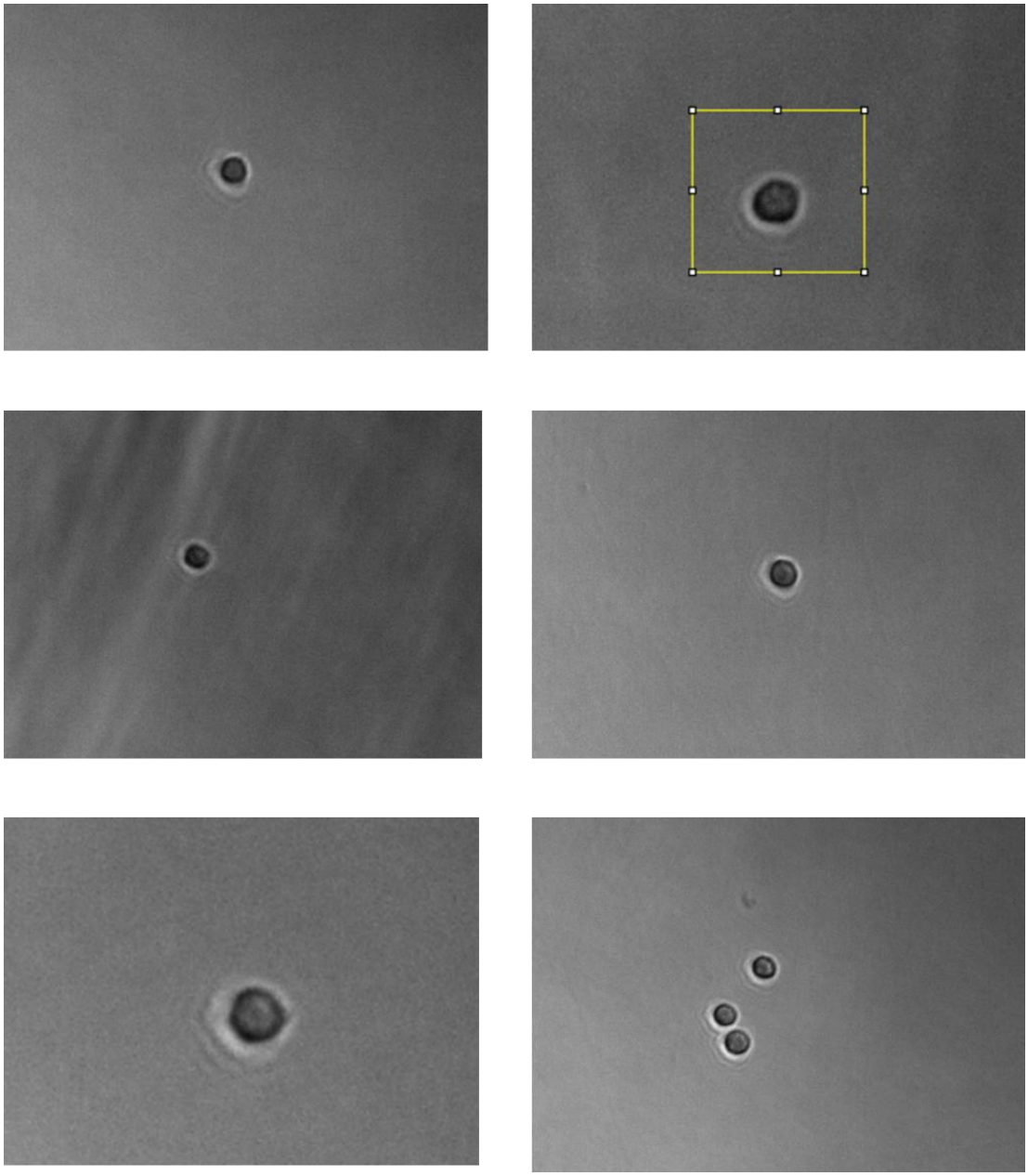

Fig 6.5 Variability in cloning efficiency not due to FACS Melody flow cytometer. Images of wells as viewed with bottom up microscope. *All of 48 images had single cells except for one well which had three cells sorted to it. This gave the flow cytometer a sorting accuracy of 98%.*

Of the 48 wells imaged, only one well had more than a single cell. This gave a sorting accuracy of 98% which meant the FACS Melody was not having enough impact to produce the variability in number of clonal outgrowths observed between sorts.

6.2.4 Cloning in Ex-Cell CHO cloning media

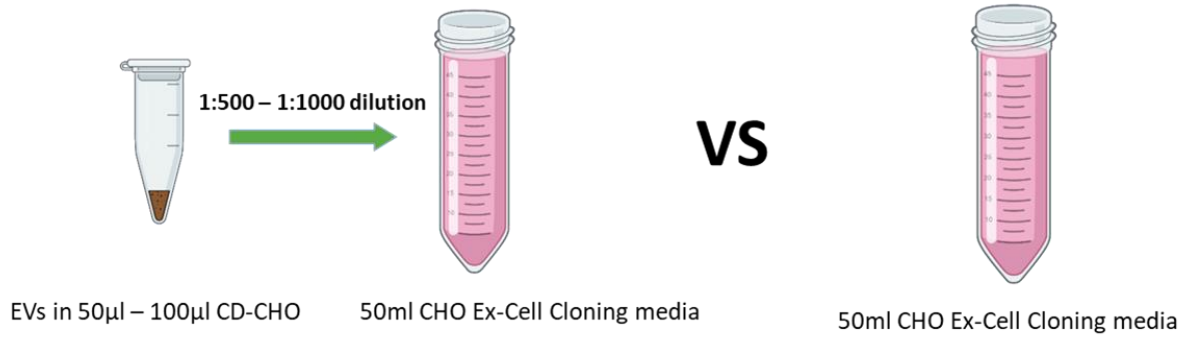

Fig 6.6 Dilution of sEVs re-suspended in Ex-Cell media. *sEVs re-suspended in CD-CHO diluted to 50ml in Ex-Cell CHO Cloning media for supplemented plates compared to 50ml Ex-Cell CHO Cloning media with no additions.*

As CD-CHO is a growth media and not optimal for culture of single cells, it was decided that Ex-Cell CHO Cloning Media (Ex-Cell) would be better suited. To determine if this media gave consistency between different rounds of sorting and to see if sEVs could improve the number of clonal outgrowths, three rounds of sorting were performed where the purified sEVs were diluted to 50ml in Ex-Cell CHO Cloning media (as shown in **Fig 6.6**) and compared to blank Ex-Cell CHO Cloning Media. 96-well plates were seeded on Day 0 with 100µl per well of either sEV supplemented or blank Ex-Cell CHO Cloning media. For the second and third round of sorting, larger numbers of plates were used to capture any possible variation.

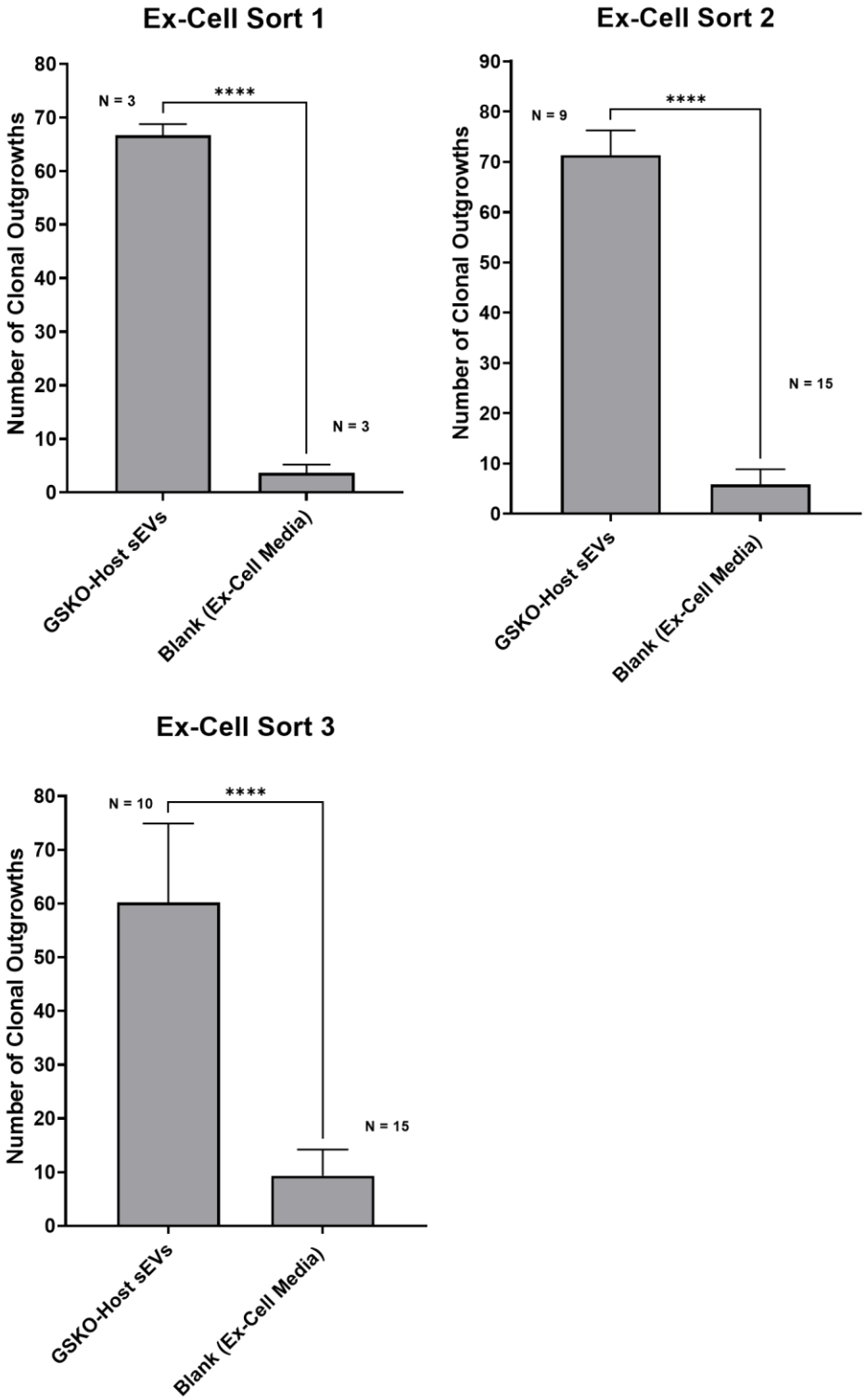

Fig 6.7 Ex-Cell gave consistent cloning efficiencies with sEVs diluted in Ex-Cell having a significantly greater efficiency. *Three rounds of single cell sorting performed in Ex-Cell CHO Cloning media comparing the number of clonal outgrowths in GSKO-Host sEVs to Blank Ex-Cell CHO Cloning Media. Independent two-tailed t-test used to test for statistical significance in each sort.*

The three rounds of sorting revealed that Ex-Cell gave consistent numbers of clonal outgrowths between rounds of sorting. There also appeared to be a large significant increase in the number of clonal outgrowths which were visible on Day 14 on the Clone Select Imager (CSI) for sEV supplemented plates.

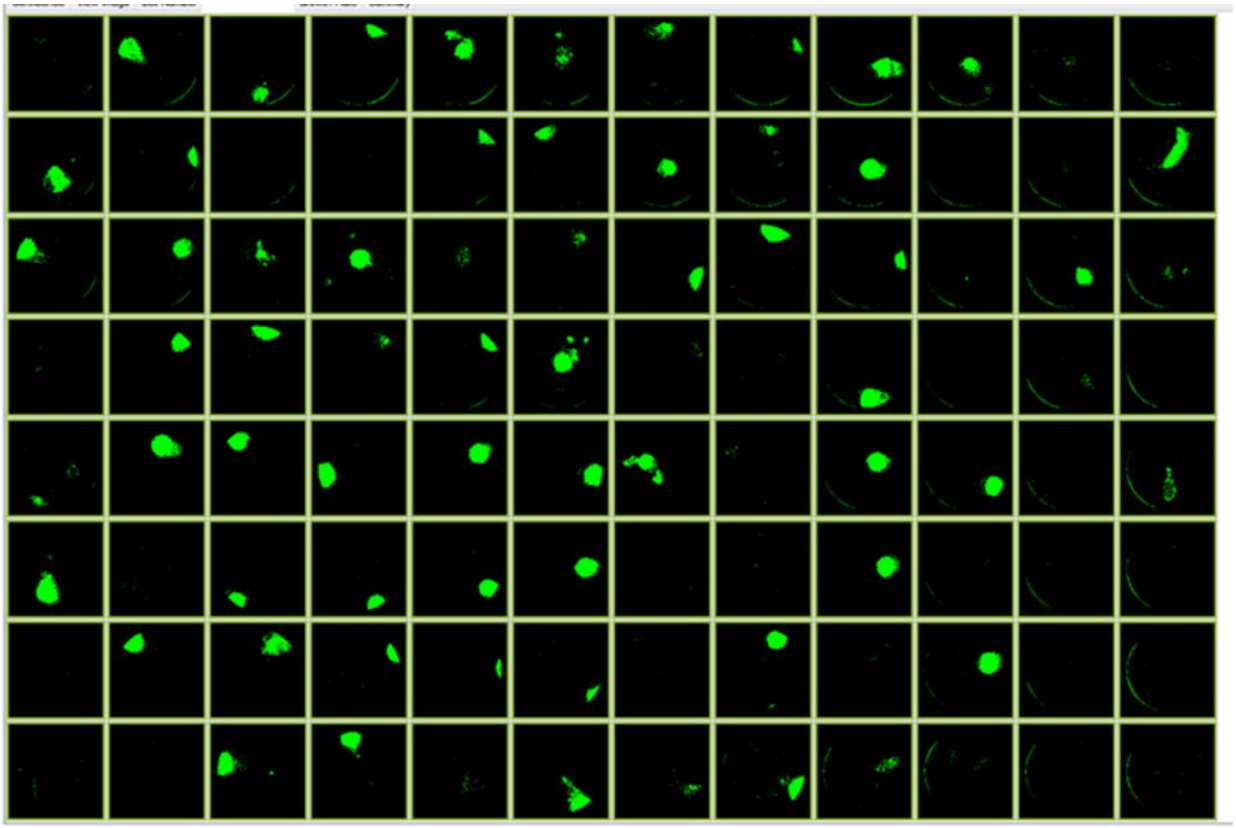

Fig 6.8 sEV supplemented plates had more visually detectable outgrowths. *CHO-A Clonal outgrowths in GSKO-Host sEV supplemented plate as imaged by CSI.*

Across the three rounds of sorting, the average number of clonal outgrowths was 65.63 +/- 11.42 in the sEV supplemented plates compared to 7.21 +/- 4.29 in the Blank Ex-Cell plates. This equated to an average cloning efficiency of 68.36% vs 7.5%.

While the sEV supplemented plates had enabled clone survival and initial growth, additional feed on Day 14 was needed to both mitigate evaporation in the wells and boost growth of the cells further to become confluent in the well. A subsection of these plates had each well fed either 50µl of Ex-Cell Cloning media or CD-CHO growth media on Day 14 to see if this could promote further cell growth.

A)

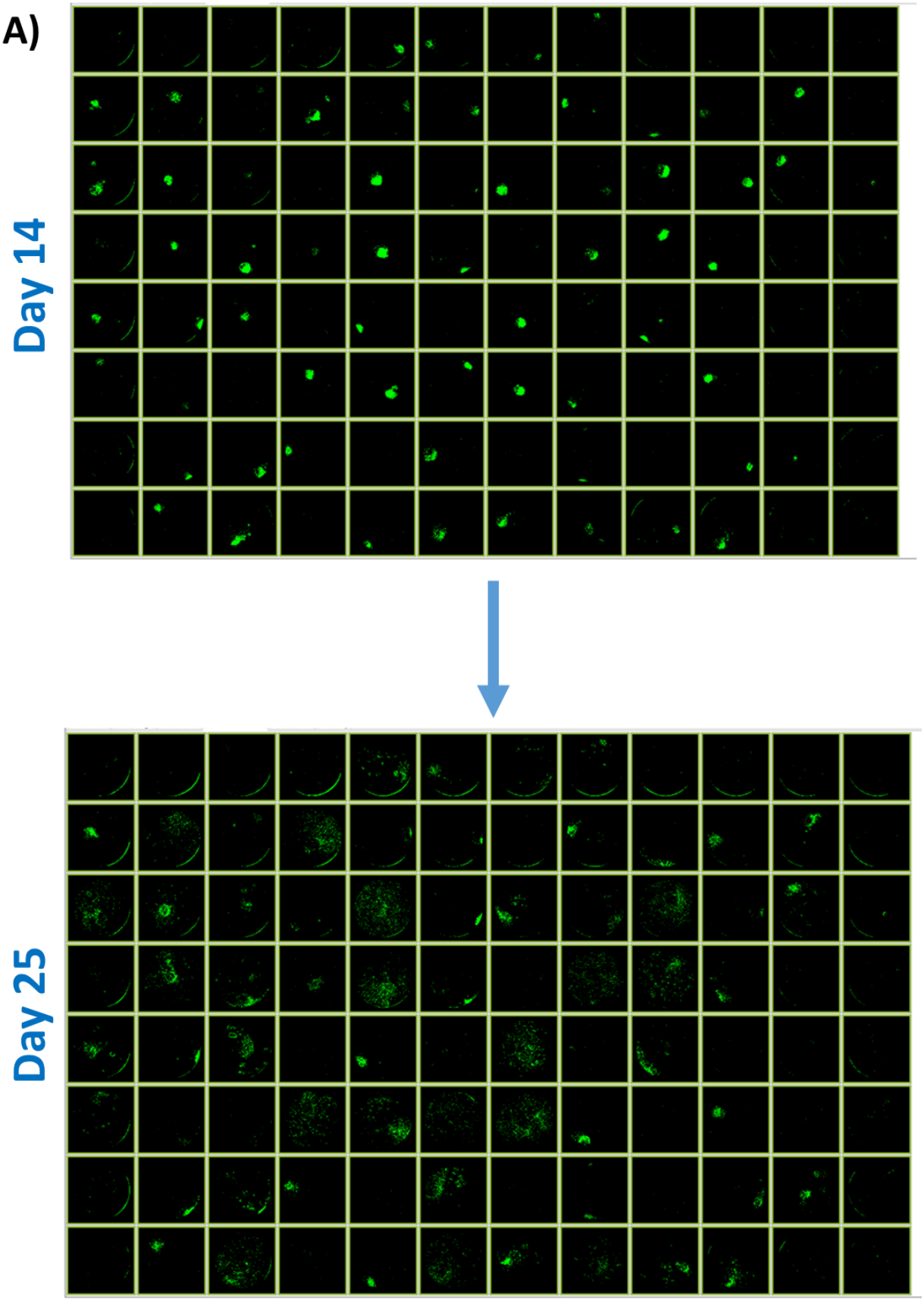

B)

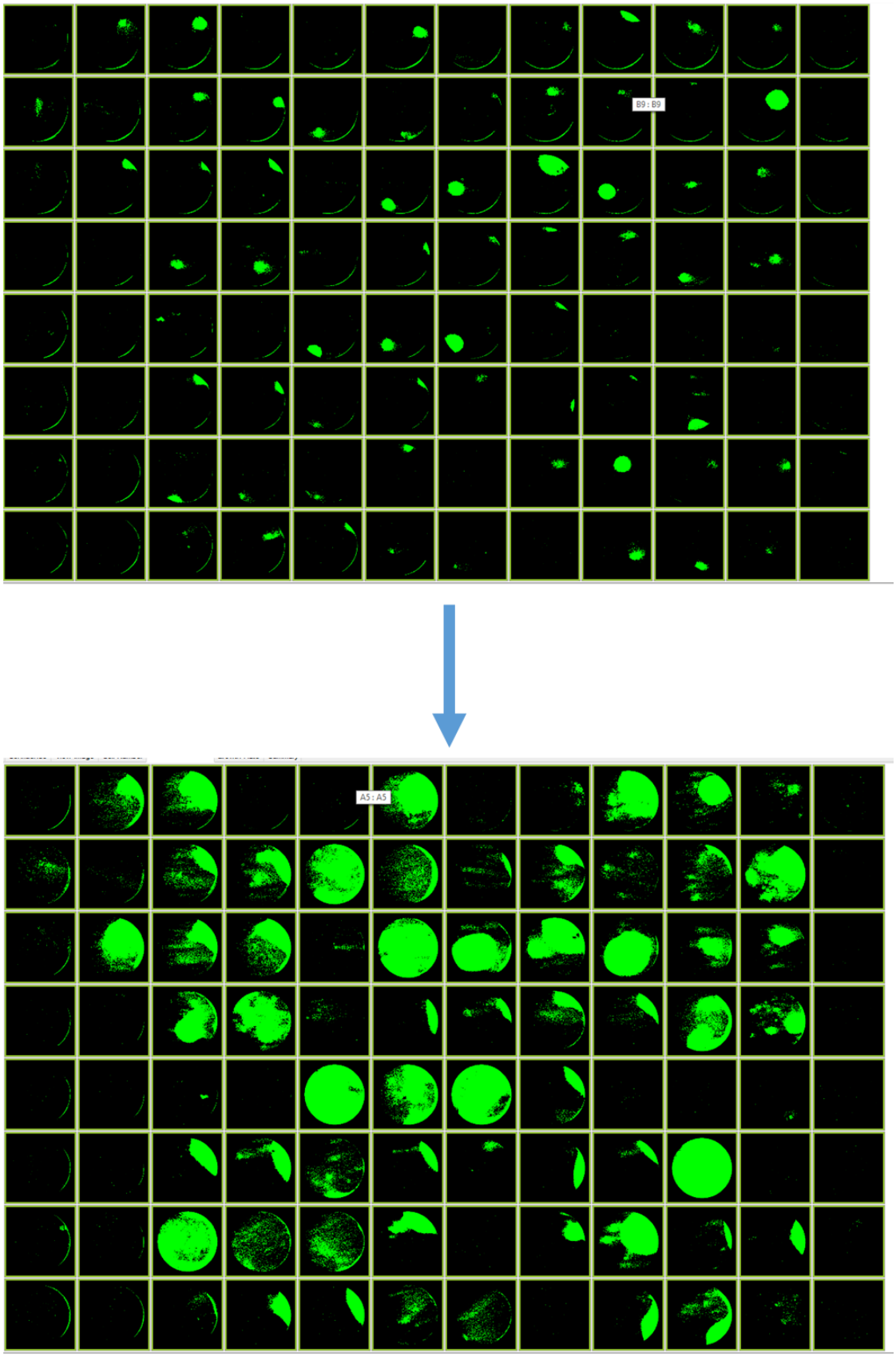

Fig 6. 9 CD-CHO feed on Day 14 enabled several of the wells to become confluent by Day 19. *(A) Confluency of wells imaged by CSI on Day 14 and Day 25 post 50µl feed with Ex-Cell (B) Confluency of wells imaged by CSI on Day 14 and Day 19 post 50µl feed with CD-CHO.*

Feeding with Ex-Cell did not increase the confluency of wells with the spreading out of the colonies on Day 25 likely to be from the addition of volume to the well on Day 14. On the other hand, CD-CHO feeding on Day 14 further augmented cell growth and several of the wells had achieved near full confluency by Day 19. This showed the clones supplemented with GSKO-Host sEVs were not only surviving the initial sorting process, but were also capable of growth.

6.2.5 Quantifying the effects of feeding and sEV supplementation

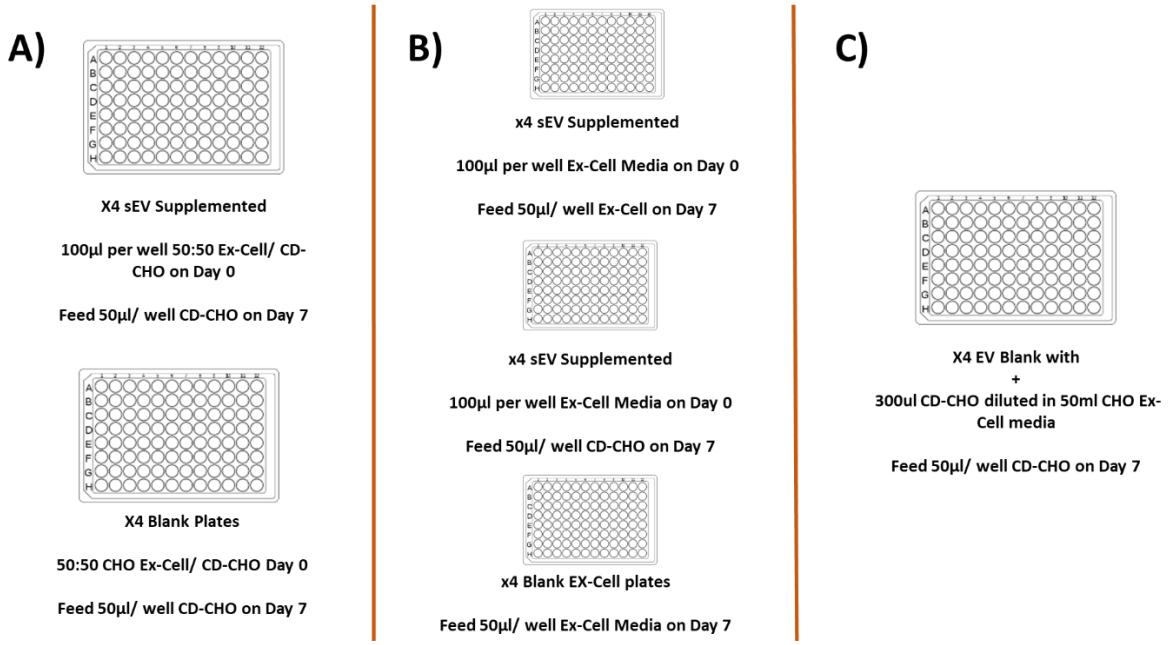

Fig 6.10 Different strategies for achieving confluent wells at a quicker rate. *(A) Plates were seeded with a 50:50 mix of CD-CHO and Ex-Cell CHO cloning media on Day 0 with feeding of 50µl per well CD-CHO on Day 7. (B) Plates seeded with Ex-Cell CHO Cloning media and fed with either Ex-Cell CHO Cloning media or CD-CHO on Day 7. (C) 300µl CD-CHO diluted to 50ml with Ex-Cell CHO Cloning media to give a concentration of 0.6% CD-CHO.*

Two more rounds of sorting were carried out. The first round (See **Fig 6.10**) was to determine what feeding strategy on Day 7 best supported growth of the clonal outgrowths and if more fully confluent wells could be achieved by Day 14. It also aimed to see if the small volume of CD-CHO that the sEVs were diluted in had any impact on the number of clonal outgrowths given that cloning with entirely CD-CHO was adverse to clone survival.

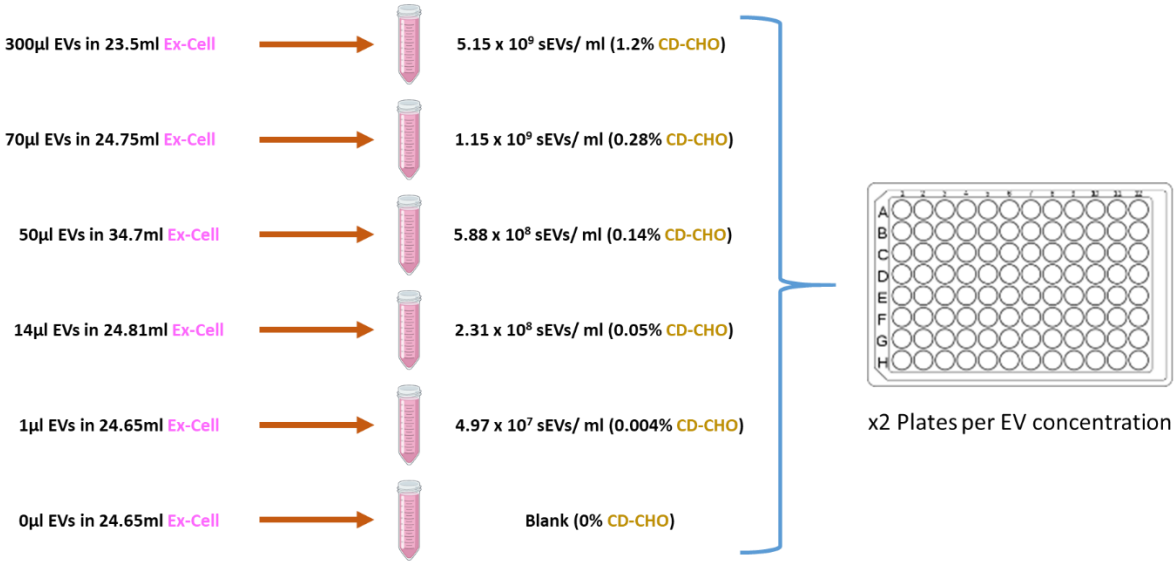

Fig 6.11 Concentration gradient of sEVs in second round of sorting.

The second round of sorting looked at the number of clonal outgrowths that different concentrations of sEVs supplementation obtained (See **Fig 6.11**). The concentrations tested ranged from 10 times fewer EVs/ml to 10 times the number of EVs/ml. With 5 x 10^8 EVs/ml already having been observed to produce a high cloning efficiency, double and half this concentration were also tested.

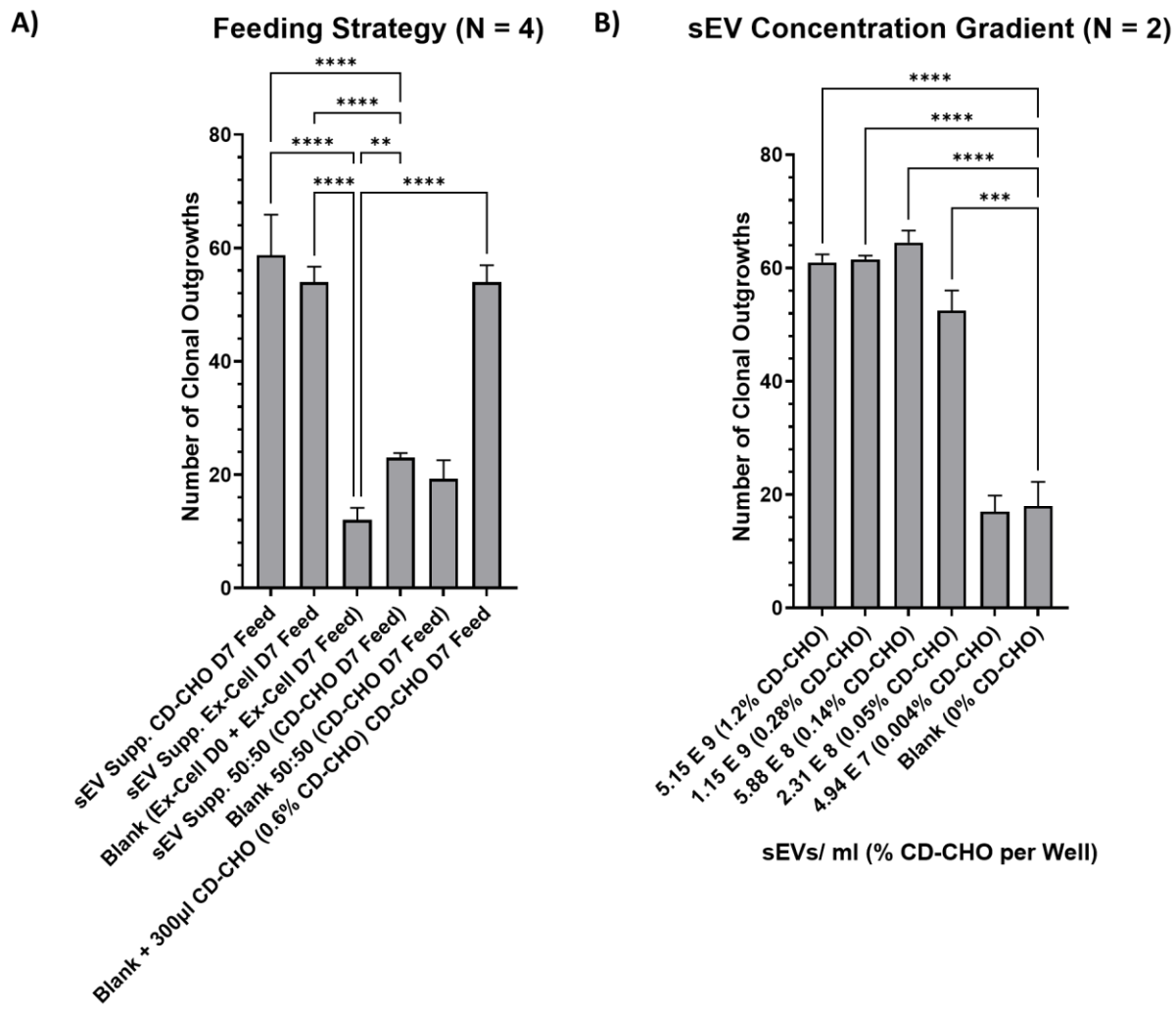

Fig 6.12 Very small concentrations of CD-CHO rather than sEVs responsible for increased cloning efficiency. *(A) Sort 1: To determine optimal feeding strategy for CHO-A clones in both supplemented and blank plates. Plates supplemented with Ex-Cell that contained 0.6% CD-CHO had equivalent cloning efficiency to sEV supplemented plates. (B) Sort 2: Concentration gradient of sEVs. As little as 0.05% CD-CHO in Ex-Cell was enough to increase cloning efficiency.*

Sort 1 provided a surprising finding that 300µl of CD-CHO diluted to 50ml in Ex-Cell increased cloning efficiency to the same as that of sEV supplemented plates. In addition to this, both sEV supplemented and non-supplemented plates seeded with a 50:50 mix of CD-CHO and Ex-Cell CHO cloning media also had comparable cloning efficiency. The sEV Supp. 50:50 plates had a significant increase in the number of clonal outgrowths over blank plates seeded with just Ex-Cell CHO Cloning media. This

therefore meant that it was not sEVs which were generating the increased number of clonal outgrowths. Instead, CD-CHO, when highly diluted in combination with the Ex-Cell CHO Cloning media, was enough to dramatically increase the number of clonal outgrowths. The feeding strategy employed did not impact the number of clonal outgrowths as seen in **Fig 6.12** (A). With the exception of a handful of wells, the CD-CHO fed plates were slightly more confluent than the Ex-Cell fed plates (see **Fig 6.13**).

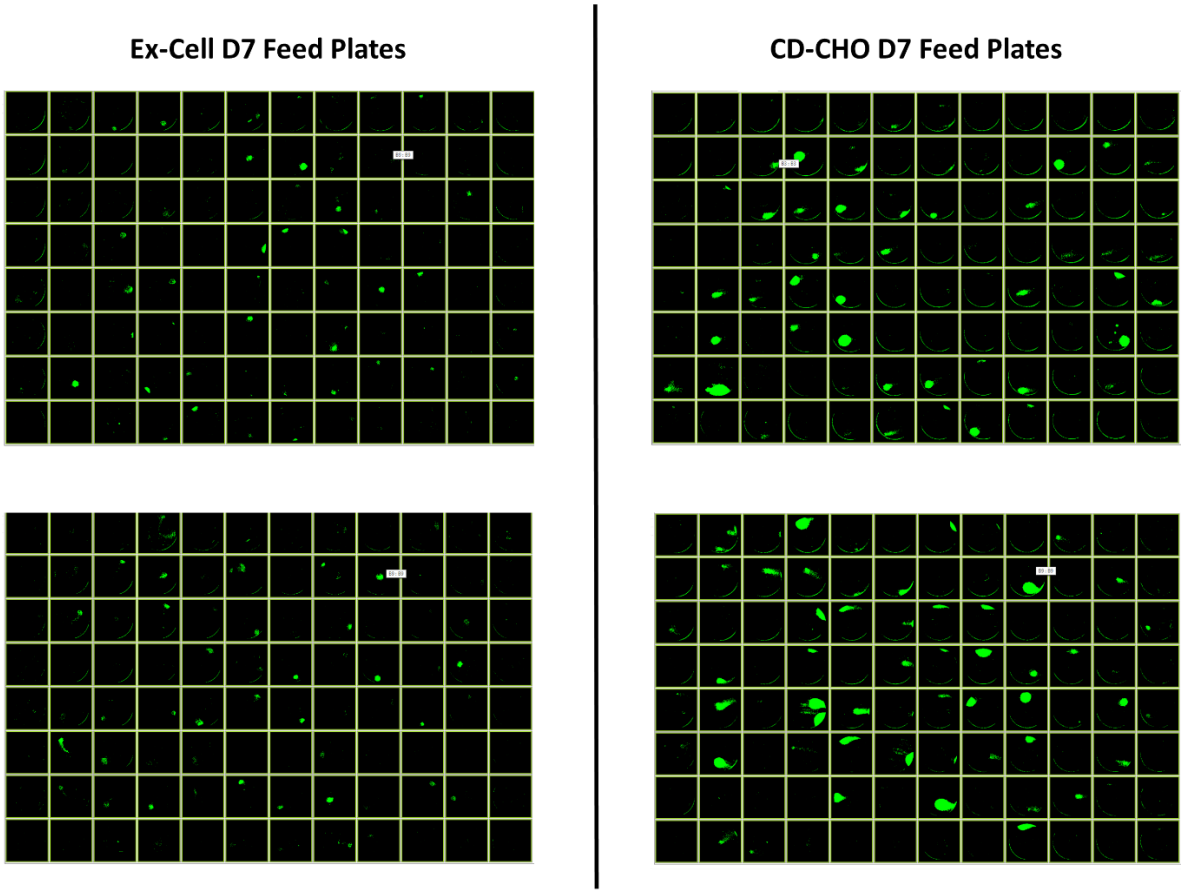

Fig 6.13 CD-CHO feeding on Day 7 had only small impact on confluency of wells by Day 14. Day 14 images of two plates seeded with Ex-Cell CHO Cloning media and fed with Ex-Cell CHO Cloning media on Day 7 (left) and two plates seeded with Ex-Cell CHO Cloning media and fed CD-CHO on Day 7 (right).

The ability of diluted CD-CHO in Ex-Cell CHO Cloning media to enhance cloning efficiency was further highlighted in the concentration gradient in **Fig 6.12** (B). The concentration of sEVs/ ml had no impact on the number of clonal outgrowths. Instead, when the concentration of CD-CHO that the sEVs were re-suspended in decreased below 0.05%, the number of clonal outgrowths was comparable to blank Ex-Cell CHO

Cloning media. However, the number of clonal outgrowths was consistent between 0.05% and 1.2% CD-CHO. This would indicate that the number outgrowths which survive sorting and subsequently grow are dependent on the nutrient concentration of the media in which they are grown. The observation that 50:50 CD-CHO/ Ex-Cell mix in **Fig 6.12** (A) had significantly fewer clonal outgrowths is evidence that there is a threshold nutrient composition.

6.3 Discussion

The inability of CHO sEVs to promote growth wasn't altogether surprising. The hypothesis of this study was supplying sEVs in a ratio several times greater than what was found naturally accumulated in the extracellular environment would potentially impact on growth as the sEVs would "accelerate" the delivery of pro-growth stimuli. This was essentially how Takagi *et al.* (2021) increased growth where they showed increased concentrations of sEV containing polymer fraction positively correlated with growth. However, their purification method likely contained several co-isolates other than sEVs which may have contributed to their finding. The time-point from which sEVs were isolated was also speculated to yield growth promoting stimuli. Yet the analysis in 3.2.5.1 showed sEVs maintain a broadly consistent small RNA composition with the miRNA profile changing little throughout the fed-batch process. This is potentially true of the protein cargo of sEVs also. Therefore, sEVs are unlikely to contribute to the exponential growth in the cells they are isolated from. Rather, this is driven from other autocrine signaling, nutrient metabolism or other intracellular processes.

Another caveat to this study was that the cells were suspension adapted but cultured in static conditions. This was seen in how they less than doubled every 24 hours and suggests the conditions used were not favourable to growth. A better approach would be to use 96 deep-well plates or 24-well plates which could be shaken to keep the cells suspended. Yet the issue with this is the larger volume required for each well means greater quantities of sEVs are needed to achieve the same numbers of sEVs per cell. This was beyond the scope of this project as it requires larger scale purification methods. It also raises the question as to whether using sEVs as media additives to promote growth would be viable in large scale biopharmaceutical

manufacturing given the extremely large cell densities achieved in industrial scale processes (Kunert and Reinhart, 2016). Even if it is a case of achieving the right sEV : cell ratio in optimal conditions for growth, this may be difficult to achieve at the necessary scale.

It was clear from the cloning sorts that sEVs do not promote clonal outgrowth. The sEVs re-suspended in CD-CHO did not give a substantial increase over Ex-Cell CHO Cloning media supplemented with a comparable quantity of blank CD-CHO. The fact as little as 0.05% CD-CHO in Ex-Cell CHO Cloning media could increase cloning efficiency from 10% to approximately 55% was an interesting finding in itself. Just using CD-CHO as a cloning medium gave poor and highly variable cloning efficiency. Even as much as 50% CD-CHO had considerably lower cloning efficiency than <1.2% concentrations. This suggests there is a nutrient balance which is optimal for the CHO-A cell line when cloning.

The Ex-Cell CHO cloning media contains plant hydrolysates which are generated by a combination of enzymatic digestion and acid hydrolysis of plant proteins. Hydrolysates contain a variety of amino acids, carbohydrates and peptides which have been shown to be anti-apoptotic and preventative of oxidative stress. The caveat to their use is they are not chemically defined yet they are less likely to cause contamination due to their non-animal source which has made them a serum substitute (Ho *et al.*, 2021). These hydrolysates, amongst other proprietary components of the Ex-Cell media, are what enable it support single cell survival and initial clonal outgrowth. Yet it lacked the necessary composition to maintain clonal outgrowth beyond initial survival as feeding additional Ex-Cell CHO cloning media on Day 14 didn't allow the cells to grow further. This is possibly why very small concentrations of CD-CHO dramatically increased the number of clonal outgrowths. When just using blank Ex-Cell CHO cloning media, a selection process was put in place where, despite its pro-survival composition, only clones with an innately strong ability to grow in non-optimal nutrient compositions could form clonal outgrowths. Adding a small concentration of CD-CHO decreased this selection pressure as clones less able to adapt to the cloning media, missing adequate nutrients for growth, now have enough nutrients from CD-CHO to form outgrowths. Once these pro-growth nutrients are expended, the outgrowths cease expanding. However, it was noted that feeding on Day 7 with 50 µl CD-CHO produced slightly larger outgrowths. It may well

be the case that seeding with a lower volume of Ex-Cell CHO Cloning media on Day 0 and feeding with an even larger volume of CD-CHO on Day 7 would further expand the size of the outgrowth by Day 14. This would also have the potential benefit of adequately reducing the adaptation required when moving cells from cloning media to growth media which can impact on cell productivity (Sabourin and Shapiro, 2011; Lim et al., 2013; Ho et al., 2021).

Similar observations to these have been made by Sabourin and Shapiro (2011) when comparing cloning efficiency of cells passaged in different growth medias prior to sorting by limiting dilution. In their study, the cells were diluted in growth media which was then further diluted 1:200 in cloning media to obtain the desired cell concentration for limiting dilution. However, they noted that there wasn't a one-size fits all as CHO-S and CHO-DG44 produced different cloning efficiencies in identical media compositions. While they didn't test CHO cell lines making different IgG mAbs, they did show that the same cell line producing EPO had a different cloning efficiency to when it produced IgG. Therefore, different products may also result in differing cloning efficiencies.

While it was outside the scope of this study to look at cloning efficiency in different combinations of medias and growth medias, it is clear that the nutrient composition of the media is perhaps the most critical factor in the cloning efficiency achieved. More so than the sorting technique or the cell's innate ability to grow as a single clone. It therefore raises the question as to what contents of serum and conditioned media allow them to be so beneficial to single cell clone survival. This results of this study suggest that sEVs are not one of the beneficial agents in either serum or conditioned media. It is likely other autocrine factors secreted by the cell that are present in serum and conditioned media are what drives clonal outgrowth. In the case of conditioned media, there may also be a benefit from the nutrient content of the media which may is depleted enough to be favourable to single cell growth. Yet secreted factors from cells grown in the condition media are most likely to be the driver in promoting clonal outgrowth. Indeed, there might not be one single factor in serum or conditioned media that promotes clonal outgrowth; it could well be a combination. The outcome of this study suggested a better approach to improving cloning efficiency in cell line development would be to mix cloning media with growth media in a ratio that is optimal for the cell line being used. Chemically defined cloning media should be used where

possible and is available on the market such as Cellvento® 4CHO-C Cloning Medium (Cat No: 14390C-500ML, Merck Life Sciences, Gillingham, UK). This eliminates risks associated with non-chemically defined cloning medias. For non-manufacturing or research purposes where chemically defined media may not be available, only low risk additives such as plant hydrolysates should be used.

Chapter 7

Conclusions and Future Works

7.1 Conclusions

7.1.1 CHO EV secretion in Biopharmaceutical Manufacturing

sEV accumulation in the cell culture environment increases up to early stationary phase of fed-batch. After this, the quantity of sEVs per cell stays relatively constant. In the case of lEVs, the concentration per cell increases gradually until early stationary phase. After this in late stationary/ early death phase, there is a dramatic increase in the number of particles and protein content detected in this fraction. However, it is unknown as to what proportion of this fraction is composed of lEVs as there is increased protein content in all UC fractions due to increased cell death at this phase. It was notable that cells grown in the Lonza fed-batch system produced far greater quantities of sEVs/ cell. This was observed in the both the CHO-X cell lines and the Non-X GS-Null which is a pool. Thus it is likely that media composition and feeding can dramatically alter the quantities of sEVs obtained.

7.1.2 sEV miRNA composition is constant through-out a fed-batch

The majority of sEV miRNA content stays broadly consistent in both terms of what miRNAs are present and their relative expression levels throughout fed-batch manufacturing process. However, there are some additional miRNAs detectable at the early and late stationary phases which could not be detected in exponential phase. The greatest difference in miRNA expression occurs at late stationary/ early death phase which is perhaps reflective of the increased cell death and stress at this stage of fed-batch. The greatest differences in miRNA abundance is also noted in the less

abundant miRNAs. It is unknown whether these are true differences in quantities or the sensitivity of the library prep kits used overstates these changes in quantity.

Small RNA-seq analysis of miRNAs in CHO sEVs predicts them to target and inhibit mRNA transcripts of genes involved in proliferation and apoptosis. This functionality is evident when sEVs are depleted from CHO fed-batch at early stationary phase. Cell death occurs at a quicker rate when sEVs are depleted. This is unique to sEVs as when lEVs are depleted, it reduces cell death and increases the duration of the fed-batch where cells maintain high viability. This suggests that sEVs maintain cell viability throughout a fed-batch process and are utilised by the cells to ensure they are homgeneous in their behaviour. However, it appears that this functionality has an upper threshold as further increasing the quantity of sEVs in the extracellular environment had no beneficial effect to cell growth or viability. It also did not improve low density cell growth or cloning efficiency when sEVs were supplemented to cultures in quantities far greater than what would naturally be present in the culture environment of cells grown in CD-CHO.

It is likely that all CHO cell lines utilise sEVs in a similar way. This is because no difference in miRNA composition was found between a producer cell line and a host cell line. This is despite all the adaptations required by the producer cell line during cell line development. The lipid composition did vary between sEVs from different cell lines. This is perhaps an expected observation given that the lipid composition of CHO cells themselves can vary between cell lines.

7.1.3 Variation in sEV secretion between CHO cell lines

This upper threshold of functionality for sEVs is further illustrated in how different CHO cell lines can have different quantities of sEVs/ cell. Poor producer cell lines appear to have far greater sEV secretion than strong producer cell lines. This is evident in both the observed quantities of sEVs/ cell for high qP cell lines and in how EVB genes are downregulated in these cell lines. The differences in EV secretion overall may perhaps be of further consideration when choosing a cell line for mAb production.

7.2 Future Work

7.2.1 Measuring EV Abundance with an EV specific counting method

While NTA is considered one of the main techniques for quantifying EV abundance. A more EV specific quantification method would better illustrate and orthogonally validate how EV accumulation changes during the course of a fed-batch. This would eliminate cell health as a factor and how cellular debris may be contributing to the total particle count in late stage fed-batch. The NanoAnalyzer can be further optimised to enable even more specific quantification than what was attempted in 5.2.2. CFSE+ particles are a useful measurement of purity as only whole sEVs should be detectable to the NanoAnalyzer. However, there are some lipid debris which may also have enough esterases that react with the dye. An even more specific EV quantification method would involve the use of antibodies targeting the three tetraspanins such as CD9, CD81 and CD63; each of which conjugated to a different fluorophore. Whilst this assay would require optimisation to ensure correct quantities of detection antibody are used, it would allow for a more accurate quantification of EV quantity with a measure of purity as non-EV particles would have no tetraspanin present. Depending on the quantity of EVs produced by a cell line, a far smaller volume than that purified in the studies presented here may be used where only a 10,000g centrifugation step is needed to isolate sEVs in the supernatant and lEVs in the pellet. Antibodies targeting the selected tetraspanins could then be directly added to the 10,000g supernatant to bind to sEVs which would then be analysed by the NanoAnalyzer. For lEVs, they could simply be re-suspended in media or PBS before detection antibody addition. The advantage of this lower volume requirement would mean more regular sampling of EV abundance could be attempted in a manner that is higher throughput than using traditional EV purification methods.

7.2.2 Characterisation of lEV RNA content

While it was outside the scope of this project to characterise the RNA content of lEVs, given the importance of sEVs to fed-batch viability, it raises the question as to what

function lEVs are serving in the fed-batch if any. As lEVs are larger than sEVs, they may carry larger RNA species such as mRNA in addition to miRNAs. This was shown to be the case by Busch et al. (2022) yet only from a single time-point in the fed-batch. It may be the case that lEV RNA content varies much more than the sEV RNA content as the fed-batch moves through different phases of growth. It may also vary more between different cell lines.

The purification of lEVs would require a combination of two purification techniques. Firstly, immunoprecipitation, as described in 1.4.3., to remove the lEVs from non-EV material present in the supernatant. Then a round of centrifugation at 10,000g to isolate them from sEVs. In addition to characterizing RNA, this method of purification could also enable more accurate quantification of lEV accumulation by NTA. This is because late stage fed-batch cellular debris would be removed.

7.2.3 Repeat EV Depletion Experiment with EV specific purification method

While UC was shown to be efficient at pelleting sEVs, it would be desirable for the EV depletion experiment to be performed with an EV purification that is more specific to EVs based on their composition; rather than relying on physical size or density. This is to eliminate the possibility that something co-isolating with the sEVs is responsible for prolonging the lifespan of the fed-batch when it is removed. This could be done with immunoprecipitation. This in itself would show if sEVs are the active agent causing this effect. As a further validation, the sEVs purified by immunoprecipitation could then be supplemented back into cultures which have had their EVs depleted either by immunoprecipitation or UC.

It is also desirable to investigate the effects of depleting sEVs at earlier stages in the fed-batch and observe how this impacts growth and viability. This would further allude to what cellular processes the sEVs are impacting. It may be the case that no impact on cell viability is witnessed, however, cell growth or titre may be altered

7.2.4 Engineering CHO EVs to contain beneficial factors

CHO cells have been engineered to contain enzymes for treating lysosomal storage disorders which are functionally active in human cells (Seras-Franzoso *et al.*, 2021). From a mAb manufacturing perspective, this same approach could be leveraged to create a cell line which packages proteins and miRNAs that increase productivity into EVs. This could be done by fusing the protein of interest or RNA binding domain for the miRNA of interest to a protein that is abundantly loaded into EVs; such as TSG101 or Syntenin-1.

Alternatively, gene therapies could be loaded into CHO EVs for treatment of disease in humans. As has been mentioned previously, CHO cells can be grown to far larger cell densities than human cell lines. This makes them ideal EV factories as they will yield greater quantities of EVs than human cell lines in conditioned media. The observation that the Lonza fed-batch system produced larger quantities of sEVs/ ml than CD-CHO with Efficient Feed B suggests that further studying which media components could further augment EV secretion and enhance the EV yield obtained from CHO. However, a caveat to using CHO EVs to treat humans is that large quantities may stimulate an immunogenic response due to them containing non-human proteins.

7.2.5 Downregulating CHO EV Secretion to Enhance Productivity

From the observation that high qP clones have downregulated EVB, an investigation into what EVB genes specifically impact qP should be carried out. This could be screened for using RNAi targeting EVB genes and measuring the effect on growth, viability and titre. Genes found to be beneficial to productivity could then be knocked out by techniques such as CRISPR-Cas. Alternatively, overexpression of miRNAs which inhibit expression of the EVB gene may be used.

7.2.6 CHO EV Profiles as Indicators of Productivity

A study which includes a larger number of producer cell lines than in Chapter 5 should be carried out to assess how great the negative correlation of sEVs/ cell is with qP.

This should include cell lines secreting different ETE and DTE mAb products to determine if the observation is product specific or if EVB negatively impacts a cell's productive capacity. If the correlation is similar to what has been observed in Chapter 5, then EV secretion may be an indicator of productivity for a cell line.

7.2.7 Investigating How Culture Conditions Impact EV Profile

Additional experiments could look to see how common process alterations in biopharmaceutical manufacturing impact EV quantity and composition. This includes pH shifts, temperature shifts and feeding regimes. If it is possible to control and measure dissolved oxygen content, then variations in this process parameter could also be measured. These parameters are often fine-tuned to maximise product titre. Examining how they impact EV yield may further allude to how cells secreting large amounts of mAb product utilise their EVB machinery.

Bibliography

Agromayor, M. *et al.* (2012) 'The UBAP1 subunit of ESCRT-I interacts with ubiquitin via a SOUBA domain', *Structure*. Elsevier, 20(3), pp. 414–428. doi: 10.1016/j.str.2011.12.013.

Alonso Y Adell, M., Migliano, S. M. and Teis, D. (2016) 'ESCRT-III and Vps4: a dynamic multipurpose tool for membrane budding and scission', *The FEBS Journal*. Blackwell Publishing Ltd, 283(18), pp. 3288–3302. doi: 10.1111/febs.13688.

Anand, S. *et al.* (2019) 'Ticket to a bubble ride: Cargo sorting into exosomes and extracellular vesicles', *Biochimica et Biophysica Acta (BBA) - Proteins and Proteomics*. Elsevier. doi: 10.1016/J.BBAPAP.2019.02.005.

Andrews, S. *et al.* (2021) 'Priming of MSCs with inflammation-relevant signals affects extracellular vesicle biogenesis, surface markers, and modulation of T cell subsets', *Journal of Immunology and Regenerative Medicine*. Elsevier, 13, p. 100036. doi: 10.1016/J.REGEN.2020.100036.

Arab, T. *et al.* (2021) 'Characterization of extracellular vesicles and synthetic nanoparticles with four orthogonal single-particle analysis platforms', *Journal of Extracellular Vesicles*. John Wiley & Sons, Ltd, 10(6), p. e12079. doi: 10.1002/JEV2.12079.

Ardito, F. *et al.* (2017) 'The crucial role of protein phosphorylation in cell signaling and its use as targeted therapy (Review)', *International Journal of Molecular Medicine*. Spandidos Publications, 40(2), p. 271. doi: 10.3892/IJMM.2017.3036.

Atienzar-Aroca, S. *et al.* (2016) 'Oxidative stress in retinal pigment epithelium cells increases exosome secretion and promotes angiogenesis in endothelial cells', *Journal of Cellular and Molecular Medicine*. Wiley-Blackwell, 20(8), p. 1457. doi: 10.1111/JCMM.12834.

Bachurski, D. *et al.* (2019) 'Extracellular vesicle measurements with nanoparticle tracking analysis–An accuracy and repeatability comparison between NanoSight NS300 and ZetaView', *Journal of Extracellular Vesicles*. Taylor and Francis Ltd., 8(1). doi: 10.1080/20013078.2019.1596016/SUPPL_FILE/ZJEV_A_1596016_SM3642.PDF.

Badhwar, A. P. and Haqqani, A. S. (2020) 'Biomarker potential of brain-secreted extracellular vesicles in blood in Alzheimer's disease', *Alzheimer's & Dementia : Diagnosis, Assessment & Disease Monitoring*. Wiley-Blackwell, 12(1). doi: 10.1002/DAD2.12001.

Baietti, M. F. *et al.* (2012) 'Syndecan-syntenin-ALIX regulates the biogenesis of exosomes', *Nature Cell Biology*. Nature Publishing Group, 14(7), pp. 677–685. doi: 10.1038/ncb2502.

Bano, R., Ahmad, F. and Mohsin, M. (2021) 'A perspective on the isolation and characterization of extracellular vesicles from different biofluids', *RSC Advances*. Royal Society of Chemistry, 11(32), pp. 19598–19615. doi: 10.1039/D1RA01576A.

Becker, M. *et al.* (2019) 'The less the better: How suppressed base addition boosts production of monoclonal antibodies with Chinese hamster ovary cells', *Frontiers in Bioengineering and Biotechnology*. Frontiers Media S.A., 7(APR), p. 76. doi: 10.3389/FBIOE.2019.00076/BIBTEX.

Beekman, P. *et al.* (2019) 'Immuno-capture of extracellular vesicles for individual multi-modal characterization using AFM, SEM and Raman spectroscopy', *Lab on a Chip*. The Royal Society of Chemistry, 19(15), pp. 2526–2536. doi: 10.1039/C9LC00081J.

Belliveau, J. and Papoutsakis, E. T. (2022) 'Extracellular vesicles facilitate large-scale dynamic exchange of proteins and RNA among cultured Chinese hamster ovary and human cells', *Biotechnology and Bioengineering*. John Wiley & Sons, Ltd, 119(5), pp. 1222–1238. doi: 10.1002/BIT.28053.

Benedikter, B. J. *et al.* (2017) 'Ultrafiltration combined with size exclusion chromatography efficiently isolates extracellular vesicles from cell culture media for compositional and functional studies', *Scientific Reports 2017 7:1*. Nature Publishing Group, 7(1), pp. 1–13. doi: 10.1038/s41598-017-15717-7.

Benesova, S., Kubista, M. and Valihrach, L. (2021) 'Small RNA-Sequencing: Approaches and Considerations for miRNA Analysis', *Diagnostics*. Multidisciplinary Digital Publishing Institute (MDPI), 11(6). doi: 10.3390/DIAGNOSTICS11060964.

Bhome, R. *et al.* (2018) 'Exosomal microRNAs (exomiRs): Small molecules with a big role in cancer', *Cancer Letters*. Elsevier, 420, p. 228. doi:

10.1016/J.CANLET.2018.02.002.

Boodhoo, K. V. K. *et al.* (2022) 'Bioprocess intensification: A route to efficient and sustainable biocatalytic transformations for the future', *Chemical Engineering and Processing - Process Intensification*. Elsevier, 172, p. 108793. doi: 10.1016/J.CEP.2022.108793.

Bost, J. P. *et al.* (2022) 'Growth Media Conditions Influence the Secretion Route and Release Levels of Engineered Extracellular Vesicles', *Advanced Healthcare Materials*. John Wiley & Sons, Ltd, 11(5), p. 2101658. doi: 10.1002/ADHM.202101658.

Brown, A. J. *et al.* (2014) 'Synthetic promoters for CHO cell engineering', *Biotechnology and Bioengineering*. John Wiley & Sons, Ltd, 111(8), pp. 1638–1647. doi: 10.1002/bit.25227.

Bunnell, T. M. *et al.* (2011) 'β-Actin specifically controls cell growth, migration, and the G-actin pool', *Molecular Biology of the Cell*. The American Society for Cell Biology , 22(21), pp. 4047–4058. doi: 10.1091/MBC.E11-06-0582/ASSET/IMAGES/LARGE/4047FIG7.JPEG.

Busch, D. J. *et al.* (2022) 'Identification of RNA content of CHO-derived extracellular vesicles from a production process', *Journal of Biotechnology*. Elsevier, 348, pp. 36–46. doi: 10.1016/J.JBIOTEC.2022.03.004.

Buschmann, D. *et al.* (2018) 'Evaluation of serum extracellular vesicle isolation methods for profiling miRNAs by next-generation sequencing', *Journal of Extracellular Vesicles*. Taylor and Francis Ltd., 7(1). doi: 10.1080/20013078.2018.1481321/SUPPL_FILE/ZJEV_A_1481321_SM9097.ZIP.

Calzada, E., Onguka, O. and Claypool, S. M. (2016) 'Phosphatidylethanolamine Metabolism in Health and Disease', *International review of cell and molecular biology*. NIH Public Access, 321, p. 29. doi: 10.1016/BS.IRCMB.2015.10.001.

Campos-Silva, C. *et al.* (2019) 'High sensitivity detection of extracellular vesicles immune-captured from urine by conventional flow cytometry', *Scientific Reports 2019 9:1*. Nature Publishing Group, 9(1), pp. 1–12. doi: 10.1038/s41598-019-38516-8.

Carnino, J. M., Lee, H. and Jin, Y. (2019) 'Isolation and characterization of extracellular vesicles from Broncho-Alveolar lavage fluid: A review and comparison of different

methods', *Respiratory Research*. BioMed Central, 20(1), pp. 1–11. doi: 10.1186/S12931-019-1210-Z/TABLES/3.

Carrara, S. C. *et al.* (2021) 'Recombinant antibody production using a dual-promoter single plasmid system', *Antibodies*. MDPI AG, 10(2). doi: 10.3390/ANTIB10020018/S1.

Carrasquillo, R. *et al.* (2012) 'SNF8, a member of the ESCRT-II complex, interacts with TRPC6 and enhances its channel activity', *BMC Cell Biology*. BioMed Central, 13, p. 33. doi: 10.1186/1471-2121-13-33.

Chen, D. *et al.* (2018) 'miR-27b-3p inhibits proliferation and potentially reverses multi-chemoresistance by targeting CBLB/GRB2 in breast cancer cells', *Cell Death & Disease 2018 9:2*. Nature Publishing Group, 9(2), pp. 1–13. doi: 10.1038/s41419-017-0211-4.

Chen, F. *et al.* (2011) 'The Combined Effect of Sodium Butyrate and Low Culture Temperature on the Production, Sialylation, and Biological Activity of an Antibody Produced in CHO Cells', *Biotechnology and Bioprocess Engineering*, 16, pp. 1157–1165. doi: 10.1007/s12257-011-0069-8.

Chen, Y. S. *et al.* (2020) 'Exosomes in clinical trial and their production in compliance with good manufacturing practice', *Tzu Chi Medical Journal*. Wolters Kluwer Medknow Publications, pp. 113–120. doi: 10.4103/tcmj.tcmj_182_19.

Cheng, Y. and Schorey, J. S. (2013) 'Exosomes carrying mycobacterial antigens can protect mice against *Mycobacterium tuberculosis* infection', *European Journal of Immunology*. Wiley-VCH Verlag, 43(12), pp. 3279–3290. doi: 10.1002/eji.201343727.

Chipman, L. B. and Pasquinelli, A. E. (2019) 'MiRNA Targeting – Growing Beyond the Seed', *Trends in genetics : TIG*. NIH Public Access, 35(3), p. 215. doi: 10.1016/J.TIG.2018.12.005.

Chiu, J. *et al.* (2017) 'Knockout of a difficult-to-remove CHO host cell protein, lipoprotein lipase, for improved polysorbate stability in monoclonal antibody formulations', *Biotechnology and Bioengineering*. John Wiley and Sons Inc., 114(5), pp. 1006–1015. doi: 10.1002/bit.26237.

Choezom, D. and Gross, J. C. (2022) 'Neutral sphingomyelinase 2 controls exosome

secretion by counteracting V-ATPase-mediated endosome acidification', *Journal of cell science*. J Cell Sci, 135(5). doi: 10.1242/JCS.259324.

Chuo, S. T. Y., Chien, J. C. Y. and Lai, C. P. K. (2018) 'Imaging extracellular vesicles: Current and emerging methods', *Journal of Biomedical Science*. BioMed Central Ltd., 25(1), pp. 1–10. doi: 10.1186/S12929-018-0494-5/FIGURES/3.

Chusainow, J. *et al.* (2009) 'A study of monoclonal antibody-producing CHO cell lines: What makes a stable high producer?', *Biotechnology and Bioengineering*, 102(4), pp. 1182–1196. doi: 10.1002/bit.22158.

Clarke, C. *et al.* (2011) 'Large scale microarray profiling and coexpression network analysis of CHO cells identifies transcriptional modules associated with growth and productivity', *Journal of Biotechnology*. Elsevier, 155(3), pp. 350–359. doi: 10.1016/J.JBIOTEC.2011.07.011.

Clarke, C. *et al.* (2012) 'Integrated miRNA, mRNA and protein expression analysis reveals the role of post-transcriptional regulation in controlling CHO cell growth rate', *BMC Genomics 2012 13:1*. BioMed Central, 13(1), pp. 1–14. doi: 10.1186/1471-2164-13-656.

Cockcroft, S. (2021) 'Mammalian lipids: structure, synthesis and function', *Essays in Biochemistry*. Portland Press Ltd, 65(5), p. 813. doi: 10.1042/EBC20200067.

Colombo, M., Raposo, G. and Théry, C. (2014) 'Biogenesis, Secretion, and Intercellular Interactions of Exosomes and Other Extracellular Vesicles', *http://dx.doi.org/10.1146/annurev-cellbio-101512-122326*. Annual Reviews , 30, pp. 255–289. doi: 10.1146/ANNUREV-CELLBIO-101512-122326.

Coudert, L. *et al.* (2021) 'The ESCRT-0 subcomplex component Hrs/Hgs is a master regulator of myogenesis via modulation of signaling and degradation pathways', *BMC Biology*. BioMed Central Ltd, 19(1), pp. 1–28. doi: 10.1186/S12915-021-01091-4/FIGURES/3.

Crawford, S. *et al.* (2010) 'Effect of increased extracellular ca on microvesicle production and tumor spheroid formation.', *Cancer microenvironment : official journal of the International Cancer Microenvironment Society*. Springer, 4(1), pp. 93–103. doi: 10.1007/s12307-010-0049-0.

Dai, B. *et al.* (2020) 'The Cell Type–Specific Functions of miR-21 in Cardiovascular Diseases', *Frontiers in Genetics*. Frontiers, 0, p. 1237. doi: 10.3389/FGENE.2020.563166.

Dard-Dascot, C. *et al.* (2018) 'Systematic comparison of small RNA library preparation protocols for next-generation sequencing', *BMC Genomics*. BioMed Central Ltd., 19(1), pp. 1–16. doi: 10.1186/S12864-018-4491-6/FIGURES/5.

Das, T. K. *et al.* (2020) 'Stress Factors in mAb Drug Substance Production Processes: Critical Assessment of Impact on Product Quality and Control Strategy', *Journal of Pharmaceutical Sciences*. Elsevier, 109(1), pp. 116–133. doi: 10.1016/J.XPHS.2019.09.023.

Datta, A. *et al.* (2017) 'Manumycin A suppresses exosome biogenesis and secretion via targeted inhibition of Ras/Raf/ERK1/2 signaling and hnRNP H1 in castration-resistant prostate cancer cells', *Cancer Letters*. Elsevier, 408, pp. 73–81. doi: 10.1016/J.CANLET.2017.08.020.

Deaton, A. M. and Bird, A. (2011) 'CpG islands and the regulation of transcription', *Genes and Development*. Cold Spring Harbor Laboratory Press, 25(10), pp. 1010–1022. doi: 10.1101/gad.2037511.

Declerck, P. *et al.* (2017) 'The Language of Biosimilars: Clarification, Definitions, and Regulatory Aspects', *Drugs*. Springer International Publishing, pp. 671–677. doi: 10.1007/s40265-017-0717-1.

Deville, S. *et al.* (2021) 'Comparison of extracellular vesicle isolation and storage methods using high-sensitivity flow cytometry', *PLOS ONE*. Public Library of Science, 16(2), p. e0245835. doi: 10.1371/JOURNAL.PONE.0245835.

Dilsiz, N. (2020) 'Role of exosomes and exosomal microRNAs in cancer', *Future Science OA*. Future Science Group, 6(4). doi: 10.2144/FSOA-2019-0116.

Ding, J., Li, X. and Hu, H. (2016) 'TarPmiR: A new approach for microRNA target site prediction', *Bioinformatics*. Oxford University Press, 32(18), pp. 2768–2775. doi: 10.1093/bioinformatics/btw318.

Dinkins, M. B., Wang, G. and Bieberich, E. (2017) 'Sphingolipid-enriched extracellular vesicles and Alzheimer's disease: A decade of research', *Journal of Alzheimer's*

disease : JAD. NIH Public Access, 60(3), p. 757. doi: 10.3233/JAD-160567.

Drobnik, J. and Stebel, A. (2017) 'Tangled history of the European uses of Sphagnum moss and sphagnol', *Journal of Ethnopharmacology*. Elsevier Ireland Ltd, pp. 41–49. doi: 10.1016/j.jep.2017.07.025.

Dumont, J. *et al.* (2016) 'Human cell lines for biopharmaceutical manufacturing: history, status, and future perspectives.', *Critical reviews in biotechnology*. Taylor & Francis, 36(6), pp. 1110–1122. doi: 10.3109/07388551.2015.1084266.

Eaton, S. L. *et al.* (2014) 'A Guide to Modern Quantitative Fluorescent Western Blotting with Troubleshooting Strategies', *Journal of Visualized Experiments : JoVE*. MyJoVE Corporation, (93), p. e52099. doi: 10.3791/52099.

Eitan, E. *et al.* (2016) 'Impact of lysosome status on extracellular vesicle content and release', *Ageing Research Reviews*. Elsevier, 32, pp. 65–74. doi: 10.1016/J.ARR.2016.05.001.

Elsherbini, A. and Bieberich, E. (2018) 'Ceramide and Exosomes: A Novel Target in Cancer Biology and Therapy', *Advances in Cancer Research*. Academic Press Inc., 140, pp. 121–154. doi: 10.1016/bs.acr.2018.05.004.

Esparza, J. (2020) 'Early vaccine advocacy: Medals honoring Edward Jenner issued during the 19th century', *Vaccine*. Elsevier Ltd, 38(6), pp. 1450–1456. doi: 10.1016/j.vaccine.2019.11.077.

Essandoh, K. *et al.* (2015) 'Blockade of exosome generation with GW4869 dampens the sepsis-induced inflammation and cardiac dysfunction', *Biochimica et Biophysica Acta (BBA) - Molecular Basis of Disease*. Elsevier, 1852(11), pp. 2362–2371. doi: 10.1016/J.BBADIS.2015.08.010.

Fan, L. *et al.* (2012) 'Improving the efficiency of CHO cell line generation using glutamine synthetase gene knockout cells', *Biotechnology and Bioengineering*. John Wiley & Sons, Ltd, 109(4), pp. 1007–1015. doi: 10.1002/bit.24365.

Fan, L. *et al.* (2013) 'Development of a highly-efficient CHO cell line generation system with engineered SV40E promoter', *Journal of Biotechnology*. Elsevier, 168(4), pp. 652–658. doi: 10.1016/j.jbiotec.2013.08.021.

Feng, Y.-H. and Tsao, C.-J. (2016) 'Emerging role of microRNA-21 in cancer

(Review)', *Biomedical Reports*. Spandidos Publications, 5(4), pp. 395–402. doi: 10.3892/BR.2016.747.

Ferreira, J. V. *et al.* (2022) 'LAMP2A regulates the loading of proteins into exosomes', *Science Advances*. American Association for the Advancement of Science, 8(12). doi: 10.1126/SCIADV.ABM1140.

Fischer, S. *et al.* (2015) 'Unveiling the principle of microRNA-mediated redundancy in cellular pathway regulation', *http://dx.doi.org/10.1080/15476286.2015.1017238*. Taylor & Francis, 12(3), pp. 238–247. doi: 10.1080/15476286.2015.1017238.

Fortunato, D. *et al.* (2021) 'Opportunities and pitfalls of fluorescent labeling methodologies for extracellular vesicle profiling on high-resolution single-particle platforms', *International Journal of Molecular Sciences*. MDPI, 22(19), p. 10510. doi: 10.3390/IJMS221910510/S1.

Frankel, E. B. and Audhya, A. (2018) 'ESCRT-dependent cargo sorting at multivesicular endosomes', *Seminars in Cell & Developmental Biology*. Academic Press, 74, pp. 4–10. doi: 10.1016/J.SEMCDB.2017.08.020.

Fu, F. *et al.* (2018) 'Circulating Exosomal miR-17-5p and miR-92a-3p Predict Pathologic Stage and Grade of Colorectal Cancer', *Translational Oncology*. Elsevier, 11(2), pp. 221–232. doi: 10.1016/J.TRANON.2017.12.012.

Gámez-Valero, A. *et al.* (2016) 'Size-Exclusion Chromatography-based isolation minimally alters Extracellular Vesicles' characteristics compared to precipitating agents', *Scientific Reports 2016 6:1*. Nature Publishing Group, 6(1), pp. 1–9. doi: 10.1038/srep33641.

Gammell, P. *et al.* (2007) 'Initial identification of low temperature and culture stage induction of miRNA expression in suspension CHO-K1 cells', *Journal of Biotechnology*. Elsevier, 130(3), pp. 213–218. doi: 10.1016/J.JBIOTEC.2007.04.020.

Gardiner, C. *et al.* (2013) 'Extracellular vesicle sizing and enumeration by nanoparticle tracking analysis', *Journal of Extracellular Vesicles*. Co-Action Publishing, 2(1). doi: 10.3402/JEV.V2I0.19671/SUPPL_FILE/ZJEV_A_11815495_SM0001.DOCX.

Garrido-Cano, I. *et al.* (2018) 'Involvement of miR-99a in resistance to chemotherapy in triple-negative breast cancer', *Annals of Oncology*. Elsevier BV, 29, p. vi32. doi:

10.1093/annonc/mdy314.040.

Gaynes, R. (2017) ‘The discovery of penicillin—new insights after more than 75 years of clinical use’, *Emerging Infectious Diseases*. Centers for Disease Control and Prevention (CDC), 23(5), pp. 849–853. doi: 10.3201/eid2305.161556.

Ge, X. *et al.* (2019) ‘Circular RNA expression alterations in extracellular vesicles isolated from murine heart post ischemia/reperfusion injury’, *International Journal of Cardiology*. Elsevier, 296, pp. 136–140. doi: 10.1016/J.IJCARD.2019.08.024.

Ghossoub, R. *et al.* (2014a) ‘Syntenin-ALIX exosome biogenesis and budding into multivesicular bodies are controlled by ARF6 and PLD2’, *Nature Communications 2014 5:1*. Nature Publishing Group, 5(1), pp. 1–12. doi: 10.1038/ncomms4477.

Ghossoub, R. *et al.* (2014b) ‘Syntenin-ALIX exosome biogenesis and budding into multivesicular bodies are controlled by ARF6 and PLD2’, *Nature Communications*. Nature Publishing Group, 5(1), pp. 1–12. doi: 10.1038/ncomms4477.

Gilgunn, S. and Bones, J. (2018) ‘Challenges to industrial mAb bioprocessing—removal of host cell proteins in CHO cell bioprocesses’, *Current Opinion in Chemical Engineering*. Elsevier Ltd, pp. 98–106. doi: 10.1016/j.coche.2018.08.001.

Gleditzsch, D. *et al.* (2019) ‘PAM identification by CRISPR-Cas effector complexes: diversified mechanisms and structures’, *RNA Biology*. Taylor and Francis Inc., pp. 504–517. doi: 10.1080/15476286.2018.1504546.

Goey, C. H. *et al.* (2017) ‘Cascading effect in bioprocessing-The impact of mild hypothermia on CHO cell behavior and host cell protein composition’, *Biotechnology and Bioengineering*. John Wiley and Sons Inc., 114(12), pp. 2771–2781. doi: 10.1002/bit.26437.

Gray, W. D., Mitchell, A. J. and Searles, C. D. (2015) ‘An accurate, precise method for general labeling of extracellular vesicles’, *MethodsX*. Elsevier, 2, pp. 360–367. doi: 10.1016/j.mex.2015.08.002.

Gurung, S. *et al.* (2021) ‘The exosome journey: from biogenesis to uptake and intracellular signalling’, *Cell Communication and Signaling 2021 19:1*. BioMed Central, 19(1), pp. 1–19. doi: 10.1186/S12964-021-00730-1.

Ha, T. K. *et al.* (2022) ‘Factors affecting the quality of therapeutic proteins in

recombinant Chinese hamster ovary cell culture', *Biotechnology Advances*. Elsevier, 54, p. 107831. doi: 10.1016/J.BIOTECHADV.2021.107831.

Hagiwara, K. *et al.* (2015a) 'Commitment of Annexin A2 in recruitment of microRNAs into extracellular vesicles', *FEBS Letters*. Wiley Blackwell, 589(24), pp. 4071–4078. doi: 10.1016/j.febslet.2015.11.036.

Hagiwara, K. *et al.* (2015b) 'Commitment of Annexin A2 in recruitment of microRNAs into extracellular vesicles', *FEBS Letters*. John Wiley & Sons, Ltd, 589(24PartB), pp. 4071–4078. doi: 10.1016/J.FEBSLET.2015.11.036.

Haimovich, G. and Gerst, J. E. (2019) 'Detection of mRNA Transfer Between Mammalian Cells in Coculture by Single-Molecule Fluorescent In Situ Hybridization (smFISH)', in *Methods in Molecular Biology*. Humana Press Inc., pp. 109–129. doi: 10.1007/978-1-4939-9674-2_8.

Hamaker, N. K. and Lee, K. H. (2018) 'Site-specific integration ushers in a new era of precise CHO cell line engineering', *Current Opinion in Chemical Engineering*. Elsevier Ltd, pp. 152–160. doi: 10.1016/j.coche.2018.09.011.

Han, L. *et al.* (2018) 'MicroRNA Let-7f-5p Promotes Bone Marrow Mesenchymal Stem Cells Survival by Targeting Caspase-3 in Alzheimer Disease Model', *Frontiers in Neuroscience*. Frontiers, 0(MAY), p. 333. doi: 10.3389/FNINS.2018.00333.

Han, S. and Rhee, W. J. (2018) 'Inhibition of Apoptosis Using Exosomes in Chinese Hamster Ovary Cell Culture', *Biotechnology and Bioengineering*. doi: 10.1002/bit.26549.

Harmati, M. *et al.* (2019) 'Small extracellular vesicles convey the stress-induced adaptive responses of melanoma cells', *Scientific Reports 2019 9:1*. Nature Publishing Group, 9(1), pp. 1–19. doi: 10.1038/s41598-019-51778-6.

Heath, N. *et al.* (2018) 'Rapid isolation and enrichment of extracellular vesicle preparations using anion exchange chromatography', *Scientific Reports 2018 8:1*. Nature Publishing Group, 8(1), pp. 1–12. doi: 10.1038/s41598-018-24163-y.

Heinzelman, P. (2018) 'Magnetic Particle-Based Immunoprecipitation of Nanoscale Extracellular Vesicles from Biofluids', *Methods in Molecular Biology*. Humana Press, New York, NY, 1740, pp. 85–107. doi: 10.1007/978-1-4939-7652-2_8.

Henry, M. N. *et al.* (2020) ‘Attenuating apoptosis in Chinese hamster ovary cells for improved biopharmaceutical production’, *Biotechnology and Bioengineering*. John Wiley & Sons, Ltd, 117(4), pp. 1187–1203. doi: 10.1002/BIT.27269.

Herbert, Z. T. *et al.* (2020) ‘Multisite evaluation of next-generation methods for small RNA quantification’, *Journal of Biomolecular Techniques*. Association of Biomolecular Resource Facilities, 31(2), pp. 47–56. doi: 10.7171/JBT.20-3102-001/-/DC1.

Hessvik, N. P. and Llorente, A. (2017) ‘Current knowledge on exosome biogenesis and release’, *Cellular and Molecular Life Sciences 2017 75:2*. Springer, 75(2), pp. 193–208. doi: 10.1007/S00018-017-2595-9.

Hessvik, N. P. and Llorente, A. (2018) ‘Current knowledge on exosome biogenesis and release’, *Cellular and Molecular Life Sciences*. Springer International Publishing, 75(2), pp. 193–208. doi: 10.1007/s00018-017-2595-9.

Hinger, S. A. *et al.* (2018) ‘Diverse Long RNAs Are Differentially Sorted into Extracellular Vesicles Secreted by Colorectal Cancer Cells’, *Cell Reports*. Elsevier B.V., 25(3), pp. 715-725.e4. doi: 10.1016/j.celrep.2018.09.054.

Ho, Y. Y. *et al.* (2021) ‘Applications and analysis of hydrolysates in animal cell culture’, *Bioresources and Bioprocessing*. Nature Publishing Group, 8(1). doi: 10.1186/S40643-021-00443-W.

Hong, M. S. *et al.* (2018) ‘Challenges and opportunities in biopharmaceutical manufacturing control’, *Computers & Chemical Engineering*. Pergamon, 110, pp. 106–114. doi: 10.1016/J.COMPCHEMENG.2017.12.007.

Hood, J. L., Scott, M. J. and Wickline, S. A. (2014) ‘Maximizing exosome colloidal stability following electroporation’, *Analytical Biochemistry*. Academic Press, 448, pp. 41–49. doi: 10.1016/J.AB.2013.12.001.

Hossler, P., Khattak, S. F. and Li, Z. J. (2009) ‘Optimal and consistent protein glycosylation in mammalian cell culture’, *Glycobiology*, 19(9), pp. 936–949. doi: 10.1093/glycob/cwp079.

Hsu, C. *et al.* (2010) ‘Regulation of exosome secretion by Rab35 and its GTPase-activating proteins TBC1D10A–C’, *The Journal of Cell Biology*. The Rockefeller University Press, 189(2), p. 223. doi: 10.1083/JCB.200911018.

Hu, J. *et al.* (2021) 'Flotillin-1 Interacts With and Sustains the Surface Levels of TRPV2 Channel', *Frontiers in Cell and Developmental Biology*. Frontiers Media S.A., 9, p. 184. doi: 10.3389/FCELL.2021.634160/BIBTEX.

Hussein, N. A. E. M. *et al.* (2017) 'Plasma miR-22-3p, miR-642b-3p and miR-885-5p as diagnostic biomarkers for pancreatic cancer', *Journal of Cancer Research and Clinical Oncology*. Springer Verlag, 143(1), pp. 83–93. doi: 10.1007/S00432-016-2248-7/FIGURES/4.

Hyenne, V., Labouesse, M. and Goetz, J. G. (2018) 'The Small GTPase Ral orchestrates MVB biogenesis and exosome secretion', *Small GTPases*. Taylor & Francis, 9(6), p. 445. doi: 10.1080/21541248.2016.1251378.

Iavello, A. *et al.* (2016) 'Role of Alix in miRNA packaging during extracellular vesicle biogenesis', *International Journal of Molecular Medicine*. Spandidos Publications, 37(4), pp. 958–966. doi: 10.3892/ijmm.2016.2488.

Jackson, C. E. *et al.* (2017) 'Effects of Inhibiting VPS4 Support a General Role for ESCRTs in Extracellular Vesicle Biogenesis', *Biophysical Journal*. Biophysical Society, 113(6), pp. 1342–1352. doi: 10.1016/j.bpj.2017.05.032.

Jadhav, V. *et al.* (2012) 'A screening method to assess biological effects of microRNA overexpression in Chinese hamster ovary cells', *Biotechnology and Bioengineering*. John Wiley & Sons, Ltd, 109(6), pp. 1376–1385. doi: 10.1002/BIT.24490.

Jawa, V. *et al.* (2016) 'Evaluating Immunogenicity Risk Due to Host Cell Protein Impurities in Antibody-Based Biotherapeutics', *AAPS Journal*. Springer New York LLC, 18(6), pp. 1439–1452. doi: 10.1208/s12248-016-9948-4.

Jiang, M. *et al.* (2019) 'MiR-92a Family: A Novel Diagnostic Biomarker and Potential Therapeutic Target in Human Cancers', *Frontiers in Molecular Biosciences*. Frontiers, 0, p. 98. doi: 10.3389/FMOLB.2019.00098.

Jiang, Z. and Sharfstein, S. T. (2008) 'Sodium butyrate stimulates monoclonal antibody over-expression in CHO cells by improving gene accessibility', *Biotechnology and Bioengineering*, 100(1), pp. 189–194. doi: 10.1002/bit.21726.

Johnson, K. C. *et al.* (2011) 'Conserved MicroRNAs in Chinese hamster ovary cell lines', *Biotechnology and Bioengineering*. John Wiley & Sons, Ltd, 108(2), pp. 475–

480. doi: 10.1002/BIT.22940.

Ju, Y. *et al.* (2021) 'The Role of Exosome and the ESCRT Pathway on Enveloped Virus Infection', *International Journal of Molecular Sciences*. Multidisciplinary Digital Publishing Institute (MDPI), 22(16). doi: 10.3390/IJMS22169060.

Kakarla, R. *et al.* (2020) 'Apoptotic cell-derived exosomes: messages from dying cells', *Experimental & Molecular Medicine 2020 52:1*. Nature Publishing Group, 52(1), pp. 1–6. doi: 10.1038/s12276-019-0362-8.

Kang, P.-C. *et al.* (2018) 'miR-191 Inhibition Induces Apoptosis Through Reactivating Secreted Frizzled-Related Protein-1 in Cholangiocarcinoma', *Cellular Physiology and Biochemistry*. Karger Publishers, 49(5), pp. 1933–1942. doi: 10.1159/000493654.

Kang, R. *et al.* (2011) 'The Beclin 1 network regulates autophagy and apoptosis', *Cell Death and Differentiation*. Nature Publishing Group, 18(4), p. 571. doi: 10.1038/CDD.2010.191.

Kao, C. Y. and Papoutsakis, E. T. (2019) 'Extracellular vesicles: exosomes, microparticles, their parts, and their targets to enable their biomanufacturing and clinical applications', *Current Opinion in Biotechnology*. Elsevier Ltd, pp. 89–98. doi: 10.1016/j.copbio.2019.01.005.

Kapuralin, K. *et al.* (2015) 'STAM2, a member of the endosome-associated complex ESCRT-0 is highly expressed in neurons', *Molecular and Cellular Neuroscience*. Academic Press, 67, pp. 104–115. doi: 10.1016/J.MCN.2015.06.009.

Keller, M. D. *et al.* (2020) 'Decoy exosomes provide protection against bacterial toxins', *Nature 2020 579:7798*. Nature Publishing Group, 579(7798), pp. 260–264. doi: 10.1038/s41586-020-2066-6.

Kellner, K. *et al.* (2018) 'Targeting miRNAs with CRISPR/Cas9 to Improve Recombinant Protein Production of CHO Cells', in. Humana Press, New York, NY, pp. 221–235. doi: 10.1007/978-1-4939-8730-6_15.

Kelly, P. S. *et al.* (2014) 'Conserved microRNA function as a basis for Chinese hamster ovary cell engineering', *Biotechnology Letters 2014 37:4*. Springer, 37(4), pp. 787–798. doi: 10.1007/S10529-014-1751-7.

Kenny, N. J. *et al.* (2015) 'The phylogenetic utility and functional constraint of

microRNA flanking sequences', *Proceedings of the Royal Society B: Biological Sciences*. The Royal Society, 282(1803). doi: 10.1098/RSPB.2014.2983.

Keysberg, C. *et al.* (2021) 'Exploring the molecular content of CHO exosomes during bioprocessing', *Applied Microbiology and Biotechnology*. Springer Science and Business Media Deutschland GmbH, 105(9), pp. 3673–3689. doi: 10.1007/S00253-021-11309-8/FIGURES/4.

Kim, J. *et al.* (2014) 'Enhanced shedding of extracellular vesicles from amoeboid prostate cancer cells: Potential effects on the tumor microenvironment', *Cancer Biology & Therapy*. Taylor & Francis, 15(4), p. 409. doi: 10.4161/CBT.27627.

Kim, K. *et al.* (2021) 'Cyclic tangential flow filtration system for isolation of extracellular vesicles', *APL Bioengineering*. American Institute of Physics, 5(1), p. 16103. doi: 10.1063/5.0037768.

Kim, T. K. and Eberwine, J. H. (2010) 'Mammalian cell transfection: The present and the future', *Analytical and Bioanalytical Chemistry*. Springer, 397(8), pp. 3173–3178. doi: 10.1007/s00216-010-3821-6.

Kim, Y. J. *et al.* (2013) 'Autophagy and its implication in Chinese hamster ovary cell culture', *Biotechnology Letters*. Springer, 35(11), pp. 1753–1763. doi: 10.1007/S10529-013-1276-5/TABLES/1.

Kim, Y. J. *et al.* (2020) 'Rich production media as a platform for CHO cell line development', *AMB Express 2020 10:1*. SpringerOpen, 10(1), pp. 1–13. doi: 10.1186/S13568-020-01025-3.

Kinch, M. S. (2015) 'An overview of FDA-approved biologics medicines', *Drug Discovery Today*. Elsevier Current Trends, 20(4), pp. 393–398. doi: 10.1016/J.DRUDIS.2014.09.003.

Knarr, M. *et al.* (2020) 'miR-181a initiates and perpetuates oncogenic transformation through the regulation of innate immune signaling', *Nature Communications 2020 11:1*. Nature Publishing Group, 11(1), pp. 1–21. doi: 10.1038/s41467-020-17030-w.

Kong, D. H. *et al.* (2018) 'Emerging Roles of Vascular Cell Adhesion Molecule-1 (VCAM-1) in Immunological Disorders and Cancer', *International Journal of Molecular Sciences*. Multidisciplinary Digital Publishing Institute (MDPI), 19(4). doi:

10.3390/IJMS19041057.

Kowal, E. J. K. *et al.* (2017) 'Extracellular Vesicle Isolation and Analysis by Western Blotting', *Methods in molecular biology (Clifton, N.J.)*, 1660, pp. 143–152. doi: 10.1007/978-1-4939-7253-1_12.

Kowal, J., Tkach, M. and Théry, C. (2014) 'Biogenesis and secretion of exosomes', *Current Opinion in Cell Biology*. Elsevier Current Trends, 29(1), pp. 116–125. doi: 10.1016/J.CEB.2014.05.004.

Kumar, N. *et al.* (2016) 'Exploring Packaged Microvesicle Proteome Composition of Chinese Hamster Ovary Secretome', *J Bioprocess Biotech*, 6, p. 274. doi: 10.4172/2155-9821.1000274.

Kunert, R. and Reinhart, D. (2016) 'Advances in recombinant antibody manufacturing', *Applied Microbiology and Biotechnology*. Springer, 100(8), p. 3451. doi: 10.1007/S00253-016-7388-9.

Lai, T., Yang, Y. and Ng, S. K. (2013) 'Advances in Mammalian cell line development technologies for recombinant protein production.', *Pharmaceuticals (Basel, Switzerland)*. Multidisciplinary Digital Publishing Institute (MDPI), 6(5), pp. 579–603. doi: 10.3390/ph6050579.

Lalonde, M.-E. and Durocher, Y. (2017) 'Therapeutic glycoprotein production in mammalian cells', *Journal of Biotechnology*. Elsevier, 251, pp. 128–140. doi: 10.1016/J.JBIOTEC.2017.04.028.

Larios, J. *et al.* (2020) 'ALIX- And ESCRT-III-dependent sorting of tetraspanins to exosomes', *Journal of Cell Biology*. Rockefeller University Press, 219(3). doi: 10.1083/JCB.201904113/133723/ALIX-AND-ESCRT-III-DEPENDENT-SORTING-OF.

Latifkar, A. *et al.* (2019) 'New insights into extracellular vesicle biogenesis and function', *Journal of cell science*. NLM (Medline). doi: 10.1242/jcs.222406.

Le, K. *et al.* (2019) 'Assuring Clonality on the Beacon Digital Cell Line Development Platform'. doi: 10.1002/biot.201900247.

Lee, J. S. *et al.* (2015) 'Site-specific integration in CHO cells mediated by CRISPR/Cas9 and homology-directed DNA repair pathway', *Scientific Reports*.

Nature Publishing Group, 5. doi: 10.1038/srep08572.

Lee, S. A., Choi, C. and Yoo, T. H. (2021) 'Extracellular vesicles in kidneys and their clinical potential in renal diseases', *Kidney Research and Clinical Practice*. Korean Society of Nephrology, 40(2), p. 194. doi: 10.23876/J.KRCP.20.209.

Li, J. *et al.* (2015) 'Serum-free culture alters the quantity and protein composition of neuroblastoma-derived extracellular vesicles', *Journal of Extracellular Vesicles*. Co-Action Publishing, 4(2015), pp. 1–12. doi: 10.3402/JEV.V4.26883/SUPPL_FILE/ZJEV_A_11815563_SM0001.PDF.

Li, K. *et al.* (2018) 'Cushioned–Density Gradient Ultracentrifugation (C–DGUC): a Refined and High Performance Method for the Isolation, Characterization & Use of Exosomes', *Methods in molecular biology (Clifton, N.J.)*. NIH Public Access, 1740, p. 69. doi: 10.1007/978-1-4939-7652-2_7.

Li, L. and Luo, Z. (2017) 'Dysregulated MIR-27a-3p promotes nasopharyngeal carcinoma cell proliferation and migration by targeting MapklO', *Oncology Reports*. Spandidos Publications, 37(5), pp. 2679–2687. doi: 10.3892/OR.2017.5544/HTML.

Li, S. P. *et al.* (2018) 'Exosomal cargo-loading and synthetic exosome-mimics as potential therapeutic tools', *Acta Pharmacologica Sinica*. Nature Publishing Group, pp. 542–551. doi: 10.1038/aps.2017.178.

Li, X. *et al.* (2019) 'miR-92a-3p promotes the proliferation, migration and invasion of esophageal squamous cell cancer by regulating PTEN', *International Journal of Molecular Medicine*. Spandidos Publications, 44(3), p. 973. doi: 10.3892/IJMM.2019.4258.

Liangsupree, T., Multia, E. and Riekkola, M. L. (2021) 'Modern isolation and separation techniques for extracellular vesicles', *Journal of Chromatography A*. Elsevier, 1636, p. 461773. doi: 10.1016/J.CHROMA.2020.461773.

Lim, U. M. *et al.* (2013) 'Identification of autocrine growth factors secreted by CHO cells for applications in single-cell cloning media', *Journal of Proteome Research*. American Chemical Society, 12(7), pp. 3496–3510. doi: 10.1021/PR400352N/SUPPL_FILE/PR400352N_SI_001.PDF.

Livshts, M. A. *et al.* (2015) 'Isolation of exosomes by differential centrifugation:

Theoretical analysis of a commonly used protocol', *Scientific Reports 2015 5:1*. Nature Publishing Group, 5(1), pp. 1–14. doi: 10.1038/srep17319.

Logozzi, M. *et al.* (2020) 'Immunocapture-based ELISA to characterize and quantify exosomes in both cell culture supernatants and body fluids', *Methods in enzymology*. Methods Enzymol, 645, pp. 155–180. doi: 10.1016/BS.MIE.2020.06.011.

Loh, W. P., Yang, Y. and Lam, K. P. (2017) 'miR-92a enhances recombinant protein productivity in CHO cells by increasing intracellular cholesterol levels', *Biotechnology Journal*. John Wiley & Sons, Ltd, 12(4), p. 1600488. doi: 10.1002/BIOT.201600488.

Lucchetti, D., Fattorossi, A. and Sgambato, A. (2019) 'Extracellular Vesicles in Oncology: Progress and Pitfalls in the Methods of Isolation and Analysis', *Biotechnology Journal*. John Wiley & Sons, Ltd, 14(1), p. 1700716. doi: 10.1002/BIOT.201700716.

Luo, L.-J. *et al.* (2017) 'The inhibition role of miR-22 in hepatocellular carcinoma cell migration and invasion via targeting CD147', *Cancer Cell International 2017 17:1*. BioMed Central, 17(1), pp. 1–9. doi: 10.1186/S12935-016-0380-8.

Maccani, A. *et al.* (2014) 'Identification of microRNAs specific for high producer CHO cell lines using steady-state cultivation', *Applied Microbiology and Biotechnology 2014 98:17*. Springer, 98(17), pp. 7535–7548. doi: 10.1007/S00253-014-5911-4.

Macías, M. *et al.* (2019) 'Comparison of six commercial serum exosome isolation methods suitable for clinical laboratories. Effect in cytokine analysis', *Clinical Chemistry and Laboratory Medicine*. De Gruyter, 57(10), pp. 1539–1545. doi: 10.1515/CCLM-2018-1297/PDF.

Mathieu, M. *et al.* (2019) 'Specificities of secretion and uptake of exosomes and other extracellular vesicles for cell-to-cell communication', *Nature Cell Biology*. Nature Publishing Group, pp. 9–17. doi: 10.1038/s41556-018-0250-9.

Mathieu, M. *et al.* (2021) 'Specificities of exosome versus small ectosome secretion revealed by live intracellular tracking of CD63 and CD9', *Nature Communications 2021 12:1*. Nature Publishing Group, 12(1), pp. 1–18. doi: 10.1038/s41467-021-24384-2.

McAndrews, K. M. and Kalluri, R. (2019) 'Mechanisms associated with biogenesis of exosomes in cancer', *Molecular Cancer*. BioMed Central, 18(1), p. 52. doi:

10.1186/s12943-019-0963-9.

McNamara, R. P. *et al.* (2018) ‘Large-scale, cross-flow based isolation of highly pure and endocytosis-competent extracellular vesicles’, *Journal of Extracellular Vesicles*. Taylor and Francis Ltd., 7(1), p. 1541396. doi: 10.1080/20013078.2018.1541396/SUPPL_FILE/ZJEV_A_1541396_SM3970.ZIP.

de Menezes-Neto, A. *et al.* (2015) ‘Size-exclusion chromatography as a stand-alone methodology identifies novel markers in mass spectrometry analyses of plasma-derived vesicles from healthy individuals’, *Journal of Extracellular Vesicles*. Taylor & Francis, 4(1), p. 27378. doi: 10.3402/jev.v4.27378.

Miao, W. *et al.* (2020) ‘MiR-27b-3p suppresses glioma development via targeting YAP1’, *https://doi.org/10.1139/bcb-2019-0300*. NRC Research Press 1840 Woodward Drive, Suite 1, Ottawa, ON K2C 0P7 , 98(4), pp. 466–473. doi: 10.1139/BCB-2019-0300.

Mitra, S. and Murthy, G. S. (2022) ‘Bioreactor control systems in the biopharmaceutical industry: a critical perspective’, *Systems Microbiology and Biomanufacturing*. Springer, 2(1), pp. 91–112. doi: 10.1007/S43393-021-00048-6/TABLES/1.

Moghadasi, S. *et al.* (2021) ‘A paradigm shift in cell-free approach: the emerging role of MSCs-derived exosomes in regenerative medicine’, *Journal of Translational Medicine 2021 19:1*. BioMed Central, 19(1), pp. 1–21. doi: 10.1186/S12967-021-02980-6.

Momen-Heravi, F. (2017) ‘Isolation of Extracellular Vesicles by Ultracentrifugation’, *Methods in molecular biology (Clifton, N.J.)*. Humana Press, New York, NY, 1660, pp. 25–32. doi: 10.1007/978-1-4939-7253-1_3.

Morita, E. *et al.* (2007) ‘Identification of Human MVB12 Proteins as ESCRT-I Subunits that Function in HIV Budding’, *Cell Host and Microbe*. NIH Public Access, 2(1), pp. 41–53. doi: 10.1016/j.chom.2007.06.003.

Morrow, T. and Felcone, L. H. (2004) ‘Defining the difference: What Makes Biologics Unique’, *Biotechnology Healthcare*. MediMedia, USA, 1(4), p. 24. Available at: /pmc/articles/PMC3564302/ (Accessed: 30 May 2022).

Mulcahy, L. A., Pink, R. C. and Carter, D. R. F. (2014) ‘Routes and mechanisms of

extracellular vesicle uptake', *https://doi.org/10.3402/jev.v3.24641*. Taylor & Francis, 3(1). doi: 10.3402/JEV.V3.24641.

Muralidharan-Chari, V. *et al.* (2009) 'ARF6-regulated shedding of tumor cell-derived plasma membrane microvesicles.', *Current biology : CB*. NIH Public Access, 19(22), pp. 1875–85. doi: 10.1016/j.cub.2009.09.059.

Muralidharan-Chari, V. *et al.* (2010) 'Microvesicles: mediators of extracellular communication during cancer progression.', *Journal of cell science*. Company of Biologists, 123(Pt 10), pp. 1603–11. doi: 10.1242/jcs.064386.

Nabhan, J. F. *et al.* (2012) 'Formation and release of arrestin domain-containing protein 1-mediated microvesicles (ARMMs) at plasma membrane by recruitment of TSG101 protein.', *Proceedings of the National Academy of Sciences of the United States of America*. National Academy of Sciences, 109(11), pp. 4146–51. doi: 10.1073/pnas.1200448109.

Nagpal, N. and Kulshreshtha, R. (2014) 'miR-191: an emerging player in disease biology', *Frontiers in Genetics*. Frontiers, 0(APR), p. 99. doi: 10.3389/FGENE.2014.00099.

Nagyova, M. *et al.* (2014) 'A comparative study of PKH67, DiI, and BrdU labeling techniques for tracing rat mesenchymal stem cells', *In Vitro Cellular and Developmental Biology - Animal*. Springer New York LLC, 50(7), pp. 656–663. doi: 10.1007/S11626-014-9750-5/FIGURES/4.

Nakai, W. *et al.* (2016) 'A novel affinity-based method for the isolation of highly purified extracellular vesicles', *Scientific Reports 2016 6:1*. Nature Publishing Group, 6(1), pp. 1–11. doi: 10.1038/srep33935.

Neville, J. J. *et al.* (2017) 'Ubiquitous Chromatin-opening Elements (UCOEs): Applications in biomanufacturing and gene therapy', *Biotechnology Advances*. Elsevier Inc., pp. 557–564. doi: 10.1016/j.biotechadv.2017.05.004.

van Niel, G. *et al.* (2011) 'The tetraspanin CD63 regulates ESCRT-independent and dependent endosomal sorting during melanogenesis', *Developmental cell*. NIH Public Access, 21(4), p. 708. doi: 10.1016/J.DEVCEL.2011.08.019.

Nishida-Aoki, N. *et al.* (2020) 'Lipidomic Analysis of Cells and Extracellular Vesicles

from High- and Low-Metastatic Triple-Negative Breast Cancer', *Metabolites*. Multidisciplinary Digital Publishing Institute (MDPI), 10(2). doi: 10.3390/METABO10020067.

Noh, S. M., Shin, S. and Lee, G. M. (2018) 'Comprehensive characterization of glutamine synthetase-mediated selection for the establishment of recombinant CHO cells producing monoclonal antibodies', *Scientific Reports*. Nature Publishing Group, 8(1), pp. 1–11. doi: 10.1038/s41598-018-23720-9.

Novgorodov, S. A. *et al.* (2016) 'Lactosylceramide contributes to mitochondrial dysfunction in diabetes', *Journal of Lipid Research*. American Society for Biochemistry and Molecular Biology, 57(4), p. 546. doi: 10.1194/JLR.M060061.

O'Brien, J. *et al.* (2018) 'Overview of MicroRNA Biogenesis, Mechanisms of Actions, and Circulation', *Frontiers in Endocrinology*. Frontiers Media SA, 9(AUG), p. 402. doi: 10.3389/FENDO.2018.00402.

O'Brien, K. *et al.* (2020) 'RNA delivery by extracellular vesicles in mammalian cells and its applications', *Nature Reviews Molecular Cell Biology 2020 21:10*. Nature Publishing Group, 21(10), pp. 585–606. doi: 10.1038/s41580-020-0251-y.

Ostrowski, M. *et al.* (2009) 'Rab27a and Rab27b control different steps of the exosome secretion pathway', *Nature Cell Biology 2010 12:1*. Nature Publishing Group, 12(1), pp. 19–30. doi: 10.1038/ncb2000.

Ostrowski, M. *et al.* (2010) 'Rab27a and Rab27b control different steps of the exosome secretion pathway', *Nature Cell Biology*. Nature Publishing Group, 12(1), pp. 19–30. doi: 10.1038/ncb2000.

Pandey, L. M. (2022) 'Physicochemical factors of bioprocessing impact the stability of therapeutic proteins', *Biotechnology Advances*. Elsevier, 55, p. 107909. doi: 10.1016/J.BIOTECHADV.2022.107909.

Paolicelli, R. C., Bergamini, G. and Rajendran, L. (2019) 'Cell-to-cell Communication by Extracellular Vesicles: Focus on Microglia', *Neuroscience*. Elsevier Ltd, pp. 148–157. doi: 10.1016/j.neuroscience.2018.04.003.

Parimon, T. *et al.* (2018) 'Syndecan-1 Controls Lung Tumorigenesis by Regulating miRNAs Packaged in Exosomes', *The American Journal of Pathology*. American

Society for Investigative Pathology, 188(4), p. 1094. doi: 10.1016/J.AJPATH.2017.12.009.

de Paula Silva, E. *et al.* (2021) 'Extracellular vesicles cargo from head and neck cancer cell lines disrupt dendritic cells function and match plasma microRNAs', *Scientific Reports 2021 11:1*. Nature Publishing Group, 11(1), pp. 1–16. doi: 10.1038/s41598-021-97753-y.

Peng, L. *et al.* (2017) 'A simple, rapid method for evaluation of transfection efficiency based on fluorescent dye', *Bioengineered*. Taylor & Francis, 8(3), pp. 225–231. doi: 10.1080/21655979.2016.1222995.

Peng, R. W., Abellan, E. and Fussenegger, M. (2011) 'Differential effect of exocytic SNAREs on the production of recombinant proteins in mammalian cells', *Biotechnology and Bioengineering*. John Wiley & Sons, Ltd, 108(3), pp. 611–620. doi: 10.1002/BIT.22986.

Pérez-Rodriguez, S. *et al.* (2021) 'Compartmentalized Proteomic Profiling Outlines the Crucial Role of the Classical Secretory Pathway during Recombinant Protein Production in Chinese Hamster Ovary Cells', *ACS Omega*. American Chemical Society, 6(19), pp. 12439–12458. doi: 10.1021/ACSOMEGA.0C06030/SUPPL_FILE/AO0C06030_SI_002.XLSX.

Petricciani, J. and Sheets, R. (2008) 'An overview of animal cell substrates for biological products', *Biologicals*. Academic Press, 36(6), pp. 359–362. doi: 10.1016/j.biologicals.2008.06.004.

Pollet, H. *et al.* (2018) 'Plasma Membrane Lipid Domains as Platforms for Vesicle Biogenesis and Shedding?', *Biomolecules*. Multidisciplinary Digital Publishing Institute, 8(3), p. 94. doi: 10.3390/biom8030094.

Potla, P., Ali, S. A. and Kapoor, M. (2021) 'A bioinformatics approach to microRNA-sequencing analysis', *Osteoarthritis and Cartilage Open*. Elsevier, 3(1), p. 100131. doi: 10.1016/J.OCARTO.2020.100131.

Raja, S. A. *et al.* (2019) 'Increased expression levels of Syntaxin 1A and Synaptobrevin 2/Vesicle-Associated Membrane Protein-2 are associated with the progression of bladder cancer', *Genetics and Molecular Biology*. Sociedade Brasileira

de Genética, 42(1), p. 40. doi: 10.1590/1678-4685-GMB-2017-0339.

Randek, J. and Mandenius, C. F. (2017) 'On-line soft sensing in upstream bioprocessing', *http://dx.doi.org/10.1080/07388551.2017.1312271*. Taylor & Francis, 38(1), pp. 106–121. doi: 10.1080/07388551.2017.1312271.

Rani, S. *et al.* (2015) 'Mesenchymal stem cell-derived extracellular vesicles: Toward cell-free therapeutic applications', *Molecular Therapy*. Nature Publishing Group, pp. 812–823. doi: 10.1038/mt.2015.44.

Ridsdale, A. *et al.* (2006) 'Cholesterol Is Required for Efficient Endoplasmic Reticulum-to-Golgi Transport of Secretory Membrane Proteins', *Molecular Biology of the Cell*. American Society for Cell Biology, 17(4), p. 1593. doi: 10.1091/MBC.E05-02-0100.

Rikkert, L. G. *et al.* (2019) 'Quality of extracellular vesicle images by transmission electron microscopy is operator and protocol dependent', *Journal of Extracellular Vesicles*. Wiley-Blackwell, 8(1). doi: 10.1080/20013078.2018.1555419.

Rita Costa, A. *et al.* (2010) 'Guidelines to cell engineering for monoclonal antibody production', *European Journal of Pharmaceutics and Biopharmaceutics*. Elsevier, pp. 127–138. doi: 10.1016/j.ejpb.2009.10.002.

Rizzetto, S. *et al.* (2017) 'Impact of sequencing depth and read length on single cell RNA sequencing data of T cells', *Scientific Reports 2017 7:1*. Nature Publishing Group, 7(1), pp. 1–11. doi: 10.1038/s41598-017-12989-x.

Robbins, P. D. and Morelli, A. E. (2014) 'Regulation of Immune Responses by Extracellular Vesicles', *Nature reviews. Immunology*. NIH Public Access, 14(3), p. 195. doi: 10.1038/NRI3622.

Rosa-Fernandes, L. *et al.* (2017) 'A Perspective on Extracellular Vesicles Proteomics.', *Frontiers in chemistry*. Frontiers Media SA, 5, p. 102. doi: 10.3389/fchem.2017.00102.

Ryan, M. B. and Corcoran, R. B. (2018) 'Therapeutic strategies to target RAS-mutant cancers', *Nature Reviews Clinical Oncology 2018 15:11*. Nature Publishing Group, 15(11), pp. 709–720. doi: 10.1038/s41571-018-0105-0.

Sabourin, M. and Shapiro, R. (2011) 'Differential cell culture media requirements of CHO-S and CHO DG44 cells for single cell cloning A simple met hod for enriching

populat ions of t ransfect ed CHO cells for cells of higher specific produc…', *Bioprocess Technical*, 9(11), pp. 44–51. Available at: www.isTockphoTo.com (Accessed: 31 August 2022).

Sadowska, A. *et al.* (2021) 'Transcriptional profiling of Chinese hamster ovary (CHO) cells exposed to 2,3,7,8-tetrachlorodibenzo-p-dioxin (TCDD)', *Reproductive Toxicology*. Pergamon, 104, pp. 143–154. doi: 10.1016/J.REPROTOX.2021.07.012.

Saheera, S. *et al.* (2021) 'Extracellular vesicle interplay in cardiovascular pathophysiology', *American Journal of Physiology - Heart and Circulatory Physiology*. American Physiological Society, 320(5), pp. H1749–H1761. doi: 10.1152/AJPHEART.00925.2020/ASSET/IMAGES/LARGE/AJPHEART.00925.2020_F003.JPEG.

Schmidt, O. and Teis, D. (2012) 'The ESCRT machinery', *Current Biology*. Cell Press, p. R116. doi: 10.1016/j.cub.2012.01.028.

Seras-Franzoso, J. *et al.* (2021) 'Extracellular vesicles from recombinant cell factories improve the activity and efficacy of enzymes defective in lysosomal storage disorders', *Journal of Extracellular Vesicles*. Wiley-Blackwell, 10(5). doi: 10.1002/JEV2.12058.

Sha, S., Bhatia, H. and Yoon, S. (2018) 'An RNA-seq based transcriptomic investigation into the productivity and growth variants with Chinese hamster ovary cells', *Journal of Biotechnology*. Elsevier, 271, pp. 37–46. doi: 10.1016/J.JBIOTEC.2018.02.008.

Sheedy, P. and Medarova, Z. (2018) 'The fundamental role of miR-10b in metastatic cancer', *American Journal of Cancer Research*. e-Century Publishing Corporation, 8(9), p. 1674. Available at: /pmc/articles/PMC6176190/ (Accessed: 31 August 2021).

Shelke, G. V. *et al.* (2014) 'Importance of exosome depletion protocols to eliminate functional and RNA-containing extracellular vesicles from fetal bovine serum', *Journal of Extracellular Vesicles*. Wiley-Blackwell, 3(1). doi: 10.3402/JEV.V3.24783.

Shi, X. *et al.* (2019) 'Research progress on the PI3K/AKT signaling pathway in gynecological cancer (Review)', *Molecular Medicine Reports*. Spandidos Publications, 19(6), pp. 4529–4535. doi: 10.3892/MMR.2019.10121/HTML.

da Silva Novaes, A. *et al.* (2019) 'Influence of high glucose on mesangial cell-derived

exosome composition, secretion and cell communication', *Scientific Reports 2019 9:1*. Nature Publishing Group, 9(1), pp. 1–13. doi: 10.1038/s41598-019-42746-1.

Skotland, T. *et al.* (2020) 'An emerging focus on lipids in extracellular vesicles', *Advanced Drug Delivery Reviews*. Elsevier, 159, pp. 308–321. doi: 10.1016/J.ADDR.2020.03.002.

St Amand, M. M. *et al.* (2014) 'Controllability analysis of protein glycosylation in CHO cells.', *PloS one*. Public Library of Science, 9(2), p. e87973. doi: 10.1371/journal.pone.0087973.

Staubach, S. *et al.* (2021) 'Scaled preparation of extracellular vesicles from conditioned media', *Advanced Drug Delivery Reviews*. Elsevier, 177, p. 113940. doi: 10.1016/J.ADDR.2021.113940.

Stefani, F. *et al.* (2011) 'UBAP1 is a component of an endosome-specific ESCRT-I complex that is essential for MVB sorting', *Current Biology*. Elsevier, 21(14), pp. 1245–1250. doi: 10.1016/j.cub.2011.06.028.

Sticht, C. *et al.* (2018) 'miRWalk: An online resource for prediction of microRNA binding sites', *PLOS ONE*. Public Library of Science, 13(10), p. e0206239. doi: 10.1371/JOURNAL.PONE.0206239.

Sun, Y., Saito, K. and Saito, Y. (2022) 'Lipidomic Analysis of Extracellular Vesicles Isolated from Human Plasma and Serum'. Humana, New York, NY, pp. 157–173. doi: 10.1007/978-1-0716-2341-1_12.

Szabo, G. and Momen-Heravi, F. (2017) 'Extracellular vesicles in liver disease', *Nature reviews. Gastroenterology & hepatology*. NIH Public Access, 14(8), p. 455. doi: 10.1038/NRGASTRO.2017.71.

Széliová, D. *et al.* (2020) 'What CHO is made of: Variations in the biomass composition of Chinese hamster ovary cell lines', *Metabolic Engineering*. Academic Press, 61, pp. 288–300. doi: 10.1016/J.YMBEN.2020.06.002.

Tadauchi, T. *et al.* (2019) 'Utilizing a regulated targeted integration cell line development approach to systematically investigate what makes an antibody difficult to express', *Biotechnology Progress*. John Wiley and Sons Inc., 35(2), p. e2772. doi: 10.1002/btpr.2772.

Tai, H. C. and Schuman, E. M. (2008) ‘Ubiquitin, the proteasome and protein degradation in neuronal function and dysfunction’, *Nature Reviews Neuroscience 2008 9:11*. Nature Publishing Group, 9(11), pp. 826–838. doi: 10.1038/nrn2499.

Takagi, M. *et al.* (2021) ‘Polymer fraction including exosomes derived from Chinese hamster ovary cells promoted their growth during serum-free repeated batch culture’, *Journal of Bioscience and Bioengineering*. Elsevier, 131(2), pp. 183–189. doi: 10.1016/J.JBIOSC.2020.09.011.

Tancini, B. *et al.* (2019) ‘Insight into the Role of Extracellular Vesicles in Lysosomal Storage Disorders’, *Genes*. Multidisciplinary Digital Publishing Institute (MDPI), 10(7). doi: 10.3390/GENES10070510.

Tao, J. *et al.* (2015) ‘MiR-27b-3p suppresses cell proliferation through targeting receptor tyrosine kinase like orphan receptor 1 in gastric cancer’, *Journal of Experimental and Clinical Cancer Research*. BioMed Central Ltd., 34(1), pp. 1–13. doi: 10.1186/S13046-015-0253-3/FIGURES/7.

Teng, F. and Fussenegger, M. (2021) ‘Shedding Light on Extracellular Vesicle Biogenesis and Bioengineering’, *Advanced Science*. John Wiley & Sons, Ltd, 8(1), p. 2003505. doi: 10.1002/ADVS.202003505.

Thane, K. E., Davis, A. M. and Hoffman, A. M. (2019) ‘Improved methods for fluorescent labeling and detection of single extracellular vesicles using nanoparticle tracking analysis’, *Scientific Reports 2019 9:1*. Nature Publishing Group, 9(1), pp. 1–13. doi: 10.1038/s41598-019-48181-6.

Théry, C. *et al.* (2018) ‘Minimal information for studies of extracellular vesicles 2018 (MISEV2018): a position statement of the International Society for Extracellular Vesicles and update of the MISEV2014 guidelines’, *Journal of Extracellular Vesicles*. Taylor & Francis, 7(1), p. 1535750. doi: 10.1080/20013078.2018.1535750.

Tiszlavicz, Á. *et al.* (2022) ‘Distinct Cellular Tools of Mild Hyperthermia-Induced Acquired Stress Tolerance in Chinese Hamster Ovary Cells’, *Biomedicines*. MDPI AG, 10(5), p. 1172. doi: 10.3390/BIOMEDICINES10051172/S1.

Tkach, M. *et al.* (2017) ‘Qualitative differences in T-cell activation by dendritic cell-derived extracellular vesicle subtypes’, *The EMBO Journal*. EMBO, 36(20), pp. 3012–

3028. doi: 10.15252/embj.201696003.

Torralba, D. *et al.* (2018) ‘Priming of dendritic cells by DNA-containing extracellular vesicles from activated T cells through antigen-driven contacts’, *Nature Communications*. Nature Publishing Group, 9(1), pp. 1–17. doi: 10.1038/s41467-018-05077-9.

Torres, M. and Dickson, A. J. (2022) ‘Combined gene and environmental engineering offers a synergetic strategy to enhance r-protein production in Chinese hamster ovary cells’, *Biotechnology and Bioengineering*. John Wiley & Sons, Ltd, 119(2), pp. 550–565. doi: 10.1002/BIT.28000.

Tricarico, C., Clancy, J. and D’Souza-Schorey, C. (2017) ‘Biology and biogenesis of shed microvesicles’, *Small GTPases*. Taylor and Francis Inc., pp. 220–232. doi: 10.1080/21541248.2016.1215283.

Tsai, T. F. *et al.* (2018) ‘miR-99a-5p acts as tumor suppressor via targeting to mTOR and enhances RAD001-induced apoptosis in human urinary bladder urothelial carcinoma cells’, *OncoTargets and therapy*. Dove Press, 11, p. 239. doi: 10.2147/OTT.S114276.

Tschuschke, M. *et al.* (2020) ‘Inclusion Biogenesis, Methods of Isolation and Clinical Application of Human Cellular Exosomes’, *Journal of Clinical Medicine*. Multidisciplinary Digital Publishing Institute (MDPI), 9(2), p. 436. doi: 10.3390/JCM9020436.

TT, V. *et al.* (2021) ‘miR-10a as a therapeutic target and predictive biomarker for MDM2 inhibition in acute myeloid leukemia’, *Leukemia*. Leukemia, 35(7), pp. 1933–1948. doi: 10.1038/S41375-020-01095-Z.

Urquhart, L. (2022) ‘Top companies and drugs by sales in 2021’, *Nature Reviews Drug Discovery*. Nature Research, 21(4), p. 251. doi: 10.1038/D41573-022-00047-9.

Vader, P. *et al.* (2016) ‘Extracellular vesicles for drug delivery’, *Advanced Drug Delivery Reviews*. Elsevier, 106, pp. 148–156. doi: 10.1016/j.addr.2016.02.006.

Veith, N. *et al.* (2016) ‘Mechanisms underlying epigenetic and transcriptional heterogeneity in Chinese hamster ovary (CHO) cell lines’, *BMC Biotechnology*. BioMed Central Ltd., 16(1), p. 6. doi: 10.1186/s12896-016-0238-0.

Vestad, B. *et al.* (2017) ‘Size and concentration analyses of extracellular vesicles by nanoparticle tracking analysis: a variation study’, *Journal of Extracellular Vesicles*. Taylor and Francis Ltd., 6(1). doi: 10.1080/20013078.2017.1344087/SUPPL_FILE/ZJEV_A_1344087_SM3610.DOCX.

Vidal, M. (2019) ‘Exosomes: Revisiting their role as “garbage bags”’, *Traffic*. Blackwell Munksgaard, 20(11), pp. 815–828. doi: 10.1111/TRA.12687/.

Voronina, E. V. *et al.* (2016) ‘Design of a stable cell line producing a recombinant monoclonal anti-TNFα antibody based on a CHO cell line’, *SpringerPlus*. SpringerOpen, 5(1). doi: 10.1186/s40064-016-3213-2.

Vulpis, E. *et al.* (2019) ‘Cancer Exosomes as Conveyors of Stress-Induced Molecules: New Players in the Modulation of NK Cell Response’, *International Journal of Molecular Sciences*. Multidisciplinary Digital Publishing Institute (MDPI), 20(3). doi: 10.3390/IJMS20030611.

Walsh, G. (2002) ‘Biopharmaceuticals and biotechnology medicines: An issue of nomenclature’, *European Journal of Pharmaceutical Sciences*. Elsevier, pp. 135–138. doi: 10.1016/S0928-0987(01)00222-6.

Walsh, G. (2018) ‘Biopharmaceutical benchmarks 2018’, *Nature Biotechnology*. Nature Publishing Group, 36(12), pp. 1136–1145. doi: 10.1038/nbt.4305.

Wang, G. *et al.* (2022) ‘miR-99a-5p: A Potential New Therapy for Atherosclerosis by Targeting mTOR and Then Inhibiting NLRP3 Inflammasome Activation and Promoting Macrophage Autophagy’, *Disease Markers*. Edited by A. Singh, 2022, pp. 1–13. doi: 10.1155/2022/7172583.

Wang, J. *et al.* (2017) ‘Molecular mechanisms and clinical applications of miR-22 in regulating malignant progression in human cancer (Review)’, *International Journal of Oncology*. Spandidos Publications, 50(2), pp. 345–355. doi: 10.3892/IJO.2016.3811.

Wang, Y. *et al.* (2010) ‘Past, present and future applications of flow cytometry in aquatic microbiology’, *Trends in Biotechnology*. Elsevier Current Trends, 28(8), pp. 416–424. doi: 10.1016/J.TIBTECH.2010.04.006.

Webber, J. and Clayton, A. (2013) ‘How pure are your vesicles?’, *Journal of extracellular vesicles*. Taylor & Francis, 2. doi: 10.3402/jev.v2i0.19861.

Wei, J. xing *et al.* (2015) 'Vps4A functions as a tumor suppressor by regulating the secretion and uptake of exosomal microRNAs in human hepatoma cells', *Hepatology*. John Wiley and Sons Inc., 61(4), pp. 1284–1294. doi: 10.1002/HEP.27660/SUPPINFO.

Wei, Z. and Liu, H. T. (2002) 'MAPK signal pathways in the regulation of cell proliferation in mammalian cells', *Cell Research 2002 12:1*. Nature Publishing Group, 12(1), pp. 9–18. doi: 10.1038/sj.cr.7290105.

Weinguny, M. *et al.* (2020) 'Directed evolution approach to enhance efficiency and speed of outgrowth during single cell subcloning of Chinese Hamster Ovary cells', *Computational and Structural Biotechnology Journal*. Elsevier, 18, pp. 1320–1329. doi: 10.1016/J.CSBJ.2020.05.020.

Whitham, M. *et al.* (2018) 'Extracellular Vesicles Provide a Means for Tissue Crosstalk during Exercise', *Cell Metabolism*. Cell Press, 27(1), pp. 237-251.e4. doi: 10.1016/j.cmet.2017.12.001.

Williams, J. A., Carnes, A. E. and Hodgson, C. P. (2009) 'Plasmid DNA vaccine vector design: Impact on efficacy, safety and upstream production', *Biotechnology Advances*. Elsevier, pp. 353–370. doi: 10.1016/j.biotechadv.2009.02.003.

Wright, P. M., Seiple, I. B. and Myers, A. G. (2014) 'The Evolving Role of Chemical Synthesis in Antibacterial Drug Discovery', *Angewandte Chemie (International ed. in English)*. NIH Public Access, 53(34), p. 8840. doi: 10.1002/ANIE.201310843.

Xing, H. *et al.* (2021) 'Crosstalk between exosomes and autophagy: A review of molecular mechanisms and therapies', *Journal of Cellular and Molecular Medicine*. Wiley-Blackwell, 25(5), p. 2297. doi: 10.1111/JCMM.16276.

Xu, R. *et al.* (2018) 'Extracellular vesicles in cancer — implications for future improvements in cancer care', *Nature Reviews Clinical Oncology*. Nature Publishing Group, pp. 617–638. doi: 10.1038/s41571-018-0036-9.

Yang, X. *et al.* (2021) 'MiR-22-3p suppresses cell growth via MET/STAT3 signaling in lung cancer', *American Journal of Translational Research*. e-Century Publishing Corporation, 13(3), p. 1221. Available at: /pmc/articles/PMC8014426/ (Accessed: 27 July 2022).

Yao, Z. *et al.* (2019) 'Label-Free Proteomic Analysis of Exosomes Secreted from THP-1-Derived Macrophages Treated with IFN-α Identifies Antiviral Proteins Enriched in Exosomes', *Journal of Proteome Research*. American Chemical Society, 18(3), pp. 855–864. doi: 10.1021/acs.jproteome.8b00514.

Yu, Z. *et al.* (2020) 'Reduced oligodendrocyte exosome secretion in multiple system atrophy involves SNARE dysfunction', *Brain*. Oxford Academic, 143(6), pp. 1780–1797. doi: 10.1093/BRAIN/AWAA110.

Yuk, I. H. *et al.* (2015) 'More similar than different: Host cell protein production using three null CHO cell lines', *Biotechnology and Bioengineering*. John Wiley and Sons Inc., 112(10), pp. 2068–2083. doi: 10.1002/bit.25615.

Zavec, A. B. *et al.* (2016) 'Extracellular vesicles concentration is a promising and important parameter for industrial bioprocess monitoring', *Biotechnology Journal*. John Wiley & Sons, Ltd, 11(5), pp. 603–609. doi: 10.1002/BIOT.201500049.

Zboray, K. *et al.* (2015) 'Heterologous protein production using euchromatin-containing expression vectors in mammalian cells', *Nucleic Acids Research*. Oxford Academic, 43(16), pp. e102–e102. doi: 10.1093/NAR/GKV475.

Zhao, F. *et al.* (2020) 'Characterization of serum small extracellular vesicles and their small RNA contents across humans, rats, and mice', *Scientific Reports 2020 10:1*. Nature Publishing Group, 10(1), pp. 1–16. doi: 10.1038/s41598-020-61098-9.

Zheng, D. *et al.* (2021) 'The Role of Exosomes and Exosomal MicroRNA in Cardiovascular Disease', *Frontiers in Cell and Developmental Biology*. Frontiers Media S.A., 8, p. 1810. doi: 10.3389/FCELL.2020.616161/BIBTEX.

Zhou, L. *et al.* (2016) 'MiR-27a-3p functions as an oncogene in gastric cancer by targeting BTG2', *Oncotarget*. Impact Journals, LLC, 7(32), p. 51943. doi: 10.18632/ONCOTARGET.10460.

Zhu, J. *et al.* (2012) 'Recombinant human albumin supports single cell cloning of CHO cells in chemically defined media', *Biotechnology Progress*. American Chemical Society (ACS), 28(3), pp. 887–891. doi: 10.1002/BTPR.1549.

Appendix

Appendix A: Differentially expressed miRNAs on Day 8 compared to Day 5

Significant Differentially Expressed miRNAs on Day 8			
miRNA	**BaseMean**	**log2FoldChange**	**padj**
cgr-miR-141-3p	27.51009479	6.235263029	3.15E-05
cgr-miR-409-3p	11.12379453	5.976792157	0.000167
cgr-miR-143-3p	31.99806823	2.875331873	0.001336
cgr-miR-1285	36.31309481	2.439230972	0.001604
cgr-miR-296-3p	55.85795561	1.779516444	5.53E-10
cgr-miR-3068-3p	33.98231673	1.774726703	0.004305
cgr-miR-146a-5p	132.7525789	1.381303544	3.22E-06
cgr-miR-103-3p	1545.052622	1.190659771	4.7E-09
cgr-miR-344-3p	56.21104403	1.165684624	0.005929
cgr-miR-3535	94.87018582	1.05098245	0.00791
cgr-miR-320a-3p	6143.382461	0.936665282	4.25E-41
cgr-miR-23b-3p	746.3533	0.879645877	3.03E-17
cgr-miR-3074-1-5p	755.7640734	0.841134585	0.000414
cgr-miR-378	673.9429583	0.841057288	1.49E-09
cgr-miR-3074-2-5p	755.6827737	0.833761057	0.000463
cgr-miR-146b-5p	8525.623291	0.820535262	0.000573
cgr-miR-221-3p	22215.53468	0.807881719	1.18E-12
cgr-miR-298-5p	1358.731655	0.791362563	7.1E-20
cgr-miR-30c-1-3p	56.22867291	0.756948927	0.010018
cgr-miR-100-5p	1757.691673	0.715209735	2.25E-05
cgr-let-7c-1-5p	182.2949355	0.639395114	0.0014
cgr-miR-181d-5p	4197.350118	0.636908851	3.32E-08
cgr-let-7a-2	224.1079648	0.600782157	0.001157
cgr-miR-6092-3p	40.62303819	0.560261587	0.042531
cgr-miR-181c-3p	24307.33959	0.537960668	4.43E-05
cgr-miR-486-5p	19387.5498	0.520586633	1.99E-13
cgr-let-7c-2-3p	324.1766429	0.478842866	0.002016
cgr-miR-1839-5p	631.8770373	0.474271759	0.000841
cgr-miR-423-5p	6549.237214	0.472632553	5.53E-10
cgr-miR-410-3p	894.2114625	0.445243261	5.66E-05
cgr-miR-1260-5p	815.5641589	0.410019341	0.001589
cgr-miR-29a-3p	11708.0047	0.384042341	0.000306
cgr-miR-27b-3p	40030.80594	0.365481445	1.56E-07
cgr-let-7g-5p	20129.65167	0.358534223	4.67E-05
cgr-miR-125b-3p	6463.967488	0.344442962	1.57E-05
cgr-miR-744-5p	333.3383453	0.340376352	0.023913
cgr-let-7a-1-5p	28547.05633	0.312434027	0.046382
cgr-miR-10b-5p	464877.2776	0.270574611	0.018399

cgr-miR-151-3p	27149.52378	0.265288638	8.39E-08
cgr-miR-125b-2-5p	673.4375555	0.264232266	0.039406
cgr-miR-10a-5p	103122.3141	0.263235796	0.000966
cgr-miR-196b-5p	1075.196255	0.262069431	0.041728
cgr-miR-26a-2-5p	7435.776734	0.258726935	0.001649
cgr-let-7f-3p	158960.6495	0.25527502	0.026493
cgr-miR-21-5p	223038.5602	0.161663599	0.038731
cgr-miR-23a-5p	4652.937942	0.150369924	0.047978
cgr-miR-199a-3p	3707.191755	-0.130898436	0.009455
cgr-miR-194-5p	1515.499772	-0.162608304	0.007325
cgr-miR-27a-3p	19616.45536	-0.199943897	0.016894
cgr-miR-125a-5p	1144.263191	-0.243339005	0.00673
cgr-miR-106b-3p	1080.059312	-0.271514812	0.00917
cgr-miR-26b-5p	1679.371486	-0.278106277	0.016894
cgr-miR-28-3p	9156.004321	-0.314371741	2.16E-07
cgr-miR-16-5p	20784.69499	-0.325251403	0.00598
cgr-miR-155-5p	173.2792408	-0.368932816	0.040959
cgr-miR-22-3p	432692.9569	-0.374514477	1.42E-07
cgr-miR-615-3p	295.7449634	-0.401651811	0.004028
cgr-miR-374-5p	517.886979	-0.420036283	0.007998
cgr-miR-542-3p	1083.51719	-0.462721941	0.000771
cgr-miR-328-3p	489.6076346	-0.463820572	0.004028
cgr-miR-92b-3p	303.4513966	-0.477936525	0.000483
cgr-miR-215-3p	970.7650336	-0.486973826	5.4E-07
cgr-miR-139-5p	211.4814576	-0.489344762	0.001815
cgr-miR-674-3p	162.0814265	-0.49061818	0.009457
cgr-miR-99b-3p	77.48064213	-0.496122989	0.048913
cgr-miR-186-5p	21044.59067	-0.536043759	1.19E-25
cgr-miR-34b-5p	2938.136494	-0.548992305	5.3E-12
cgr-miR-92a-3p	140725.3984	-0.556894188	9.73E-18
cgr-miR-30e-5p	12824.93034	-0.581006516	4.28E-08
cgr-miR-301a-3p	6358.217731	-0.591584667	9.21E-16
cgr-miR-1343-3p	43.60375108	-0.614978289	0.043208
cgr-miR-350-5p	95.95595019	-0.69771049	0.00165
cgr-miR-191-5p	45115.38819	-0.70108489	5.51E-10
cgr-miR-17-5p	840.8987206	-0.722211944	1.09E-14
cgr-miR-484-5p	295.2369555	-0.72763319	0.000071
cgr-miR-30c-2-5p	2493.895118	-0.83379412	3.5E-18
cgr-miR-30b-5p	1335.740289	-0.843786183	1.26E-06
cgr-miR-93-5p	6931.016458	-0.859658032	2.27E-13
cgr-miR-450a-5p	1008.38082	-0.861461166	8.61E-08
cgr-miR-497-5p	154.5235125	-0.862995665	0.000218
cgr-miR-20a-5p	372.8737239	-0.896475281	3.05E-12
cgr-miR-130a-3p	36.6564201	-1.059997885	0.001275
cgr-miR-1306-5p	21.08489248	-1.10122438	0.039285
cgr-miR-18a-5p	92.93241536	-1.104521314	1.19E-08

cgr-miR-664-3p	180.8547115	-1.150621021	1.18E-05
cgr-miR-193a-3p	328.9503518	-1.26099595	1.93E-05
cgr-miR-149-5p	1837.217701	-1.381674501	2.89E-39
cgr-miR-503	11685.97079	-1.433426224	1.5E-104
cgr-miR-450b-5p	2216.666691	-1.619917033	2.35E-42

Appendix B: Significantly Differentially Expressed miRNAs on Day 12 relative to Day 8

Significant Differentially Expressed miRNAs on Day 12			
miRNA	**BaseMean**	**log2FoldChange**	**padj**
cgr-let-7e	9.783598267	8.376149636	1.23E-08
cgr-miR-147-3p	9.51986006	8.168458778	1.54E-06
cgr-miR-338	8.813187775	8.121838927	2.19E-07
cgr-miR-219b	8.320368377	8.013198135	4.68E-07
cgr-miR-138-5p	4.888788903	6.806939896	0.000141
cgr-miR-137-3p	4.250092069	6.601664696	0.000136
cgr-miR-331-3p	12.22695999	5.783443326	0.002419
cgr-miR-1903	71.22097695	3.261593517	5.43E-06
cgr-miR-29b-2	19.03489536	2.839024469	0.000862
cgr-miR-24-1	6.672909662	2.819008043	0.003258
cgr-miR-190b-5p	278.4196634	2.615180749	8.84E-40
cgr-miR-210	128.3390866	2.585714411	9.14E-27
cgr-miR-378	673.9429583	2.24494011	1.34E-75
cgr-miR-103-3p	1545.052622	2.095810411	4.37E-27
cgr-miR-141-3p	27.51009479	2.050605032	0.003165
cgr-miR-3102-3p	77.28889133	1.910564765	9.96E-12
cgr-miR-199a-2	16.09380381	1.787421388	0.02394
cgr-miR-107-3p	1880.154954	1.762180934	1.02E-21
cgr-miR-32-5p	125.8061082	1.729925292	2.78E-11
cgr-miR-193a-3p	328.9503518	1.703634033	4.98E-09
cgr-miR-101a-5p	1647.946044	1.56375457	2.23E-26
cgr-miR-23b-5p	746.3533	1.555210947	2.21E-65
cgr-miR-455-5p	60.99325156	1.500104132	1.59E-09
cgr-miR-324-5p	40.89793118	1.480474993	6.08E-07
cgr-miR-26a-1-5p	217.7815643	1.344118245	5.42E-17
cgr-miR-664-5p	180.8547115	1.331687772	2.38E-07
cgr-miR-154-5p	29.3959545	1.216521055	0.042096
cgr-miR-29a-5p	11708.0047	1.198066299	3.72E-33
cgr-miR-574-5p	543.6007005	1.068644885	1.27E-21
cgr-let-7c-2-5p	324.1766429	1.05434354	4.22E-14
cgr-miR-344-5p	56.21104403	1.048617804	0.00916
cgr-miR-34a-5p	42.42544259	1.011446625	0.045298

cgr-miR-16-2-5p	42.30356298	0.95418675	0.034817
cgr-miR-221-5p	22215.53468	0.951280623	4.32E-17
cgr-miR-23a-5p	4652.937942	0.914404212	2.01E-44
cgr-miR-100-5p	1757.691673	0.878673677	7.97E-08
cgr-miR-99b-5p	77.48064213	0.823020098	0.000989
cgr-miR-3074-1-5p	755.7640734	0.806232425	0.000587
cgr-miR-3074-2-5p	755.6827737	0.804864602	0.000587
cgr-miR-19b-5p	15788.23394	0.796626844	2.25E-05
cgr-miR-33-5p	178.5623424	0.78401972	0.000326
cgr-miR-1343-5p	43.60375108	0.76383836	0.015758
cgr-miR-365-5p	89.48567389	0.754805053	0.00938
cgr-miR-26a-2-5p	7435.776734	0.734627648	4.23E-22
cgr-let-7c-1-5p	182.2949355	0.722284238	0.000109
cgr-let-7a-2-5p	224.1079648	0.703283124	4.26E-05
cgr-miR-369-5p	53.56114754	0.694069986	0.031708
cgr-miR-24-5p	1069.738303	0.668678849	2.46E-13
cgr-miR-320a-5p	6143.382461	0.666445616	1.86E-22
cgr-let-7i-5p	631.7722844	0.661200603	2.25E-12
cgr-miR-193b-5p	189.9935667	0.656737688	0.01392
cgr-miR-342-5p	110.2795644	0.656167812	0.001133
cgr-miR-31-5p	9676.749608	0.652038012	5.96E-23
cgr-let-7b-5p	5471.579056	0.630877343	1.55E-05
cgr-miR-199a-3p	3707.191755	0.617210246	5.96E-44
cgr-miR-194-5p	1515.499772	0.609174659	4.1E-31
cgr-miR-1839-5p	631.8770373	0.589675712	1.06E-05
cgr-miR-30b-5p	1335.740289	0.588578206	0.000756
cgr-miR-196b-5p	1075.196255	0.558498027	1.93E-06
cgr-miR-181c-3p	24307.33959	0.554980383	1.69E-05
cgr-miR-350-5p	95.95595019	0.53479795	0.016433
cgr-miR-22-3p	432692.9569	0.506040716	2.08E-13
cgr-miR-99a-5p	416.0810394	0.490855309	0.039231
cgr-miR-27a-3p	19616.45536	0.479391658	2.96E-10
cgr-miR-674-3p	162.0814265	0.475638391	0.010803
cgr-miR-196a-5p	4228.019904	0.440289226	0.000469
cgr-miR-192-5p	7313.706481	0.422255168	1.52E-05
cgr-miR-484-5p	295.2369555	0.399103168	0.031511
cgr-miR-34b-5p	2938.136494	0.387295483	1.05E-06
cgr-miR-139-5p	211.4814576	0.36934143	0.017664
cgr-miR-652-3p	985.9489123	0.362507536	1.8E-06
cgr-miR-125a-5p	1144.263191	0.330497989	7.92E-05
cgr-miR-29b-3p	338.7360927	0.322063579	0.001464
cgr-miR-101b-3p	15537.44698	0.225599126	0.00029
cgr-miR-106b-3p	1080.059312	0.21998592	0.029121
cgr-let-7g-5p	20129.65167	0.211314615	0.015743

cgr-miR-140-5p	4740.169838	0.113033997	0.045972
cgr-miR-21-5p	223038.5602	-0.153585616	0.036441
cgr-miR-10a-5p	103122.3141	-0.224659119	0.008924
cgr-miR-298-5p	1358.731655	-0.229144343	0.008854
cgr-miR-186-5p	21044.59067	-0.23575339	5.43E-06
cgr-miR-181a-5p	101007.9582	-0.26729685	0.006654
cgr-miR-423-5p	6549.237214	-0.295943608	8.88E-05
cgr-miR-181b-5p	4021.37077	-0.301558533	0.020459
cgr-miR-125b-2-5p	673.4375555	-0.303020589	0.01176
cgr-miR-93-5p	6931.016458	-0.315064854	0.009304
cgr-miR-340-5p	1225.225772	-0.316046444	0.001264
cgr-miR-28-3p	9156.004321	-0.322995757	4.72E-08
cgr-miR-10b-5p	464877.2776	-0.328056554	0.001026
cgr-miR-30d-3p	535.5756432	-0.386812983	0.01184
cgr-miR-98-5p	2527.391727	-0.397896458	6.35E-05
cgr-miR-26b-5p	1679.371486	-0.417895558	0.000191
cgr-miR-34c-5p	53731.81123	-0.418488515	1.95E-06
cgr-miR-92a-3p	140725.3984	-0.419811598	8.26E-11
cgr-miR-149-5p	1837.217701	-0.439153497	5.93E-05
cgr-miR-16-5p	20784.69499	-0.449586362	8.54E-05
cgr-miR-486-5p	19387.5498	-0.478358617	8.65E-12
cgr-miR-146b-5p	8525.623291	-0.501285444	0.036088
cgr-miR-151-3p	27149.52378	-0.563913517	6.19E-33
cgr-miR-425-5p	737.789245	-0.584747382	1.68E-06
cgr-miR-146a-5p	132.7525789	-0.597125673	0.036753
cgr-miR-872-5p	3047.023164	-0.619921837	2.25E-05
cgr-miR-215-3p	970.7650336	-0.691301988	4.85E-13
cgr-miR-181d-5p	4197.350118	-0.758031591	1.48E-11
cgr-miR-671-3p	316.7148807	-0.765937855	8.33E-06
cgr-miR-195-5p	168.5775715	-0.766046944	7.98E-06
cgr-miR-222-3p	514.4185634	-0.7985393	1.5E-17
cgr-miR-20a-5p	372.8737239	-0.822150816	5.13E-10
cgr-miR-744-5p	333.3383453	-0.878009452	5.22E-10
cgr-miR-17-5p	840.8987206	-0.896447741	2.37E-21
cgr-miR-30e-5p	12824.93034	-0.908954779	6.39E-19
cgr-miR-296-3p	55.85795561	-0.970670906	0.000136
cgr-miR-301a-3p	6358.217731	-1.086767639	7.66E-51
cgr-miR-497-5p	154.5235125	-1.166569024	1.33E-06
cgr-miR-410-3p	894.2114625	-1.189318933	2.1E-29
cgr-miR-148b-3p	2157.300024	-1.23587702	2.94E-64
cgr-miR-1260-5p	815.5641589	-1.262879471	1.83E-24
cgr-miR-542-3p	1083.51719	-1.464240032	2.37E-28
cgr-miR-322-5p	5973.731666	-1.585293901	9.75E-64
cgr-miR-15b-5p	862.120109	-1.635509971	2.84E-48

cgr-miR-191-5p	45115.38819	-1.809388137	2.65E-60
cgr-miR-503	11685.97079	-2.342768548	1.1E-266
cgr-miR-1285	36.31309481	-2.37289071	0.001466
cgr-miR-450b-5p	2216.666691	-3.02939949	6.4E-128

Appendix C: Significantly Differentially Expressed miRNAs in GSKO-Host sEVs compared to CHO-A sEVs

Upregulated/ Downregulated miRNAs in GSKO-Host sEVs vs CHO-A sEVs			
miRNA	**BaseMean**	**log2FoldChange**	**padj**
miR-215-3p	392.7156703	2.165376669	6.88416E-12
miR-450a-5p	2379.609269	-1.188503816	7.40071E-10
miR-93-5p	3811.113955	1.177518104	3.92082E-09
miR-101a -5p	105.2333534	1.872980655	1.49654E-07
miR-322-5p	2291.115242	-0.714680301	5.82568E-07
miR-139-5p	650.4056217	-0.965975102	1.22087E-06
miR-152-3p	321.2701195	-1.180816905	5.08061E-06
miR-149-5p	1168.66769	0.870137951	6.46119E-06
miR-125b-2-5p	954.1601847	-1.060993531	1.23958E-05
miR-100 -5p	7055.104124	-0.790423742	1.66278E-05
miR-27b-3p	8815.355532	0.586184871	1.94362E-05
miR-125b-3p	11186.74042	-0.471201226	2.71992E-05
miR-194-5p	590.5104218	1.383189147	0.000163965
miR-146a-5p	339.0275394	0.92382008	0.000380642
miR-674-3p	737.1257224	-0.909200279	0.000487149
miR-19b-5p	160.4079647	2.102829173	0.001362315
miR-9-5p	65.65435245	-1.137054141	0.001362315
miR-92a-3p	19833.92097	0.570702221	0.001473337
miR-30a-5p	78.75086163	-1.266020196	0.003108149
miR-1249-3p	12.85969388	4.852686048	0.003116662
miR-486-5p	970.7575304	0.606923351	0.005637
miR-450b-5p	1486.347167	-0.734425056	0.005899455
miR-664-5p	70.39053246	0.974356655	0.009122051
miR-872-5p	2833.768147	0.41599155	0.009122051
miR-99a-5p	33699.91967	-0.651099398	0.014582658
miR-222-3p	559.2291886	-0.541063116	0.01798043
miR-542-3p	727.0593198	-0.762473624	0.01994599
miR-365-5p	33.32445146	0.31730266	0.029603797
miR-499-5p	142.8984568	0.66311262	0.030296563
miR-181a-5p	4379.778634	-0.527263109	0.031339471
miR-30d-3p	415.1784754	-0.578837454	0.038342277
miR-29a-3p	6262.644347	0.38696419	0.039847437
miR-451a-5p	15.06089448	0.115786178	0.044696214

Appendix D: Significantly Differential Expressed miRNAs in GSKO-Host Intracellular miRNA composition compared to GSKO-Host sEVs

Upregulated/ Downregulated miRNAs in GSKO-Host Cells vs GSKO Host sEVs			
miRNA	**BaseMean**	**log2FoldChange**	**padj**
cgr-miR-322-5p	2291.115242	1.791325646	2.37E-44
cgr-miR-222-3p	559.2291886	1.965128184	1.07E-23
cgr-miR-27a-5p	30239.71914	-1.475643081	7.07E-19
cgr-miR-30d-3p	415.1784754	1.940032349	9.29E-16
cgr-miR-22-3p	12586.56854	-1.420978766	1.04E-15
cgr-miR-674-3p	737.1257224	-1.900450763	6.07E-15
cgr-miR-34c-5p	18420.23564	1.399072435	7.17E-15
cgr-miR-17-5p	2037.503255	2.120937893	1.09E-14
cgr-miR-99a-5p	33699.91967	-1.865440578	3.55E-14
cgr-miR-503	4776.601412	0.839516463	4.32E-13
cgr-miR-125b-3p	11186.74042	0.676728872	9.45E-11
cgr-let-7d-5p	7203.171151	1.073945323	1.29E-10
cgr-miR-20a-5p	2444.487222	1.970768163	3E-10
cgr-miR-328-3p	2199.77385	1.309734823	3.24E-10
cgr-miR-16-5p	1199.082856	1.44349326	3.57E-10
cgr-miR-9-5p	65.65435245	-1.921017176	8.86E-10
cgr-miR-15b-5p	515.7511434	1.49308049	2.71E-09
cgr-miR-181b-5p	760.735186	-0.831007442	3.03E-09
cgr-miR-186-5p	2741.06186	-2.041174243	7.8E-09
cgr-miR-192-5p	2922.163057	-1.152361518	0.000000102
cgr-let-7a-1-5p	22061.60428	0.881932138	0.000000137
cgr-miR-542-3p	727.0593198	1.635309472	0.000000602
cgr-miR-409-3p	14.80745468	7.360177716	0.00000102
cgr-miR-744-5p	704.1472283	0.905215053	0.00000135
cgr-miR-148a-3p	43.94339905	-2.254476837	0.00000321
cgr-miR-146b-5p	6585.442655	-1.119178912	0.0000057
cgr-miR-365-3p	33.32445146	8.026858638	0.0000221
cgr-miR-874-3p	12.0073877	6.871260372	0.0000257
cgr-miR-152-3p	321.2701195	0.971397003	0.0000298
cgr-miR-486-5p	970.7575304	0.844028529	0.0000359
cgr-miR-148b-3p	2780.427224	0.747375879	0.0000364
cgr-miR-410-3p	27.85662444	-2.228590985	0.0000733
cgr-miR-7b-5p	68.59534631	1.737822533	0.0000746
cgr-miR-1249-3p	12.85969388	6.01253662	0.0000944
cgr-let-7i	654.9319897	-1.09645243	0.0000949
cgr-miR-130a-3p	53.80697851	-2.177461298	0.000130397
cgr-miR-378	204.7529686	-0.947010381	0.000140723
cgr-let-7f-3p	78863.85345	0.646953729	0.000144186
cgr-miR-93-5p	3811.113955	0.74352813	0.000145137
cgr-miR-107-3p	91.66631793	1.41278896	0.000158698

cgr-miR-103-3p	95.01239368	3.577718055	0.000182213
cgr-miR-29a-5p	6262.644347	-0.625157538	0.000196212
cgr-miR-149-5p	1168.66769	-0.678297342	0.000281642
cgr-miR-374-5p	749.011004	1.062174257	0.000304461
cgr-miR-125a-5p	767.9745805	0.694747629	0.000402267
cgr-miR-215-5p	392.7156703	-1.080910292	0.000402267
cgr-miR-92b-5p	9.863162798	6.3063502	0.000402267
cgr-miR-32-5p	85.56338983	-1.183276017	0.000744636
cgr-miR-339-5p	20.759599	6.97799271	0.000789491
cgr-miR-19b	160.4079647	1.95849473	0.001232184
cgr-miR-615-5p	451.9558633	0.777607654	0.001333041
cgr-miR-199a-5p	3485.237437	0.53996959	0.001566439
cgr-miR-146a-5p	339.0275394	-0.748115352	0.002421548
cgr-miR-92a-3p	19833.92097	0.518301878	0.002432489
cgr-miR-423-5p	6457.732783	0.489916933	0.002972692
cgr-miR-98-5p	1767.922286	0.492877025	0.003282818
cgr-miR-101a-5p	105.2333534	-0.968061919	0.004773455
cgr-miR-450a-5p	2379.609269	-0.537917332	0.005015047
cgr-miR-365-2-5p	6.39481158	5.123832707	0.005442851
cgr-miR-301a-5p	50.15560626	1.853513055	0.007610893
cgr-miR-26a-1-3p	245.0645751	-0.700189876	0.00806854
cgr-miR-29b-3p	174.953528	0.775511099	0.009095185
cgr-miR-671-5p	108.5025036	1.616216864	0.00943558
cgr-miR-320a	2275.538402	0.450650074	0.009675587
cgr-miR-344-5p	68.68914306	0.733563555	0.009684566
cgr-miR-28-5p	1703.23326	0.306457426	0.010807569
cgr-miR-125b-2	954.1601847	0.5876596	0.012029838
cgr-miR-25-3p	10603.05396	-0.304464524	0.013092795
cgr-miR-193a-3p	18.24829452	-0.792815055	0.01648386
cgr-miR-574-5p	522.1676724	-0.792746255	0.01648386
cgr-miR-652-3p	2137.243672	0.323926057	0.01648386
cgr-miR-30c-2-5p	3594.761012	-0.312891117	0.018123851
cgr-miR-330-3p	161.198801	0.671349532	0.018123851
cgr-miR-1839-5p	52.56076841	1.3592168	0.019255908
cgr-miR-21-5p	158651.2519	0.640072847	0.021267071
cgr-miR-210-5p	12.25345401	1.074313933	0.021635117
cgr-miR-30a-5p	78.75086163	-0.890562723	0.022934607
cgr-miR-455-5p	326.004739	0.562887661	0.024638285
cgr-miR-31-5p	418.0668234	0.961515313	0.027043968
cgr-miR-369-5p	7.251760362	2.768825017	0.034283036
cgr-miR-181a-5p	4379.778634	-0.490589466	0.035939114
cgr-miR-340-5p	286.6637731	0.69412414	0.036385627
cgr-miR-296-3p	34.3095184	1.85198447	0.041116901
cgr-miR-15a-5p	4.289728479	1.986741719	0.042119189
cgr-miR-3072-3p	3.906135271	2.110409393	0.044487566
cgr-miR-137-3p	4.601301412	1.333207951	0.047502668

cgr-miR-191-5p	10139.92657	-0.534157247	0.049099744

Appendix E: Large difference in number of annotated reads in each library. (A) Library 1 in Chapter 3. (B) Library 2 in Chapter 4.

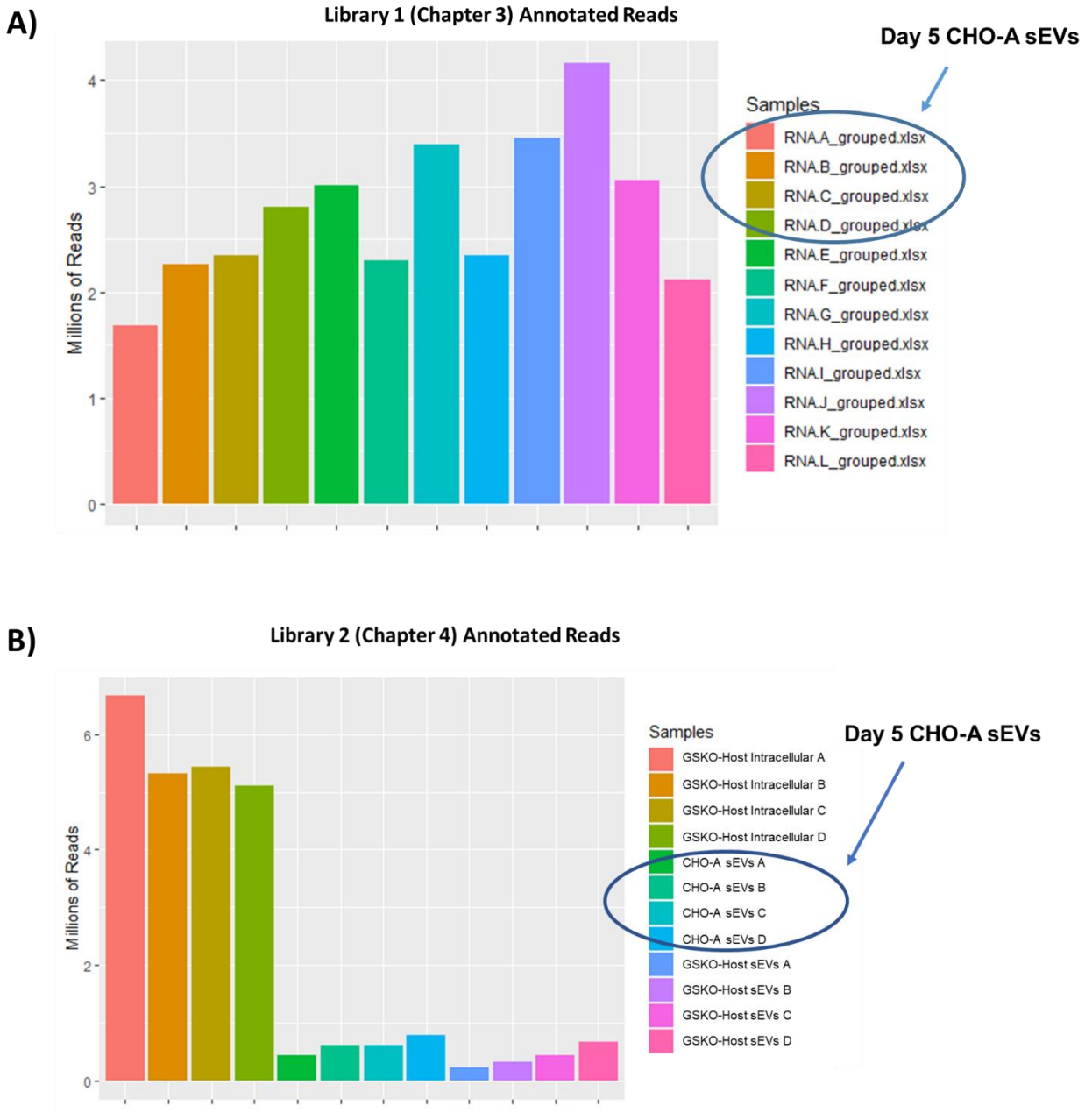

Appendix F: Azenta (Genewiz) Quality Control report on samples from (A) Library 1 in Chapter 3 and (B) Library 2 in Chapter 4.

A)

Sample ID	Barcode Sequence	# Reads	Yield (Mbases)	Mean Quality Score	% Bases >= 30
RNA-A	CCGTCC	21,391,138	6,417	29.83	59.54
RNA-B	GTAGAG	19,767,393	5,930	29.43	58
RNA-C	GTCCGC	20,108,675	6,033	29.52	58.32
RNA-D	GTGAAA	23,982,770	7,195	29.24	57.3
RNA-E	GTGGCC	23,599,007	7,080	29.54	58.39
RNA-F	GTTTCG	17,676,528	5,303	29.52	58.28
RNA-G	CGTACG	25,181,902	7,555	29.7	58.94
RNA-H	GAGTGG	19,830,621	5,949	29.99	60.07
RNA-I	GGTAGC	21,867,097	6,560	29.43	57.97
RNA-J	ACTGAT	21,027,019	6,308	29.29	57.49
RNA-K	ATGAGC	24,481,240	7,344	29.34	57.64
RNA-L	ATTCCT	12,777,283	3,833	29.44	58.02

Name	Number of reads	Avg.length	Number of reads after trim	Percentage trimmed	Avg.length after trim
RNA-A	42,782,276	150	9,544,867	22.31%	21.7
RNA-B	39,534,786	150	9,946,449	25.16%	22
RNA-C	40,217,350	150	9,409,614	23.40%	21.9
RNA-D	47,965,540	150	11,862,309	24.73%	21.8
RNA-E	47,198,014	150	11,100,321	23.52%	22
RNA-F	35,353,056	150	8,439,405	23.87%	22
RNA-G	50,363,804	150	10,849,921	21.54%	22
RNA-H	39,661,242	150	8,687,824	21.91%	22
RNA-I	43,734,194	150	10,776,310	24.64%	21.5
RNA-J	42,054,038	150	11,314,201	26.90%	21.5
RNA-K	48,962,480	150	11,391,146	23.27%	21.5
RNA-L	25,554,566	150	6,474,175	25.33%	21.6

B)

Name	Number of reads	Avg.length	Number of reads after trim	Percentage trimmed	Avg.length after trim
GSKO-Host Intracellular A	53,751,142	150	13,211,399	24.58%	21.7
GSKO-Host Intracellular B	38,459,002	150	10,826,372	28.15%	21.8
GSKO-Host Intracellular C	37,280,162	150	10,732,505	28.79%	21.8
GSKO-Host Intracellular D	34,243,012	150	10,482,581	30.61%	21.8
CHO-A sEVs A	40,304,458	150	9,199,458	22.82%	21.3
CHO-A sEVs B	39,690,304	150	8,920,749	22.48%	21.6
CHO-A sEVs C	47,878,848	150	9,872,289	20.62%	21.6
CHO-A sEVs D	43,519,756	150	9,365,963	21.52%	21.8
GSKO-Host sEVs A	52,925,992	150	9,434,217	17.83%	20.8
GSKO-Host sEVs B	41,629,186	150	9,122,756	21.91%	20.9
GSKO-Host sEVs C	40,453,648	150	8,534,844	21.10%	21.2
GSKO-Host sEVs D	40,005,560	150	8,939,616	22.35%	21.5

Name	Number of reads	Avg.length	Number of reads after trim	Percentage trimmed	Avg.length after trim
GSKO-Host Intracellular A	53,751,142	150	13,211,399	24.58%	21.7
GSKO-Host Intracellular B	38,459,002	150	10,826,372	28.15%	21.8
GSKO-Host Intracellular C	37,280,162	150	10,732,505	28.79%	21.8
GSKO-Host Intracellular D	34,243,012	150	10,482,581	30.61%	21.8
CHO-A sEVs A	40,304,458	150	9,199,458	22.82%	21.3
CHO-A sEVs B	39,690,304	150	8,920,749	22.48%	21.6
CHO-A sEVs C	47,878,848	150	9,872,289	20.62%	21.6
CHO-A sEVs D	43,519,756	150	9,365,963	21.52%	21.8
GSKO-Host sEVs A	52,925,992	150	9,434,217	17.83%	20.8
GSKO-Host sEVs B	41,629,186	150	9,122,756	21.91%	20.9
GSKO-Host sEVs C	40,453,648	150	8,534,844	21.10%	21.2
GSKO-Host sEVs D	40,005,560	150	8,939,616	22.35%	21.5

Appendix G: Values and code used to generate correlations summary matrix

Cell Line	D5 Titre (sEV Flasks)	D10 Titre (RNA-seq Flasks)	D5 qP (sEV Flasks) - pg/cell/day	D10 qP (RNA-seq Flasks) - pg/cell/day	Average specific glucose consumption rate	IVCD	Cell Volume (cm3)	sEVs/ Cell	Growth Rate (cells/ ml/ day)
X4 (1)	0.330690764	2.5171	23.30588659	36.5681844	0.157445586	16.295	2804.739583	247682.7094	0.630834041
X4 (2)	0.353254846	2.476	28.11053012	34.41256579	0.184193554	13.13	2756.93256	258098.8917	0.589656535
X3 (1)	0.709843393	6.3279	49.87905301	42.66764467	0.210140941	17.56	2804.739583	81997.57134	0.48053371
X3 (2)	0.765224706	6.0009	50.52369851	62.38151402	0.238759564	17.225	2902.00527	77297.73463	0.50647125
X2 (1)	0.864066665	6.0075	74.56817892	91.87256452	0.199211326	12.9	2902.00527	78086.85446	0.612945029
X2 (2)	0.735238908	5.9211	58.72254036	83.0212071	0.191921763	13.53	2853.096107	56172.04301	0.654238323
X1 (1)	0.519360297	5.7729	54.44374571	106.5185715	0.293567165	9.51	4124.180143	49652.77778	0.57880809
X1 (2)	0.655581404	5.3529	73.31268124	109.7419879	0.219523677	9.185	4124.180143	38821.13821	0.58591643
Non-X GS-NULL (1)					0.140044226	9.106	2951.470213	92029.40053	0.571516387
Non-X GS-NULL (2)					0.18244519	9.34	2804.739583	62278.80658	0.640530598
PARENTAL (1)					0.16760256	6.573	3001.494077	32341.52652	0.558938719
PARENTAL (2)					0.166956681	5.885	2853.096107	24389.67136	0.587420438
GS-NULL 1 (1)					0.171945671	7.921	2709.671897	64540.98916	0.627655746
GS-NULL 1 (2)					0.132655661	8.339	2526.030043	67174.06261	0.575980092
GS-NULL 2 (1)					0.14361555	10.896	2616.77709	33010.56338	0.667464795
GS-NULL 2 (2)					0.161352126	8.843	2662.954453	49890.96573	0.611724272

RStudio Code:

```
correlations_summary <- read_csv("correlations_summary_no_names.csv")

#Generates object in R with csv file containing values as seen in above.

library(RColorBrewer)

#Contains a pallete of colours for generating graphics in RStudio.

library(readr)

#Makes rectangular data out of csv files which is needed for matrix generation.

library(Hmisc)

#Load Hmisc library which contains functions needed to generate matrix graphic.

significant_matrix <- rcorr(as.matrix(correlations_summary, use = "complete.obs"))

#Converts correlations_summary into a matrix which can be graphed using functions in the Hmisc library.
```

```
corrplot(significant_matrix$r, method = "color", type="upper", order="hclust", col = brewer.pal(n=8, name = "RdYlBu"), tl.cex = 0.6, tl.col = "black", addCoef.col = 1, number.cex = 0.6, p.mat = significant_matrix$P, sig.level = 0.05, insig = "blank")

#Corrplot function in Hmisc generates a graphic showing the Pearson co-efficient correlations between variables in the matrix. “Method” makes the graph in colour
```

Appendix H: (A) VCD of EV Depletion Experiment Donor Flasks, (B) % Viability of EV Depletion Donor Flasks, (C) Repeat EV Depletion Donor Flasks VCD, (D) % Viability of Repeat EV Depletion Flasks

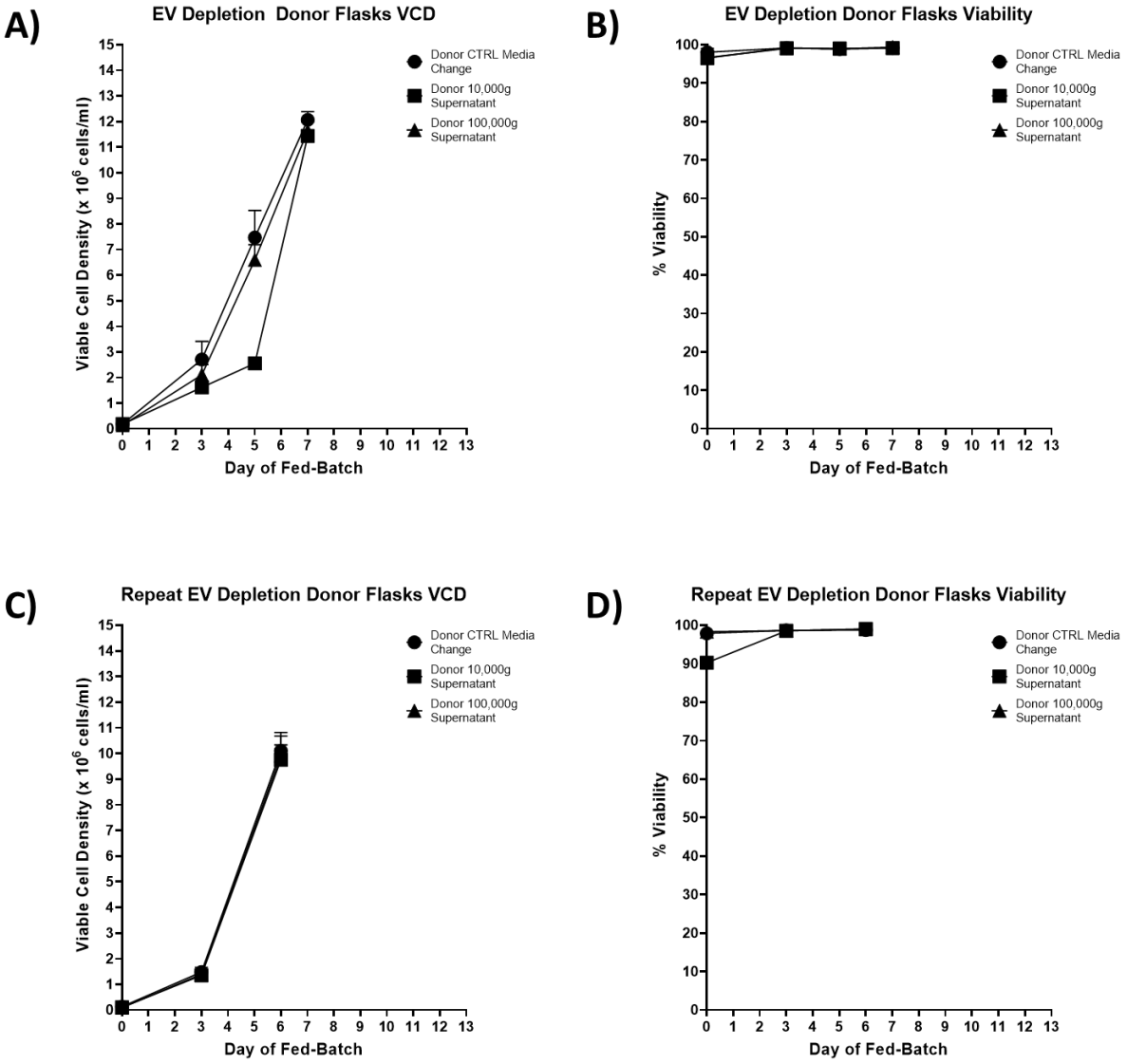

Appendix H: Fold changes of genes significantly differentiated in expression Chapter 5. The fold changes of significantly differentially expressed genes in each category show that the majority of genes had relatively small changes in expression. Wald's Test used to determine statistically significant upregulated and downregulated genes with Benjamini-Hochberg correction for multiple comparisons.